AD NUMBER

AD824865

NEW LIMITATION CHANGE

TO

Approved for public release, distribution unlimited

FROM

Distribution authorized to U.S. Gov't. agencies and their contractors; Test and Evaluation; Nov 1967. Other requests shall be referred to the Air Force Flight Dynamics Laboratory, Attn: FDD, Wright-Patterson AFB, OH 45433.

AUTHORITY

AFFDL, per ltr, 31 May 1973

AFFDL-TR-67-123
VOLUME I

PROJECT HICAT
AN INVESTIGATION OF HIGH ALTITUDE CLEAR AIR TURBULENCE

WALTER M. CROOKS, FREDERIC M. HOBLIT, DAVID T. PROPHET, et al

LOCKHEED-CALIFORNIA COMPANY

TECHNICAL REPORT AFFDL-TR-67-123
VOLUME I

NOVEMBER 1967

AIR FORCE FLIGHT DYNAMICS LABORATORY
RESEARCH AND TECHNOLOGY DIVISION
AIR FORCE SYSTEMS COMMAND
WRIGHT-PATTERSON AIR FORCE BASE, OHIO

NOTICE

When Government drawings, specifications, or other data are used for any purpose other than in connection with a definitely related Government procurement operation, the United States Government thereby incurs no responsibility nor any obligation whatsoever; and the fact that the Government may have formulated, furnished, or in any way supplied the said drawings, specifications, or other data, is not to be regarded by implication or otherwise as in any manner licensing the holder or any other person or corporation, or conveying any rights or permission to manufacture, use, or sell any patented invention that may in any way be related thereto.

Copies of this report should not be returned unless return is required by security considerations, contractual obligations, or notice on a specific document.

300 - January 1967 - CO455 - 18-385

PROJECT HICAT
AN INVESTIGATION OF HIGH ALTITUDE CLEAR AIR TURBULENCE

WALTER M. CROOKS, FREDERIC M. HOBLIT, DAVID T. PROPHET, et al

VOLUME I

FOREWORD

This report was prepared by the Lockheed-California Company, Burbank, California, for the Air Force Flight Dynamics Laboratory, Wright-Patterson Air Force Base, Ohio, under Contract AF33(657)-11143. The contract was for "Redirection and Addition of Effort to the Maintenance of Instrumentation and Equipment for Collection of High Altitude Clear Air Turbulence Data", Project No. 1469. Turbulence research is presently being conducted by the Air Force Flight Dynamics Laboratory under the ALLCAT Program, ADP 682E. The Lockheed-California Company report number is LR 20771, dated 10 July 1967. This report covers work conducted from 12 February 1965 through 10 July 1967.

Air Force Flight Dynamics Laboratory management responsibility was under the ALLCAT Program Director, Mr. E. Brazier, with Mr. N. V. Loving as the Technical Coordinator. Initially the Air Force Project Engineer was Mr. N. V. Loving; Mr. J. P. Boone later assumed responsibility for the Project. The Lockheed-California Company Program Manager was Mr. C. B. Fabian with Mr. W. M. Crooks as the Technical Leader.

All HICAT aircraft operations and field team logistics support were under the direction of Lt Col J. J. King, USAF, Air Force Flight Test Center, VSTOL Branch Flight Operations, Edwards Air Force Base, California.

Special acknowledgements are due to the New Zealand Meteorological Services at Wellington and the Christchurch personnel who developed the local forecasts, and in Australia, the Australian Bureau of Meteorology. Particular thanks are due Mr. Anthony Powell of the Australian Bureau of Meteorology who prepared the high altitude forecasts and the flight plans, and to Mr. C. K. Rider of the Structures Division of the Australian Aeronautical Research Laboratories who helped analyze the meteorological data in Australia.

Acknowledgement is made for the valuable assistance of the following Lockheed-California Company personnel: Mr. R. E. Storey, data analysis; Messrs. D. W. Thompson and P. L. Underwood, field team operation; Messrs. R. H. Cook, H. J. Cail, and R. C. Quist, instrumentation; Messrs. R. D. Baker, E. A. Goulette, and P. J. Tersigni, data processing; Messrs. G. E. Abrahms and W. W. Hildreth, meteorology; and Mr. R. P. Boal, editor.

This report consists of three volumes. Volume I contains the main body of the report plus Appendix I, HICAT Test Summary, Appendix II, Instrumentation System, Appendix III, Data Processing, and Appendix IV, Derivation of Gust Velocity Equations. Volume II contains Appendix V, HICAT Flight Test Log, Appendix VI, Time Histories, Appendix VII, Gust Velocity Power Spectra, and

Appendix VIII, Mathematically Defined Gust Velocity Power Spectral Density Curves. Volume III contains Appendix IX, Flight Descriptions and Flight Track Maps and Appendix X, Meteorological Data Tables.

This technical report has been reviewed and is approved.

James C. Horsley Jr.

JAMES C. HORSLEY, JR., Major, USAF
Chief, Experimental Mechanics Branch
Structures Division

ABSTRACT

This report describes the high altitude clear air turbulence (HICAT) flight investigation with primary emphasis upon the results achieved since 15 February 1965. On this date the program was redirected to utilize a new digital instrumentation system for the measurement of CAT in the wavelength range from about 100 feet to 60,000 feet. The program effort required the measurement of CAT velocity components at altitudes of 45,000 to 70,000 feet in seven geographic areas. Instrumentation carried aboard the HICAT aircraft, an Air Force U-2, consisted of a PCM System, an Inertial Navigation System, aerodynamic and aircraft response sensors including a fixed vane gust probe, oscillograph recorder, and a digital magnetic tape recorder.

The program objective is to determine the statistical characteristics of high altitude CAT so as to improve structural design criteria. Overall, 29.2 hours of high altitude CAT were located and recorded in flights covering over 256,000 miles from bases in California, Massachusetts, Alaska, Hawaii, Puerto Rico, New Zealand, and Australia. Actual vertical, lateral, and longitudinal gust velocity time histories have been calculated from the measurements and used to obtain gust velocity power spectra. Derived equivalent gust velocities were also calculated and peak counted. Meteorological factors were considered in categorizing and correlating data. Time histories and power spectra are found in Volume II of this report, while meteorological data and flight track maps are included in Volume III.

Distribution of this abstract is unlimited.

TABLE OF CONTENTS

		Page
	VOLUME I	
SECTION I	INTRODUCTION	1
	BACKGROUND	1
	HICAT PROGRAM HISTORY	2
SECTION II	INSTRUMENTATION SYSTEM	5
SECTION III	DATA ACQUISITION	7
	HICAT BASES OF OPERATION	7
	HICAT PILOTS	7
	HICAT FLIGHT SCHEDULING	7
	HICAT FLIGHT PROCEDURES	9
	HICAT SEARCH STATISTICS	10
SECTION IV	DATA PROCESSING	13
	GENERAL	13
	DATA ACQUISITION AT THE FIELD SITE	13
	DATA OPERATIONS	13
	DATA EDITING	15
	PCM DATA PROCESSING GROUND STATION	15
	COMPUTER SYSTEM OPERATIONS	15
	BASIC DATA REDUCTION	16
	EVALUATION OF TURBULENCE INTENSITY	16
	GUST VELOCITY COMPUTATION	17
	POWER SPECTRAL COMPUTATION	17
SECTION V	ANALYSIS METHODS	21
	GENERAL	21
	DATA EDITING	21
	TURBULENCE SAMPLE LENGTH DISTRIBUTION	22
	GUST VELOCITY DETERMINATION	23
	DERIVED EQUIVALENT GUST VELOCITY, U_{de}	23
	GUST VELOCITY COMPONENT EQUATIONS	26
	PEAK COUNTING	26
	POWER SPECTRAL ANALYSIS	28
	POWER SPECTRA	28
	SPECTRAL RELIABILITY	29
	SPECTRAL RMS VALUES	33

TABLE OF CONTENTS (Continued)

		Page
SECTION VI	PRESENTATION AND DISCUSSION OF RESULTS	35
	GENERAL	35
	HICAT TEST SUMMARY	35
	TURBULENCE SAMPLE DISTRIBUTIONS	36
	LENGTH	36
	THICKNESS	37
	DISTRIBUTION OF TURBULENCE BY ALTITUDE	39
	GUST VELOCITY TIME HISTORIES	39
	PEAK COUNTS	40
	GUST VELOCITY SPECTRA	53
	GUST VELOCITY SPECTRA PLOTS	53
	MATHEMATICALLY DEFINED GUST VELOCITY POWER SPECTRAL DENSITY CURVES	53
	AVERAGE SPECTRAL SHAPE	59
	SPECIAL STATISTICS	69
	PROBABILITY DISTRIBUTIONS OF RMS GUST VELOCITY	69
	ISOTROPY	76
	STATIONARITY	82
	PEAK COUNT COMPARISON	88
	ERROR ASSESSMENT	89
	ALIASING ERRORS	89
	GUST VELOCITY ERRORS IN ROLLER COASTER MANEUVERS	92
	GUST VELOCITY RESOLUTION	93
	GUST VELOCITY MEASUREMENT ACCURACY	105
	RECAPITULATION	105
SECTION VII	METEOROLOGICAL ASPECTS	107
	GENERAL	107
	SAMPLING SITE SELECTION	107
	FORECASTING PROCEDURES	109
	EVALUATION OF METHODS	112
	METEOROLOGICAL DATA	113
	ANALYSIS AND INTERPRETATION	113
SECTION VIII	CONCLUSIONS	121
APPENDIX I	HICAT TEST SUMMARY TABLE	125
APPENDIX II	INSTRUMENTATION SYSTEM	146
	GENERAL DESCRIPTION	146
	FUNCTIONAL DESCRIPTION OF AIRBORNE EQUIPMENT	146
	TIME CODE GENERATOR	174
	AIRBORNE SENSORS	176
	RECORDERS	187
	POWER SUPPLY	188

TABLE OF CONTENTS (Concluded)

		Page
	FUNCTIONAL DESCRIPTION OF GROUND EQUIPMENT	191
	FIELD TEST EQUIPMENT	191
	PCM GROUND STATION	193
	OPERATIONAL PROCEDURES	196
	PREFLIGHT	196
	PRESTART CHECK	200
	POSTFLIGHT	200
	CALIBRATION PROCEDURES	201
	PCM SYSTEM	201
	LN-3/PCM SYSTEM	204
APPENDIX III	DATA PROCESSING	207
	COMPUTING METHODS	207
	NUMERICAL FILTERING	207
	NUMERICAL INTEGRATION	210
	AERODYNAMIC CALCULATIONS	211
	GUST VELOCITY	214
	WIND VELOCITY	216
	POWER SPECTRA	217
	STATISTICAL COUNTING METHODS	219
	COMPUTER PROGRAMS	221
	HICAT BASIC DATA PROGRAM	221
	HICAT GUST VELOCITY PROGRAM	232
	HICAT SPECTRAL ANALYSIS PROGRAM	234
	STATISTICAL ANALYSIS PROGRAM	237
APPENDIX IV	DERIVATION OF GUST VELOCITY EQUATIONS	240
	REFERENCES	254
	VOLUME II	
APPENDIX V	HICAT FLIGHT TEST LOG	1
APPENDIX VI	TIME HISTORIES	16
APPENDIX VII	GUST VELOCITY POWER SPECTRA	236
APPENDIX VIII	MATHEMATICALLY DEFINED GUST VELOCITY POWER SPECTRAL DENSITY CURVES	483
	VOLUME III	
APPENDIX IX	FLIGHT DESCRIPTIONS AND FLIGHT TRACK MAPS	1
APPENDIX X	METEOROLOGICAL DATA TABLES	234

ILLUSTRATIONS

FIGURE		PAGE
1	Schedule of HICAT Operations	8
2	HICAT Double-X Search Pattern	10
3	CAT Percentage by Base	11
4	Data Acquisition at the Field Site	14
5	Data Processing Flow Chart	18
6	HICAT Aircraft Lift Curve versus Mach Number	27
7	Eighty Percent Confidence Limits as a Function of Degrees of Freedom	30
8	CAT Sample Length Distribution, Time	31
9	CAT Sample Length Distribution, Miles	36
10	Distribution of the Thickness of Turbulent Regions	37
11	Distribution of Flight Miles by Altitude Band for Each Base	38
12	Distribution of CAT Miles by Altitude Band for Each Base	38
13	Percent Turbulence Time versus Altitude	39
14	Typical Time History - Test 102, Run 2, Gust Velocities	42
15	Typical Time History - Test 102, Run 2, Flight Parameters	43
16	Frequency of Exceedance of U_{de} per Flight Mile, Various Locations	44
17	Frequency of Exceedance of U_{de} per Mile in Turbulence, Various Locations	44
18	Frequency of Exceedance of U_{de} per Flight Mile Test 155, Run 2 (Ramey AFB)	45
19	Frequency of Exceedance of CG Normal Acceleration per Flight Mile, Test 155, Run 2 (Ramey AFB)	45
20	Frequency of Exceedance of U_{de} per Flight Mile, Comparison of HICAT with TN D-548	46
21	Frequency of Exceedance of U_{de} per Flight Mile in Turbulence, Comparison of HICAT with TN D-548	47
22	Frequency of Exceedance of U_{de} per Flight Mile in Turbulence, Comparison of HICAT with TN D-548 for Locations Giving Most Severe Turbulence	47
23	Frequency of Exceedance of U_{de} per Flight Mile for Various Altitude Bands	49
24	Frequency of Exceedance of U_{de} per Flight Mile for Various Altitude Bands, Comparison of HICAT with TN D-548	49
25	Distribution of Flight Miles by Altitude Band	50
26	Distribution of Turbulence Miles by Altitude Band	51
27	Percent Turbulence Time versus Altitude	52
28	Comparison of Highest Measured U_{de} Values with Current Design Requirements	52
29	Typical Power Spectra of Vertical, Lateral, and Longitudinal Gust Velocity Components (Test 102, Run 2)	54
30	Comparison of Gust Velocity Power Spectral Envelopes	55
31	Comparison of Three Mathematically Defined Gust Power Spectral Density Curves, m = -1.667, L = 1000 ft and ∞	56

ILLUSTRATIONS (Continued)

FIGURE		PAGE
32	Example of Fairing of Gust Velocity Power Spectral Density Curves	61
33	Cumulative Probability of Power Spectral Density; Vertical, Lateral, and Longitudinal Gust, Maximum λ = 2000 Ft	63
34	Cumulative Probability of Power Spectral Density; Vertical, Lateral, and Longitudinal Gust, Maximum λ = 10,000 Ft	64
35	Cumulative Probability of Power Spectral Density; Vertical Gust, Maximum λ = 40,000 Ft	65
36	Average Power Spectral Density; Based on Cumulative Probability, Maximum λ = 2000 Ft	66
37	Average Power Spectral Density; Based on Cumulative Probability, Vertical Gust, Maximum λ = 10,000 Ft	68
38	Average Power Spectral Density; Based on Cumulative Probability, Vertical Gust, Maximum λ = 40,000 Ft	70
39	Direct-Average Power Spectral Density 3 Components, Maximum λ = 40,000 Ft	71
40	Comparison of Power Spectral Density for 3 Components, Cumulative Probability of .1 at 2 wavelengths	72
41	Cumulative Probability Distributions of RMS 2 Gust Velocities for All Runs Analyzed	74
42	Cumulative Probability Distributions of RMS 2 Gust Velocities for Those Runs for Which All Three Components Are Available	74
43	Probability Distribution of Gust Velocity Component Ratios, RMS 2	79
44	Probability Distribution of Gust Velocity Component Ratios, RMS 10	80
45	Probability Distribution of Gust Velocity Component Ratios, RMS 40	81
46	Theoretical Effect of Nonstationarity on U_{de} Exceedance Curves	86
47	Frequency of Exceedance of U_{de} and Comparison with Rice's Equation	87
48	Comparison of Frequency of Exceedance of U_{de} Based on Positive Slope Crossing and Mean Crossing Procedures	90
49	Roller Coaster Maneuver Gust Velocity Time History - Test 110, Run 3	94
50	Roller Coaster Maneuver Gust Velocity Time History - Test 114, Run 19	96
51	Roller Coaster Maneuver Gust Velocity Time History - Test 142, Run 5	98
52	Roller Coaster Maneuver Gust Velocity Time History - Test 172, Run 3	100
53	Terrain Classification of CAT Encounters	118
54	Aircraft Instrumentation Location Diagram	148

ILLUSTRATIONS (Continued)

FIGURE		PAGE
55	Instrumentation Hatch	149
56	Aft View of Instrumentation J-Box	149
57	View of Magnetic Tape Recorder, LN-3 Stable Platform and SPARMO Radiation Instrumentation (Lower Left)	150
58	HICAT Digital Instrumentation System	151
59	PCM Package	153
60	Time Code Generator	153
61	Instrumentation Control Panels in Cockpit	154
62	PCM Control Panel	154
63	Phase Response of HICAT Passive Low Pass Filter at Room Temperature	155
64	Amplitude Response of HICAT Passive Low Pass Filter at Room Temperature	155
65	Power Spectrum of Alpha-Vane Force	156
66	Power Spectrum of Beta-Vane Force	157
67	Power Spectrum of Indicated Airspeed	158
68	Power Spectrum of Gust Probe Normal Acceleration	159
69	Power Spectrum of Gust Probe Lateral Acceleration	160
70	Power Spectrum of Vertical Acceleration	161
71	Power Spectrum of CG Normal Acceleration	162
72	Power Spectrum of CG Lateral Acceleration	163
73	Power Spectrum of CG Longitudinal Acceleration	164
74	Power Spectrum of Pitch Rate	165
75	Power Spectrum of Roll Rate	166
76	Power Spectrum of Yaw Rate	167
77	Power Spectrum of Pitch Angle	168
78	Power Spectrum of Roll Angle	169
79	Power Spectrum of Heading Sine	170
80	Power Spectrum of Heading Cosine	171
81	Power Spectrum of X Velocity	172
82	Power Spectrum of Y Velocity	173
83	Airborne Data Frame and Tape Format	175
84	Double Beam Sensor with Strain Gage Installation for Shear Measurement	177
85	Angular Deflection of Simple Sensor	177
86	HICAT Gust Probe and Boom Installation on Nose of U-2	179
87	HICAT Gust Sensors	179
88	Typical CG Accelerometer Installation	180
89	Rosemount Total Temperature Probe	180
90	Instrumentation in Aircraft Nose Compartment	181
91	Block Diagram of SPARMO Radiation Counter	185
92	Oscillograph Installation	190
93	Instrumentation Inverter	190
94	PCM Field Checkout Unit	192
95	Gyro Bias Test Set Used With LN-3 System	194
96	HICAT Data Processing Ground Station	197
97	PCM Ground Station	198

ILLUSTRATIONS (Concluded)

FIGURE		PAGE
98	Organization of Field Operation Data	199
99	Sample Field Calibration Data Sheet	202
100	Numerical Filtering Transfer Functions	209
101	Amplitude Ratio Comparison of Simpson's One-Third Rule and Trapezoidal Integrations	212
102	Example of Peak Count Method	220
103	Example of Level-Crossing Count Method	220
104	Ground Station Tape Format	223
105	Basic Data Tables	229
106	Data Acquisition and Reduction of Analog Channel Measurements	230

TABLES

TABLE		PAGE
I	HICAT Instrumentation List	6
II	Determination of Minimum Turbulence Sample Length, $T_{n_{Min}}$	30
III	Turbulence Samples for Spectral Analysis	32
IV	Runs Used for Analysis	67
V	Turbulence Classification According to Terrain	114
VI	HICAT Instrumentation List and Sensor Characteristics	147
VII	Bit Usage of 10 PCM System Digital Channels	183
VIII	Typical PCM Analog Channel Usage	189
IX	Low-Pass Numerical Filtering Cutoff Frequencies of Basic Measurements	210

SYMBOLS

a_F	Longitudinal acceleration in aircraft axes (ft/sec^2); positive forward.
a_L	Lateral acceleration in aircraft axes (ft/sec^2); positive to the right.
a_N	Normal acceleration in aircraft axes (ft/sec^2); positive upward.
a_V	Vertical acceleration in aircraft axes (ft/sec^2); positive upward.
a_X	Aircraft longitudinal acceleration in the horizontal plane (ft/sec^2); positive forward.
a_Y	Aircraft lateral acceleration in the horizontal plane (ft/sec^2); positive to the right.
a_Z	Vertical acceleration in earth reference axes (ft/sec^2); positive upward.
$\bar{c}$	Mean aerodynamic chord.
C_{L_α}	Wing lift curve slope (1/rad).
C_{N_α}	Alpha-vane rate-of-change of normal force coefficient with angle-of-attack (1/rad).
C_{N_β}	Beta-vane rate-of-change of normal force coefficient with side-slip angle (1/rad).
f	Cyclic frequency (cycles/sec).
f_c	Numerical filtering cutoff frequency (cycles/sec).
f_s	Sampling frequency = $1/\Delta t$ (samples/sec).
f_t	Numerical filtering termination frequency (cycles/sec).
$F(\ )$	Probability distribution function.
F_I	Vane inertial force (lb).
F_N	Vane normal force (lb).
$F_{N_{M\alpha}}$	Measured alpha-vane normal force (lb); positive up.

SYMBOLS

$F_{N_{M\beta}}$	Measured beta-vane normal force (lb); positive to the left.
g	Acceleration-of-gravity (ft/sec^2).
$g(\ )$	Statistical frequency of occurrence.
$G(\ )$	Statistical frequency of exceedance.
$h(t)$	Time domain weighting function of numerical filter (1/sec).
$H(f)$	Transfer function designed for numerical filter.
$H^*(f)$	Transfer function of numerical filtering weights.
H_{pc}	Corrected pressure altitude (ft).
H_{pn}	Indicated pressure altitude (ft).
k	Degrees of freedom.
k_b	Fuselage flexibility factor (rad/ft/sec^2).
K_g	Gust alleviation factor = $.88\,\mu g/(5.3 + \mu g)$.
L	Scale of turbulence (ft).
L_h	Raw power spectral estimates.
L_x	Moment arm from gust probe to accelerometer location (ft).
m	Number of spectral estimates, or slope of the power spectral density high frequency asymptote on a log-log plot, or mass of gust sensing vane (lb-sec^2/ft).
M_i	Indicated mach number.
M_T	True Mach number.
$N(\ )$	Frequency of exceedance per unit time = $G(\ )/T_N$.
n	Horizontal distance (meters).
P_a	Ambient pressure (lb/ft^2).
P_s	Static pressure (lb/ft^2).
q_c	Differential pressure (lb/ft^2).

SYMBOLS

$R(\tau)$	Autocorrelation function.
R_p	Estimates of autocorrelation function.
S	Wing area (ft^2).
S_V	Vane area (ft^2).
t	Time (sec).
t_a	Ambient temperature (deg C).
t_t	Total temperature (deg C).
T_n	Elapsed time of a data run (sec).
U_{AG_X}, U_F	Longitudinal gust component in earth reference axes measured in the horizontal plane parallel to the average grid heading of the aircraft over the duration of a run (fps); positive aft.
U_{AG_Y}, U_L	Lateral gust component in earth reference axes measured in the horizontal plane and perpendicular to the average grid heading of the aircraft over the duration of the run (fps); positive to the left.
U_{AG_Z}, U_V	Vertical gust component in earth reference axes measured perpendicular to the horizontal plane (fps); positive upward.
U_{de}	Derived equivalent gust velocity (fps); positive upward.
V	Wind velocity vector (meters per second).
V_e	Equivalent airspeed (fps).
V_g	Geostrophic wind velocity vector (meters per second).
V_{in}	Indicated airspeed (fps).
V_T	True airspeed (fps).
$V_{X'}$	Aircraft grid-X-velocity in earth reference axes (fps); positive to the east.
$V_{Y'}$	Aircraft grid-Y-velocity in earth reference axes (fps); positive to the north.

SYMBOLS

w_n	Numerical filtering weights.
W	Aircraft weight (lb).
$W_I(f)$	Transfer function of ideal integration = $1/2\pi f$.
$W_s(f)$	Transfer function of Simpson's one-third rule integration.
$W_T(f)$	Transfer function of trapezoidal rule integration.
z	Height (meters)
α	Angle-of-attack (rad); positive for relative wind upward.
β	Sideslip angle (rad); positive for relative wind from the right.
γ	Inclination with respect to the horizontal of the instantaneous relative wind (rad).
δ_E	Elevator angle (deg).
δH_p	Altitude static position error correction (ft).
δM	Mach number static position error correction.
Δ	Incremental value. When used for time series data, increments are with respect to mean or linear trend of data.
Δt	Sampling interval (sec.)
∇	Laplacian operator.
ϵ_{ij}	Error resulting from instrumentation resolution (ft/sec) where i refers to the gust velocity component and j refers to each term in the first-order gust velocity equations.
η	Wind direction angle (deg); clockwise from north to the direction the wind is blowing.
θ	Aircraft pitch angle (rad); positive nose up.
θ_M	Aircraft pitch angle measured by inertial platform (rad); positive nose up.
$\dot{\theta}$	Aircraft pitch rate (rad/sec).
λ	Turbulence wavelength (ft).
Λ	Aircraft heading angle (rad); clockwise from north.

SYMBOLS

μ_g	Aircraft mass ratio - $2W/\rho g C_{L_\alpha} c S$.
ρ	Air density ($lb\text{-}sec^2/ ft^4$).
ρ_o	Air density at sea level ($lb\text{-}sec^2/ft^4$).
σ	Air density ratio, ρ/ρ_o.
σ_s	Standard root-mean-square deviation.
σ_w	Standard deviation of any gust velocity component, w. (ft/sec).
σ_y	Standard deviation of y (ft/sec).
τ	Time lag (sec).
ϕ	Aircraft roll angle (rad); positive right wing down.
ϕ_M	Aircraft roll angle measured by inertial platform (rad); positive right wing down.
$\dot{\phi}$	Aircraft roll rate (rad/sec).
$\Phi( )$	Power spectral function.
Φh	Power spectral estimates.
Φ_{xy_h}	Cross-spectral estimates.
ψ	Aircraft yaw angle (rad); positive nose right.
$\dot{\psi}$	Aircraft yaw rate (rad/sec).
ω	Angular frequency (rad/sec).
Ω	Reduced frequency = $2\pi/\lambda$ (rad/ft).
	A bar over a symbol indicates a mean value.
	A caret over a symbol indicates that a filtering transformation has been performed.

SECTION I

INTRODUCTION

BACKGROUND

A distinguishing characteristic of advanced flight vehicles is the increased size of their operating envelope in terms of speed and altitude. Optimum design of such a vehicle is essential and requires detailed knowledge of the intended operating environment.

Sometime before 1962 the Air Force Flight Dynamics Laboratory recognized the need for better definition of the atmospheric turbulence environment, particularly for altitudes above 50,000 feet (Reference 1). Information available then was derived almost entirely from NASA VGH[1] recordings acquired during 192 U-2 flights in five world areas (Reference 2). These flights were made for purposes not directly related to atmospheric turbulence or the penetration of turbulence. Only about half of the data from these flights or approximately 5-1/2 hours were for turbulence above 50,000 feet.

The Air Force realized the danger of relying solely on the acceleration response of the U-2 aircraft as a measure of turbulence at high altitudes. A supersonic or hypersonic vehicle of possibly radical configuration, flying four to ten (or more) times the speed of the U-2, will obviously have a somewhat different response to turbulence than the U-2. An aircraft flying at these high speeds would be affected much more by longer turbulence wavelengths and less by the shorter wavelengths than the relatively slow flying U-2. For these reasons, the Air Force initiated a program to measure high altitude clear air turbulence (HICAT) at altitudes above 45,000 feet in several areas of the world. The principal objective of the program was to statistically define the characteristics of high altitude CAT so as to improve structural design criteria. To accomplish this result, an Air Force U-2 was to be instrumented so that true gust velocity components encountered along the aircraft flight path could be determined.

Lockheed was directed to install and maintain the turbulence measuring instrumentation in the U-2 as well as to process and analyze the data. In this joint effort, the Air Force was to supply the instrumentation, maintain and fly the HICAT aircraft, and provide overall direction of the program. Under a separate contract (Reference 3) Lockheed was directed to utilize the data gathered in the flight program to develop a statistical model of high altitude CAT. The model would then provide meteorologists with a basis for the prediction of atmospheric regions of turbulent flow.

---

[1] Aircraft velocity, center-of-gravity acceleration, and altitude

Section I

HICAT PROGRAM HISTORY

Most of the aircraft instrumentation for the first phase of the program was provided off-the-shelf from Air Force inventory in order to keep within the modest HICAT budget. In many instances standard instruments were supplied which were not particularly intended for turbulence research. This first HICAT instrumentation system was designed so that the analog signals from the sensors modulated the output of strain controlled oscillators to produce frequency modulated signals. The fm signals were then recorded on board the aircraft with a magnetic tape recorder.

Installation of the instrumentation was begun at Edwards AFB in March 1963 and completed in February 1964. During about 8 months of this period the aircraft was required for a higher priority Air Force program and was not available for instrumentation work. During this time, it was established that the differential pressure-type gust probe supplied to the program was inoperative and unrepairable. This probe (a low altitude device originally used in the B-66B program, Reference 4) was intended for interim use only until a more sensitive probe could be purchased. However, a new differential pressure probe could not be built to meet the requirements for high altitude gust measurements because appropriate 1 psi pressure transducers were unavailable.

Consequently, at the request of the Air Force, Lockheed designed and built a high altitude gust sensor. The sensor design was based upon the fixed vane principle which had been utilized successfully in a prior investigation of tail buffeting turbulence on the USN P-3A patrol bomber. Fortunately, it was possible to adapt the fixed vane gust sensors to the nose boom previously fabricated for the differential pressure probe.

The first HICAT checkout flight occurred on 20 February 1964 and the first HICAT search on 3 April 1964. In the period ending 15 July 1964, 18 HICAT search flights were completed, 5 from Edwards Air Force Base, California, 4 from Patrick Air Force Base, Florida, and 9 from Ramey Air Force Base, Puerto Rico. In this initial phase of the program, the HICAT aircraft had to be shared on a day-to-day basis with other higher priority Air Force programs. For this reason, the flights only occasionally coincided with optimum turbulence forecasts. Nevertheless, about 6 hours of high altitude CAT of predominately light-to-moderate intensity was encountered on these flights. Turbulence in the wavelength range from 60 to 2500 feet was located and recorded approximately 14 percent of the time at altitudes above 50,000 feet. Complete documentation of this phase of the HICAT program is presented in Reference 5.

Recognizing the need for better instrumentation to obtain longer wavelength measurements, the Air Force redirected and extended the HICAT program on 15 February 1965. The redirection required installation of a new digital instrumentation system capable of measuring turbulence waves up to 60,000 feet in length. First flight with the new instrumentation occurred 8 October 1965 at Edwards Air Force Base. After several check flights, high altitude CAT search flights were resumed on 16 November 1965, and continued under the present contract until 17 February 1967. During this period, 114 high CAT search flights were performed along with 32 incidental flights. Over 29 hours of

CAT were recorded in the operations conducted from bases in Hawaii, New Zealand, Australia, Puerto Rico, Alaska, California, and Massachusetts. This redirected phase of the HICAT program is the subject of the present report.

On 13 March 1967, the HICAT program was again extended, this time under a new Air Force contract (Reference 6). In this extension the HICAT search flights will be continued from new bases in Great Britain, Louisiana, Maine, Panama, Florida, the Mediterranean area, and the Okinawa area. The new contract provides for more extensive and detailed analysis than was possible under the present contract. The analysis undertaken in connection with the new contract will, of course, consider the data presented in this report as well as the new data.

SECTION II

INSTRUMENTATION SYSTEM

The primary airborne data acquisition system is a digital pulse code modulation (PCM) system. The system accepts both analog and digital data signals from various remote sources in the test aircraft and processes them into a digital format at 25 samples per second. Data from this system is recorded on 1-inch magnetic tape in a parallel format which comprises 10 data bits, one parity bit, and one synchronizing clock bit. The analog data signals are also recorded concurrently in analog form on an oscillograph for purposes of quick-look analysis and data sensor performance evaluation after each flight. These data signals are supplied to the oscillograph following the low-pass presample filtering that takes place within the PCM system. The major components of the instrumentation system are housed in the aircraft Q-bay just behind the pilot. The basic HICAT instrumentation list is shown in Table I.

Analog data signals are routed to the PCM system from a variety of sensors located throughout the test aircraft. A gust probe designed specifically for the purpose provides measurement of airspeed and gust forces. An inertial navigation system provides information on aircraft attitude, acceleration, velocity, and horizontal displacement. Additional acceleration, temperature, angular rate, altitude, and control surface position information is supplied from other sensors appropriately located throughout the aircraft. Each analog signal is conditioned to a 0- to +5-volt level prior to entry into the PCM system. Signal conditioning equipment includes attenuation networks, dc amplifiers, and phase sensitive demodulators. The PCM system also accommodates five channels of external digital information which is entered directly into the system through switch closures on the pilot's control panel and other remote locations.

The digital magnetic tape generated in the airborne system is subsequently processed through a PCM ground station. This equipment decommutates the time-multiplexed data and makes it available to a buffer-formatter which assembles the data into a preprogrammed computer-compatible format. Under control of the formatter, an output tape deck generates a gapped-format magnetic tape which is then processed through digital computing equipment. The ground station also provides for limited visual display and digital-to-analog conversion of selected data channels. The airborne oscillograms are used as editing aids preparatory to ground station processing.

Details of the airborne, ground station, and field checkout systems are presented in Appendix II.

Section II

TABLE I. HICAT INSTRUMENTATION LIST

Measurement	Data Source
Alpha - Vane normal force	Vane - gust probe
Beta - Vane lateral force	Vane - gust probe
Probe normal acceleration	Accelerometer - gust probe
Probe lateral acceleration	Accelerometer - gust probe
CG normal acceleration	Accelerometer - FS 408
CG lateral acceleration	Accelerometer - FS 408
CG longitudinal acceleration	Accelerometer - FS 408
Left wing nodal acceleration	Accelerometer - left wing
Right wing nodal acceleration	Accelerometer - right wing
Indicated airspeed	Δ pressure sensor - probe
Coarse altitude	Pressure sensor - nose
Fine altitude	Pressure sensor - nose
Vernier altitude	Δ Pressure sensor - nose
Total temperature	Temperature sensor - nose
Pitch rate	Gyro - nose
Roll rate	Gyro - nose
Yaw rate	Gyro - nose
Left aileron position	Potentiometer - left wing
Elevator position	Potentiometer - tail
Rudder position	Potentiometer - tail
Fuel counter	Flowmeter and counter - fuselage
Pitch angle	Stable platform - Q-bay
Roll angle	Stable platform - Q-bay
Heading sine	Stable platform - Q-bay
Heading cosine	Stable platform - Q-bay
Vertical acceleration	Stable platform - Q-bay
X velocity	Stable platform - Q-bay
Y velocity	Stable platform - Q-bay
X distance	Stable platform - Q-bay
Y distance	Stable platform - Q-bay
Al radiation count	SPARMO system - Q-bay
Bi radiation count	SPARMO system - Q-bay
Te radiation count	SPARMO system - Q-bay

SECTION III

DATA ACQUISITION

HICAT BASES OF OPERATION

The data acquisition phase of the HICAT program was designed to obtain CAT search flights in various areas of the world over all types of terrain. Whenever possible the optimum season for high altitude CAT in a particular region was selected on the basis of the best available meteorological opinion. The actual selection of a particular base of operation was made by the Air Force consistent with the requirements for U-2 operations. In the current program HICAT searches have been conducted from the following bases:

- Edwards Air Force Base, Edwards, California, U.S.A.
- Hickam Air Force Base, Honolulu, Hawaii, U.S.A.
- Christchurch International Airport, Christchurch, New Zealand
- Royal Australian Air Force Base, Laverton, Victoria, Australia
- Hanscom Field, Bedford, Massachussetts, U.S.A.
- Ramey Air Force Base, Aquadilla, Puerto Rico, U.S.A.
- Elmendorf Air Force Base, Anchorage, Alaska, U.S.A.

The schedule of HICAT operations is shown in Figure 1. Note that approximately a month or more of search flight operations was carried out at each base.

HICAT PILOTS

The U-2 HICAT flights were performed by Edwards Air Force Flight Test Center V/STOL Operations Branch pilots under the command of Lt. Col. James J. King. Pilots flying HICAT missions in addition to Lt. Col. King were the following: Majors W. H. Shawler, F. J. Cuthill, C. Rosburg, and A. P. Johnson together with Captains R. B. Lowell, F. J. Davey, and T. H. Smith. Major Rosburg also flew B-47 support missions in New Zealand.

HICAT FLIGHT SCHEDULING

When the program began, it was thought that HICAT flights would be made at optimum times during the day as determined by a meteorologist or a forecaster. The realities of remote flight test operations and the limitations of

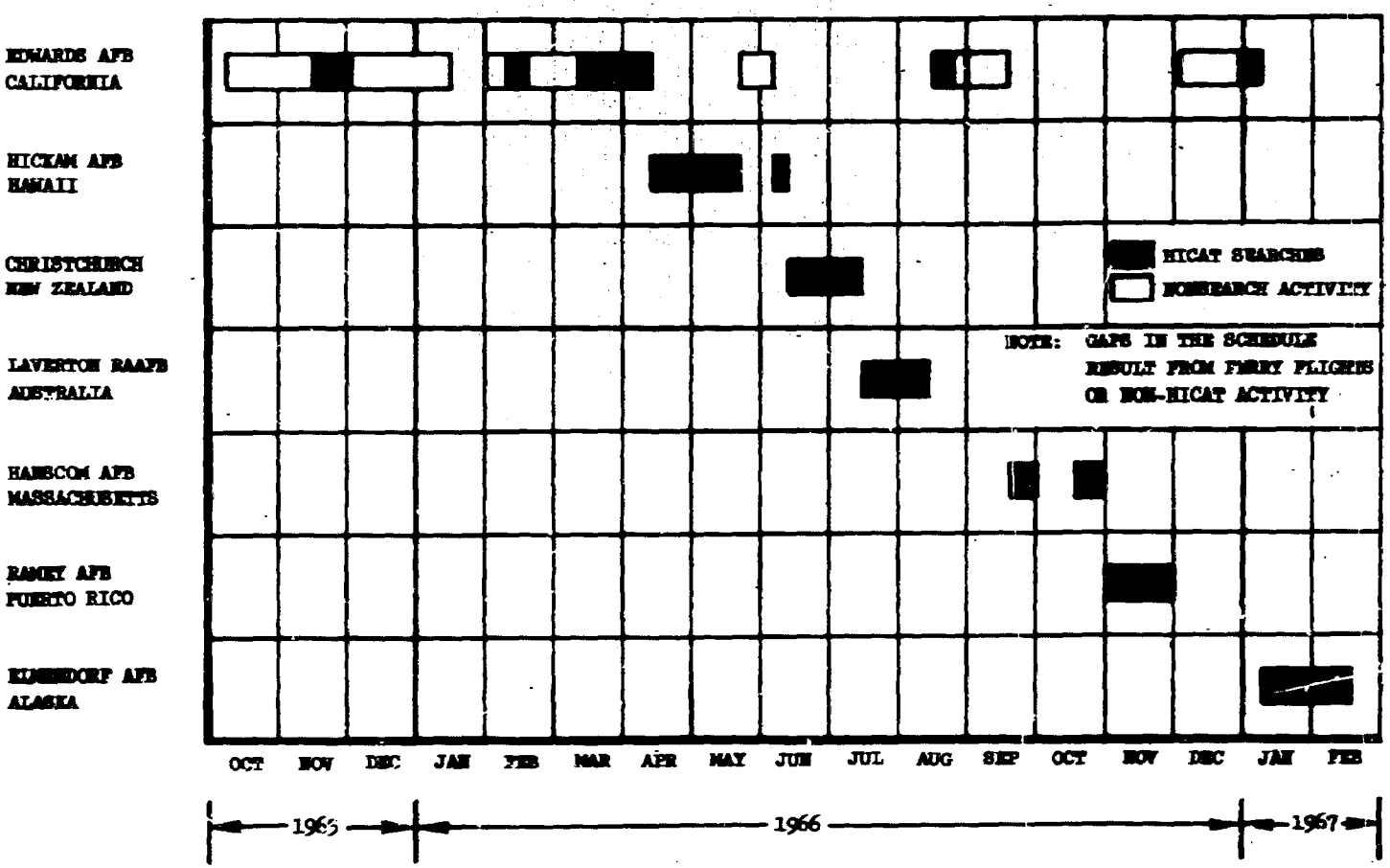

Figure 1. Schedule of HICAT Operations

meteorological forecasts resulted in some practical compromises. Aircraft, instrumentation, and weather permitting, flights were scheduled Monday through Friday as long as two or more pilots were available. (When only one pilot was available, as was the case in Australia, only three flights a week were planned.) Normally, HICAT flights were scheduled only during daytime hours with the takeoff at about 10 AM local time.

HICAT FLIGHT PROCEDURES

On a day of a flight, a flight plan was prepared, based upon a CAT forecast derived from the most recent weather observations. The pilot was then briefed on the high altitude CAT conditions predicted en route and any special flight tests to be performed.

If the flight was to be over water and more than 200 miles from land, an additional aircraft was required to patrol the search area to provide navigational aid and air rescue support. A B-47 jet was used for this purpose in New Zealand and a C-97 Air Rescue transport in Puerto Rico and Alaska.

The flights usually began about midmorning as mentioned above and were of three to six hours duration. The instrumentation was operated continuously throughout the flight. The aircraft normally began the CAT searches at an altitude of about 50,000 feet. If no turbulence was encountered, the aircraft alternately climbed and descended in the altitude range above 50,000 feet while en route. If significant CAT was encountered, fairly level straight runs were made through the turbulence. During these runs, the autopilot was turned off and control activity minimized. In order to define the CAT area a double X-pattern was frequently flown with upwind, crosswind, and downwind legs.[2] Figure 2 illustrates this pattern. If the turbulence covered a wide area and appeared sufficiently intense, the pattern was repeated at another altitude.

CAT intensity was usually evaluated subjectively by the pilot as well as from a mechanical cockpit accelerometer. Pertinent weather observations (i.e., winds, clouds, etc.) were noted along with necessary flight and navigational information. On most flights the pilot also took 35mm color photographs of the clouds (if any) in the vicinity of the CAT area.

During many of the flights when the air was especially smooth, control pulses and smooth symmetric pitch maneuvers (roller coasters) were performed. This was done in order to check the polarity and behavior of the instrumentation as well as to check the efficacy of the gust velocity determination (See Gust Velocity Errors in Roller Coaster Maneuvers, Section VI).

At the end of a HICAT flight, the pilot was debriefed by the local weather personnel and the Lockheed field engineer. These meetings were tape recorded for later evaluation in conjunction with the meteorological analysis. Also, immediately after the flight, the quick-look oscillograph record was processed and examined. Turbulence penetrations were evaluated as well as the performance of the instrumentation. Peak turbulence accelerations were

[2]This pattern was flown over Mauna Loa on the island of Hawaii on most of the flights from Hickam AFB regardless of the presence of CAT.

Section III

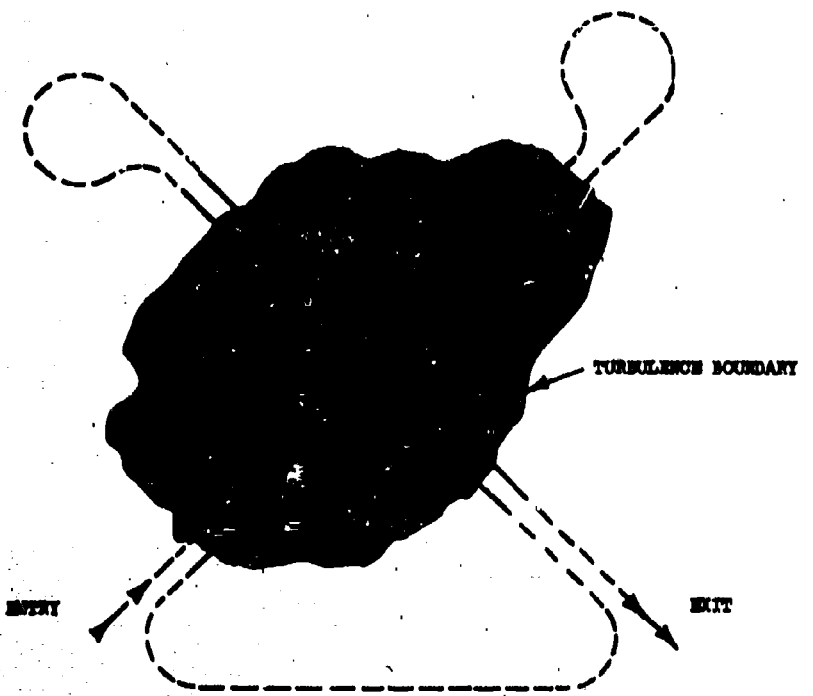

Figure 2. HICAT Double-X Pattern

determined at this time in order to classify the intensity of the CAT encounter and for comparison with the pilot's notes.

HICAT SEARCH STATISTICS

As the Flight Test Log appearing in Appendix V shows, 146 HICAT test flights were made totaling 649.5 flight hours. Of these flights, 114 were planned searches for high altitude CAT and 75 of the 114 resulted in CAT encounters ranging from light to moderate severity. In addition, high CAT was encountered in 9 of the 32 incidental flight tests. The incidental flight tests or non-search tests included aircraft check flights, instrumentation check flights, and ferry flights. Overall, 29.2 hours of high CAT were recorded, 27.1 of them resulting from planned searches based upon CAT forecasts. Figure 3 summarizes the relative success of HICAT searches at each of the bases of operation. The figure indicates that the Australian flights encountered the largest amounts of CAT and the Alaskan flights the least.

Track maps of the HICAT search flights are presented in Appendix IX along with a description of each flight from the standpoint of the meteorologist and the pilot.

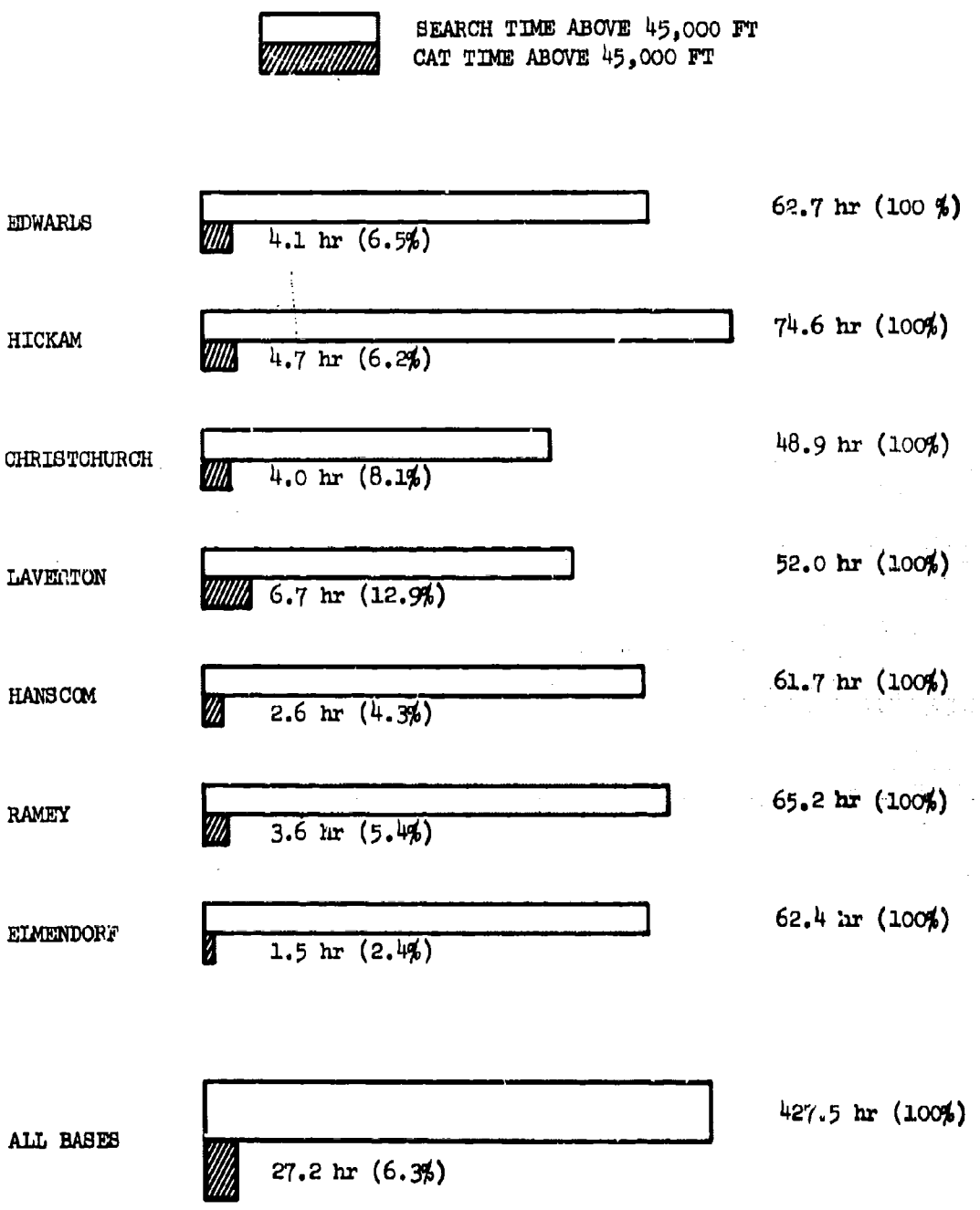

Figure 3. CAT Percentage by Base

SECTION IV

DATA PROCESSING

GENERAL

The purpose of the Data Processing phase of the HICAT program was to retrieve edited raw turbulence data recorded digitally on an airborne PCM magnetic tape, convert the data to a computer-compatible format on the HICAT PCM Ground Station, and then process it through a series of computer programs designed to provide data for a statistical analysis of high altitude clear air turbulence.

Automatic data handling techniques were essential in processing the large volume of data required for the HICAT program. The total amount of data processed was equivalent to about 27 hours of turbulence. This required the processing of approximately 100 million data points and the preparation of several thousand plots of gust velocity time histories and power spectra. An IBM System/360 Model 50/75 computer was used to process the data and to perform the statistical computations. A CALCOMP automatic plotter with magnetic tape input was used for the graphical presentation of the data.

DATA ACQUISITION

Flight test data were recorded simultaneously on both a PCM magnetic tape and an oscillogram. The PCM magnetic tape was used as the primary recording medium and the oscillogram was used for a quick-look evaluation of the test data and the instrumentation system by the field team.

After the postflight evaluation, all of the test data including the quick-look oscillogram, PCM magnetic tape, instrumentation and flight data sheets, track maps, meterological data, pilot's flight log and pilot's photos were transmitted to the HICAT project office at the Lockheed-California Company in Burbank, California, for distribution and processing. Figure 4 diagrams the data acquisition phase at the field site.

DATA OPERATIONS

In order to verify the quality of the PCM magnetic tape and check for possible malfunctions of the airborne PCM data acquisition system, the airborne PCM magnetic tape was played back through the PCM ground station as soon as it was received. The time recorded on the tape was checked by means of a translated visual display in terms of days, hours, minutes, and seconds. Each of the data channels was given a rudimentary check by means of a visual decimal display. Fourteen digital-to-analog converters on the ground station coupled to a

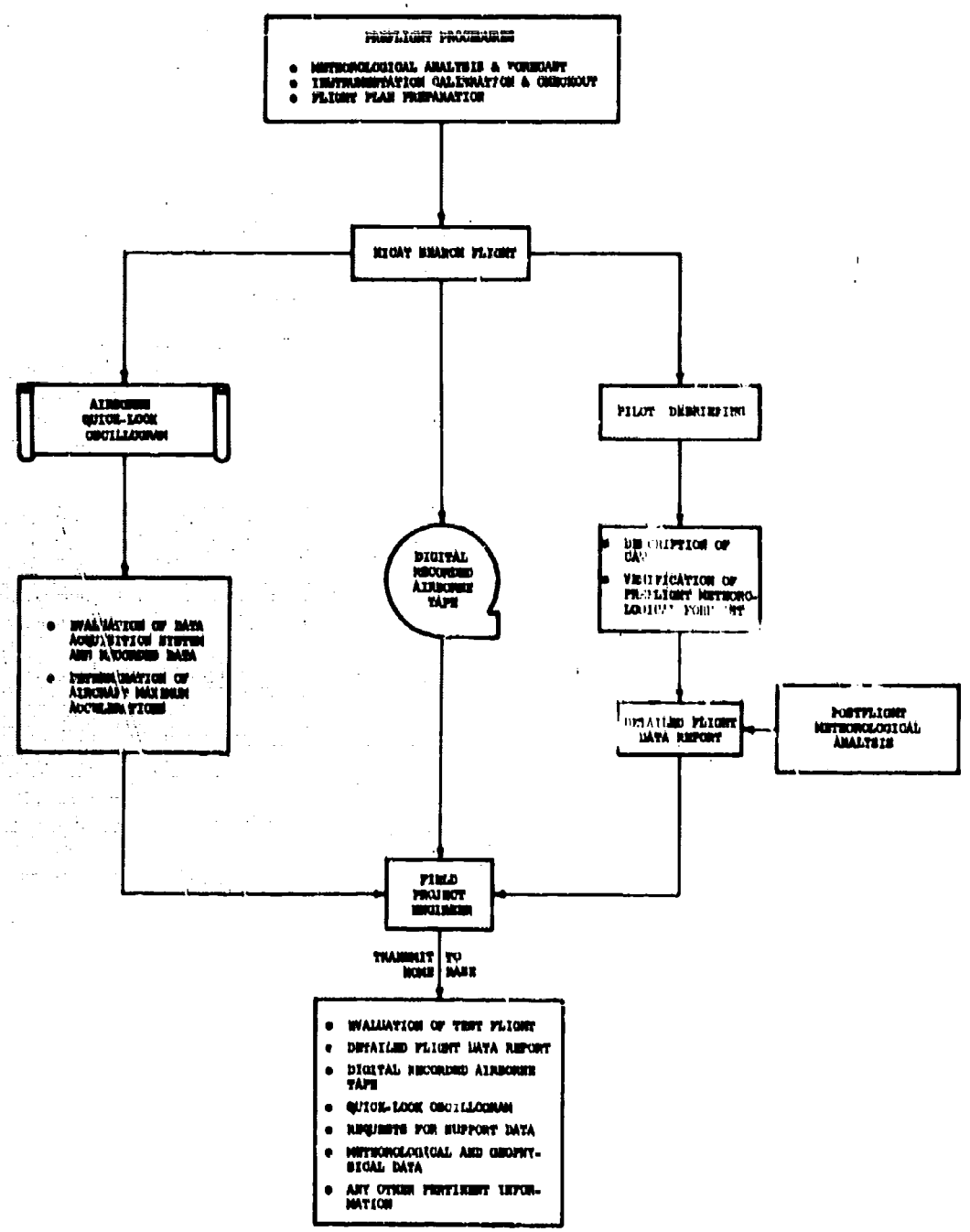

Figure 4. Data Acquisition at the Field Site

direct-write oscillograph recorder could be used for further checking and trouble shooting. Notice of any instrumentation system malfunctions discovered in this checkout was immediately transmitted back to the field team.

Instrumentation and flight data records received from the field team after each flight were appraised to obtain the current status of the instrumentation calibrations and configuration prior to the processing of any data.

DATA EDITING

The airborne oscillograph record was utilized to select data samples for computer processing. When the airborne oscillogram was unsatisfactory or missing, an oscillograph record was generated on the PCM ground station from the airborne magnetic tape. The editing process consisted of the following basic steps:

- Evaluation of instrumentation performance.
- Selection of turbulence samples to be processed and determination of their start and stop times.
- Determination of turbulence intensity and character.
- Determination of aircraft attitude and control motions during CAT penetrations.

Details of the editing process from the analysis point of view are presented in section V.

PCM DATA PROCESSING GROUND STATION

The results of the editing provided turbulence run start and stop times for processing the selected data through the PCM ground station. The ground station performed the following functions: Retrieval of data from the airborne magnetic tape, decommutation, digital-to-analog conversion with analog display, conversion of the data to computer-compatible format, and the recording of reformatted data onto computer magnetic tape. The airborne data, originally recorded on tape at 1-7/8 inches per second, was played into the ground station at 30 inches per second. This permitted the data to be converted at 16 times the real-time recording speed. The output magnetic tape from the ground station is compatible for input to the initial basic data computer program.

A more detailed description of the ground station is provided in Appendix II.

COMPUTER SYSTEM OPERATIONS

Four computer programs were designed to process and analyze the turbulence data recorded on the ground station output tapes:

- Basic data program
- Gust velocity program

- Statistical analysis program
- Spectral analysis program

A detailed description of these programs is included in Appendix III.

Reduction of the turbulence data recorded on each ground station magnetic tape culminated in the production of two additional tapes corresponding respectively to the first two programs above; (1) an intermediate tape containing the reduced basic measurement samples in engineering units, and (2) a final output tape recording the reduced measurements, the computed aerodynamic variables, the derived equivalent gust velocity, and the 3-axes gust velocity components. The analysis programs (the last two above) were designed to accept either of the two computer-generated tapes as their data source.

Figure 5 indicates the sequential operations involved in the implementation of the programs at the computer system facility.

BASIC DATA REDUCTION

The tape generated by the ground station was input to the basic data program to perform the reduction functions required for each measurement. Specifically, the program read, disassembled, and translated the packed PCM data into a standardized format configuration in the computer. The times associated with contiguous frames were monitored to ensure that the correct time interval was maintained. The measurement samples were then calibrated into engineering units. A sporadic error search of the calibrated data was initiated to detect and correct the presence of "wild point" samples. Finally, the calibrated measurement samples were low-pass filtered by applying selected sets of Martin-Graham numerical filtering weights designed to pass only the useful frequency response range of each measurement. A description of the derivation and application of the four numerical filters designed for HICAT data is given in Appendix III.

Following execution of the functions described above, the basic data were recorded on magnetic tape and tabulated in continuous time history listings. When a graphical representation was required for analysis at this point, a plot program was introduced to automatically generate fully annotated time histories of the basic data.

EVALUATION OF TURBULENCE INTENSITY

Following a review of the basic data output, the runs found to be acceptable were processed through the statistical analysis program. This program computed the derived-equivalent gust velocity and then determined the distribution characteristics of selected data utilizing two statistical counting methods. Both methods are described in Appendix III under Computing Methods. To evaluate turbulence intensity the distribution characteristics of cg accelerations and the derived equivalent gust velocity were examined. CAT runs of very low intensity usually produce poor spectra and so normally were excluded from further processing.

GUST VELOCITY COMPUTATION

The gust velocity program used the tape generated by the basic data program to compute and output on tape the following parameters for the CAT data.

- Aerodynamic variables such as V_e, H_{pc}, t_a, M_T, etc.
- Derived equivalent gust velocity
- Uncorrected gust velocity components
- Gust velocity components corrected for aircraft motion
- Wind velocity

The computing method employed to determine these parameters is presented in Appendix III under Computing Methods.

Simpson's one-third rule was used to numerically evaluate the integral terms in the gust velocity equations (see Appendix III, Computing Methods).

The gust velocity program was designed to compute the gust velocity components by several alternate methods utilizing various combinations of measurements. These options were made available so that some gust velocity components could still be obtained despite an instrument malfunction.

If desired, time history plots of gust velocities and other parameters recorded on the final data tape were generated at this time.

POWER SPECTRAL COMPUTATION

To determine the statistical characteristics of the turbulence data in the frequency domain, selected parameters recorded on the computer-generated tapes were processed through the spectral analysis program. This program employed techniques developed by Tukey to numerically evaluate power spectral estimates as defined in Appendix III under Computing Methods. The tabular listings of the spectral data were output along with spectral plots automatically generated during execution of the program.

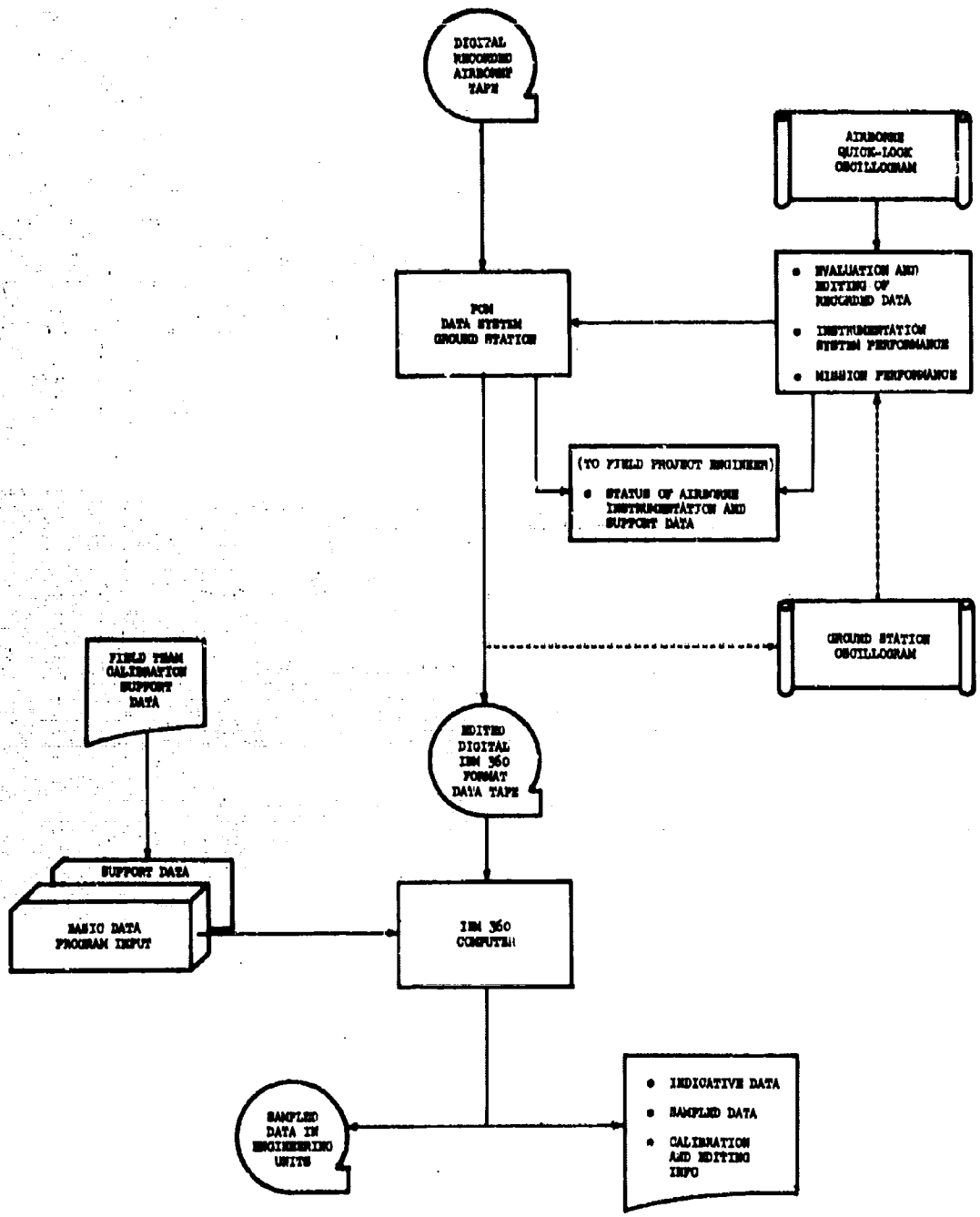

Figure 5A. Data Processing Flow Chart

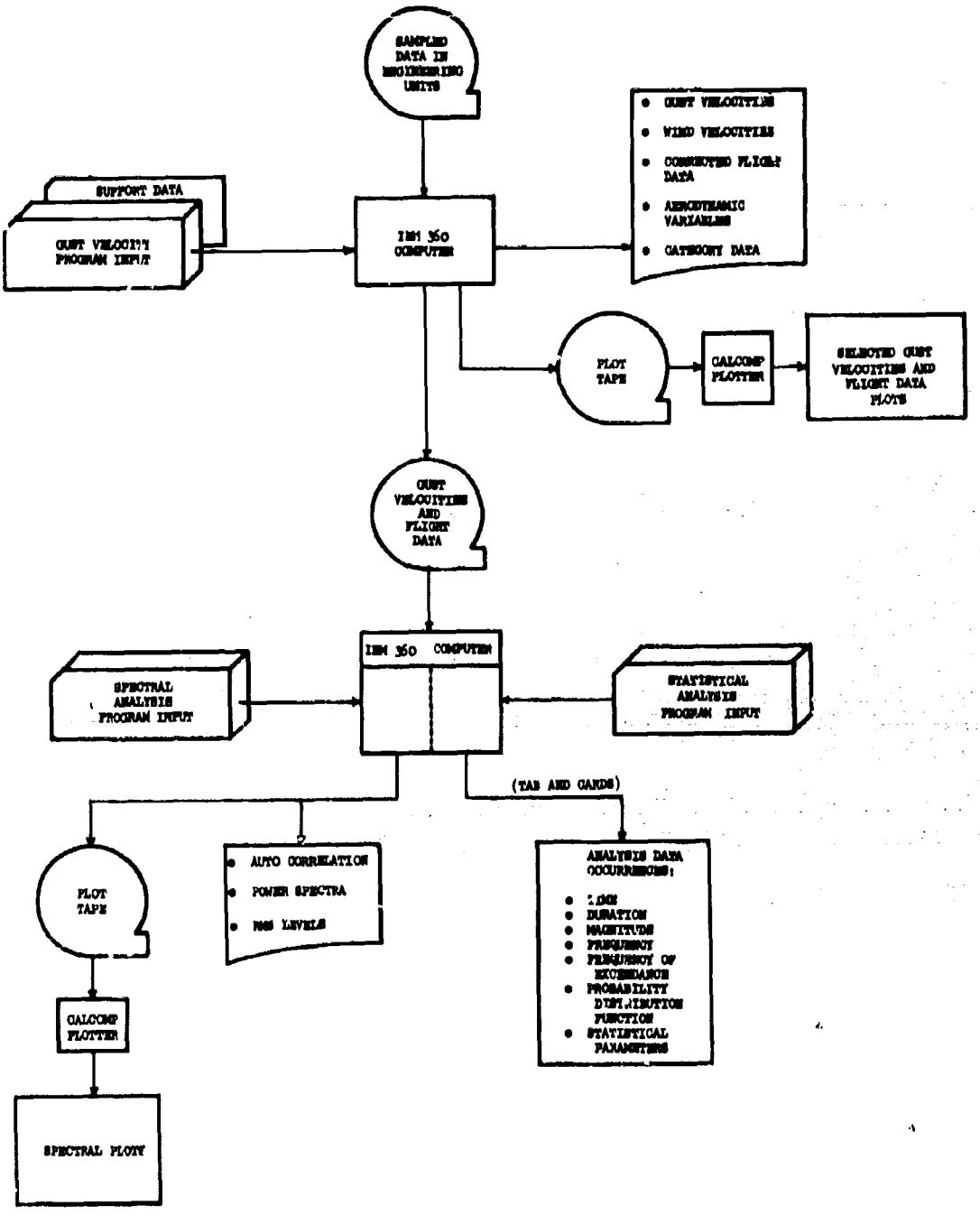

Figure 5B. Data Processing Flow Chart

SECTION V

ANALYSIS METHODS

GENERAL

The HICAT analysis constitutes one of the final steps toward the objectives stated in the Introduction, i.e., to determine the statistical characteristics of high altitude clear air turbulence so as to improve the structural design criteria for advanced flight vehicles. This objective means quantifying in some meaningful way such fundamental CAT characteristics as size, height, intensity, variation of intensity with wavelength, frequency of occurrence, gust component variability, scale, and rate of dissipation. The analysis methods used for this purpose are described in this section. They include the following:

- Data editing - the selection of CAT samples.
- Turbulence sample length distribution.
- Gust velocity determination from flight measurements.
- Derived equivalent gust velocity and cg acceleration peak and level crossing counts.
- Gust velocity power spectral analysis.

DATA EDITING

The selection of CAT samples for data processing and analysis was based upon an edit of the flight measurements recorded on the quick-look oscillogram. Turbulence samples were selected primarily from an evaluation of the cg normal acceleration response of the aircraft. The acceleration sensitivity of the oscillograph trace was approximately 0.9g per inch which provided a reading resolution of 0.01g. If continuous rapid cg acceleration disturbances were observed in excess of ±0.05g, turbulence was considered to be present. Small, high-frequency oscillations in the gust probe measurements normally provided further evidence of the presence of CAT. Usually, the pilot would confirm the presence of CAT by activating his oscillograph event marker.

A turbulent region as defined above was considered to be significant (i.e. worth processing) if frequent cg acceleration peaks of ±0.10g or more were observed.

In this event sample[3] start and stop times were noted to the nearest 5 seconds. An attempt was made to note all significant samples. However, those turbulence patches of less than 10 seconds' duration - corresponding to about one mile in physical length - were usually ignored. CAT encountered in turns, particularly unsteady turns, was usually excluded also.

Generally speaking, no special attempt was made to edit recordings that did not contain the relatively rapid oscillations normally associated with the confused mixing of turbulence - nearly always noted by the pilot. It was, of course, recognized that some long wave phenomena (e.g., gravity waves or undulance) might exist apart from those regions commonly identified as turbulent. However, no such perturbations were observed except for those rare oscillations caused by the pilot or by a malfunctioning autopilot. Nevertheless if the waves were present but so low as to pass unnoticed, then they are included in the edited data since such waves could hardly be expected to stop at the edge of a genuinely turbulent region.

Each edited sample was characterized by a subjective description of the CAT in words as well as in terms of the estimated cg acceleration peak-level. In general, the following classification, derived originally from HICAT pilots' comments, was observed:

Frequently occurring peak g increment	CAT description
±0.05 to ±0.10	Very light (VL)
±0.10 to ±0.25	Light (L)
±0.25 to ±0.50	Moderate (M)
±0.50 to ±0.75	Severe (S)
±0.75 or greater	Extreme (X)

As an aid to later analysis, the aircraft attitude during the turbulence penetration was noted, i.e., level, climbing, descending or turning. In this connection, average rates of climb or descent less than about 400 feet per minute were considered to be level.

Frequent or excessive use of the controls as evidenced by changes in control surface positions or fuel flow rate were also noted. Relatively slow, large-amplitude motions of the elevator were suspect if the turbulence was very light and occasionally resulted in a CAT sample being passed over.

TURBULENCE SAMPLE LENGTH DISTRIBUTION

In an attempt to determine the distribution of high CAT sample lengths, the following simple procedure was used to construct a cumulative histogram. All

[3]After processing in the ground station, CAT samples are usually called runs and referred to by a run number.

CAT samples from searches were classified by duration into 1-minute intervals and summed within these intervals. The cumulative sum of occurrences was then computed beginning with the number of occurrences in the highest interval. By dividing each of these values by the total number of samples, a cumulative percentage distribution was obtained of CAT sample lengths in minutes. The sample lengths in minutes were then converted to lengths in statute miles by multiplying by the average true airspeed. A similar procedure was used to obtain cumulative percentage distribution by base of operation. The resulting distributions are presented and discussed in Section VI.

GUST VELOCITY DETERMINATION

Two methods of gust velocity determination are utilized in this report. The first method relies primarily upon the measurement of the cg normal acceleration response of the aircraft to compute the derived equivalent gust velocity, U_{de}. This useful quantity is a fictitious gust velocity. The second method is much more rigorous and depends upon the simultaneous measurement of air velocities and aircraft motions to compute the true or absolute vertical, lateral, and longitudinal gust velocity components. Each of these methods is described in detail in the following paragraphs.

DERIVED EQUIVALENT GUST VELOCITY, U_{de}

The complete derivation of the formula relating the derived equivalent gust velocity, U_{de}, to the peak measured incremental cg normal acceleration, Δa_N, is contained in Reference 7. Pertinent portions of the derivation are repeated below to provide insight into the meaning of U_{de}.

The derivation is predicated on the following assumptions:

- The airplane is a rigid body.
- The airplane forward speed is constant.
- The airplane is in steady level flight prior to entry into the gust.
- The airplane can rise but cannot pitch.
- The lift on the airplane is concentrated at a single fore-aft location, i.e., penetration effects are neglected.
- The gust velocity is uniform across the span and always normal to the longitudinal axis of the airplane.
- The gust velocity profile is a one-minus-cosine shape with a 12.5 chord gradient.
- The transient lift growth functions are those for an infinite aspect ratio wing at zero Mach number.

Section V

As a result of the prescribed gust shape and the particular transient lift functions, the acceleration which would be determined from the solution to the equation of motion depends only on the following two quantities:

1. A reference acceleration, called the sharp-edged gust acceleration and defined as the acceleration which would occur if the airplane were to encounter a sharp-edged gust of velocity, U, and develop instantaneously the change in lift due to this encounter:

$$\Delta a_{N_{ref}} = \frac{C_{L_\alpha} \rho S V U}{2W}$$

2. A dimensionless mass parameter, μ_g defined as:

$$\mu_g = \frac{2W}{C_{L_\alpha} \rho c g S}$$

The solution of the equation of motion is obtained in Reference 7 as a time history of the ratio $\Delta a_N / \Delta a_{N_{ref}}$ for various values of μ_g. The maximum calculated value of this ratio for each value of μ_g is identified as the gust factor and labeled K_g. Points on the curve of K_g versus μ_g were computed one at a time, and no closed-form analytical expression for this relation is available. However, a close approximation to the curve relating K_g to the mass parameter μ_g is given by the expression

$$K_g = \frac{.88 \mu_g}{5.3 + \mu_g}$$

The maximum ag normal acceleration is thus seen to be given by

$$\Delta a_{N_{max}} = \frac{\Delta a_{N_{max}}}{\Delta a_{N_{ref}}} \Delta a_{N_{ref}}$$

$$= K_g \frac{C_{L_\alpha} \rho S V U}{2W}$$

Converting from true to equivalent airspeed, the equation becomes

$$\Delta a_{N_{max}} = K_g \frac{C_{L_\alpha} \rho_o S V_e U_{de}}{2W} \qquad (1)$$

or, rewriting to express U_{de} in terms of $\Delta a_{N_{max}}$,

$$U_{de} = \left[\frac{2W}{C_{L_\alpha} \rho_o S V_e K_g}\right] \Delta a_{N_{max}} \qquad (2)$$

The subscript "d" in U_{de} stands for derived and the "e" for equivalent. It emphasizes the fact that when U_{de} is obtained from flight measured cg normal accelerations using equation (2), it is not an actual gust velocity but a fictitious derived quantity, the derived equivalent gust velocity. It can be interpreted as the gust velocity that would produce the measured value of $\Delta a_{N_{max}}$ if the restrictions contained in the basic assumptions were met. One assumption that is not even closely met is that pertaining to gust shape; the simple one-minus-cosine shape of fixed length bears little resemblance to the actual complex gust velocity profiles measured in the atmosphere. Nevertheless, it has been found that this highly simplified theory gives a very good indication of the relative accelerations experienced in turbulence by various airplanes. As a result, it has been a very useful design tool. If statistical data on cg accelerations of existing airplanes are converted to U_{de} form by means of equation (2), then the acceleration experience of a new airplane can be predicted by means of equation (1). This approach has been used for many years both in establishing design loads and in defining repeated loads spectra for fatigue analysis; only recently has it been supplemented by newer theories that are more precise both in their description of the gust pattern and their treatment of the airplane dynamics.

It is clear, however, that the derived equivalent gust velocities inferred from cg accelerations are, in fact, fictitious gust velocities that bear little relation to actual gust velocities that might be measured directly. It is also clear from the above derivation that U_{de} should be regarded as applying only to peak values, obtained from the measured peak values of Δa_N. As a matter of convenience, however, it has become common practice to apply the bracketed term on the right-hand side of equation (2) to the entire Δa_N time history and to designate the resulting variable U_{de}. Thus, when peak values are read from the time history, no further conversion is necessary. Also, this term can be regarded as a normalizing factor which places not only peak values of acceleration, but acceleration time histories as well, on a common basis largely independent of the characteristics of any individual airplane.

In the HICAT program a time history of U_{de} is computed for each run from the measured time history of cg normal acceleration for each run. Average values are used during a run for all quantities in the expression for U_{de} except Δa_N. The parametric variations during any single run are generally small as to have

a negligible effect on the values of U_{de}. Values of S, c, and C_{L_α} used in calculating U_{de} were as follows:

$$S = 600 \text{ ft}^2, \quad c = 8.4 \text{ ft}, \quad C_{L_\alpha} \text{ as given in Figure 6.}$$

GUST VELOCITY COMPONENT EQUATIONS

The determination of the absolute gust velocity components of atmospheric turbulence from an aircraft requires the measurement of (1) the motion of the air disturbances with respect to the aircraft and (2) the motion of the aircraft with respect to the ground. In the HICAT instrumentation system the air disturbances relative to the aircraft are measured with a gust probe; the aircraft motion relative to the ground is determined by an inertial platform.

The basic equations used to determine the vertical, lateral, and longitudinal gust velocity components from the HICAT measurements are given below.

$$\Delta U_V = V_T \Delta\alpha + V_T \Delta\beta\Delta\phi - V_T \Delta\theta + \int \Delta a_Z dt + L_X \Delta\dot{\theta}$$

$$\Delta U_L = V_T \Delta\beta - V_T \Delta\alpha\Delta\phi + V_T \Delta\psi - \Delta V_X, \cos\bar{\Lambda} + \Delta V_Y, \sin\bar{\Lambda} + L_X \dot{\psi}$$

$$\Delta U_F = \Delta V_T - \Delta V_X, \sin\bar{\Lambda} - \Delta V_Y, \cos\bar{\Lambda}$$

The Δ's indicate that the components are zero-mean values with linear trends removed. The derivation of these equations is shown in considerable detail in Appendix IV.

PEAK COUNTING

The peak count analysis has two objectives:

- Determination of the level of turbulence encountered and correlation with existing data published by NASA in TN D-548.
- Determination of the stationarity of turbulence data time histories by comparing HICAT cumulative peak count distributions with peak count distributions given by theory for a stationary Gaussian process (Rice's equation).

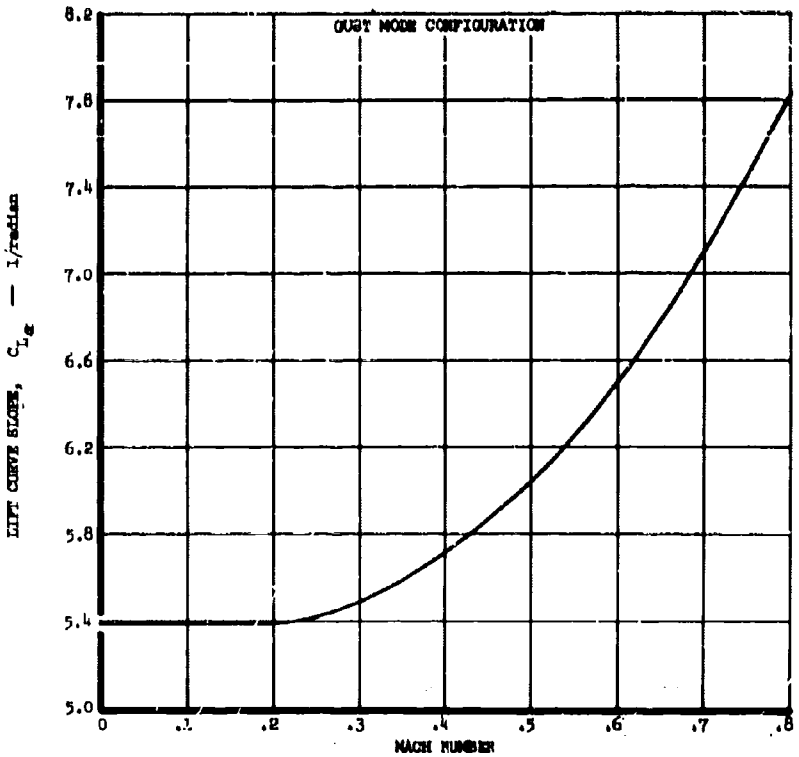

Figure 6. HICAT Aircraft Lift Curve Slope versus Mach Number

Peak counts were obtained from the low-pass-filtered time histories of normal acceleration at the airplane center of gravity, Δn_N, and of the related quantity, derived equivalent gust velocity, U_{de}.

Peak counts were not obtained of the absolute gust velocities because of the probability of large, uncertain contributions at the long wavelengths and the sensitivity of the peak count data to these large contributions. Consideration was given to the use of high-pass filtering to remove the long wavelength components from the data, but it was decided not to attempt such filtering, for two reasons. First, the proper interpretation and use of peak counts based on filtered time histories is not evident at this time. It is not clear how such peak counts might be utilized directly in developing design criteria, and inasmuch as the filter characteristic would be quite arbitrary, it is unlikely that valid comparisons could be made with peak counts obtained from other programs. Second, peak counts have been of value chiefly in establishing gust intensity statistics. In the HICAT program, there has been no attempt to obtain either a random sample of the atmosphere or one that would simulate normal aircraft operations. Consequently, in this program, peak counting has been considered to be of secondary importance, and it appears that the measure of turbulence intensities given by the U_{de} peak counts should be adequate.

Two different peak counting procedures were used. In the first, peaks were defined as maxima occurring between adjacent zero crossings, based on the time history after removal of linear trends. This definition is a common-sense one

that has been used quite generally. In obtaining the peak count, the peaks were classified by absolute magnitude within various intervals. The numbers of peaks falling in the various intervals were then accumulated, starting with the highest interval. Thus the resulting peak count curves give the number of peaks in excess of any given value of Δa_N or U_{de}.

In the second peak counting procedure, the number of positive slope crossings of positive levels defines the number of peaks in excess of that level. Similarly, negative slope crossings of negative levels define negative peaks. This peak counting technique is inherently cumulative, so that a cumulative sum is obtained by simply combining the counts of positive and negative peaks. This technique gives the kind of peak count that is predicted theoretically for a stationary Gaussian process by Rice's equation, as discussed in Section VI under Stationarity. Comparison of peak count curves obtained in this manner with the corresponding theoretical curves given by Rice's equation for the same runs provides information that can be extremely important when measured gust velocity rms values are used in establishing a model of the atmosphere for design use.

Peak counts were obtained only for the portions of the flight records identified as runs, as runs were defined under Data Editing earlier in this section. Difficulties with the airborne instrumentation precluded obtaining peak counts from some runs. Peak counts were not obtained for runs in which maneuver load factors could be misinterpreted as significant gust response. As noted earlier, the oscillograph records were edited so as to provide runs containing reasonably continuous turbulence. Accordingly, some very short bursts of rough air were not classified as runs, so peak counts were not made of these data. Finally, some runs contained anomalies such as radio transmission interference or other electrical noise which prevented their being processed. The data that were lost or discarded for these reasons amounts to a negligible percentage of the total in the peak count summary, and hence does not affect the conclusions regarding the peak count data.

The classification intervals for both peak counting techniques were 0.05g for Δa_N and 1.0 foot per second for U_{de}. A threshold was established at 10 percent of the basic interval to preclude the possibility of repeated high-frequency crossings of the mean or zero level. In the positive slope level crossing count, zero crossings were not counted so that the effective threshold was ±1 interval.

POWER SPECTRAL ANALYSIS

POWER SPECTRA

The power spectrum or power spectral density of a function (e.g., a gust velocity time history) describes the manner in which the total average power of the function (velocity amplitude squared/cycles per second) is distributed over the frequency range. In essence it provides a statistical measure of the mean square amplitude of a measurement for each of a number of narrow but discrete frequency bands. The square root of the sum of all these values over the frequency range of the spectrum gives the rms value of the spectrum data.

Normally, power spectra from uniform time series data are computed and plotted as a function of frequency in cycles per second or radians per second. However, for atmospheric turbulence, it is desirable to interpret the frequency in terms of wavelength in feet per cycle or inverse wavelength in cycles per foot. Thus, to obtain the ordinates of the spectra in cycles per foot, the ordinate and abscissa values are respectively multiplied and divided by the aircraft speed in feet per second. The average true airspeed of the aircraft was the value used for all the gust velocity spectra.

The methods used for computing power spectra and associated statistical functions are described in detail in Appendix III.

SPECTRAL RELIABILITY

One of the most important objectives of the HICAT program is to determine gust velocity spectra for turbulence waves ranging from about 100 feet to as much as 60,000 feet in length. Statistically reliable spectral determinations require that turbulence sample lengths increase in proportion to the longest wavelength of interest.

Since turbulence patches and hence turbulence recordings vary considerably in length, some patches will be too short for a reliable long wave spectral analysis but quite adequate for a medium or short wave analysis. The following table illustrates the determination of the minimum sample lengths associated with a specified long wavelength limit in the power spectrum. In constructing the table the minimum turbulence run was assumed to be of a length sufficient to contain twenty complete cycles of the longest wave.

The table assumes that the data sample rate is 12.5 samples per second (the normal HICAT rate after low pass numerical filtering) with $\Delta t = 1/12.5 = 0.08$ sec and an f_N, the Nyquist or folding frequency, of 6.25 cps. The symbols used in the table are defined as follows:

m = Total number of spectral estimates or lags = $f_N/\Delta f$.

Δf = Elementary spectral frequency band associated with each spectral power estimate = half of the spectral frequency resolution and corresponds to the plotting interval in the power spectrum.

λ Max = Longest wavelength for which a spectral power estimate is desired = 600 (assumed velocity)/Δf.

$T_{n_{Min}}$ = 20 times the length of λ Max in seconds = $20/\Delta f$ = minimum criteria.

Section V

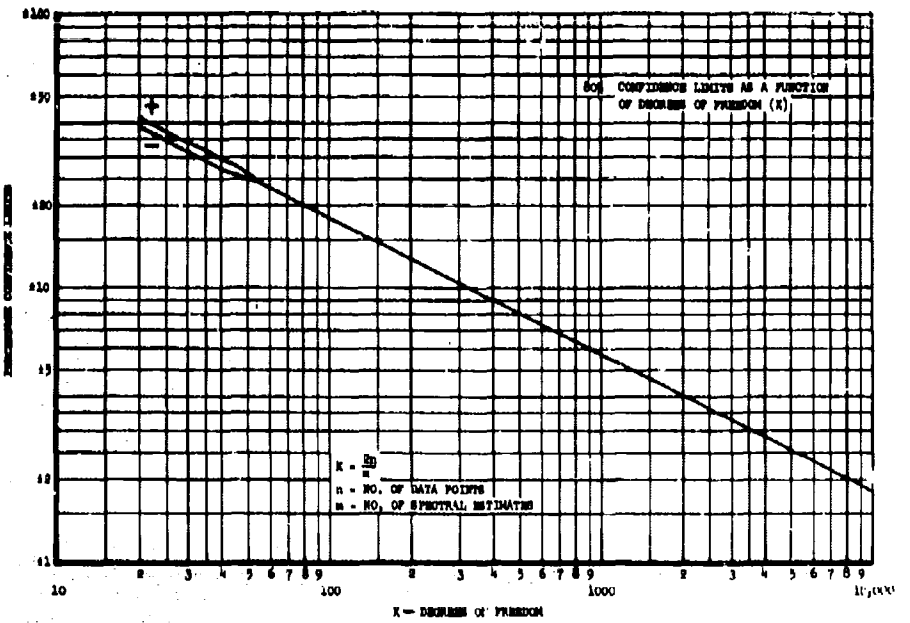

Figure 7. Eighty Percent Confidence Limits as a Function of Degrees of Freedom

Table II

DETERMINATION OF MINIMUM TURBULENCE SAMPLE LENGTH, $T_{n_{Min}}$

Analysis	m	Δf (cps)	λ Max (ft)	$T_{n_{Min}}$	
				(sec)	(min)
Short wave	25	0.250	2,400	80	1.3
Medium wave	50	0.125	4,800	160	2.7
Medium to long wave	125	0.050	12,000	400	6.7
Long wave	250	0.025	24,000	800	13.3
Long to very long wave	500	0.0125	48,000	1,600	26.7
Very long wave	625	0.010	60,000	2,000	33.3

The minimum sample lengths, $T_{n_{Min}}$, determined in the table, will provide data with 25 T_n/m or 80 statistical degrees of freedom. Hence at the 80 percent confidence level, Figure 7 (derived from the chi-square distribution data shown

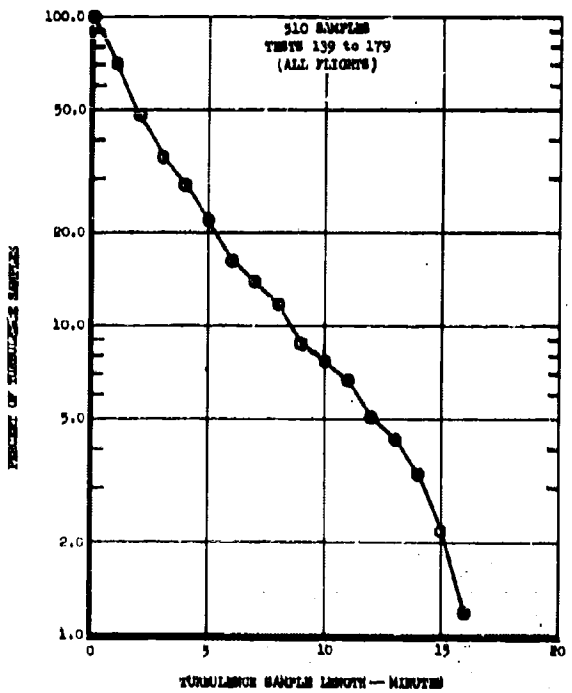

Figure 8. CAT Sample Length Distribution, Time

on page 22 of Reference 23) shows that the spectral estimates will be within 20 percent of the "true" long run average. Obviously longer samples are desirable. If the samples are twice $T_{n_{Min}}$ in length, the confidence band is reduced (improved) to about 14 percent.

The number of turbulence samples that will provide reliable spectra may be estimated[4] if the turbulence sample length distribution is known. Figure 8 shows this distribution for all the edited turbulence samples in the HICAT program.

Table III was constructed using this distribution together with the m values from Table II and applying the minimum sample length criteria, i.e., that the sample be at least 20 times the length of the longest wave, and hence that the sample spectra contain 80 or more degrees-of-freedom. The table shows the actual number of turbulence samples available for power spectral analysis in various m and wavelength categories.

For example, the table indicates that 54 turbulence samples will be between 6.7 and 13.3 minutes in length. Spectra computed from these samples with an

[4] Samples which result in invalid spectra because of insufficient gust intensity, excessive maneuvering, or instrument malfunctions must be rejected. Thus the actual number of spectra will be less than estimated.

m of 125 will have confidence bands between 14 percent and 20 percent at the 80 percent confidence level. Note that if the spectra are computed using the "m" and "T_n" combinations indicated, the confidence bands will be 20 percent or better for wavelengths up to 24,000 feet.

Table III shows the maximum value for T_n, the sample length, to be about 16 minutes. This was originally an IBM 7094 computer limitation based upon a very large value of m combined with a sampling rate of 12.5 samples per second.[5] The advent of the IBM System/360 removed this computing limitation. However, the absence of turbulence samples significantly greater than 16 minutes in length would appear to preclude the computation of 48,000 and 60,000 foot spectra unless a lower statistical reliability is accepted. The last two rows in Table III illustrate this point.

Based upon these considerations, the HICAT spectra are computed using the m and T_n combinations shown in Table III up to an m of 250. Spectra for samples longer than 13.3 minutes are also computed and plotted using an m of 500.

Table III

TURBULENCE SAMPLES FOR SPECTRAL ANALYSIS

m	λ Max ft	T_n Min	Degrees of freedom	Confidence bands at 80% level ±%	Turbulence samples* %	No.
-	-	0- 1.3	-	-	37.0	189
25	2,400	1.3- 2.7	80-160	20-14	24.4	124
50	4,800	2.7- 6.7	80-200	20-13	24.1	123
125	12,000	6.7-13.3	80-160	20-14	10.5	54
250	24,000	13.3-16.6	80-100	20-18	4.0	20
500	48,000	13.3-16.6	40-50	29-27	(4.0)	(20)
625	60,000	16.0-16.6	38-40	30-29	(1.2)	(6)
					100.0	510

*Numbers in parenthesis are already included in the m = 250 category and hence are excluded from column totals.

[5] It would, of course, have been possible to low pass filter the data again and then halve the sample rate to reduce m, the number of estimates required. This would have necessitated considerably more computing and required two spectral plots to provide essentially identical information.

SPECTRAL RMS VALUES

As explained above in the discussion of Spectral Reliability, the spectra are always computed so as to make certain that a selected minimum level of statistical reliability is obtained. This is done by varying the wavelength resolution of the spectrum to suit the turbulence sample length. In effect, this means that some spectra will extend to much lower frequencies and longer wavelengths than others. The rms values (called RMS Spectra on the plots) characterizing individual spectra are thus not comparable unless the spectra cover the same wavelength range.

To enable spectra with different low frequency limits to be compared, additional rms values were computed using the following standard long wavelength limits: 1000, 2000, 4000, 8000, 20,000 and 40,000 feet. The high frequency or short wavelength limit was established for convenience at the wavelength corresponding to 5.0 cps and thus varies slightly with aircraft speed, e.g., at 700 feet per second, 5 cps corresponds to a wavelength of 700/5 or 140 feet.

SECTION VI

PRESENTATION AND DISCUSSION OF RESULTS

GENERAL

The HICAT program results are based upon flight measurements of aircraft cg acceleration response and the true or absolute gust velocity components together with measurements of the related aerodynamic and meteorological variables. These measurements are compiled for analysis in statistical tabulations, time histories, peak counts, and gust velocity power spectra. A comprehensive presentation of all the HICAT measurements available for analysis is provided by the HICAT Test Summary, discussed briefly below and presented in Appendix I.

It is the purpose of this section of the report to describe and analyze these results with emphasis upon the point of view of the aircraft structural designer. The main features of this analysis are the following:

- A discussion and a statistical description of the length and thickness of CAT as well as its relative frequency of occurrence in various altitude bands.
- An examination of the intensity and relative frequency of occurrence of CAT per flight mile as well as within various altitude bands. This analysis is based upon U_{de} peak counts determined from time histories of the aircraft cg acceleration response. The HICAT data is compared with similar U-2 operational data collected by NASA.
- An evaluation of the true gust velocity power spectra utilizing an averaging method to obtain spectra for aircraft design. The representation of gust velocity spectra by various mathematically defined curves is also discussed.
- An examination of certain special statistical relationships of CAT to determine probability distributions of rms velocities for the three gust components, to determine the isotropy of the turbulence, and to evaluate the stationarity of the vertical gust velocity. This latter evaluation is an essential step in the application of HICAT statistics to aircraft design.

HICAT TEST SUMMARY

The HICAT Test Summary Table, Appendix I, provides a brief tabular description of all high altitude CAT encounters in order by test and run number. The

Section VI

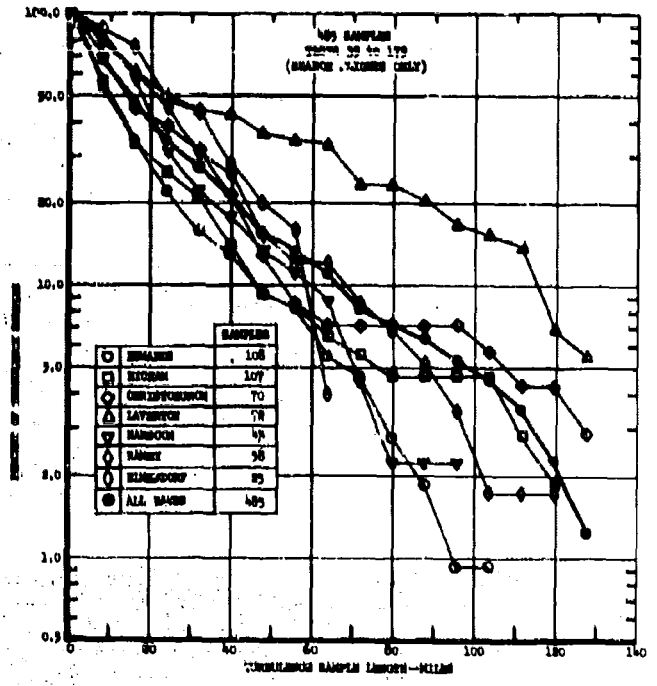

Figure 9. CAT Sample Length Distribution, Miles

table is intended to convey the scope of the results while at the same time characterizing each CAT run with sufficient detail to permit an independent assessment of the measured data.

TURBULENCE SAMPLE DISTRIBUTIONS

LENGTH

In order to provide some idea of the length of turbulent regions in the atmosphere, the sample durations were classified and converted to miles as explained in Section V.

Figure 9 shows the turbulence sample length distribution for each operational base and the sample length distribution overall. Figure 9 shows fairly clearly that more long turbulence samples were obtained in operations from Laverton, Australia, than from the other six locations. Overall, 1.25 percent of all the samples obtained in the search flights, i.e., six samples, exceeded 127 miles in length. About half of all the CAT samples encountered were 15 miles or more in length.

Admittedly, there is a slight bias in this distribution because some light, short samples were ignored. It may, however, be counterbalanced by the fact that some samples were interrupted and shortened because of the aircraft turning or radio interference in the measurements.

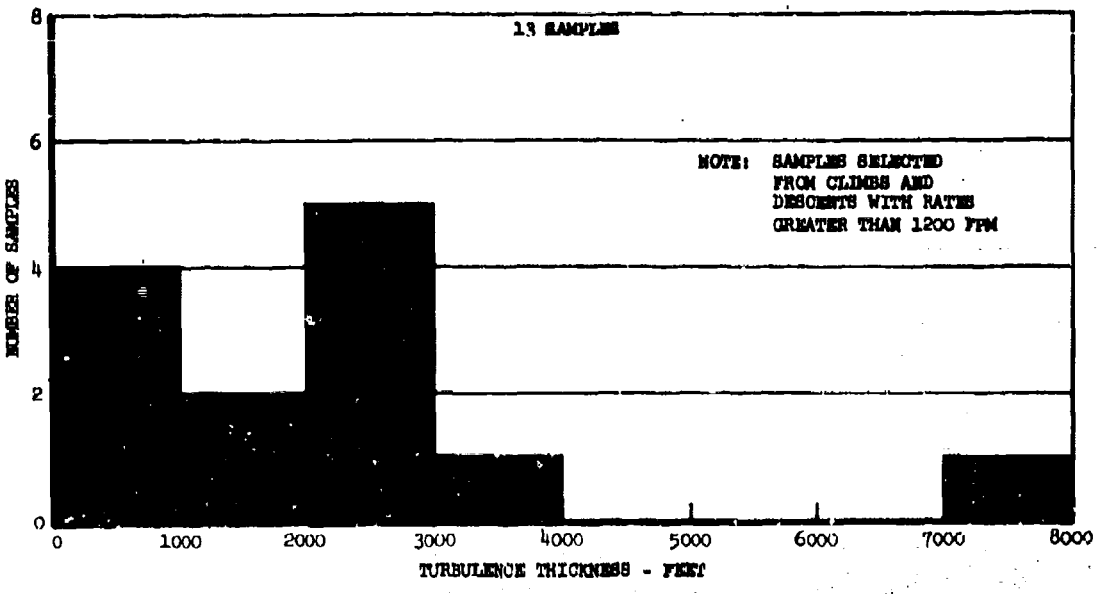

Figure 10. Distribution of the Thickness of Turbulent Regions

THICKNESS

The thickness of the turbulent regions is also of interest but cannot be as simply determined from aircraft measurements as can the horizontal length. The difficulty occurs in determining from a climbing or descending airplane which boundary of the turbulent region has been crossed; an upper or lower boundary as against a horizontal peripheral boundary.[6]

This difficulty was only approximately resolved by limiting the turbulence thickness estimates to those runs with a relatively high rate of climb or descent.

The rate of climb or descent considered acceptable (1200 fpm) provided sample durations averaging 66 seconds or about one third of the average length of a level flight sample. By this means, the probability was considerably increased that the thickness of the turbulent region was actually measured and not the length. This process, however, reduced the total number of valid thickness estimates from about 31 to only 13. The thickness distribution provided by those 13 samples is presented in Figure 10. Based on this very limited number of estimates, it appears that most turbulence regions are fairly thin, probably less than 3000 feet thick.

[6] Normally, horizontal peripheral boundaries are the only kind considered when estimating turbulence patch lengths from level flight penetrations - the possible slight slope of a turbulent band is ignored.

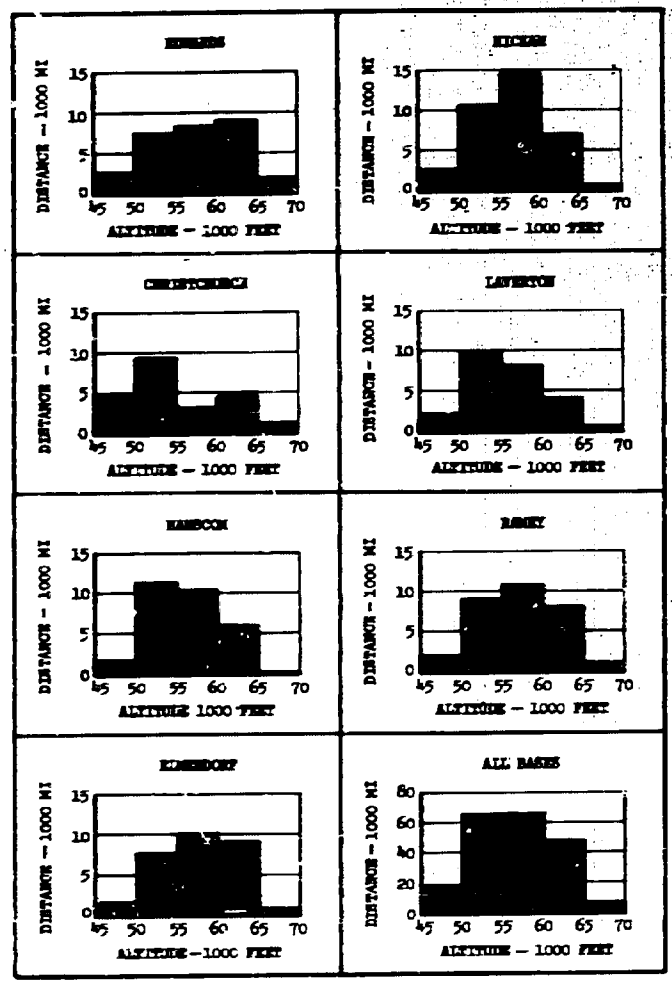

Figure 11. Distribution of Flight Miles by Altitude Band for Each Base

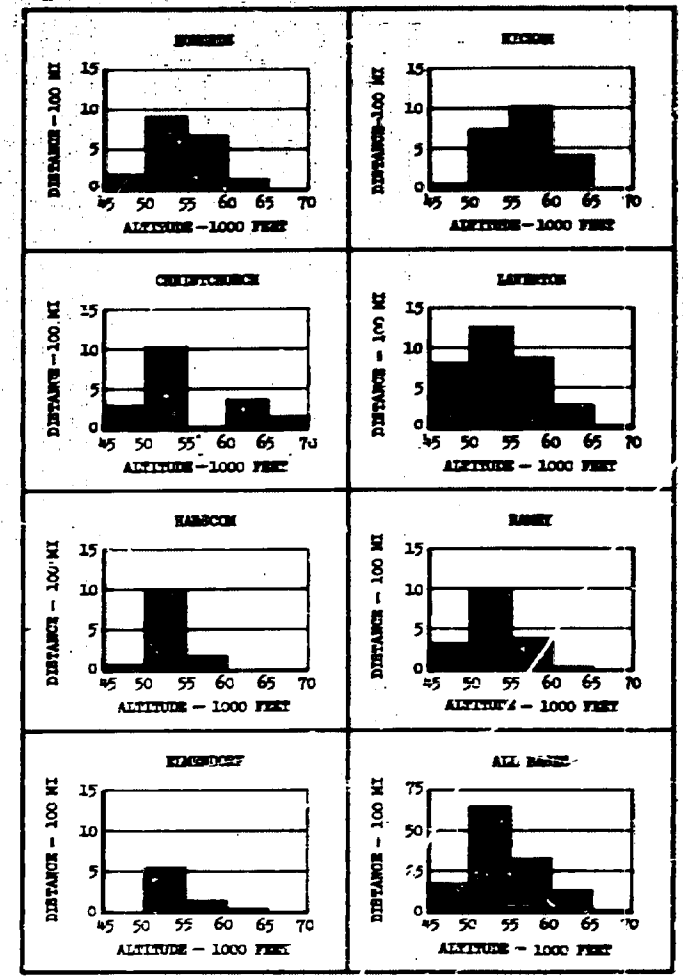

Figure 12. Distribution of CAT Miles by Altitude Band for Each Base

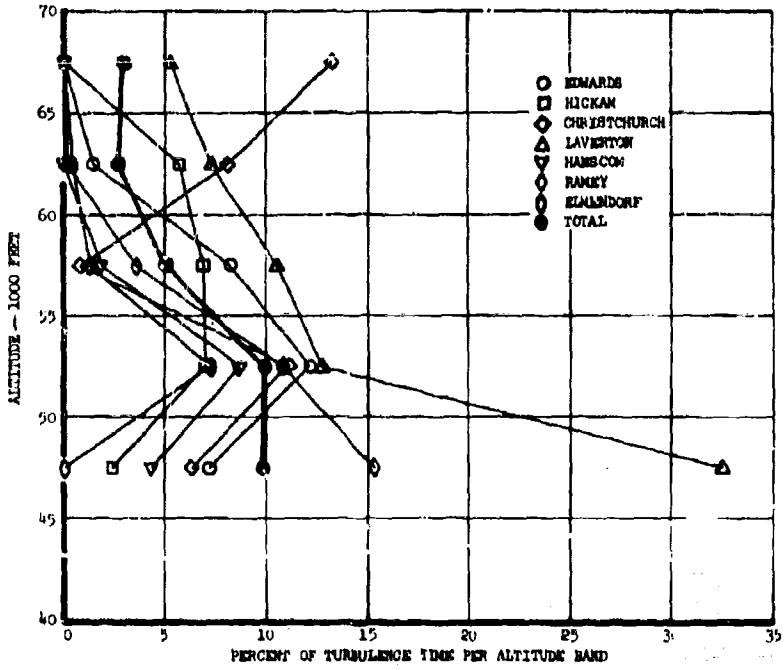

Figure 13. Percent Turbulence Time versus Altitude

DISTRIBUTION OF TURBULENCE BY ALTITUDE

The amount of turbulence encountered in a given altitude band obviously depends upon the amount of turbulence which naturally occurs in the particular band as well as the time or distance searched within the band. Figure 11 graphically depicts the number of miles flown in 5000-foot altitude bands above 45,000 feet for each base of operations and for all bases. Figure 12 shows the number of miles of turbulence encountered in the same altitude bands for each base and for all bases. Figure 13 shows the percentage of turbulence in each altitude band for each base of operations.

These latter two curves considered together appear to indicate a possible increase in the occurrence of turbulence in the 50,000 to 55,000-foot band in all but two of the areas searched. That this effect is not due to flying significantly more time in this band is shown by Figure 11, "All Bases."

GUST VELOCITY TIME HISTORIES

The gust velocity time histories are presented in Appendix VI. A gust velocity time history is shown corresponding to each run for which gust velocity power spectra are presented in Appendix VII.

A typical gust velocity time history appears in Figures 14 and 15. The first figure presents time histories of the three gust velocity components along with

derived equivalent gust velocity, corrected pressure altitude and ambient air temperature. The second figure shows the associated time histories of true airspeed, roll angle, elevator position, cg longitudinal acceleration, cg lateral acceleration and cg normal acceleration.

PEAK COUNTS

As noted in Section V, peak count data were obtained for two basic purposes:

- Obtain a general indication of the level of turbulence encountered
- Evaluate the stationarity of the time history

Results and discussion directed toward the first of these purposes are contained in this section. Results and discussion pertaining to the second appear under Stationarity later in this section under the paragraphs entitled Special Statistics.

HICAT peak count data were obtained during flights specifically directed toward locating and measuring turbulence. As a result, the HICAT data would be expected to reflect a more severe exposure than VGH data obtained in routine operations. The latter data would reflect a more random sampling of the atmosphere, or perhaps actually a bias toward less frequent and less severe turbulence. Such a bias could result from the use of turbulence avoidance procedures or from the possibility that operational missions would be less frequently carried out under the type of weather conditions likely to occur in conjunction with turbulence. Another factor that might lead to an indication of more severe exposure to turbulence in the HICAT program is that, in a number of instances, once a turbulent region was found, repeated passes were made through the same region in different directions.

On the other hand, there were two or three occasions when the pilot maneuvered the aircraft out of the turbulence because of its severity.[7] As a result, some of the higher gust velocities may have been missed. Subsequent examination of the records from these three flights indicated that the center-of-gravity accelerations that occurred before the airplane left the turbulence were comparable to - but no higher than - the most severe obtained on other runs. Further, some of the turbulence data were excluded from peak counting for the various reasons noted in the discussion of peak counting methods in Section V. This loss of data, however, is believed to have a rather small effect on the frequency of exceedance curves.

[7] Severe in the sense that airframe fatigue load damage was possible although actual cg accelerations were well below limit values.

In defining miles flown in turbulence, the miles flown are considered to be exactly those covered during "runs," as defined under Data Editing in Section VI. Generally, the criterion used as a guide in breaking the flight records into runs was that the cg acceleration trace be continuously disturbed (±0.05g) and exhibit frequent peaks in excess of ±0.10g, corresponding to an average U_{de} of about 1.7 fps. This criterion is, of course, arbitrary to begin with and also quite subjective in its application. In fact, some of the very long runs needed to establish power spectral densities at the longest wavelengths included scattered regions in which no ±0.10g peaks occurred.

The peak count data obtained in the redirected HICAT program are summarized in Figures 16 and 17. Figure 16 presents frequency of occurrence of derived equivalent gust velocity, U_{de}, per flight mile from each of the seven bases of operation , together with the summation per total flight mile. Note that the most severe turbulence was encountered during flights from Laverton, Australia, and Ramey AFB, Puerto Rico. The maximum measured incremental value of cg acceleration, 0.6g, resulted in a maximum value of U_{de} of 12.6 fps.

Figure 17 presents the program data on a per-turbulence-mile basis. The most severe turbulence on this basis was also encountered on flights from Laverton, Australia, and Ramey AFB, Puerto Rico.

The results for the run during which the maximum values of Δa_N (increment in cg normal acceleration) and U_{de} were obtained are presented in Figures 18 and 19. This run was a very short one, 42 seconds. The U_{de} exceedance curve, Figure 18, exhibits a much shallower slope than the total data from Ramey AFB presented in Figure 17. This shallower slope indicates in this case that a greater proportion of larger gust velocity increments are present. The turbulence encountered in this run is thus much more severe - actually by a factor of about 2.5 - than the average for all runs. The corresponding exceedance curve for Δa_N is shown in Figure 19. This curve is, of course, very similar to the U_{de} exceedance curve, reflecting a ratio of U_{de} to Δa_N of approximately 19.

Figure 20 presents a comparison of the HICAT peak count data, normalized to total flight miles, with similar data obtained with VGH recorder during operational U-2 flights as reported by NASA in TN D-548 (Reference 2). The influence on the TN D-548 data of the flights over Japan is quite obvious. With the Japanese data excluded, the HICAT and TN D-548 results exhibit the same slope. The difference in vertical position of the two lines indicates a different percent of time in turbulence, which can be attributed to the types of missions flown in the two programs. The HICAT airplane was in turbulence about 2.5 times as often, accounting for the nearly constant factor relating the HICAT and TN D-548 data. When the HICAT and TN D-548 data are put on a more directly comparable basis by excluding the 20,000 to 45,000 ft altitude band from the TN D-548 data, the factor of 2.5 increases to about 4.5.

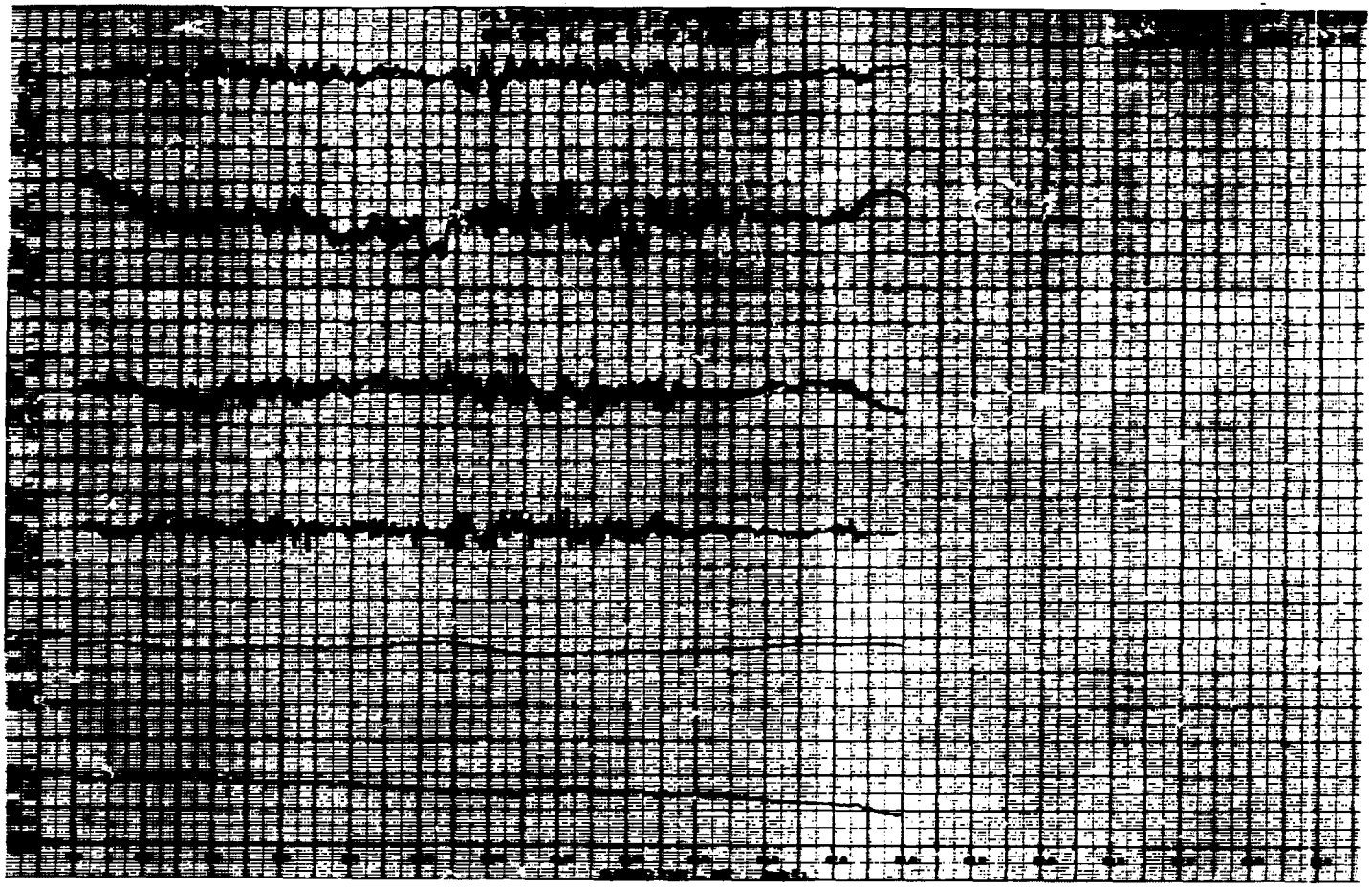

Figure 14. Typical Time History - Test 102, Run 2, Gust Velocities

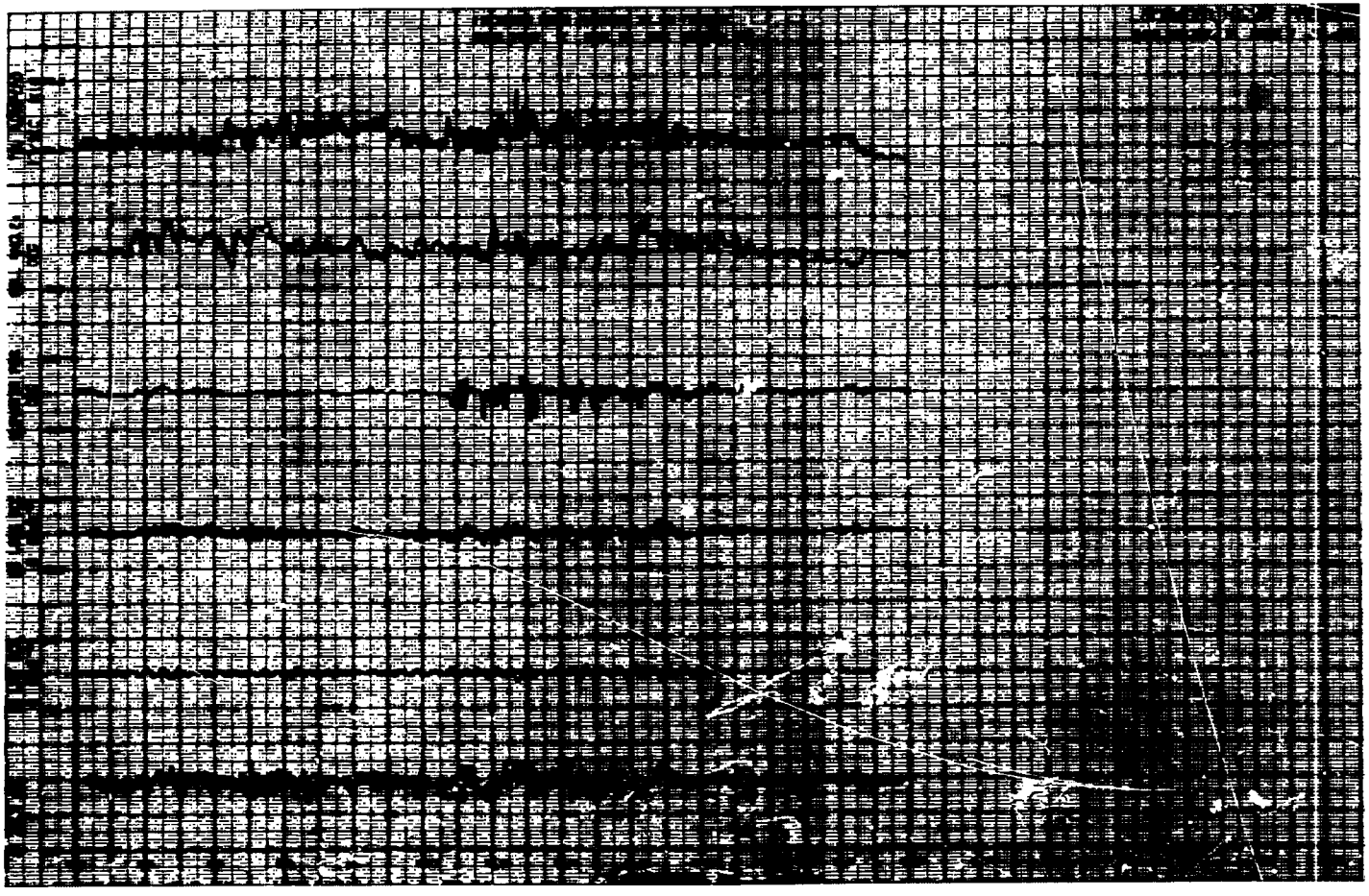

Figure 15. Typical Time History - Test 102, Run 2, Flight Parameters

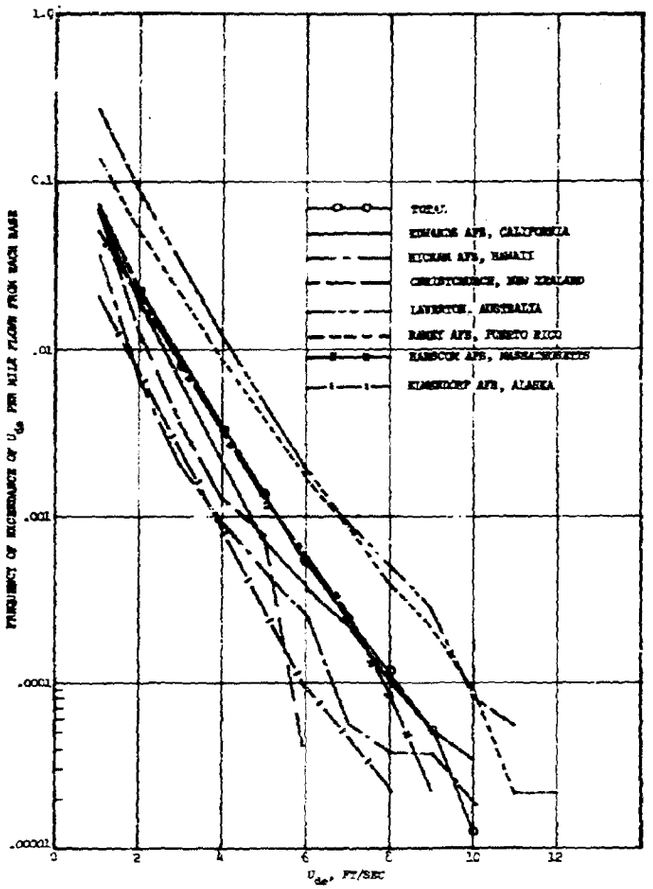

Figure 16. Frequency of Exceedance of U_{de} per Flight Mile, Various Locations

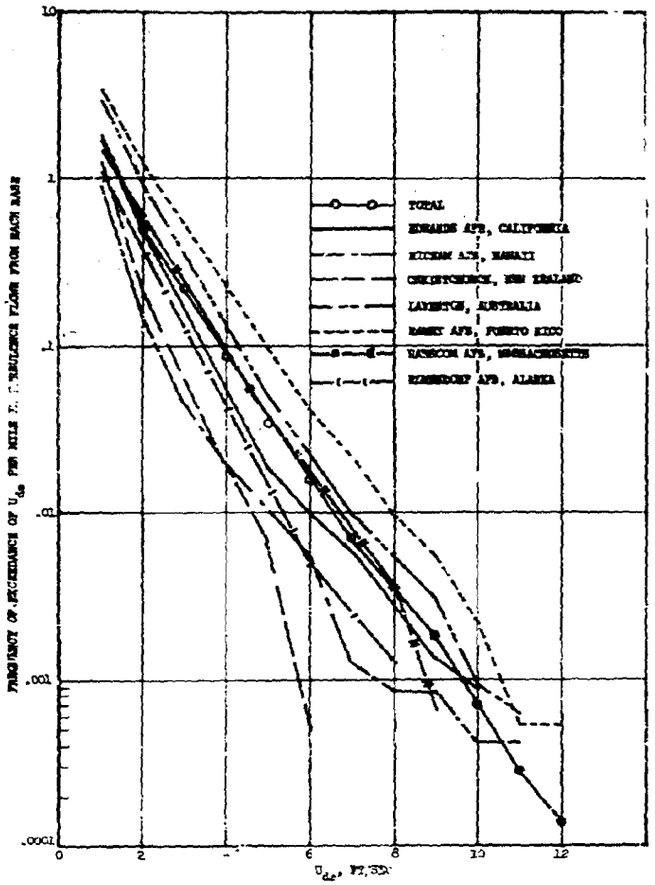

Figure 17. Frequency of Exceedance of U_{de} per Mile in Turbulence, Various Locations

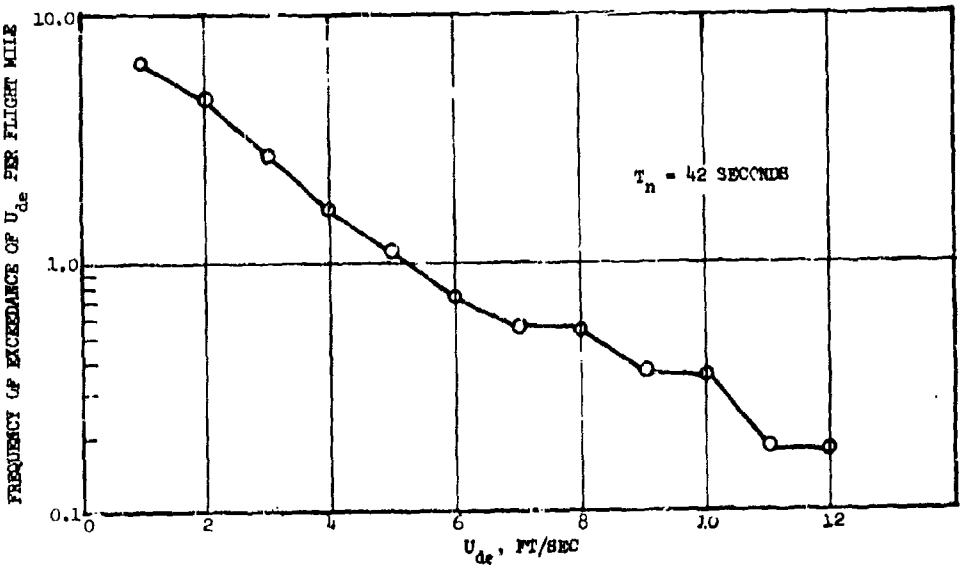

Figure 18. Frequency of Exceedance of U_{de} per Flight Mile Test 155, Run 2 (Ramey AFB)

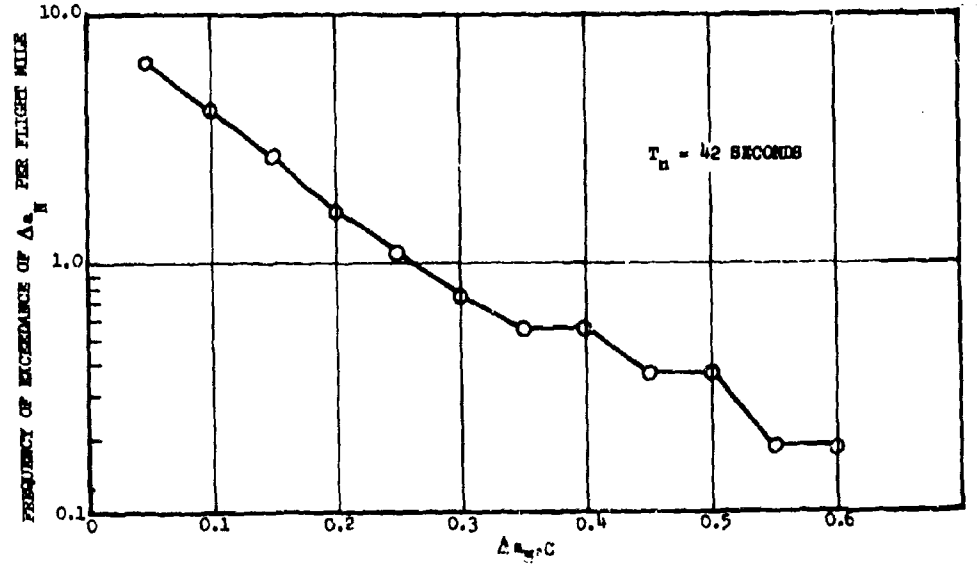

Figure 19. Frequency of Exceedance of CG Normal Acceleration per Flight Mile, Test 155, Run 2 (Ramey AFB)

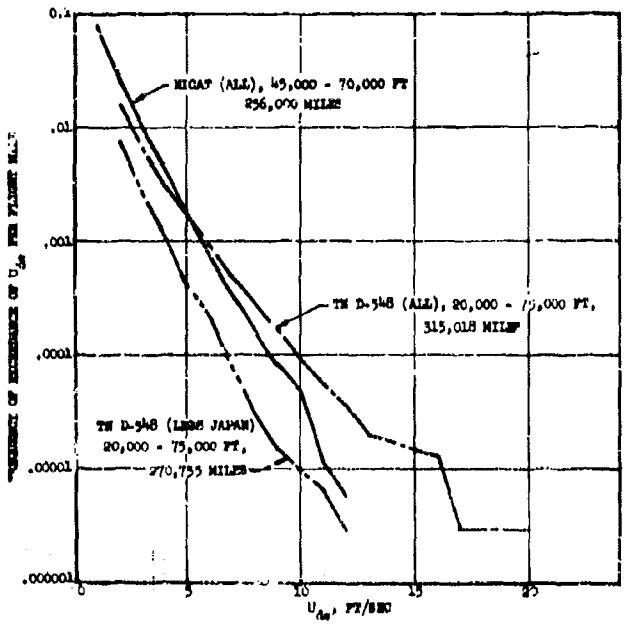

Figure 20. Frequency of Exceedance of U_{de} per Flight Mile, Comparison of HICAT with TN D-548

A comparison of the TN D-548 and HICAT data on a per-turbulence-mile basis is shown in Figure 21. With the Japanese data excluded, the agreement is very close, as would be expected in light of the discussion of the preceding figure. As noted earlier, however, the definition of miles in turbulence is rather arbitrary, and was, in fact, not identical between the two sets of data. It will be recalled that the HICAT turbulence runs were defined based on a U_{de} threshold of 1.7 fps, while the corresponding TN D-548 threshold was 2 fps.

Any difference in the number used for the miles in turbulence would be reflected in a vertical shift of the frequency-of-exceedance curves, so the close agreement is not altogether significant.

The Japanese data extracted from TN D-548 are compared in Figure 22 with the HICAT data obtained during flights from the two bases where the most severe turbulence was encountered. Comparing the "all flights" curves, it is seen that, at a given frequency of exceedance, the Japanese data are more severe by a factor of roughly 1.4. If only the one flight over Japan (CW-58-2) for which the turbulence was most severe is included, the effect is seen to be an almost uniform upward shift of the curve. These two Japan curves are only slightly less severe in slope than the curve representing the one most severe patch of turbulence measured out of Ramey AFB, test 155, run 2.

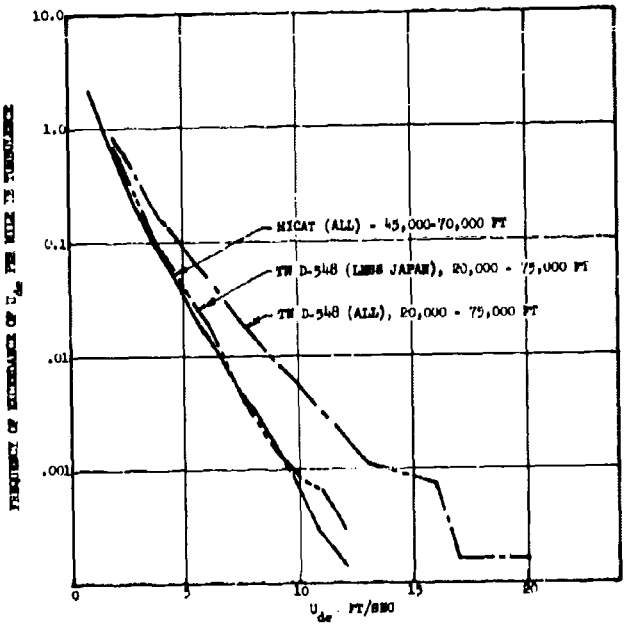

Figure 21. Frequency of Exceedance of U_{de} per Flight Mile in Turbulence, Comparison of HICAT with TN D-548

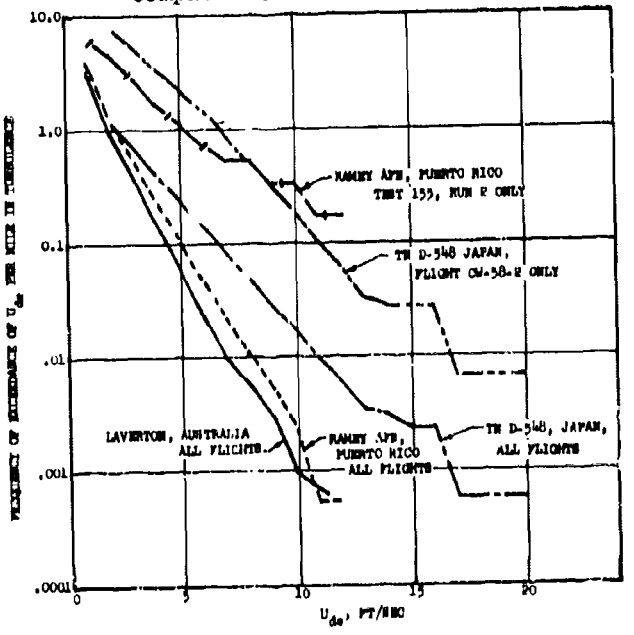

Figure 22. Frequency of Exceedance of U_{de} per Flight Mile in Turbulence, Comparison of HICAT with TN D-548 for Locations Giving Most Severe Turbulence

Section VI

The preceding discussion has been concerned with the overall HICAT peak count data, including some comparisons with the data from TN D-548. The breakdown of the data by altitude bands is presented in Figures 23 and 24. Figure 23 presents the frequency of exceedance of U_{de} by altitude band for the HICAT program. Note that the general trend is toward a generally less severe turbulence environment as altitude increases.

Figure 24 presents a comparison by altitude band of the exceedance data obtained in the HICAT program and the material reported in TN D-548. In the 40,000-60,000 ft band, the relation of the three curves is very similar to that shown in Figure 20, where the data are not separated by altitude bands and, in fact, are not for exactly the same altitude ranges. This similarity is to be expected since a major part of the more severe turbulence exposure in both programs, including the severe turbulence over Japan, occurred in this band. In the 60,000-75,000 ft band, the Japanese data still dominate the TN D-548 data, but here the HICAT exposure becomes relatively much more severe.

Figures 25 and 26 present flight and turbulence miles by altitude band for the HICAT program and from TN D-548. Note that the HICAT flights were concentrated, almost uniformly, in the altitude range 50,000-65,000 feet, and that turbulence was most prevalent in the band 50,000-55,000 feet. The TN D-548 flights were concentrated in the bands 50,000-55,000 and 60,000-65,000 feet, and turbulence was encountered mainly in the band 50,000-60,000 feet. This information concerning turbulence encounter is consistent with the data of Figure 24, which shows for both programs more frequent encounters at all gust intensities in the altitude band 40,000-60,000 feet than the 60,000-70,000 foot band.

Figure 27 compares, by altitude band, the percent of time in turbulence for the HICAT program with that for the flights reported in TN D-548, including all data from both programs. The HICAT airplane was in turbulence a higher percent of time at all altitudes above 45,000 feet. This information is consistent with the data presented in Figures 25 and 26, and with the types of missions flown in the two programs. Again it should be noted that definitions of time in turbulence are somewhat arbitrary and subjective and no effort has been made to achieve consistency between the HICAT and the TN D-548 data. However, the larger percentages of time in turbulence for the HICAT program would be expected in view of the specific effort to find and measure turbulence in this program.

Figure 28 presents the variation of U_{de} with altitude presently used in design of military aircraft (see Reference 8). Superimposed on this figure are the maximum values of U_{de} obtained in the HICAT program to date, including both the data from Test 33 reported in the HICAT interim report (Reference 5) and the data from the redirected HICAT program. Approximately 280,000 miles have been flown in HICAT flights to date (including flights made before the program redirection), and the design values of U_{de} between 45,000 and 70,000 feet have not been exceeded. A significant margin exists between the highest recorded value of U_{de} and the design value at the corresponding altitude.

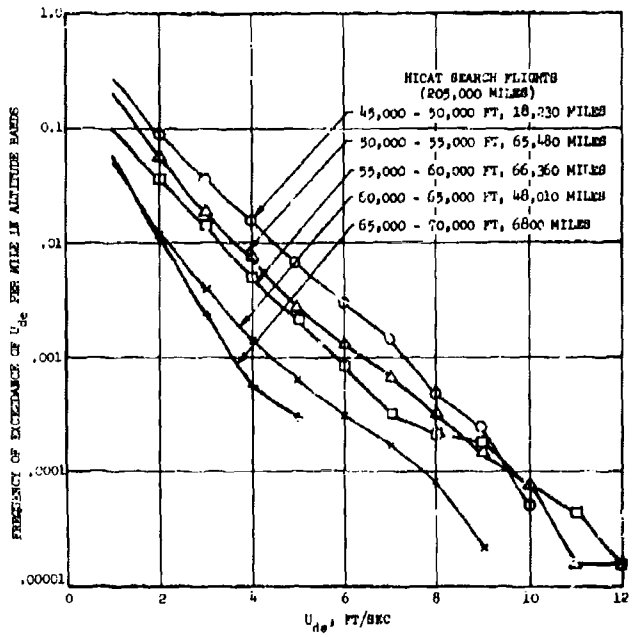

Figure 23. Frequency of Exceedance of U_{de} per Flight Mile for Various Altitude Bands

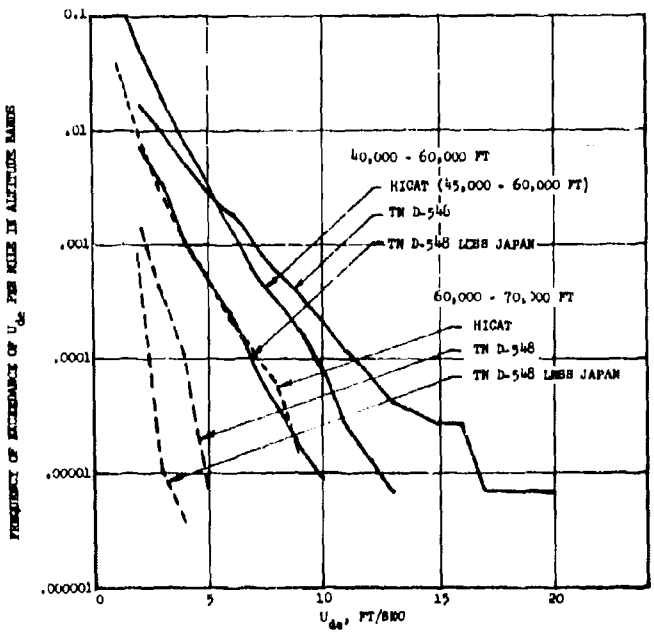

Figure 24. Frequency of Exceedance of U_{de} per Flight Mile for Various Altitude Bands, Comparison of HICAT with TN D-548

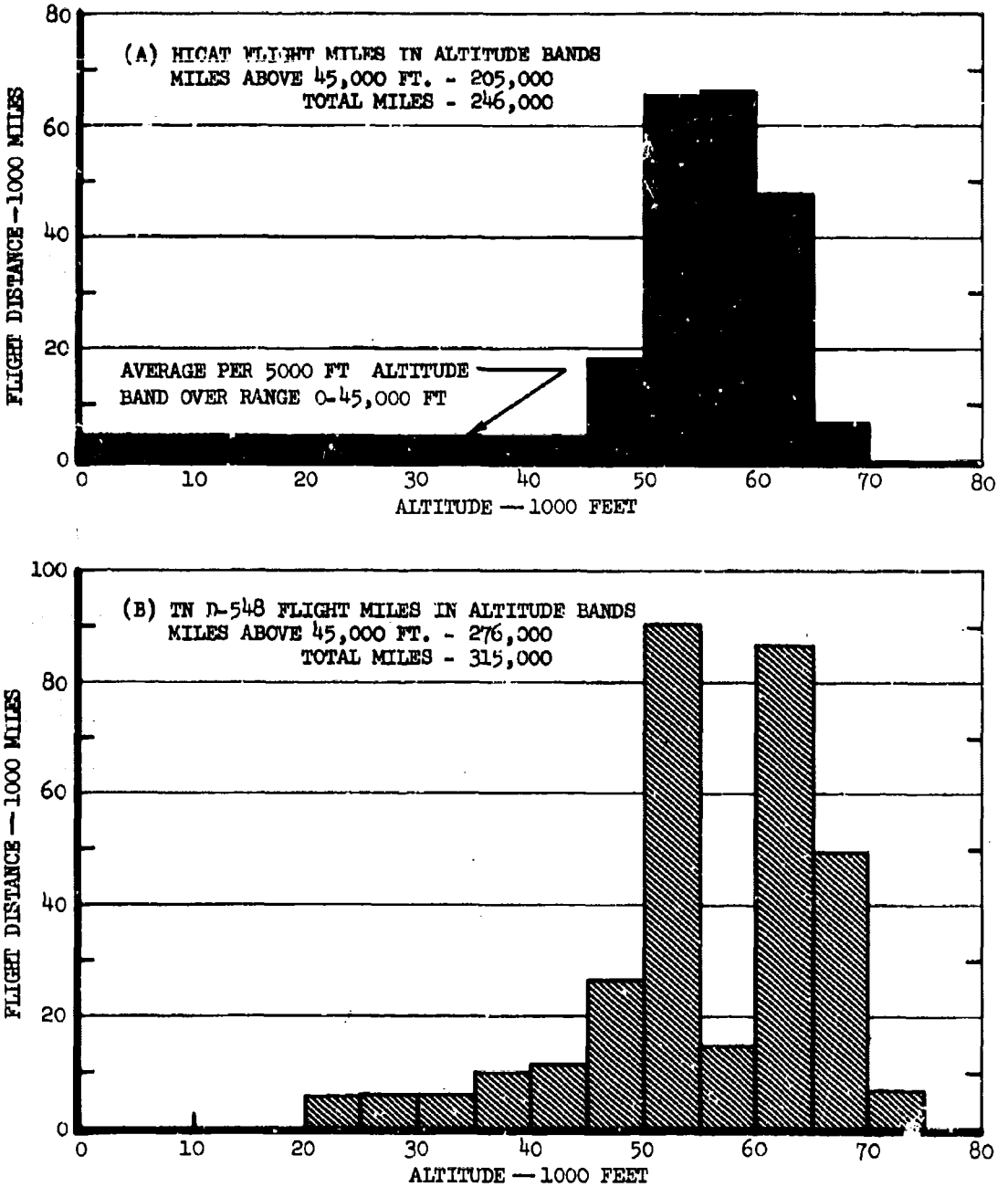

Figure 25. Distribution of Flight Miles by Altitude Band

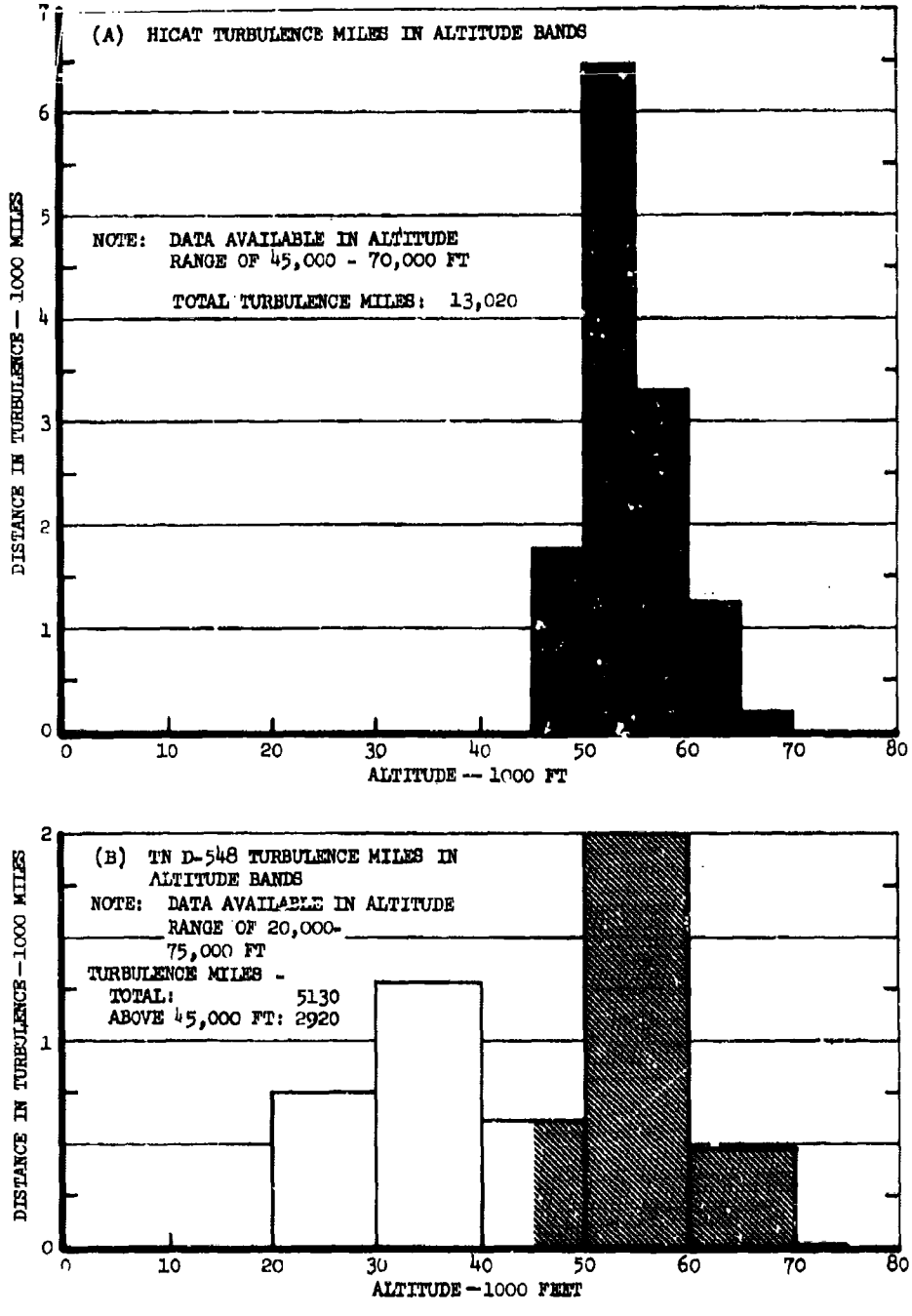

Figure 26. Distribution of Turbulence Miles by Altitude Band

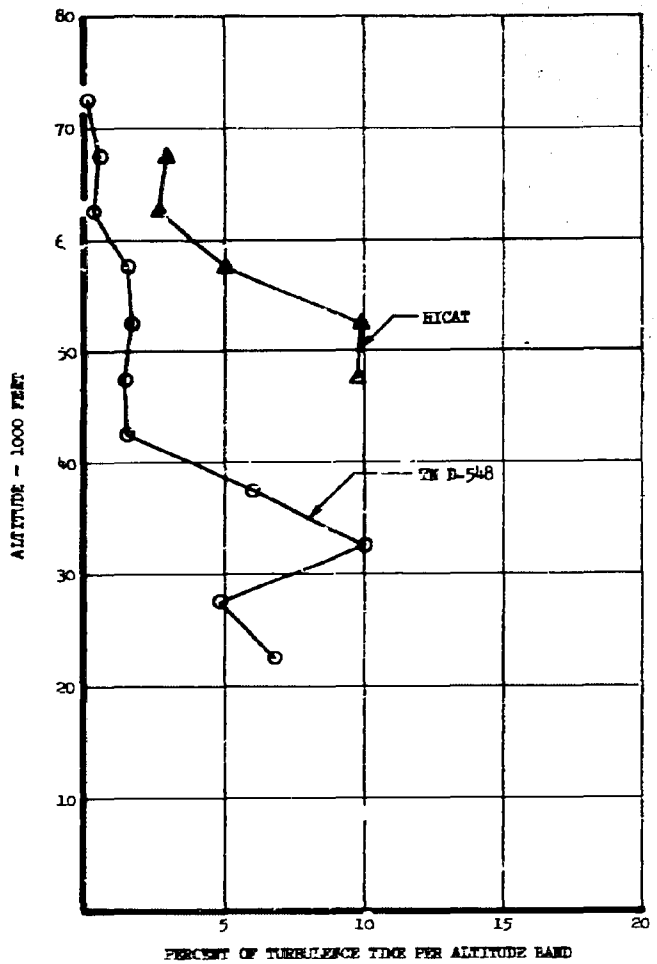

Figure 27. Percent Turbulence Time Versus Altitude

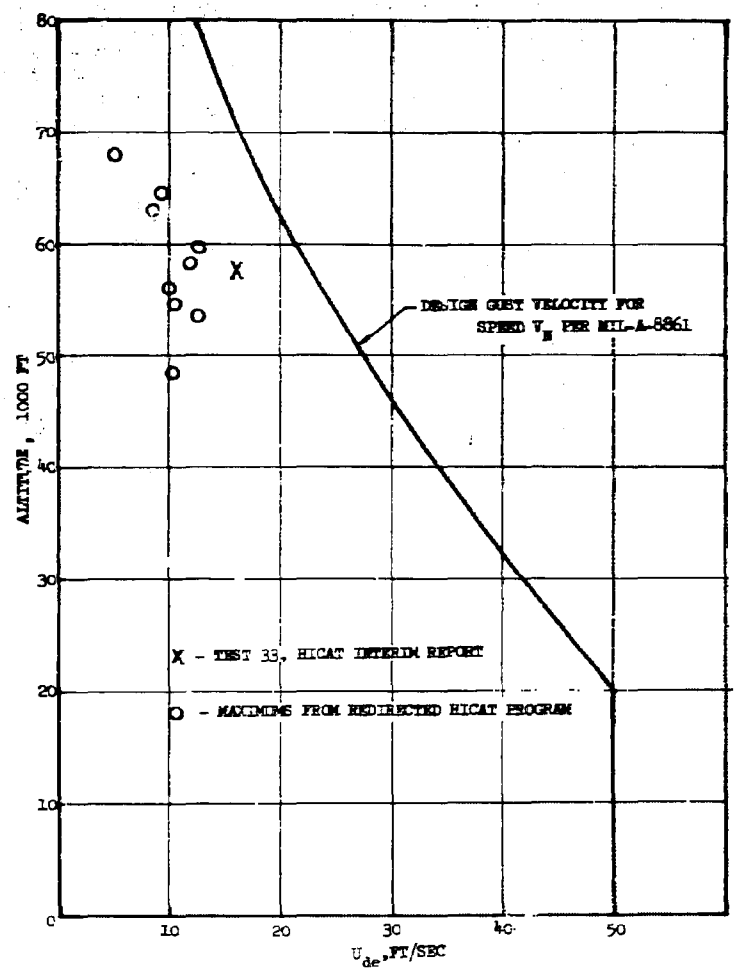

Figure 28. Comparison of Highest Measured U_{de} Values with Current Design Requirements

GUST VELOCITY SPECTRA

GUST VELOCITY SPECTRA PLOTS

The plots of the power spectra of the vertical, lateral, and longitudinal gust velocity components are presented in Appendix VII. Figure 29 of this section shows typical examples of vertical, lateral, and longitudinal spectra.[8] Note that the rms gust velocity characterizing the entire spectrum as well as the rms values for various intermediate wavelength cutoffs are tabulated on the plots. The intermediate wavelength cutoffs are abbreviated by dropping the thousands, (i.e., 1 = 1000 ft, 2 = 2000 ft, etc.). Figure 30 compares the overall envelope of all the HICAT spectra with those obtained from the Douglas NB-66B High Altitude Gust survey (Reference 9) and the Australian TOPCAT program (Reference 10). The HICAT spectra overlay the TOPCAT spectra which were also clear air but fall considerably below the upper limit of the B-66 thunderstorm data, as might be expected.

MATHEMATICALLY DEFINED GUST VELOCITY POWER SPECTRAL DENSITY CURVES

For use in aircraft design, as well as for comparison of measured data with various proposed theories, it is often desirable to represent atmospheric turbulence power spectral density curves by means of mathematical expressions.

Current theories indicate that, over a frequency range comparable to that studied in the HICAT program, the gust velocity power spectra are likely to be characterized by the following:

- At very low frequencies, a power spectral density that does not vary with frequency.
- At high frequencies, a power spectral density that varies inversely as some constant power of frequency.
- A transition between these two regions.

The mathematical expressions that are most frequently proposed to represent gust velocity power spectral densities are generally in a form such that the high-frequency exponent and the nature of the transition are defined. These expressions, however, generally contain two parameters to which any desired values may be assigned. One of these parameters, the rms value of the gust velocity (σ_w), measures the intensity of the turbulence, and the other (usually designated by the symbol L and called the scale of turbulence) is a shape parameter that defines the frequency at which the transition occurs between the horizontal and sloping regions of the curve on the usual log plot.

[8] The gust velocity time history from which these HICAT spectra were obtained appears in Figures 14 and 15.

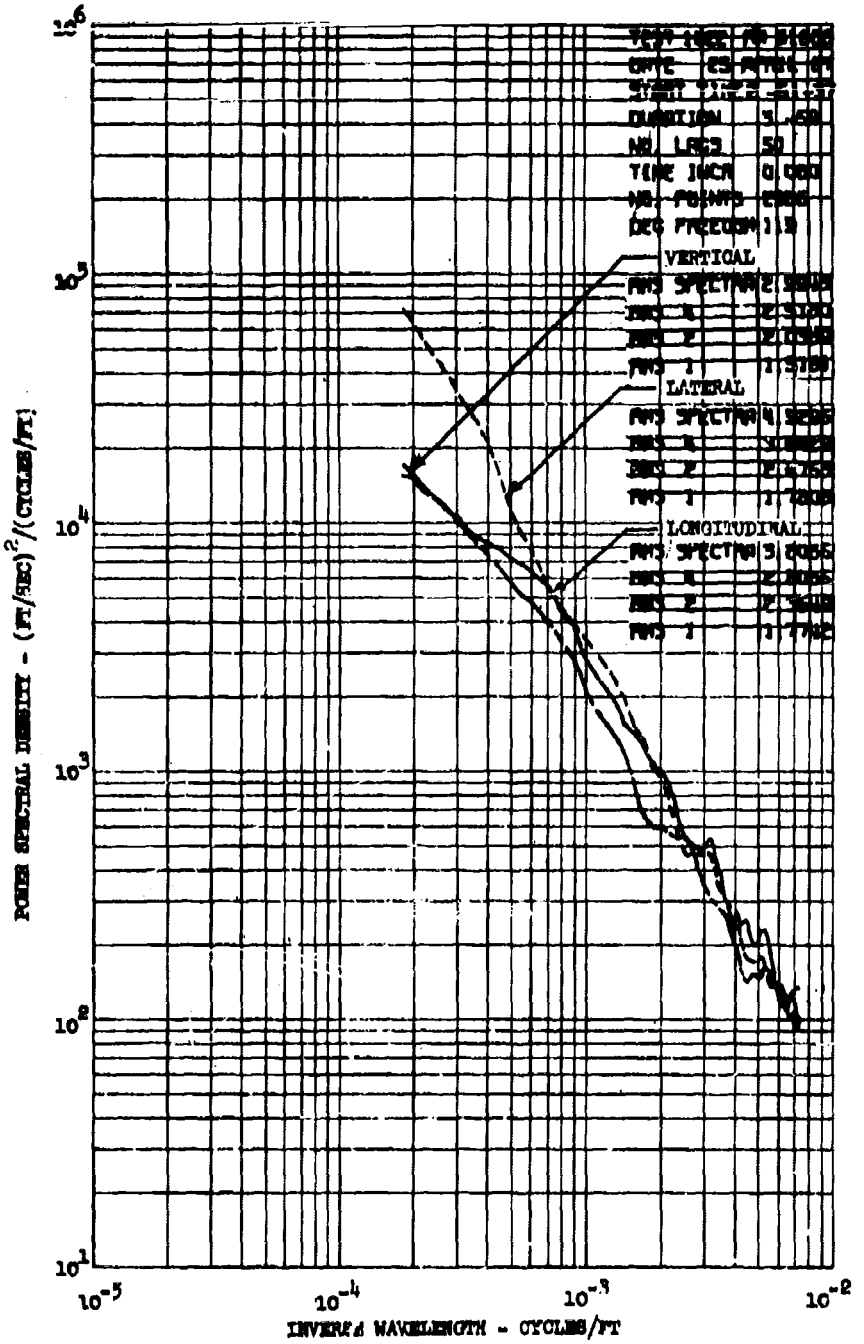

Figure 29. Typical Power Spectra of Vertical, Lateral, and Longitudinal Gust Velocity Components (Test 102, Run 2)

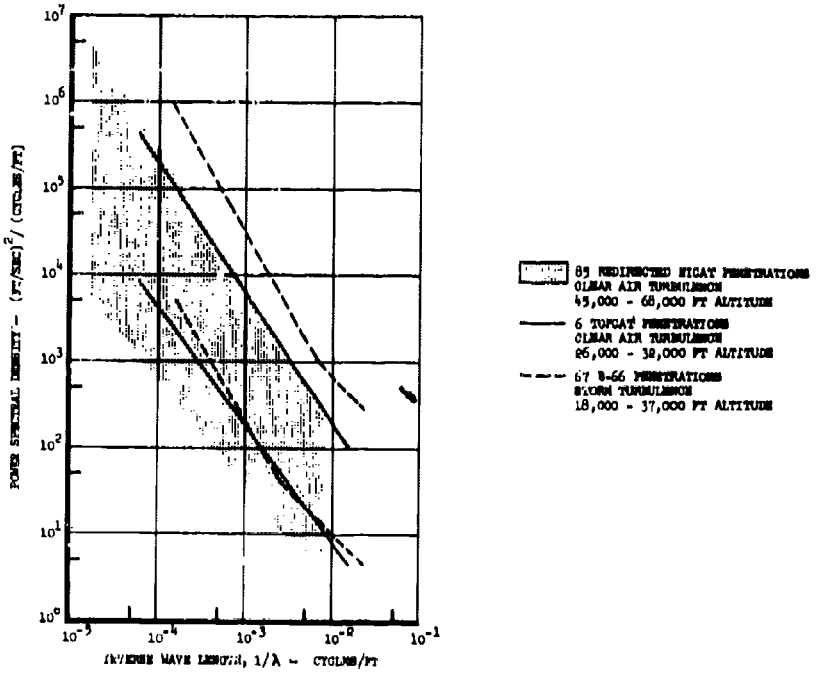

Figure 30. Comparison of Gust Velocity Power Spectral Envelopes

To assist in finding simple, mathematically-defined curves that best fit the measured shapes, several families of curves are shown in Appendix VIII. These are plotted to the same scales as the measured curves in Appendix VII to facilitate comparison (e.g., by vellum tracing). All are arbitrarily shown at a level such that the high-frequency asymptote passes through a power spectral density (psd) value of 10^3 $(fps)^2$/cpf at a frequency of 10^{-3} cpf.

Three basic families are included. For each basic family, curves are provided for high-frequency exponents, (m) of -1, -7/6, -4/3, -3/2, -5/3, -11/6, and -2, respectively. For each value of m, curves are shown for scales of turbulence, (L) of 500, 1000, 2000, 4000, and 8000 ft, and ∞. Figure 31 in this section compares the three families for an m of -5/3 and an L of 1000 ft and ∞.

The first family includes both the Von Karman spectrum (exponent = -5/3) and the Dryden spectrum (exponent = -2) as special cases. The basic equations for this family are given by Taylor in Reference 11; he credits N. I. Bullen

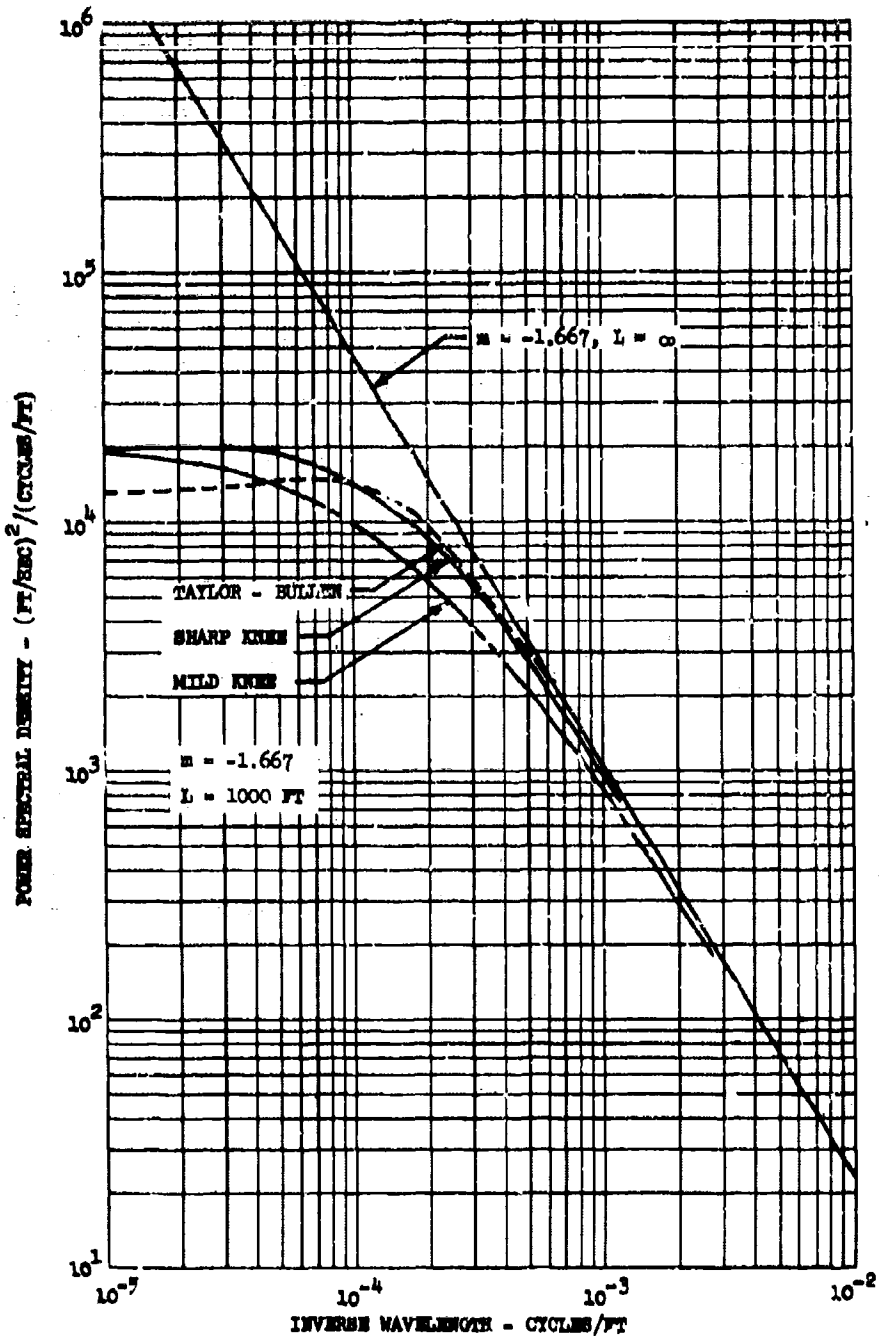

Figure 31. Comparison of Three Mathematically Defined Gust Power Spectral Density Curves, m = -1.667, L = 1000 ft and ∞

with suggesting their use. Accordingly, this family is designated herein the Taylor-Bullen family. The general form of the equation for this family is

$$\Phi(\Omega) = \frac{\sigma^2 L}{\pi} \frac{\left[1 + 2(n+1)\, b^2\right] (\Omega L)^2}{\left[1 + b^2 (\Omega L)^2\right]^{n + 3/2}} \qquad (1)$$

where n is related to the slope of the high frequency asymptote on the log-log plot, m, as follows:

$$n = \frac{1}{2}(-m - 1)$$

or conversely,

$$m = -1 - 2n$$

and b is defined by

$$b = \frac{\Gamma(n)}{\sqrt{\pi}\,\Gamma(n + 1/2)}$$

and is equal to 1/L times the constant, a, used by Taylor. Values of n, b, and b^2 for the curves shown herein are as follows:

m	n	b	b^2
-1	0	∞	∞
-7/6	1/12	4.10	16.81
-4/3	1/6	2.318	5.373
-3/2	1/4	1.671	2.792
-5/3	1/3	1.339	1.793
-11/6	5/12	1.139	1.297
-2	1/2	1.000	1.000

The resulting equations are:

$m = -1$: $\Phi(\Omega) = (\text{Constant})\frac{1}{\Omega}$

$m = -\frac{7}{6}$: $\Phi(\Omega) = \frac{\sigma^2 L}{\pi} \frac{[1 + 36.42\,(\Omega L)^2]}{[1 + 16.81\,(\Omega L)^2]^{19/12}}$

$m = -\frac{4}{3}$: $\Phi(\Omega) = \frac{\sigma^2 L}{\pi} \frac{[1 + 12.57\,(\Omega L)^2]}{[1 + 5.37\,(\Omega L)^2]^{5/3}}$

$$m = -\frac{3}{2}: \quad \Phi(\Omega) = \frac{\sigma^2 L}{\pi} \frac{[1 + 7.00\,(\Omega L)^2]}{[1 + 2.80\,(\Omega L)^2]^{7/4}}$$

$$m = -\frac{5}{3}: \quad \Phi(\Omega) = \frac{\sigma^2 L}{\pi} \frac{[1 + 4.78\,(\Omega L)^2]}{[1 + 1.79\,(\Omega L)^2]^{11/6}}$$

$$m = -\frac{11}{6}: \quad \Phi(\Omega) = \frac{\sigma^2 L}{\pi} \frac{[1 + 3.69\,(\Omega L)^2]}{[1 + 1.30\,(\Omega L)^2]^{23/12}}$$

$$m = -2: \quad \Phi(\Omega) = \frac{\sigma^2 L}{\pi} \frac{[1 + 3.00\,(\Omega L)^2]}{[1 + (\Omega L)^2]^{2}}$$

This family of equations, as proposed by Bullen and Taylor, applies to the component of turbulence perpendicular to the direction of traverse, i.e., to vertical and lateral gusts as measured in the HICAT program. Their corresponding equation for the component of turbulence in the direction of traverse - designated the longitudinal component in the HICAT program - is

$$\Phi(\Omega) = \frac{2\sigma^2 L}{\pi} \frac{1}{[1 + b^2\,(\Omega L)^2]^{n + 1/2}} \qquad (2)$$

Curves are not shown herein for this equation.

The second family is designated the sharp-knee family. This shape differs most conspicuously from the Taylor-Bullen shape in that the small hump to the left of the knee is eliminated. In addition, the frequency at which the knee occurs remains about the same for all values of m from -1 to -2; in contrast, the knee in the Taylor-Bullen family shifts to much lower frequencies as m approaches -1. The equation is simply

$$\Phi(\Omega) = \frac{\text{Constant}}{1 + (\Omega L)^{-m}} \qquad (3)$$

where (-m) = 1, 7/6, 4/3, 3/2, 5/3, 11/6, and 2. For the special case of m = -2, this equation is identical to equation (2).

The third family is designated the mild-knee family. The equation is

$$\Phi(\Omega) = \frac{\text{Constant}}{(1 + \Omega L)^{-m}}$$

For the special case of m = -2, this family yields the equation proposed by Lappe in Reference 12. The presence of a first-degree term in the denominator (with m = -2) results in a much milder knee. The sharp-knee and mild-knee families become more alike as (-m) decreases, and they are identical when

m = -1. At the frequency defined by the intersection of the low-frequency (horizontal) and high frequency asymptotes, ratios of actual psd to the value defined by the intersection are as follows:

	m = -2	m = -4/3	m = -1
Sharp-knee family	.50	.50	.50
Mild-knee family	.25	.40	.50

AVERAGE SPECTRAL SHAPE

It can be observed that the shapes of the gust velocity power spectra shown in Appendix VII display considerable variability. As a result, some sort of averaging of the many curves is desirable. Various ways of obtaining such an average are possible. One possibility would be to normalize all the curves to a consistent intensity level (by dividing by σ_w^2) and take a simple average. However, a somewhat different approach, which appears to offer several distinct advantages, is used herein.

This approach can best be understood by following the detailed description of its application to the HICAT data, given below. A brief summary at this point, however, is pertinent. From the many power spectral density (psd) curves that are to be averaged, a cumulative probability curve is prepared of the psd values read at a given frequency (inverse wavelength). This process is repeated for various frequencies covering the range of interest. A probability level is then selected, and the psd value corresponding to this probability is read from each curve. Each of the psd values read corresponds to a different frequency, and a plot versus frequency gives the desired average psd curve.

The advantages of this approach are the following:

- Under the normalizing and averaging approach, turbulence of all intensities contributes equally to the averages. But very mild turbulence is of negligible importance to airplane design and is much more subject to inaccuracy of measurement. It is therefore desirable to look separately at turbulence at various intensity levels. This is accomplished under the cumulative probability approach simply by reading power spectral densities from the probability curves at more than one probability level.

- In normalizing the power spectral densities in preparation for averaging, the vertical, lateral, and longitudinal gust power spectral densities would ordinarily each be normalized by dividing by their individual σ_w^2 value. A direct comparison of intensities in the three directions is thus lost.

- Because of uncertainty in measuring the very long wavelength components of the turbulence, the true rms value is quite uncertain. The appropriate rms to use for normalizing, therefore, is an arbitrary one

obtained by integration of the psd between appropriate limits. The value obtained will differ materially depending upon the limits selected. For example, the σ_w value obtained by integration with a lower limit at λ = 40,000 ft may be 2 to 3 times that obtained using a lower limit of 2000 feet. This vast difference in rms value that may be used to describe the same patch of turbulence has led to much confusion in the past. To minimize such confusion, great care is required in the use of rms values, and wherever their use can be avoided, it would appear desirable to do so.

- The procedure in which average psd curves are obtained from cumulative probabilities is believed to be particularly appropriate for arriving at a spectral shape for design use. For example, consider two airplanes. Airplane A feels predominantly gust frequencies over a narrow band in the vicinity of λ = 400 ft, and airplane B over a narrow band in the vicinity of λ = 20,000 ft. The design loads obtained for these two airplanes will depend upon the design gust power spectral densities at their respective frequencies. If design power spectral density curves utilize average shapes obtained as described above, the design power spectral density values will be exceeded with the same probability for both airplanes, regardless of what turbulence intensity may be selected as a design level. Clearly, the two airplanes will be of consistent strength, as desired; the possible variation of spectral shape from one patch of turbulence to another is quite unimportant. While real airplanes generally respond over broader frequency bands than assumed in this illustration, the general line of reasoning still applies and the same conclusions hold.

The spectra chosen for analysis of the HICAT data are listed in Table IV. With a few exceptions, those runs were excluded for which the RMS 2 values of vertical, lateral, and longitudinal gust velocities were all less than 1 fps. Others were excluded where there were obvious instrumentation malfunctions, or when the spectral shapes differed greatly from the norm and an instrument malfunction could not be definitely ruled out. Otherwise, all power spectra curves obtained are included.

First, all of the power spectra were faired to eliminate obvious irregularities such as the closely spaced oscillations at the high frequency end. For the most part, at the low frequency end the curves were left unfaired from the lowest frequency to a frequency four or five times this value, with the fairing becoming progressively heavier as the frequency increased beyond this point. A typical example of how the curves were faired is shown in Figure 32.

The faired curves were then read at frequencies corresponding to wavelengths of 200, 400, 1000, 2000, 4000, 10,000, 20,000, and 40,000 feet. It will be observed that all of the measured spectra provide data at wavelengths of 200, 400, 1000, and 2000 feet, while progressively fewer curves extend to wavelengths of 4000, 10,000, 20,000, and 40,000 feet.

At each of these frequencies, cumulative probability curves of power spectral density (psd) were prepared. In obtaining each probability distribution, the

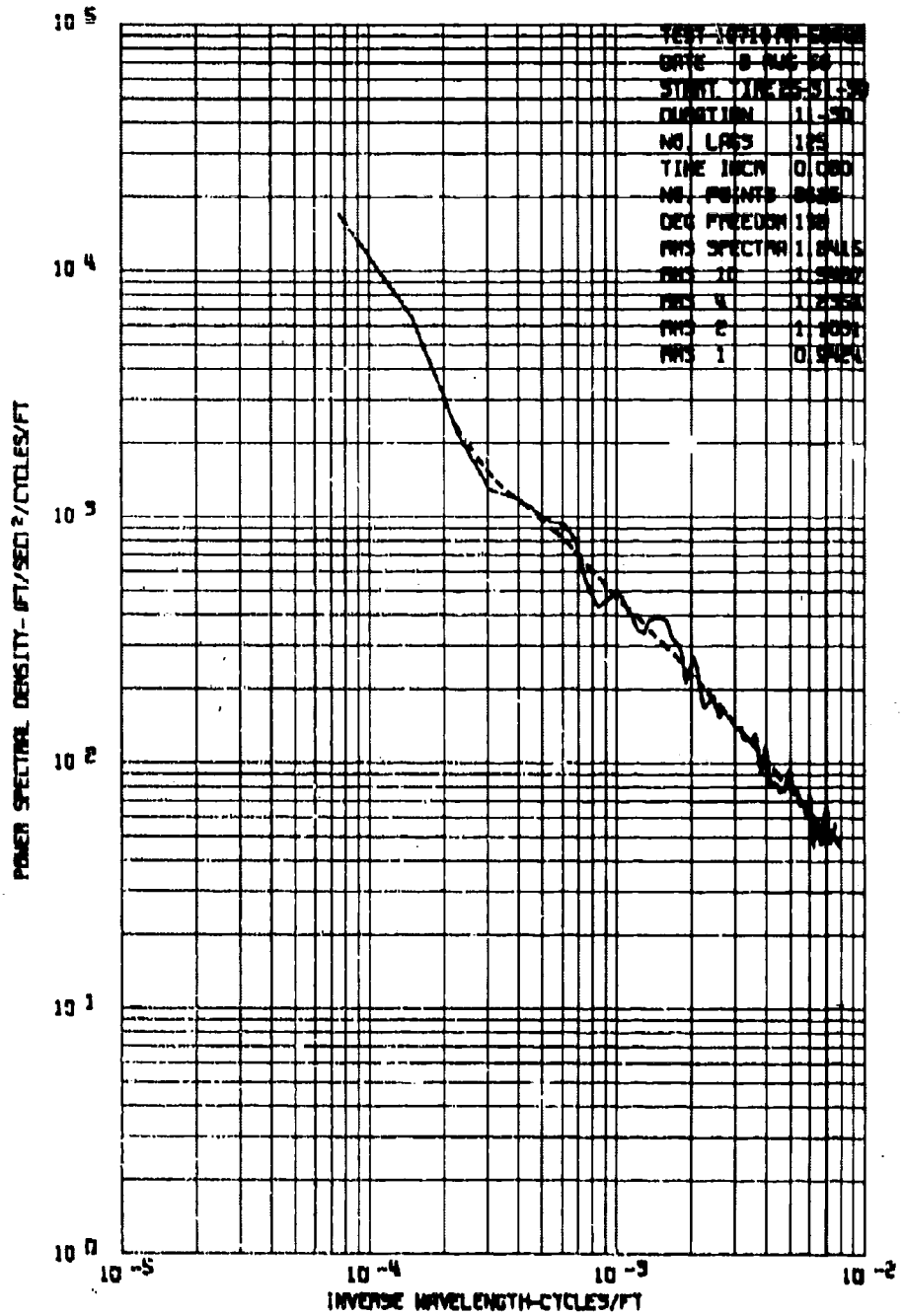

Figure 32. Example of Fairing of Gust Velocity Power Spectral Density Curves

psd values read were grouped into 7 roughly equal bands. Inasmuch as the longer runs actually represented larger samples of data, the various runs were weighted by length in accordance with the following table:

Actual duration of run, in minutes	Assumed duration of run, in minutes	Resulting number of times counted
1.33 - 3	2	1
3 - 5	4	2
5 - 7	6	3
7 - 9	8	4
9 - 11	10	5
11 - 13	12	6
13 - 16	14	7

The resulting curves are shown in Figures 33 through 35.

Figure 33 includes only wavelengths (λ) from 200 through 2000 feet and utilizes data from all the runs listed in Table IV. Figure 34 extends to a wavelength of 10,000 feet; in preparing these curves, only those runs were included for which psd values were available at λ = 10,000 ft. Because of the much smaller sample size, these curves are much less regular and it was much more difficult to establish with confidence a faired curve to represent the data. Figure 35 extends to a wavelength of 40,000 feet, for the vertical gust component only. This sample size was so small and the curves so irregular that it appeared that these data would not be of use. Accordingly, the corresponding curves for the lateral and longitudinal gust components were not prepared.

In Figure 33, each of the cumulative probability curves was faired by means of a straight line, as shown. Psd values were read as indicated by the plus symbols, at probabilities of .01, .1, and .5. The values at probabilities of .01 and .1 were read from the straight line; at a probability of .5, however, where each point represented a large sample, the value was read from the actual straight line segment through the plotted points.

At each of the three probability levels, the psd values thus read were then plotted versus inverse wavelength to give Figure 36. An average psd curve was thus obtained at each of three probability levels. The curves corresponding to the lower probability levels are most pertinent for direct practical application, as they reflect the more severe turbulence. The curves corresponding to the higher probability levels, however, are based on much more data and are statistically more reliable.

For both vertical and longitudinal gust velocities (in Figure 36), the psd curves for the three intensities are straight and parallel. The slopes, especially for the vertical gust velocity, are somewhat shallower than the -1.67 and -2.00 values currently used in design and analysis.

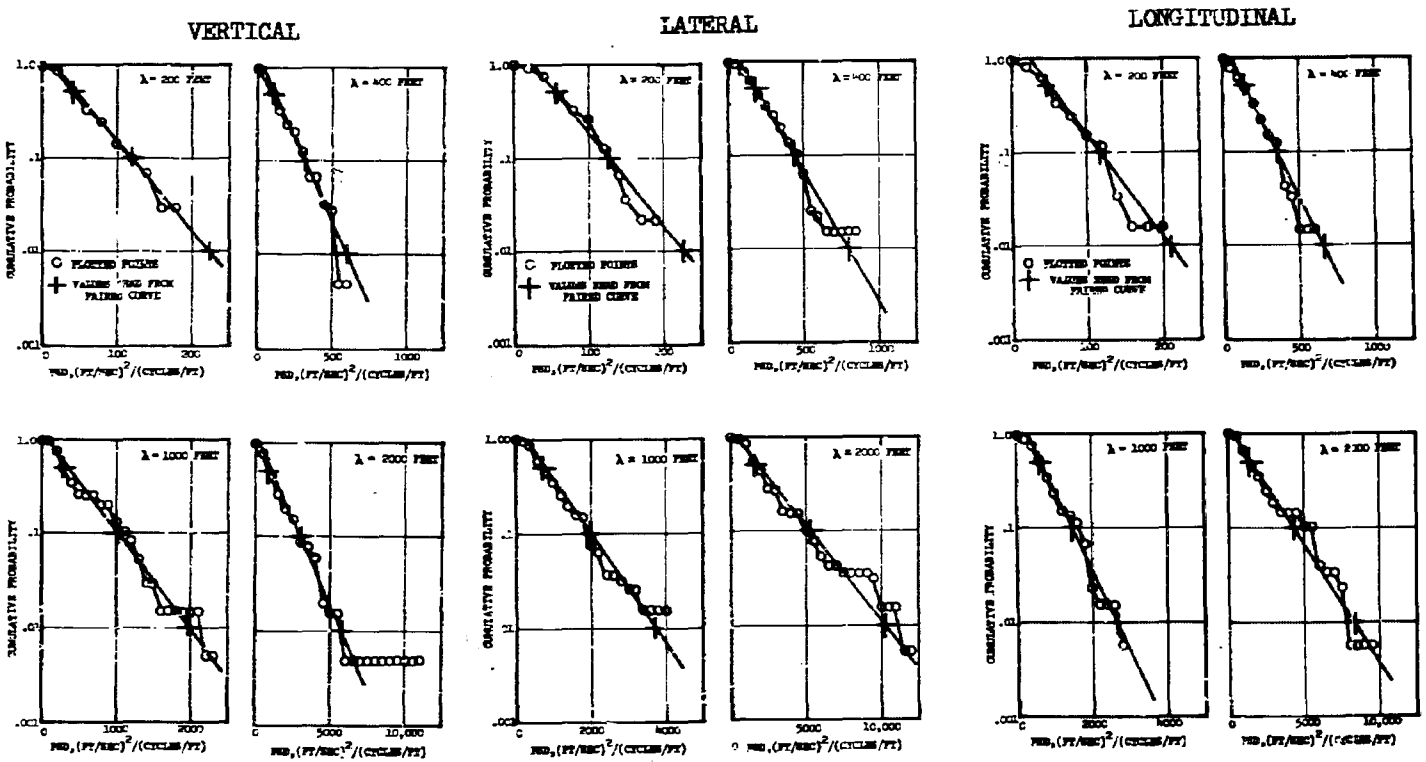

Figure 33. Cumulative Probability of Power Spectral Density; Vertical, Lateral, and Longitudinal Gusts, Maximum λ = 2000 ft

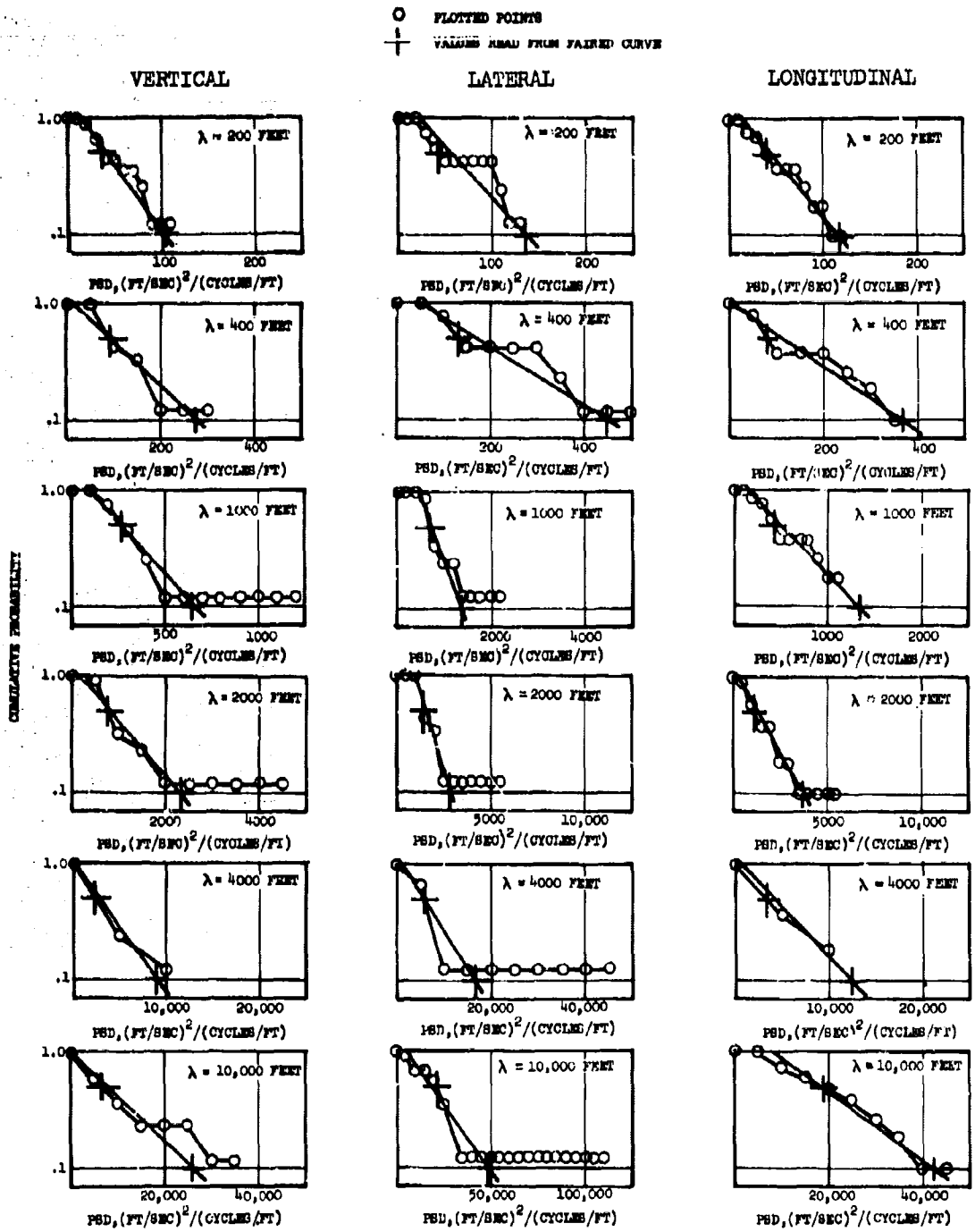

Figure 34. Cumulative Probability of Power Spectral Density, Vertical Lateral, and Longitudinal Gusts, Maximum λ = 10,000 ft.

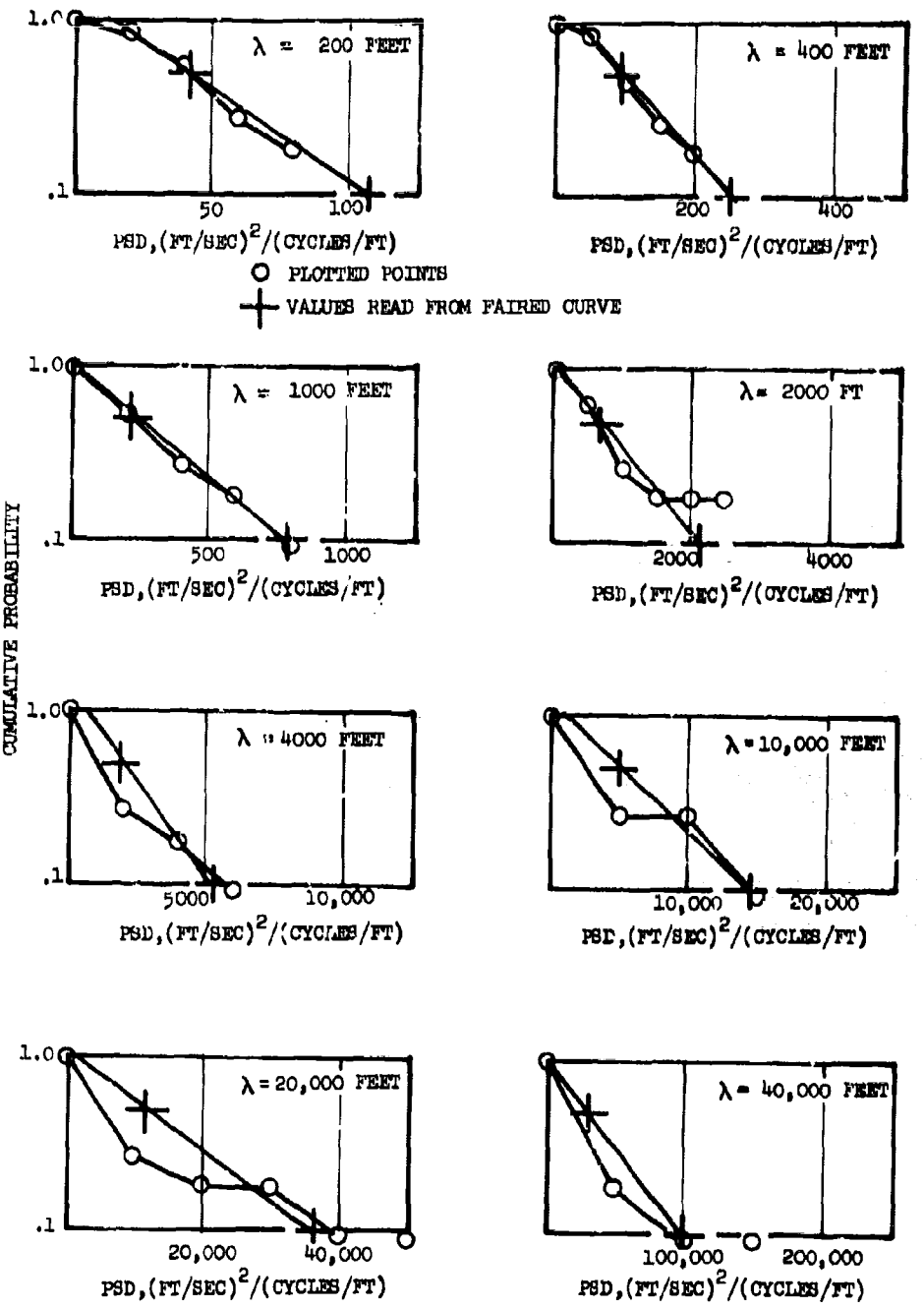

Figure 35. Cumulative Probability of Power Spectral Density, Vertical Gust, Maximum λ = 40,000 ft

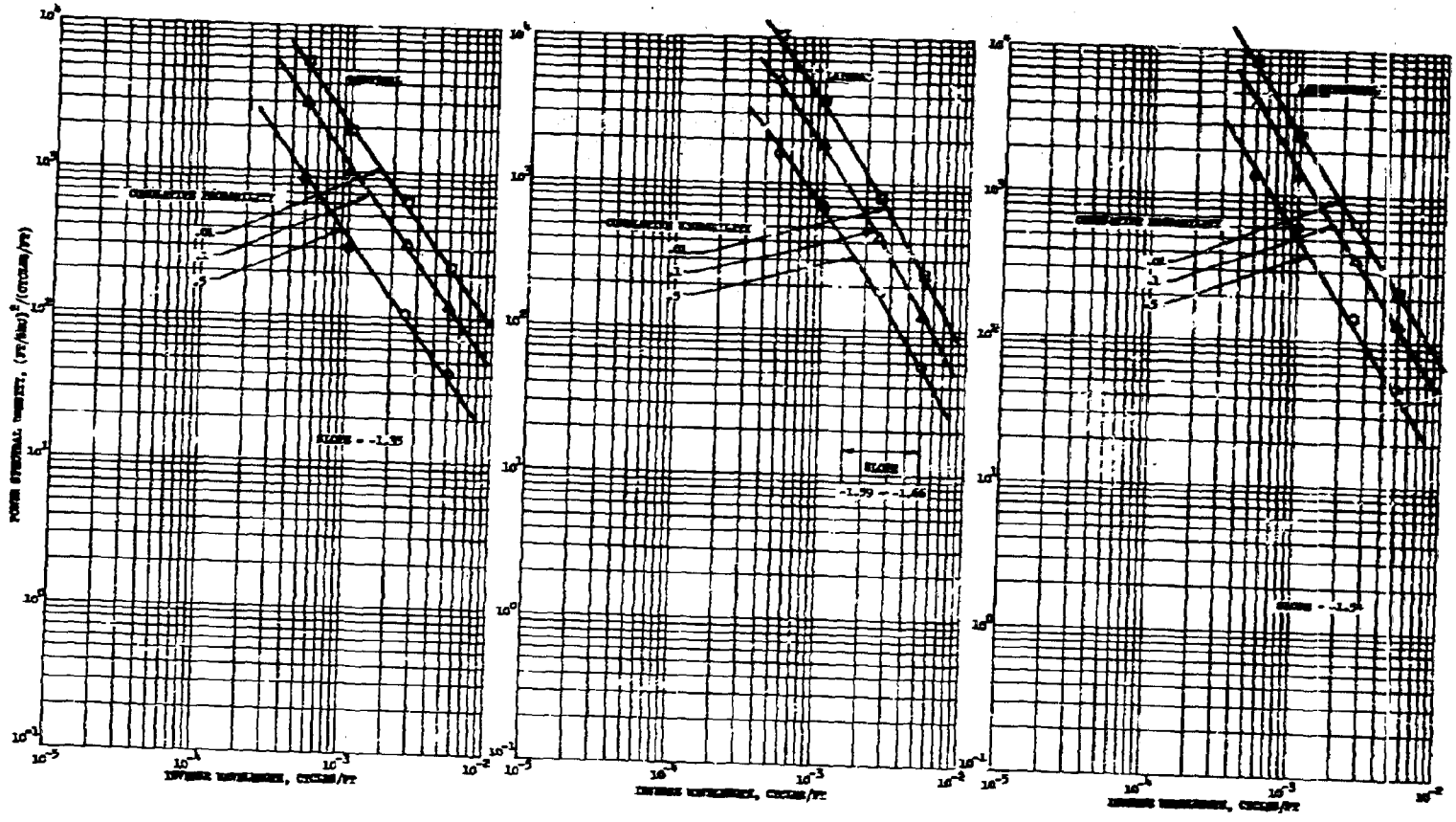

Figure 36. Average Power Spectral Density Based on Cumulative Probability, Maximum λ = 2000 ft

TABLE IV. RUNS USED FOR ANALYSIS

TEST	RUN	DATA USED			TEST	RUN	DATA USED		
		VERT	LAT	LONG.			VERT	LAT	LONG.
54	3	X	X	X	102	12	X	X	X
54	4	X	X	X	102	15	X	X	X
54	9	X	X	X	102	16	X	X	X
55	5	X	X	X	107	3	X	X	X
63	2		X	X	107	4	X	X	X
75	4	X	X	X	107	6	X	X	X
76	4	X	X	X	107	7	X		X
76	5	X	X	X	107	8	X	X	X
76	6	X	X	X	107	9	X	X	X
79	2	X	X	X	107	10	X	X	X
79	3	X	X	X	107	11	X	X	X
79	7	X	X	X	107	14	X	X	X
88	6	X	X	X	107	18	X	X	X
88	9	X	X	X	114	10	X	X	X
88	10	X	X	X	114	11	X	X	X
90	5	X	X		114	12	X	X	X
90	9	X	X		114	13	X	X	X
90	11	X	X		114	14	X	X	X
90	12	X	X		142	3	X	X	
96	12		X	X	142	4	X	X	
100	3	X	X	X	144	3	X	X	
100	5	X	X	X	147	3	X		
100	6	X	X	X	147	4	X		
100	7	X	X	X	147	5	X		
102	2	X	X	X	147	7	X		
102	3	X	X	X	147	8	X		
102	5	X	X	X	164	4	X	X	X
102	6	X	X	X	164	5	X	X	X
102	8	X	X	X	164	7	X	X	X
102	9	X	X	X					

For the lateral gust velocity, the slope is comparable to that for the longitudinal gust velocity, but varies slightly with probability level. Also, the curves in this case are not quite straight. A mild-knee shape (as defined previously in this section under Mathematically Defined Power Spectral Density Curves) with scale of turbulence of 1000 feet gives a good fit; the curvature is so slight, however, that a scale of turbulence, L, is not well defined.

The cumulative gust probability curves of Figure 34 were treated in the same way as the corresponding curves of Figure 33 except that only two of the three probability levels could be read. The resulting power spectral densities are shown in Figure 37. The trends are quite similar to those shown in Figure 36. However, the slight curvature in the lateral gust curves remains slight as the frequency range is extended to the longer wavelengths; the indicated scale of turbulence is at least 4000 feet.

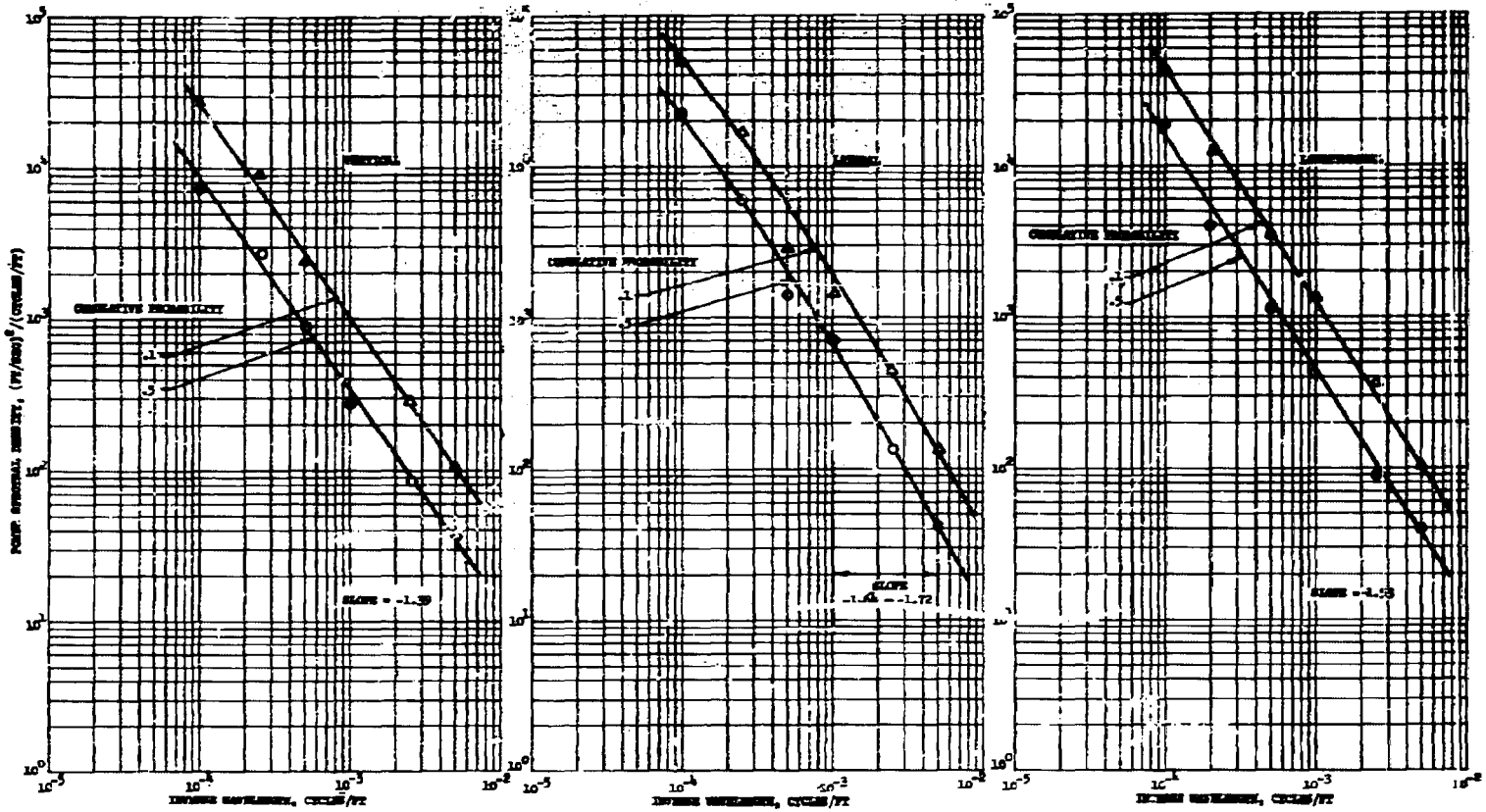

Figure 37. Average Power Spectral Density Based on Cumulative Probability, Vertical Gust, Maximum λ = 10,000 ft

The cumulative probabilities shown in Figure 35 are so irregular that somewhat more judgment seems necessary in reading the faired values at the two probability levels; consequently, it will be noted that the rules followed in the other cases are not strictly adhered to. The resulting psd curves are shown on Figure 38. Despite the considerable leeway in reading values from the probability curves, the scatter of the points on the psd plots is not excessive. The curves retain the relatively shallow slope shown in the vertical gust curves in Figure 36 and 37, and are straight through the full range of wavelengths. The indicated scale of turbulence is at least 8000 feet.

Because of the very small sample of psd curves extending to $\lambda = 40{,}000$ ft and the resulting irregularity of the cumulative probability curves, average power spectral densities over this range were also obtained by taking simple averages of the psd values at the same eight wavelengths. The same weighting factors for length of run were used as in obtaining the cumulative probability curves of Figures 33 through 35. Since the power spectral densities were not normalized before averaging, the various runs were also, in effect, weighted heavily according to intensity. This weighting is beneficial, since the more severe turbulence is more important for design and its measurement is inherently more accurate. The range of rms values for the nine runs was approximately a factor of 2 for RMS 2 and 2.5 for RMS 40.

The power spectral densities obtained in this way are shown in Figure 39. For the vertical gust velocity, the curve agrees almost exactly in shape with the curves obtained from the cumulative probabilities as shown in Figure 38. All three curves obtained by the direct-average method are essentially straight over the full range of wavelengths.

Similar comparisons of the average spectra for the vertical, lateral, and longitudinal components of turbulence for $\lambda = 2000$ and $\lambda = 10{,}000$ ft are shown in Figure 40. The curves compared are those for a cumulative probability of 0.1 previously shown in Figure 36.

In assessing the spectra shown in Figures 33 to 40, it is felt that the data up to wavelengths of 10,000 (and possibly extrapolated to 12,000 or 15,000 feet) provide valid representations of the atmosphere. At wavelengths of 20,000 feet and above the situation is less clear because the data sample is much smaller, the gust intensity level is considerably less, and the possibility of some extraneous influence is correspondingly greater. However even these latter spectra are believed to be conservative from a design standpoint.

SPECIAL STATISTICS

PROBABILITY DISTRIBUTIONS OF RMS GUST VELOCITY

Probability distributions of rms values of the three components of absolute gust velocity, for the runs identified in Table IV, are shown in Figures 41 and 42.

Cumulative probability distributions rather than probability densities are shown because this form of presentation is more amenable to drawing

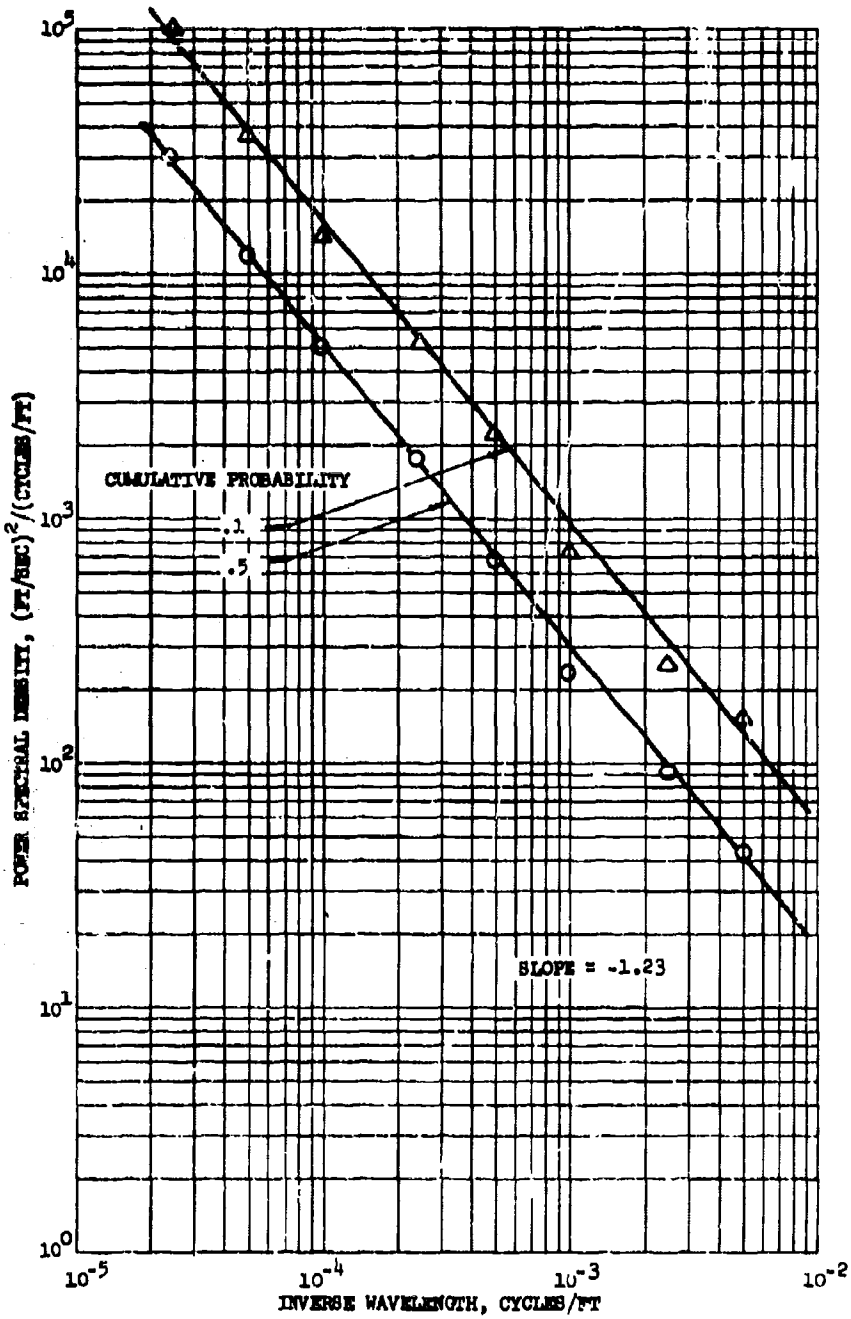

Figure 38
Average Power Spectral Density Based on Cumulative Probability, Vertical Gust, Maximum λ = 40,000 ft

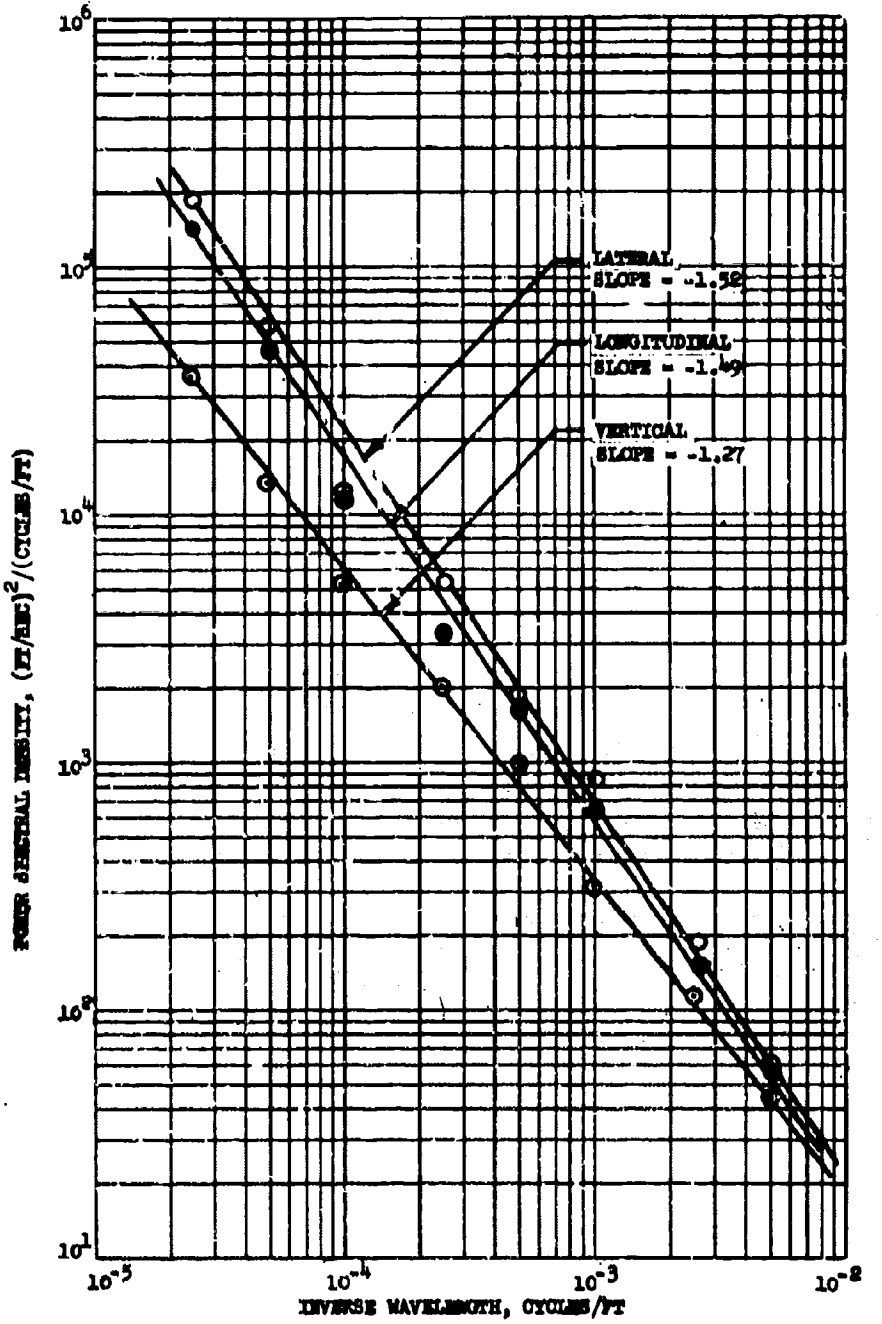

Figure 39. Direct-Average Power Spectral Density, 3 Components
Maximum λ = 40,000 ft

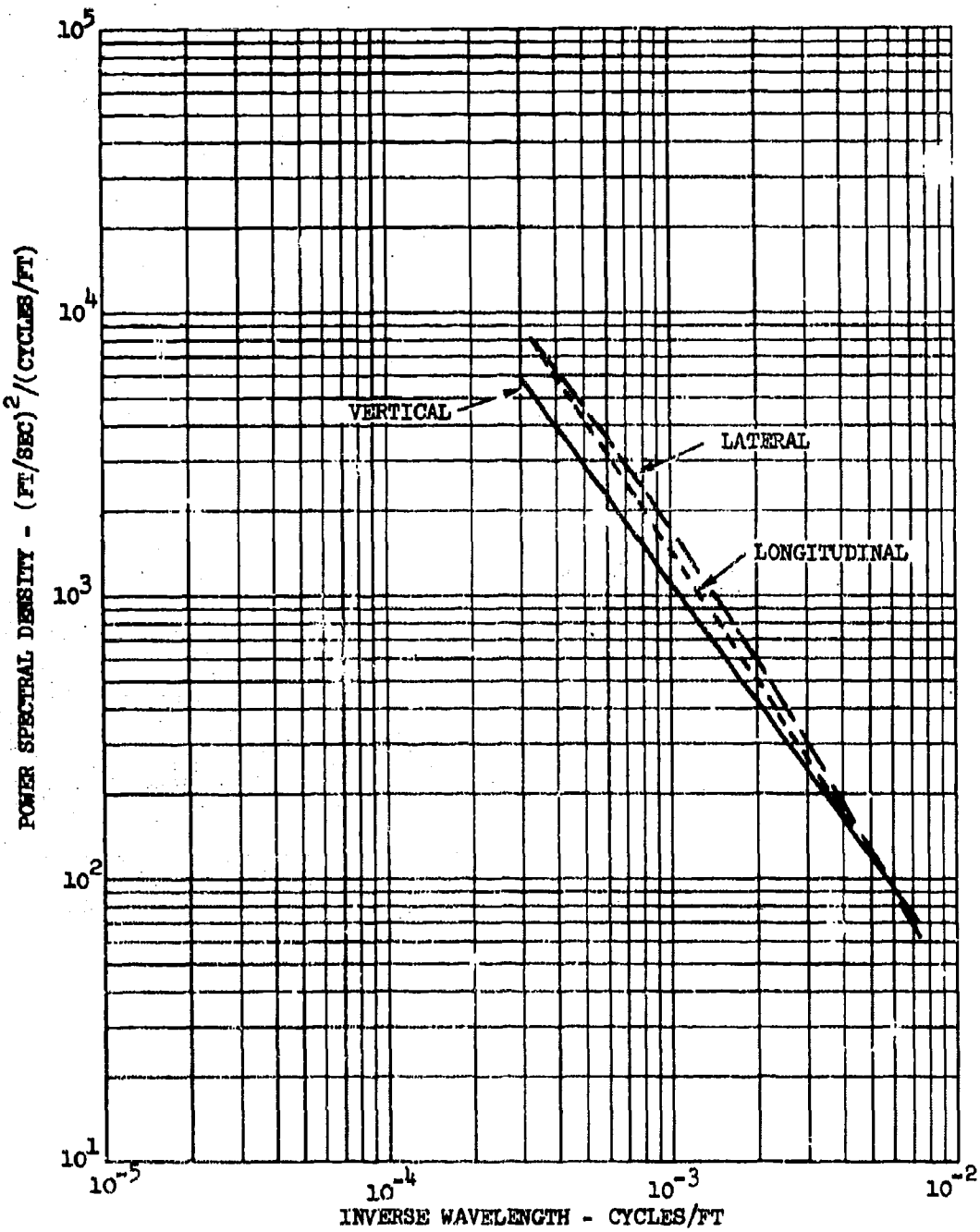

Figure 40A. Comparison of Power Spectral Densities for 3 Components, Cumulative Probability of .1, Maximum λ = 2000 ft

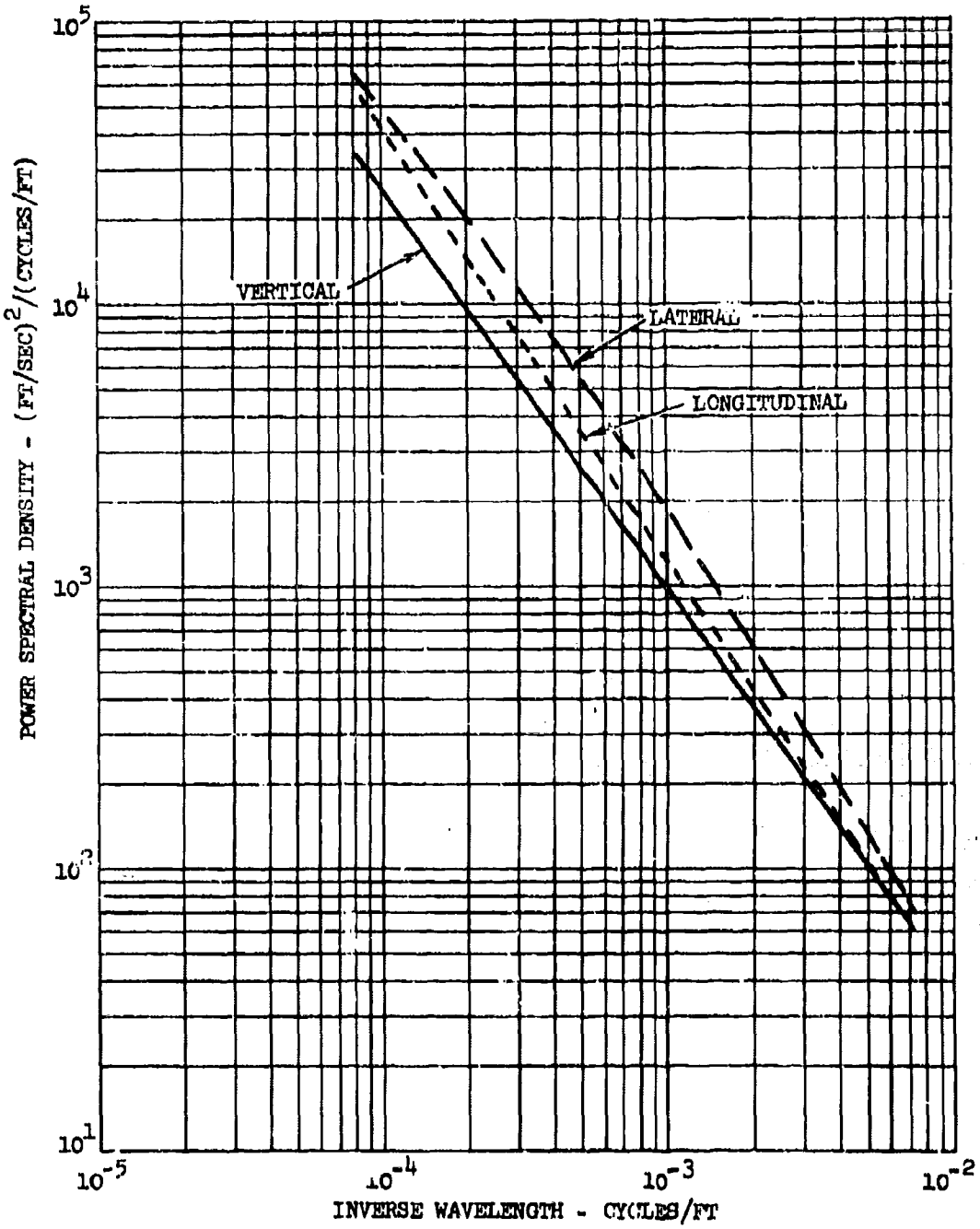

Figure 40B. Comparison of Power Spectral Densities for 3 Components, Cumulative Probability of .1, Maximum λ = 10,000 ft

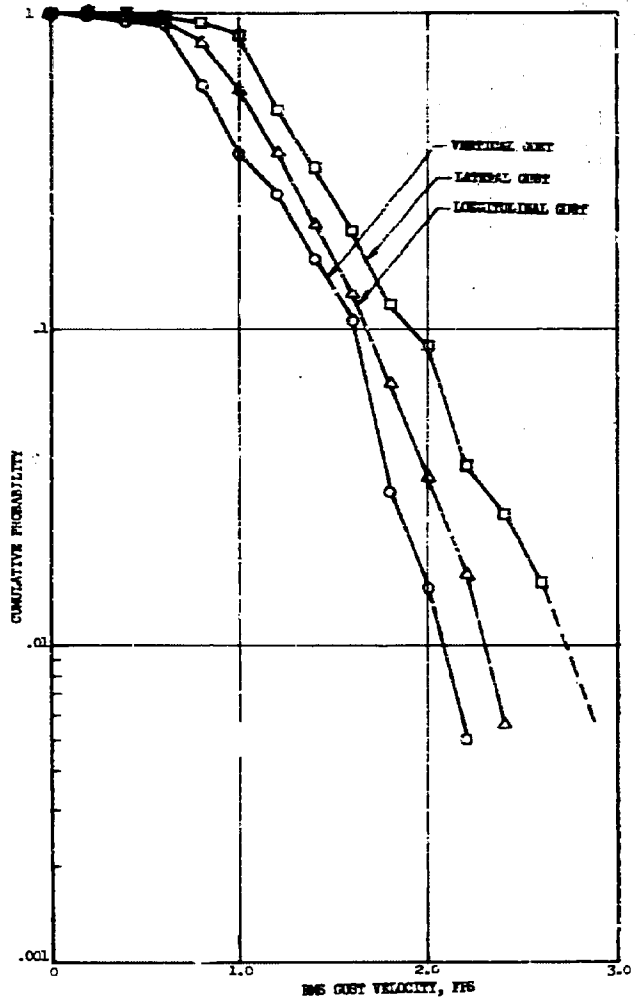

Figure 41. Cumulative Probability Distributions of 2 Gust Velocities for All Runs Analyzed

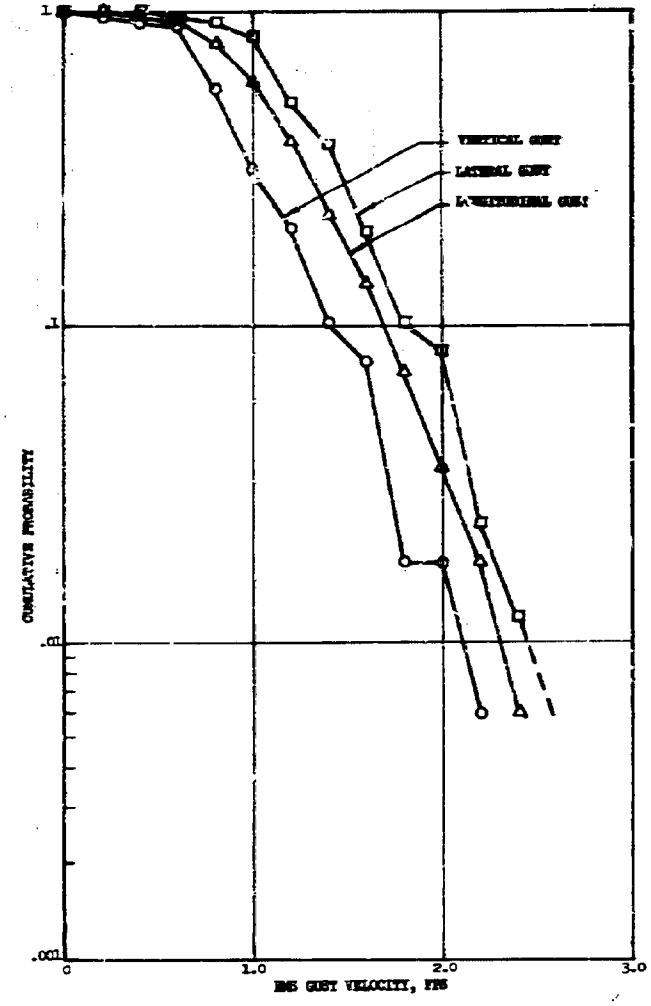

Figure 42. Cumulative Probability Distributions of RMS 2 Gust Velocities for Those Runs for Which All Three Components are Available

quantitative conclusions. For any given rms gust velocity the cumulative probability read from the appropriate curve is the probability that the given rms gust velocity is exceeded.

The rms gust velocities upon which these curves are based are the values obtained by integrating the power spectral densities over the frequency range from .0005 cycles per foot (λ = 2000 ft) to the highest frequency at which the power spectral densities were defined, corresponding to 5.00 cps and averaging about .007 cycles per foot. The low frequency limit of integration was selected as the lowest frequency common to all the power spectral densities obtained. To convert to rms values that would be obtained if various shapes of power spectral density function were fitted to the data and the integration carried out from zero to infinite frequency, the RMS 2 values would be multiplied by approximately the following factors:

Spectral Shape	Factor
Von Karman, L = 2500 ft	2.48
Dryden, L = 1000 ft	1.97
Dryden, L = 2000 ft	2.72

These were obtained from the theoretical curves noted by evaluating the ratio

$$\frac{\sqrt{\int_0^{\infty} \Phi\left(\frac{\Omega}{2\pi}\right) d\left(\frac{\Omega}{2\pi}\right)}}{\sqrt{\int_{.0005}^{.007} \Phi\left(\frac{\Omega}{2\pi}\right) d\left(\frac{\Omega}{2\pi}\right)}}$$

In obtaining the probability distributions, the variation in length of runs was accounted for approximately by weighting the various runs as follows:

Actual duration of run, in minutes	Assumed duration of run, in minutes	Resulting number of times counted
1.33 - 3	2	1
3 - 5	4	2
5 - 7	6	3
7 - 9	8	4
9 - 11	10	5
11 - 13	12	6
13 - 16	14	7

The probability distributions shown apply to the flight time included in "runs" as defined under Data Editing in Section V, and of 80 seconds or more duration. To convert to a basis of total flight time, all of the

curves would be shifted down in roughly the ratio .045, which is the ratio of time in runs of 80 seconds or more duration to the total flight time for which data are available.

The flatness of all the curves for rms gust velocities below about .5 to 1.0 fps is due at least in part to excluding data in very mild turbulence - that is, turbulence yielding peak cg accelerations less than about 0.1g.

Figure 41 includes data from all runs shown in Table IV. In order to provide a more reliable basis for judging the relative intensity of turbulence in the three directions, the probabilities were recomputed using only those runs for which data were available for all three directions, as indicated in Table IV. The results are shown in Figure 42. On this basis, the ratios between various pairs of curves are seen to be somewhat more consistent with probability level.

It should be emphasized that each rms value utilized in preparing these figures was an overall value for a given run, and that in many of the runs the rms gust velocities varied significantly during the run. If this variation were to be taken into account, the probability distributions would show much higher rms values at the low probability levels. This phenomenon is discussed in detail under Stationarity.

ISOTROPY

Knowledge of the probable isotropy of turbulence is important chiefly to provide answers to the following questions:

- First, Should the turbulence intensities used for design be the same for the three components of turbulence, vertical, lateral, and longitudinal? This question is important because design levels are ordinarily based primarily upon measurement of airplane center-of-gravity normal acceleration during a great many hours of routine operational flight. Thus, the design intensity of the vertical component of gust velocity is established fairly directly. The determination of realistic design intensities of the lateral and longitudinal components must depend upon more complete data from a much smaller sample, such as provided by the HICAT program.

- Second, Should the airplane be considered to be subjected to the design intensity of all three components of turbulence simultaneously, or when one component is at its maximum is it probable that the intensities of the other two will be significantly lower?

The isotropy of the turbulence measured in the HICAT program is indicated in this report in three ways.

First, rms values of the three components of gust velocity can be read from the cumulative probability curves of Figure 41 or Figure 42 at a given probability level and the pertinent ratios calculated. For this purpose,

Figure 42 is considered the more appropriate, as the three curves there were obtained from exactly the same runs.

It is seen first that the ratio of longitudinal to lateral gust velocity is roughly 0.93 throughout the probability range. For isotropic turbulence, ratios of the longitudinal component to the lateral or vertical component in the constant exponent region of the psd depend upon the exponent and have the following theoretical values:

Exponent	Ratio of longitudinal to lateral psd	Ratio of longitudinal to lateral spectral rms velocities
-2	2/3	.818
-5/3	3/4	.866
-3/2	4/5	.895
-4/3	6/7	.926
-1	1	1.000

The value 0.93 is in good agreement with the theoretical values in the pertinent range of exponents, namely -5/3 to -3/2. This agreement is gratifying, in that the direction of flight through the turbulence presumably is random, and therefore, on the average, the turbulence should appear isotropic in the horizontal plane.

In comparing the vertical component with the lateral or longitudinal, isotropy does not appear to be so necessary, as the mechanism generating the turbulence might well be inherently directional. Figure 42 indicates a ratio of lateral to vertical rms values ranging from about 1.45 at the higher probability (lower intensity) levels to about 1.20 at the low probability levels.

Second, in order to determine whether the isotropy picture is the same at all frequencies (inverse wavelengths), the comparative psd plots shown in Figures 39 and 40 can be examined. Figure 40A, which represents the largest sample of data, indicates that all three components have about the same intensity (as measured by psd) at the shortest wavelength at which measurements were made (100 to 150 feet). Both figures show the vertical component to decrease in intensity, relative to the lateral, as the wavelength increases.

The above approaches give information pertinent to answering the first question posed, i.e., what relative intensities of vertical and lateral gust are appropriate for design? It does not, however, shed any light on the isotropy of individual patches of turbulence.

For this latter purpose, as well as to obtain an independent indication of the average ratios amongst the three components, a third approach was followed. Ratios of longitudinal to lateral, lateral to vertical, and longitudinal to vertical spectral rms gust velocities were obtained for all the available runs listed in Table IV. Probability distributions of these ratios were then

obtained, weighted according to duration of run as described previously in the paragraph entitled Probability Distributions of RMS Gust Velocity. Plots of these probability distributions on probability paper are shown in Figures 43 through 45. The probability indicated by the curves is the probability that the ratio is less than the indicated value.

A Gaussian, or normal probability is indicated by a straight line on such a plot. The value of the variable at a probability of 50 percent is the mean. The difference between the mean and the value read at a probability of 15.9 or 84.1 percent is the standard deviation.

The probability distributions for ratios of RMS 2 values are shown in Figure 43.

The distribution for the ratio of longitudinal to lateral rms, shown in Figure 43, is almost a straight line. The mean value, 0.88, is in reasonable agreement with the ratio of 0.93 indicated by Figure 42. In 70 percent of turbulence encounters, it would be expected that the ratio of longitudinal to lateral intensities would lie between 0.88 - 0.14 = 0.72 and 0.88 + 0.14 = 1.02.

The distribution for the ratio of lateral to vertical rms also is shown in Figure 43. At the high values of the ratio, the data depart markedly from a straight line. Test and run numbers for the data defining this part of the curve are indicated. Tests 70-3 and 73-5 both have RMS 2 values well below 1 fps and as a result should perhaps not have been included. Unfortunately, this type of presentation gives equal importance to all intensity levels. In contrast, in Figure 42, a few extreme values of the ratio of lateral to vertical rms, if occurring at low intensity levels, are submerged by the many more occurrences of near-average values.

Examination of the rest of the lateral to vertical curve in Figure 43 indicates a fairly good straight line fit, with an indicated mean of 1.45. This agrees with the ratio obtained at a probability of about 0.5 from Figure 42. The variation of the ratio with turbulence intensity, shown in Figure 42, is quite possibly a real effect, and the presentation of Figure 43 inherently is dominated by the lower intensities, of less interest. The standard deviation shown in Figure 43 indicates that in 70 percent of turbulence encounters the ratio of lateral to vertical intensities should be between 1.24 and 1.66.

The above discussion of the ratio of lateral to vertical applies generally to the longitudinal-to-vertical curve in Figure 43 although the curve here is not quite as straight. The lower value of the mean, 1.32 as compared with 1.45, is consistent with a mean of less than 1.00 on the longitudinal-to-lateral curve.

Corresponding probability distribution curves based on RMS 10 and RMS 40 values are shown in Figures 44 and 45, respectively. These are not different from the curves based on RMS 2. The mean values of the ratios of lateral and longitudinal to vertical rms gust velocities are somewhat greater,

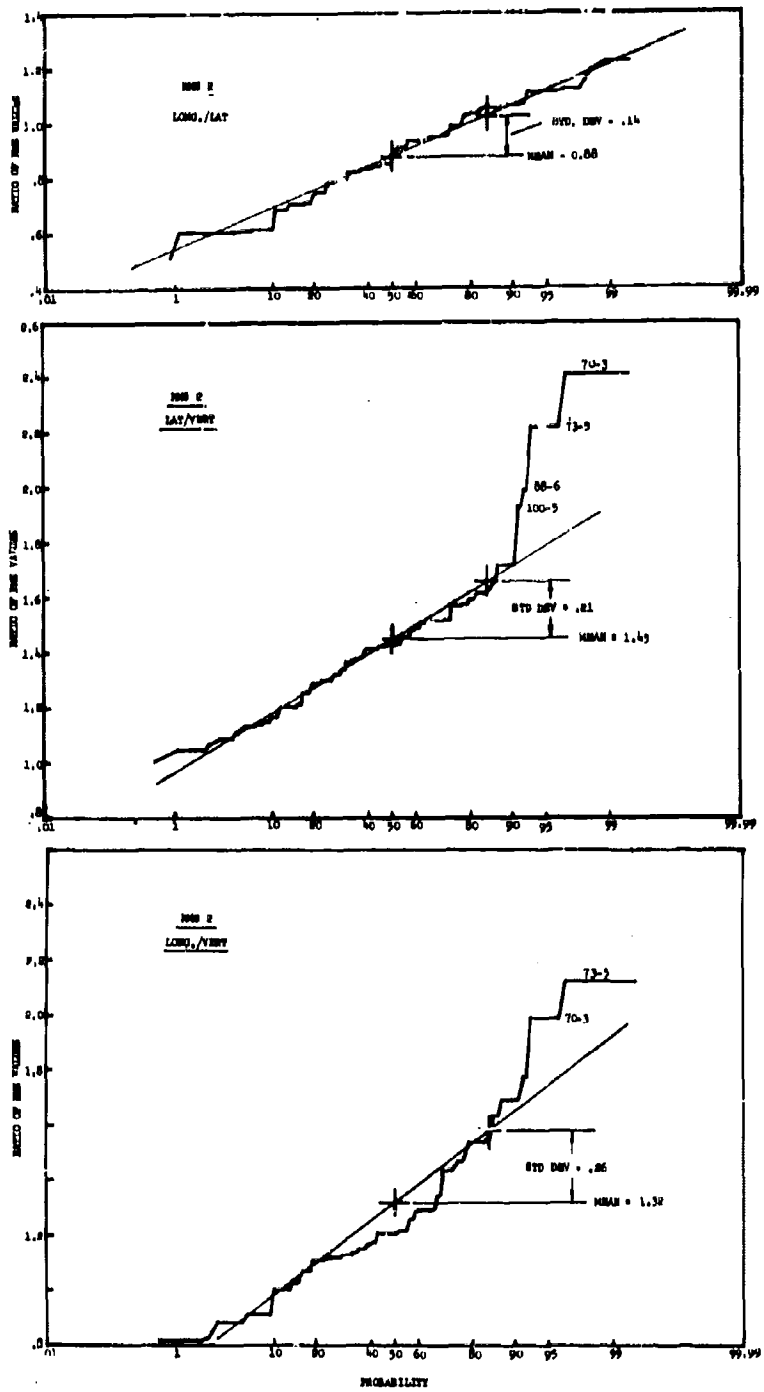

Figure 43. Probability Distribution of Gust Velocity Component Ratios, RMS 2

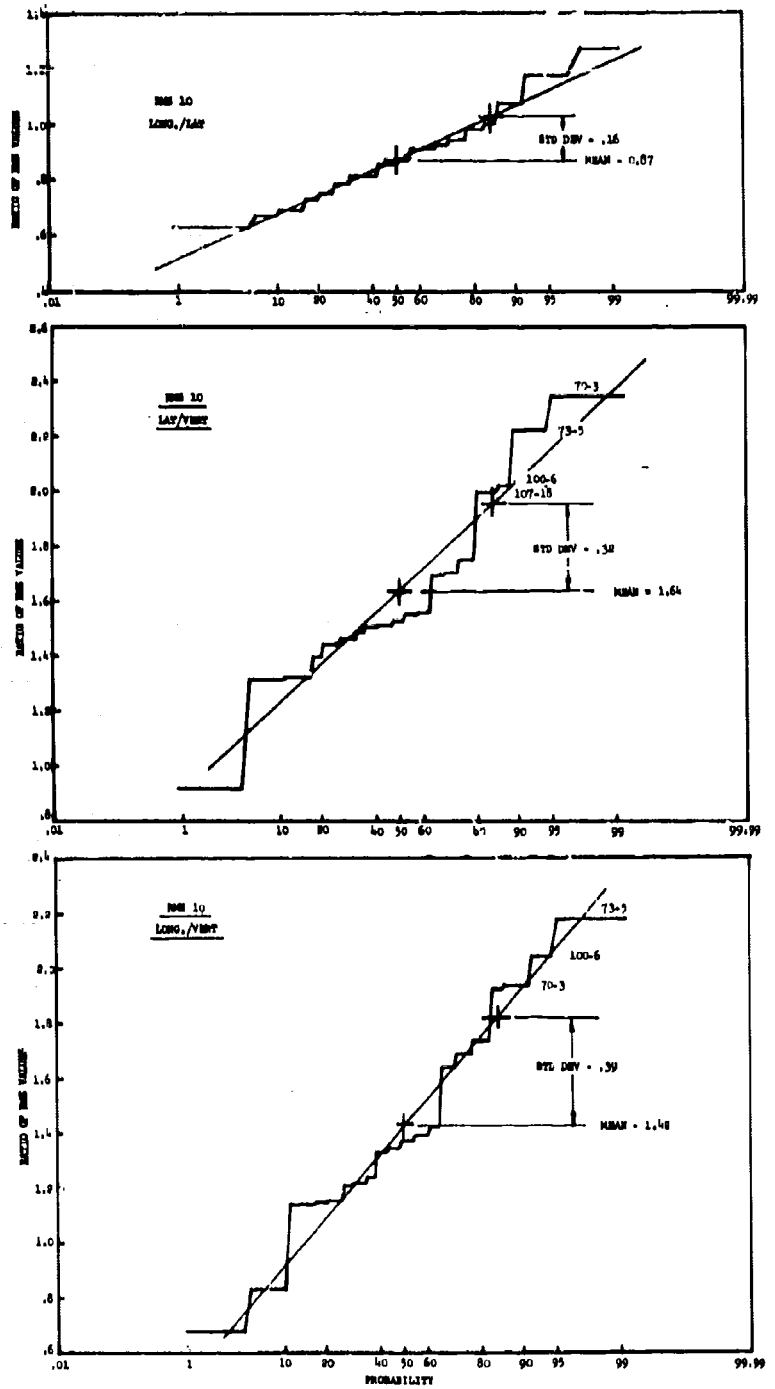

Figure 44. Probability Distribution of Gust Velocity Component Ratios, RMS 10

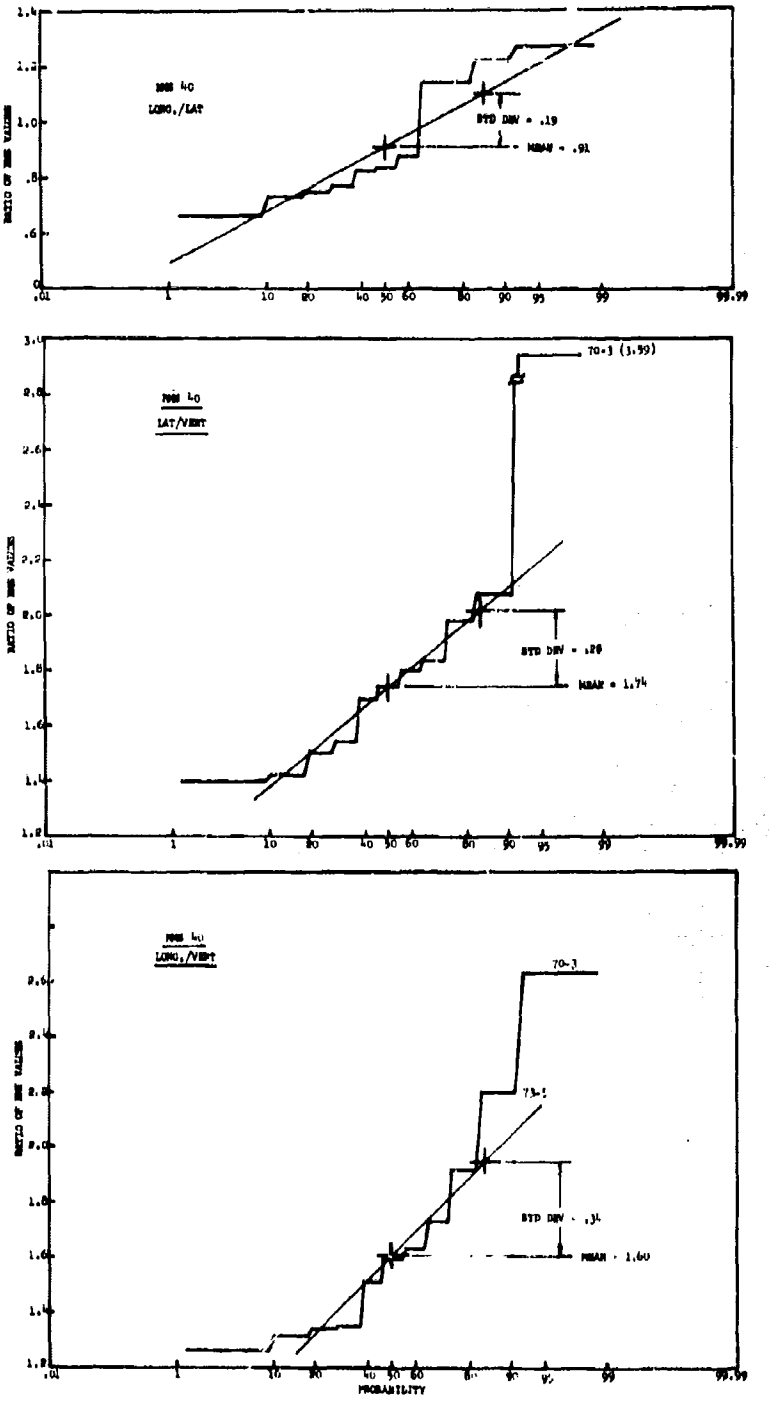

Figure 45. Probability Distribution of Gust Velocity Component Ratios, RMS 40

and the standard deviations also are greater. The extreme departures from the straight line at the high-ratio end do not appear at RMS 10, but are present again at RMS 40.

STATIONARITY

The term stationarity as used in this report refers to that property of a time history for which the statistical parameters, such as the mean, the root-mean-square (rms) value, the power spectral density, and so on, do not change with time.

In any application of measured rms gust velocity values to structural design or, perhaps to a lesser degree, to ride comfort, stationarity of the sample is of major importance. This is because of the effect stationarity has upon the relationship of peak values of load or acceleration to rms values. Rms values are of use only as a means of determining expected peak values. For establishing the strength needed to withstand one-time loading, on either a "limit" or an "ultimate" basis, the peak value expected once in some very long time, such as the desired life of the airplane, is needed. For evaluating resistance to structural fatigue, the expected frequency of occurrence of peaks over a wide range of load levels is required.

Prediction of load peaks due to turbulence is invariably based upon Rice's equation, which relates frequency of exceedance to load level and rms value:

$$N(y) = N_o e^{-\frac{1}{2}(y/\sigma_y)^2}$$

where

y = any load, stress, or other quantity varying with time

σ_y = rms value of y

$N(y)$ = average number of crossings per unit time, with positive slope, of the value y

N_o = characteristic frequency, equal to the radius of gyration of the power-spectral density function of y about zero frequency

This equation can be derived theoretically, under the assumption that the time history is stationary and Gaussian.[9] The quantity N(y), although its formal definition is not in terms of peaks, provides a good approximation to the number of peaks per unit time in excess of given values of y, for any reasonable definition of a peak. The approximation is especially good for values of y/σ_y greater than about 2 and for time histories characterized by a narrow-band power spectral density.

For flight through many patches of turbulence of various intensities, as would be experienced over the entire life of any given airplane, Rice's equation is applied, in effect, to each patch separately. The exceedances contributed by all the various patches are then added together to give a total.

If Rice's equation is plotted on coordinates of log N(y) vs y^2, the result is a straight line, as shown in Figure 46 (a). In this figure, y has been replaced by U_{de}. As noted earlier, y can be any quantity which varies in response to a varying gust velocity as an input. The incremental cg normal acceleration is such a quantity, and the derived equivalent gust velocity, U_{de}, is simply a constant times the cg acceleration.

Accordingly, if a given sample of turbulence is stationary and Gaussian, a plot of $N(U_{de})$ vs U_{de}^2 will approximate a straight line. The measured values of $N(U_{de})$ should, of course, be counts of positive slope crossings at various U_{de} levels from the time histories. In Figure 46 (a), the units of $N(U_{de})$ are crossings per duration of the run. Thus, a value of $N(U_{de}) = 1$ denotes the one highest peak in the run.

Suppose that an actual patch of turbulence consists of two portions, both stationary but of different rms levels. For example, consider a patch of which the first 90 percent yields an rms of 1.75 fps and the last 10 percent an rms of 3.50 fps. The overall rms will be

$$\sqrt{0.90 \times 1.75^2 + 0.10 \times 3.50^2} = 2.00 \text{ fps.}$$

---

[9] It should be noted, incidentally, that the Gaussian nature of the time history does not result in a Gaussian distribution of the peaks. A Gaussian time history is characterized by a Gaussian - or normal - distribution of values read from the time history, either at random or at an arbitrary uniform time interval. Rice's equation, which, as noted above, approximates the probability distribution of the peaks, has the same mathematical form as the equation for the Gaussian probability density. But Rice's equation inherently represents a cumulative distribution. When it is differentiated to give the probability density, it no longer has the Gaussian form.

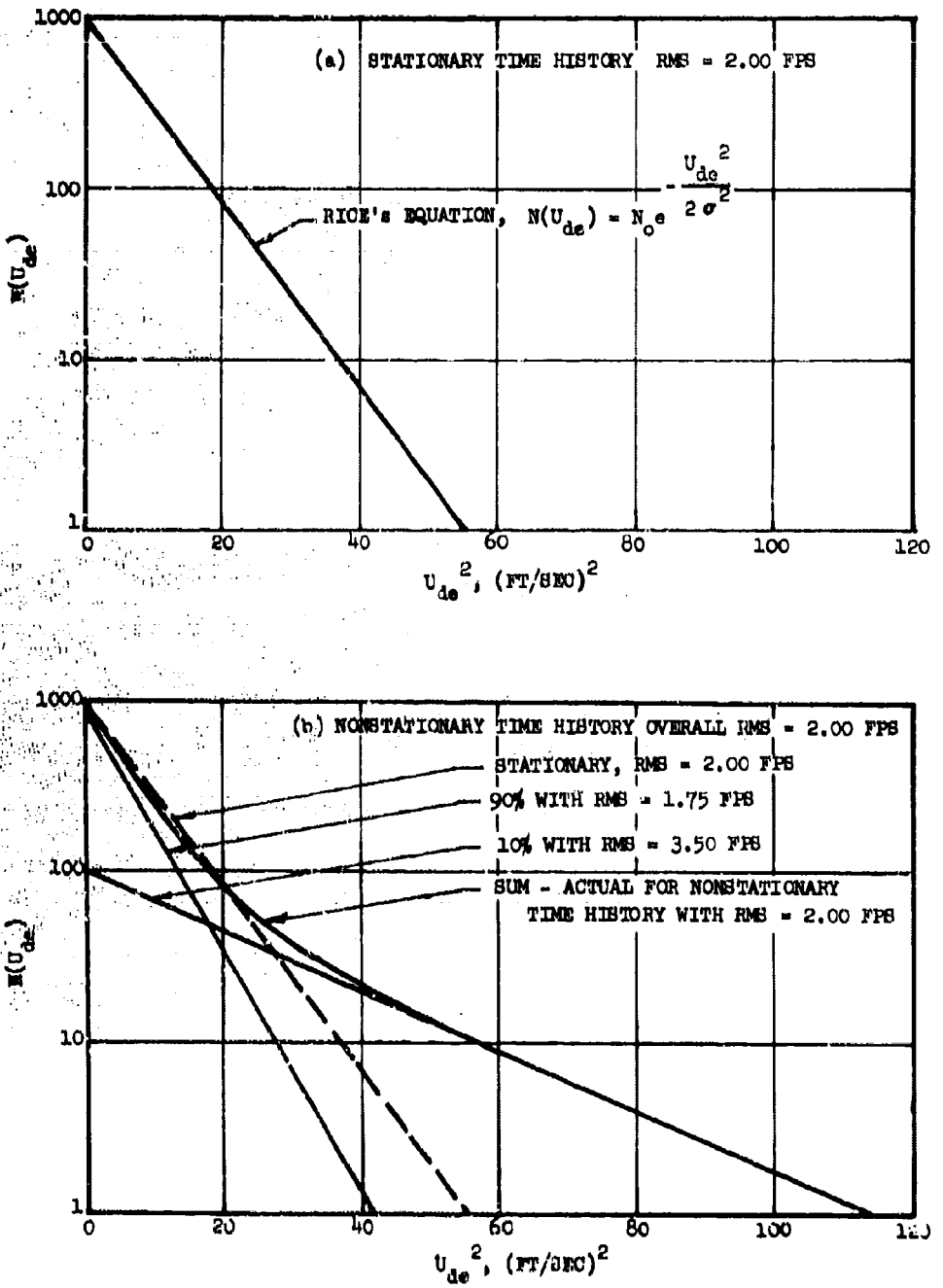

Figure 46. Theoretical Effect of Nonstationarity on U_{de} Exceedance Curves

The expected exceedance curve for such a patch can be obtained by adding together the contributions of the two parts, taking account of the relative time in each, as shown in Figure 46 (b).

The significant result shown in this figure is that the expected highest peak for the actual nonstationary patch is 45 percent higher than that obtained by application of Rice's equation to the patch as a whole. It is clear that if the only rms gust velocity considered were that for the patch as a whole, calculated airplane load peaks would be low by some 30 percent. Similarly, if rms values for many runs were obtained in the same way and a probability distribution obtained, the highest load peaks would again be substantially underpredicted.

It might be remarked that, in the example shown in Figure 46 (b), the 10 percent of the time at the high rms value need not be at either the beginning or the end of the run, but might have occurred in the middle. Or, it might have occurred in still smaller portions, distributed at intervals throughout the run. In all cases, the exceedance curve would have been the same. The only requirement is that the individual stationary portions be long enough, or the rms level vary gradually enough, so that the theoretical input-output relations for a stationary random process apply.

The same principle would apply if more than two rms levels were present. Here, the "total" curve in Figure 46 (b) would have been made up of the sum of three of more straight lines. It is interesting to note that even with a continuous variation in σ_w over the run, it is likely that the actual exceedance curve can be approximated quite closely by adding as few as two or three straight lines, representing a correspondingly small number of discrete σ_w values.

In past programs directed toward the measurement of time histories of absolute gust velocity, little attention has been given, quantitatively, to stationarity. Examination of the various gust velocities shown in Appendix VI, however, indicates that a typical run of several minutes' duration is likely to be distinctly nonstationary. Patches of relatively severe turbulence of perhaps 20 or 30 seconds' duration are interspersed with regions of comparable duration where the turbulence is clearly less severe, or even quite mild.

As suggested by Figure 46 (b), a very practical quantitative measure of stationarity is available from the frequency-of-exceedance plots, in the form of the ratio of the highest load peak to the value predicted by Rice's equation from the overall rms value. In forming this ratio, the highest load could be either the actual value or the value read from the faired exceedance curve.

Several examples of plots of $N(U_{de})$ versus U_{de}^2 from the NICAT program are shown in Figure 47. These represent the following runs:

Test and run	Location	Duration (sec)	Rms U_{de}
88-9	New Zealand	110	0.87
102-2	Australia	235	1.79
107-8	Australia	990	1.14
107-14	Australia	670	0.74
147-4	Puerto Rico	255	1.90
164-4	Alaska	215	1.42

Cases (test and run) 88-9, 107-8, 107-14, and 147-4 were selected more or less at random, covering a range of durations, locations, and rms levels. These were later found not to include the runs that appeared most stationary from their time histories. As a result, cases 102-2 and 164-4 were added.[10]

In all cases the experimental curve has the characteristic concave-upward shape indicated theoretically in Figure 46 (b). Also, in all cases, a very close fit to the test points is obtained by adding only two straight-line components, to give the curve labeled "sum." This closeness of fit is rather remarkable when one notes the many different intensities displayed in several of the time histories (Appendix VI).

The line representing Rice's equation is plotted using the U_{de} rms value obtained from the time history and an N_o value equal to the total number of peaks counted using the mean-crossing procedure.

Ratios of the U_{de} values read from the faired test-data curve and the curve of Rice's equation at $N(U_{de}) = 1$ are as follows:

Case	U_{de}^2, Test	U_{de}^2, Rice	U_{de}^2 Ratio	U_{de} Ratio
88-9	25	8	3.13	1.77
102-2	65	34	1.91	1.38
107-8	72	20	3.60	1.90
107-14	36	7.2	5.00	2.24
147-4	69	42	1.64	1.28
164-4	36	23	1.57	1.25

[10] A systematic evaluation of stationarity for all runs is beyond the scope of the present program. In fact, such an evaluation is unnecessary because no attempt was made to obtain a random sampling of turbulence intensities from which a probability distribution could be obtained that would be useful for design.

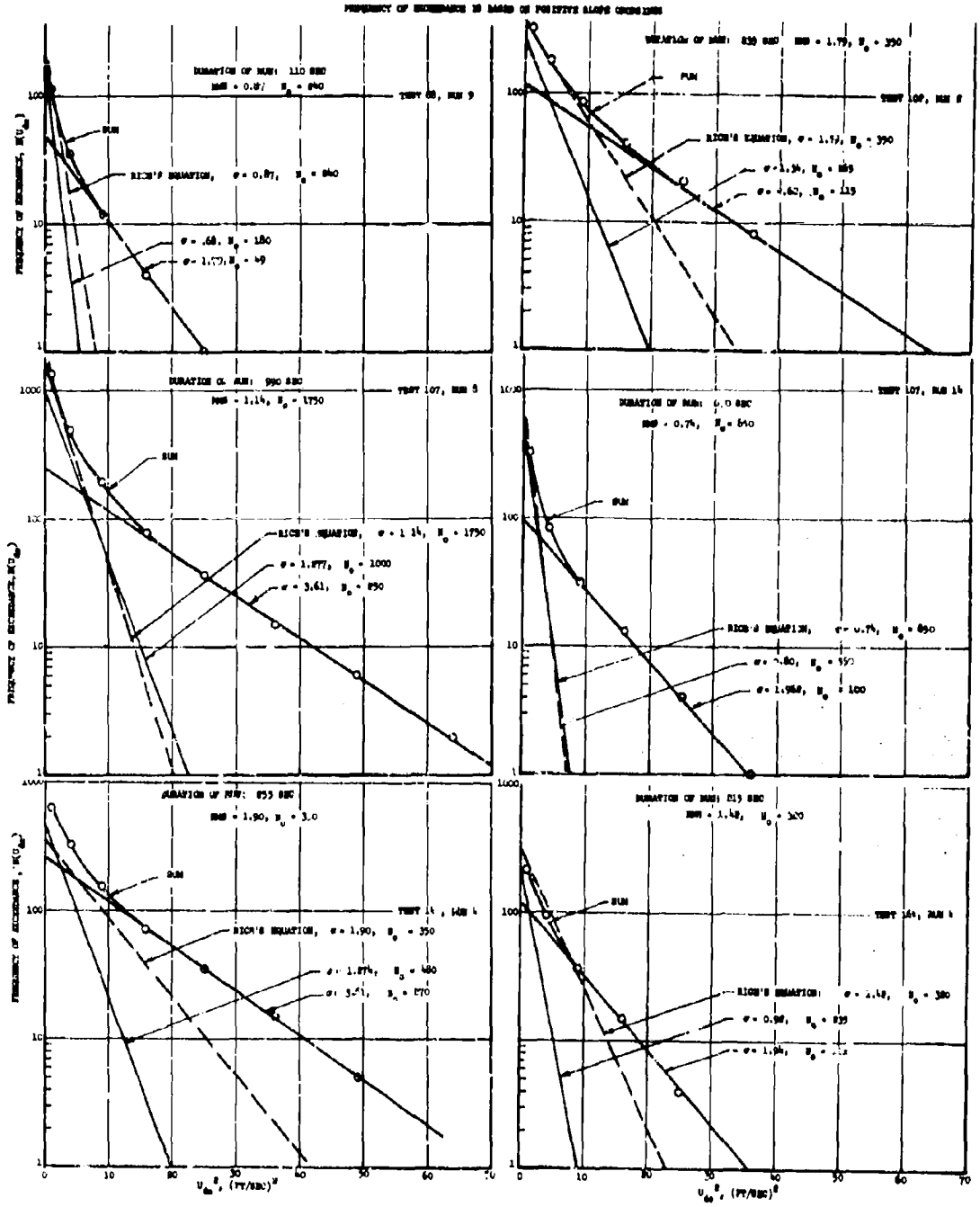

Figure 47. Frequency of Exceedance of U_{de} and Comparison with Rice's Equation

Even for the two cases for which the U_{de} time history had the appearance of rather good stationarity (102-2 and 164-4) the U_{de} ratio is substantially greater than unity, and it is approximately 2 for the two runs that appeared least stationary.

In comparison, application of the same technique to the 27 four-minute runs from the B-66 low level gust study for which U_{de} peak counts were available (Reference 13) gave ratios fairly well scattered over the range 1.05 to 1.57.

The fact that the range for the B-66 data was lower than for the HICAT data is consistent with the impression gained from examination of records of earlier low altitude test flights of Lockheed airplanes, that low altitude turbulence tends to be more nearly stationary than high altitude CAT.

Throughout the above discussion, it has been assumed that disagreement between the measured exceedance curves and the theoretical curves for a stationary Gaussian process as given by Rice's equation is due to lack of stationarity. It could, of course, be due instead to the time history being non-Gaussian. However, this distinction is believed to be of secondary importance. If the constant-rms portions into which the run is considered to be divided are vanishingly short, it might be more valid to regard the time history simply as non-Gaussian. But the assumption that the main consideration is non-stationarity is useful because it explains the shape of the exceedance curves. What is important is that, for whatever reason, the peak-to-rms ratio is not in agreement with Rice's equation, and the degree of disagreement is an important property of the turbulence.

In summary, the significant conclusions with respect to stationarity of the HICAT data are:

- Visual examination of the time histories indicates significant variations in intensity throughout each run in nearly all the HICAT tests. This variation appears to be more pronounced than that for low altitude turbulence.

- Apparently as a result primarily of this non-stationarity, the ratios of peak value to rms value for any given run, of any quantity, reflecting airplane response, are in excess of the ratios predicted by Rice's equation by factors ranging from 1.25 to 2.24.

- Any probability distribution derived from average-over-the-run gust velocity rms values will lead to a gross underprediction of the higher load peaks when applied in airplane design.

PEAK COUNT COMPARISON

Since frequency of exceedance curves are often available only on a simple peak count basis rather than as counts of positive slope crossings, it is of interest to compare the results of the two types of count. Such comparisons

are shown for the same six HICAT runs in Figure 48. The curves given by the two bases inherently coincide at both ends. The number of positive-slope zero crossings is equal to the total number of individual positive peaks (as defined under Peak Counting in Section V), and the one highest peak must define the same point on both curves. In between, the "positive-slope crossing" curve is always higher than the "mean crossing" curve. This relation must hold because wherever the time history reaches a maximum, decreases (but not to zero), and then increases to another maximum, there will be only one peak but two positive slope crossings of constant-y lines within the range of y values between the minimum and the lower of the two maximums.

The closeness of the curves given by the two bases is somewhat variable, but generally the agreement is fairly good. The maximum difference between the two curves on the frequency-of-exceedance scale ranged from a factor of 1.25 for case 164-4 to 2.20 for case 147-4.

ERROR ASSESSMENT

ALIASING ERRORS

The HICAT PCM system samples the analog data at equally spaced time intervals and for this reason may produce amplitude errors due to aliasing.[11] In order to evaluate the aliasing effect in the HICAT data a flight test was performed in which the sampling frequency was set at 50 samples per second, or twice the normal rate. By this means, the frequency content of the data could be examined out to 25 cps, i.e., to a frequency well above the 60-db attenuation point of 16.5 cps of the analog presampling filters.

The power spectral format was selected as the best means of evaluating the presence of aliasing effects. Spectra of the most critical measurements - those required in the determination of the gust velocity components - are presented in Figures 65 through 82 in Appendix II. These spectra cover the frequency band from 0.125 cps to 25.0 cps. They were obtained from a landing approach on Test 56 during which moderate turbulence was encountered. The landing approach was selected in preference to a high altitude run because the run was longer and the level of excitation was relatively high for all measurements.

Aliasing in turbulence data obtained at 25 samples per second (spc) is indicated in the present spectra by the presence of significant power at frequencies between 12.5 and 25 cps. For frequencies in this band, the frequency alias is equal to the sampling rate minus the actual frequency. For example, the

---

[11] Aliasing causes frequency components greater than half the sampling frequency to appear in the data as if they were actually less than half the sampling frequency.

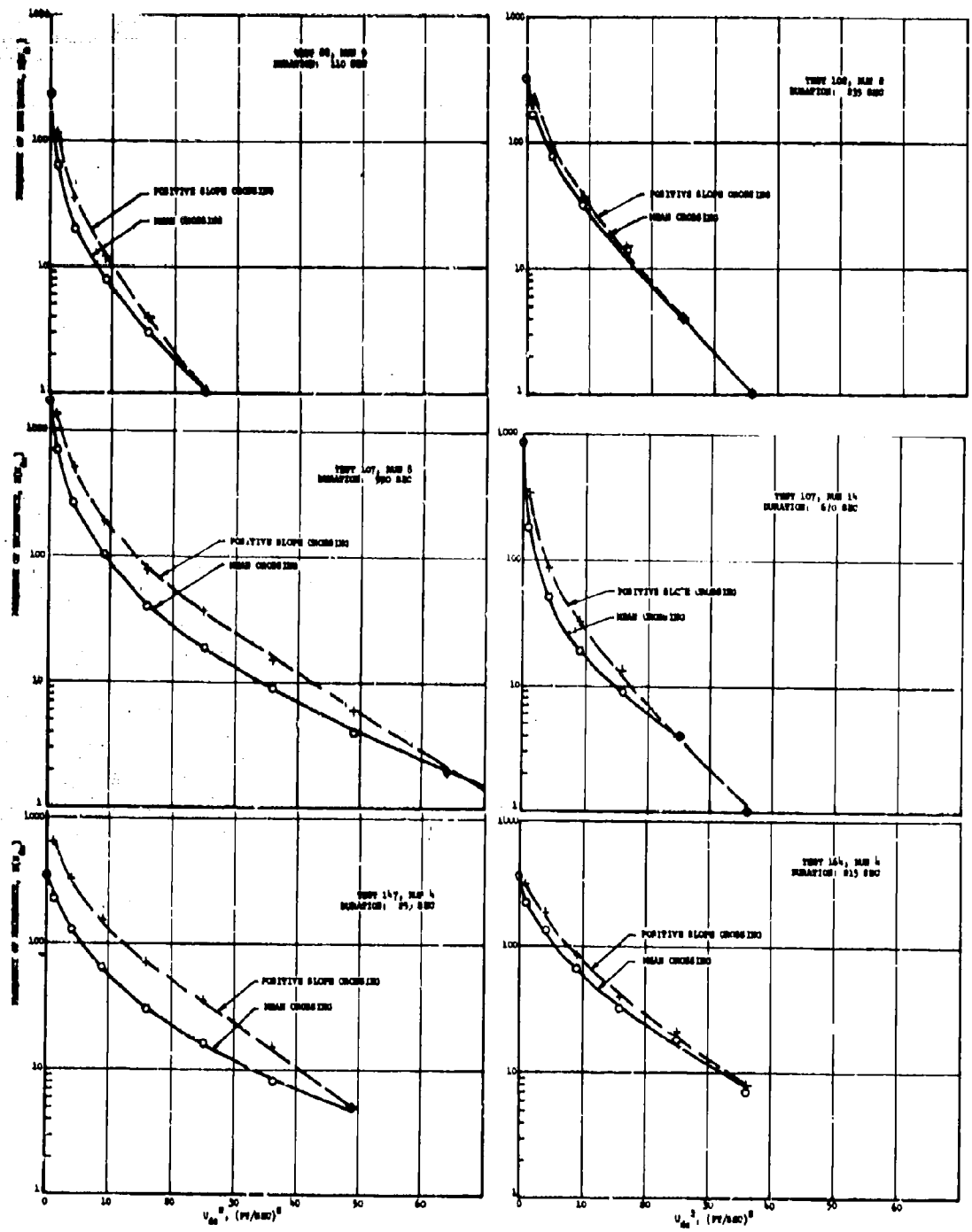

Figure 48. Comparison of Frequency of Exceedance of U_{de} Based on Positive-Slope-Crossing and Mean-Crossing Procedures

frequency alias of 20 cps when sampled at 25 sps is 25 - 20 or 5 cps. The following table lists the aliases for various frequencies:

Frequency alias (cps)	Actual frequency (cps)
0.125	24.875
1	24
2	23
3	22
4	21
5	20
6	19
7	18
8	17
9	16
10	15
11	14
12	13

Thus, the aliasing criterion of "significant power" in the present spectra depends upon the ratio of the power at the actual frequency to that at the frequency alias. If this ratio is very small, i.e., less than 1 percent, then amplitude distortion due to aliasing will be negligible. Applying this criterion to the raw data spectra shows that for most of the measurements no aliasing exists in the frequency range of interest below about 5.0 cps.[12] However, the spectra of yaw rate, pitch, roll, and heading angle (sine and cosine), Figures 76 through 80,[13] indicate aliasing distortions as high as 70 percent of the actual power at 5.0 cps. Surprisingly, this is not significant because the actual power at 5 cps in these particular spectra is itself negligible due to the lack of aircraft response in the measurements at this relatively high frequency.

The X and Y velocity spectra of Figures 81 and 82 also indicate significant aliasing distortions, in this case extending down to frequencies as low as 0.375 cps. For these two measurements, the actual aliased 25 sps spectra are shown and the distortion appears serious. As before, however, it can be observed that there is negligible response at the aliased frequencies. Therefore, it is concluded from examination of the 50 sps spectra that the normal HICAT PCM sampling rate of 25 sps is satisfactory and free of significant amplitude distortion due to aliasing.

---

[12] Frequencies above 6.0 cps are already considerably attenuated by the airborne PCM filters and are normally removed by numerical filtering as part of the HICAT data processing routine.

[13] When power spectral density values were less than the lower limit of the plots, the points were plotted at the lower limit. For the purposes of this discussion, the actual values at 5.0 cps and 20.0 cps have been printed on the figures.

Section VI

GUST VELOCITY ERRORS IN ROLLER COASTER MANEUVERS

Several times during the course of the HICAT program, smooth symmetric pitch maneuvers or roller coasters were performed in calm air to verify the performance of this instrumentation and check the gust velocity equations. It was expected that if the air were perfectly calm and the appropriate instruments were accurately calibrated and working properly, the result of the gust velocity determination would be zero or near zero, i.e., in agreement with the test conditions. In actual practice, it was found that a small but significant vertical gust velocity "error" does occur.

Figures 49 through 52 present gust velocity time histories of four separate roller coaster maneuvers taken from four different tests. Figure 49 shows a roller coaster maneuver of 205 seconds' duration with cg normal accelerations averaging about ±0.45g in amplitude and with a period of about 13 seconds. The vertical gust velocity component has a 13-second oscillation of roughly ±5 fps amplitude obviously resulting from the pilot's elevator motion.

On the other hand, the 13-second oscillation is fairly small or absent in the lateral and longitudinal gust velocity time histories. The nonzero lateral and longitudinal components appear to result from secondary effects (i.e., changes of heading, speed, altitude, etc.) rather than directly from the pitch control input.

Figure 50 shows a relatively brief, large-amplitude roller coaster from test 114, run 19. In this case, the accelerations average about ±0.85g amplitude with a 15-second period. Again, the vertical gust velocity oscillations have the same period as the control motion with an amplitude of about ±7 fps.

Figures 51 and 52 are fairly similar time histories of the roller coasters from test 142, run 5 and test 172, run 3. For these two cases, the normal accelerations are only about ±0.35g and the oscillatory period is fairly short, i.e., only 7 seconds.[14] Notice that in these two cases, the resulting vertical gust velocity "error" is much smaller, or about ±1 to ±2 fps. Unfortunately, a malfunction prevented the determination of reliable lateral and longitudinal gust velocity components for these two tests.

[14] Pilots favored this input period because airspeed was more easily controlled.

The following table summarizes the results of the roller coaster tests:

	HICAT Test Number			
Parameter	110	114	142	172
Average Osc Period (sec)	13	15	7	7
Average Δa_N (±g)	0.45	0.85	0.37	0.35
Average ΔU_V (±fps)	5.0	7.0	1.2	2.0
Average δ_E (±deg)	1.2	2.3	1.1	1.4
Average U_V/δ_E (fps/deg)	4.2	3.0	1.1	1.4

The last line of the table indicates the vertical gust velocity error per degree change of elevator angle.

It appears from the table that the gust velocity error is a function of the period of the elevator motion (and thus inversely proportional to control rate) because the smallest errors are associated with the shorter control input periods. Thus, for elevator motions of amplitude of 1 degree or less associated with oscillatory periods of 7 seconds or less, the gust velocity error appears to be small enough to ignore. However, elevator motions of similar size associated with longer periods of oscillation appear capable of causing significant errors in the vertical gust velocity measurements. Fortunately, as a result of the measurement philosophy followed during the program (see HICAT Flight Procedures in Section III), the elevator motions in turbulence are minimal. Examination of the elevator time histories of those tests used for "medium to long wave analysis" (i.e. $\lambda \geq 10{,}000$ ft.) indicates very few elevator angle excursions of a size and frequency as to cause a substantial gust velocity error.

However, if such an error is assumed to be present, it should increase the power of the vertical gust spectra at wavelengths of 10,000 feet and above. The vertical gust spectra in Figures 38 and 39 display little if any evidence of such effect. Therefore, it would appear that elevator motions are not a significant source of error in the HICAT data.

GUST VELOCITY RESOLUTION

The gust velocity resolution of the HICAT measurement system may be established from examination of the basic gust velocity equations and consideration of the resolution of the various individual measurements. The gust velocity equations are reproduced below in somewhat simplified form, ignoring second order terms.

$$\Delta U_V = V_T \Delta\alpha - V_T \Delta\theta + \int \Delta a_Z \, dt \qquad (1)$$

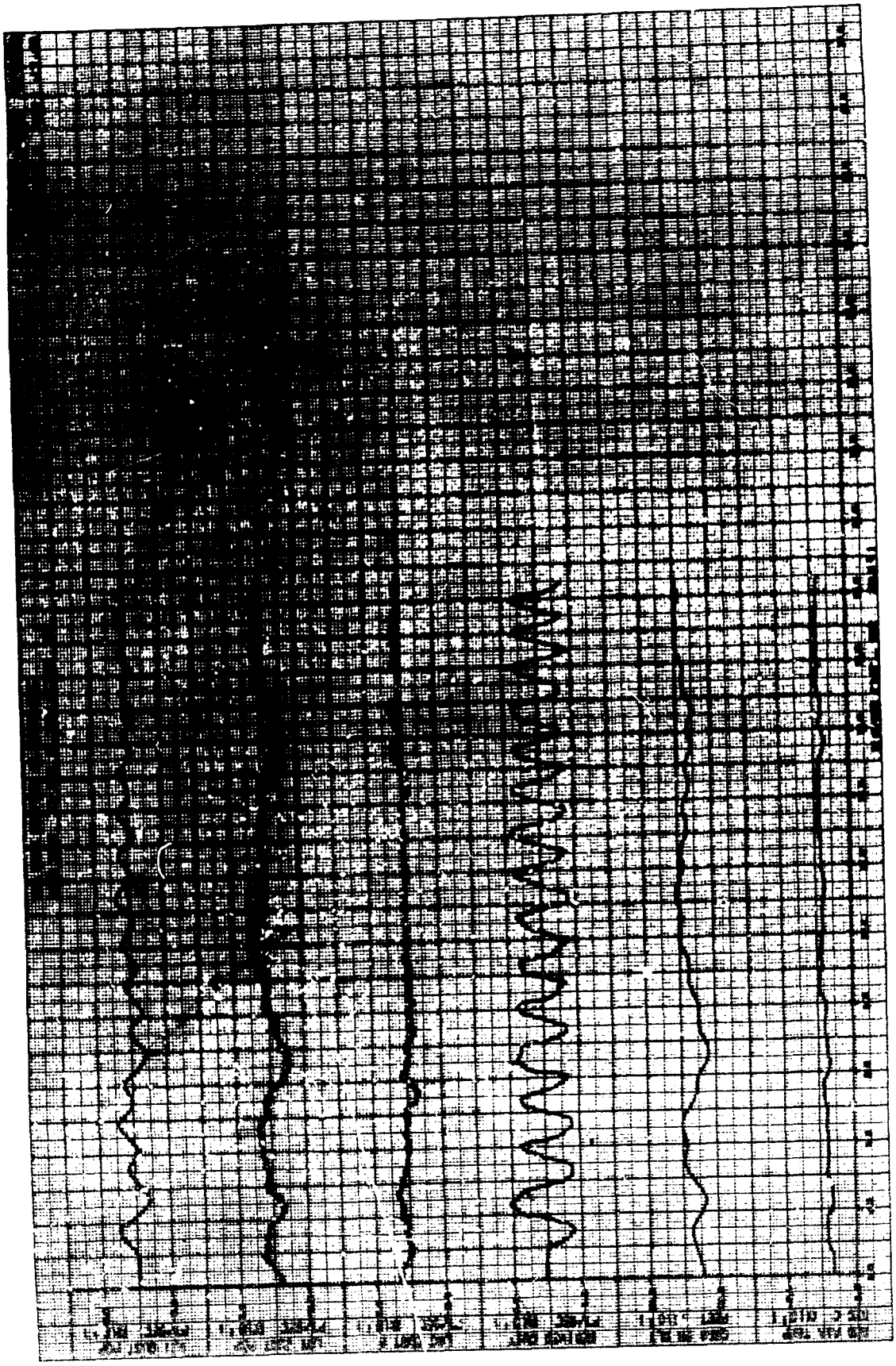

Figure 49A. Roller Coaster Maneuver Gust Velocity Time History - Test 11[illegible], Run 3

Figure 49B. Roller Coaster Maneuver Gust Velocity Time History - Test 110, Run 3

Section VI

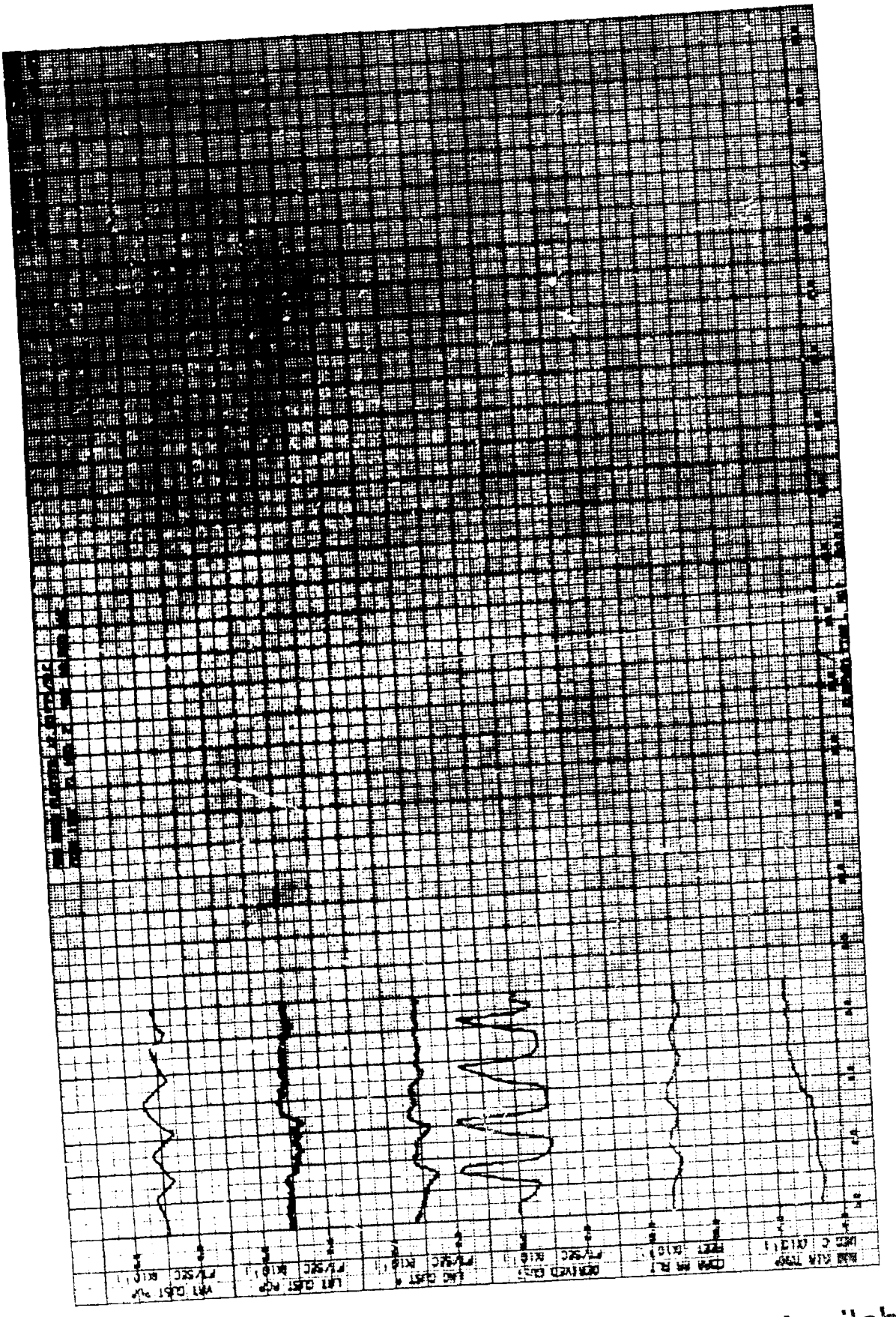

Roller Coaster Maneuver Gust Velocity Time
History - Run 10

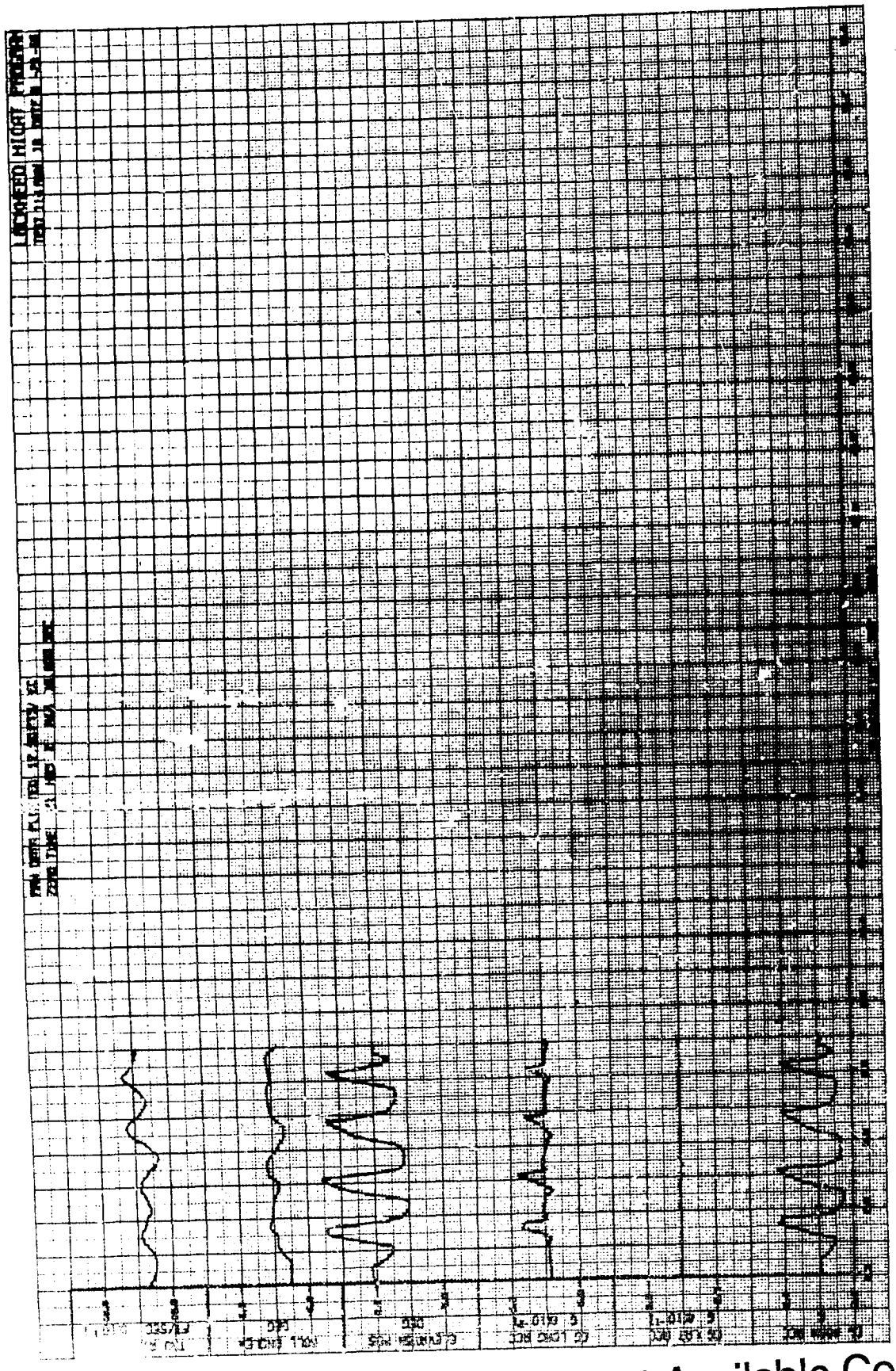

Figure 50B. Roller Coaster Maneuver Gust Velocity Time History - Test 114, Run 19

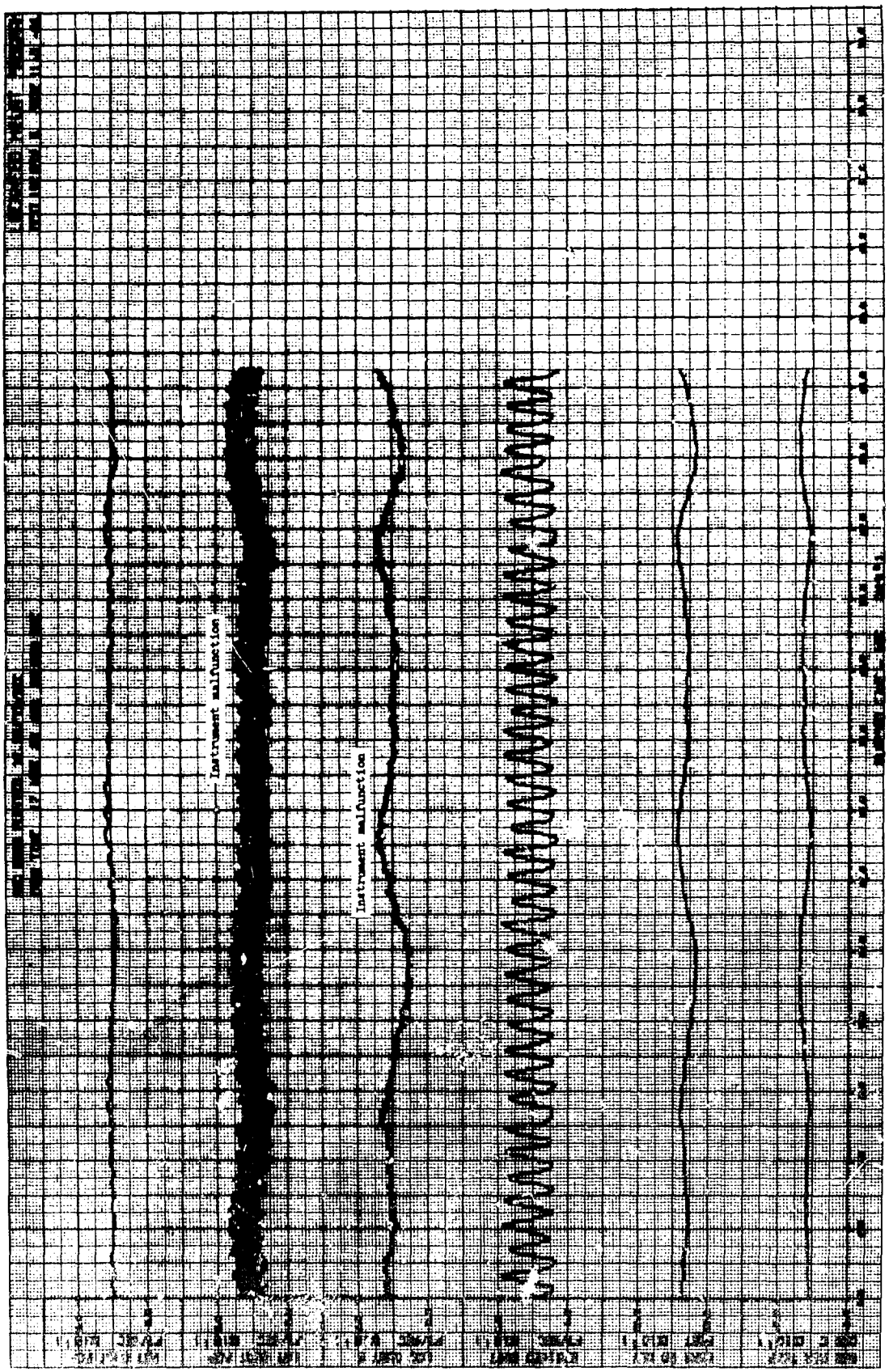

Figure 51A. Roller Coaster Maneuver Gust Velocity Time History - Test 142, Run 5

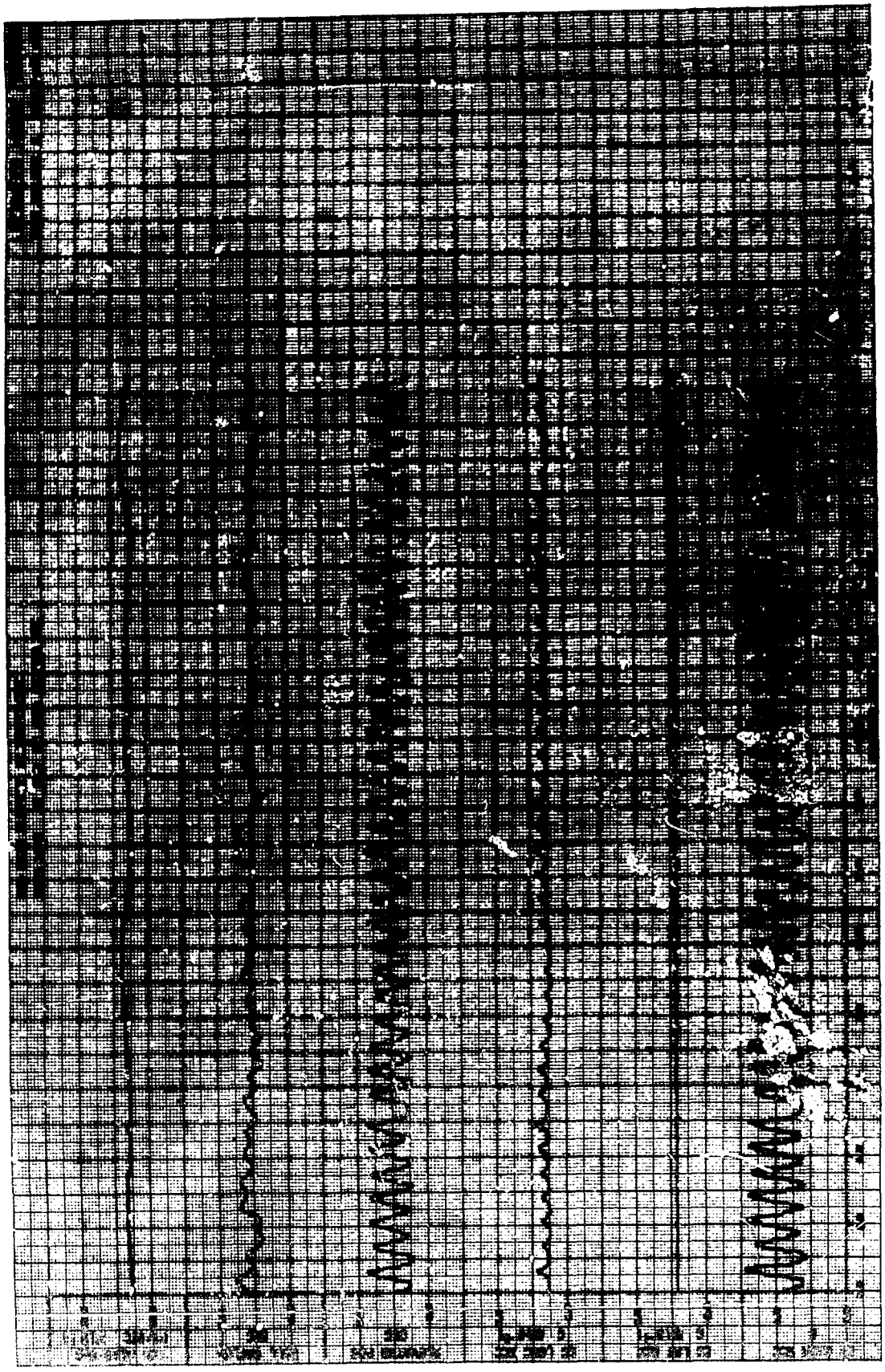

Figure 51B. Roller Coaster Maneuver Gust Velocity Time History - Test 142, Run 5

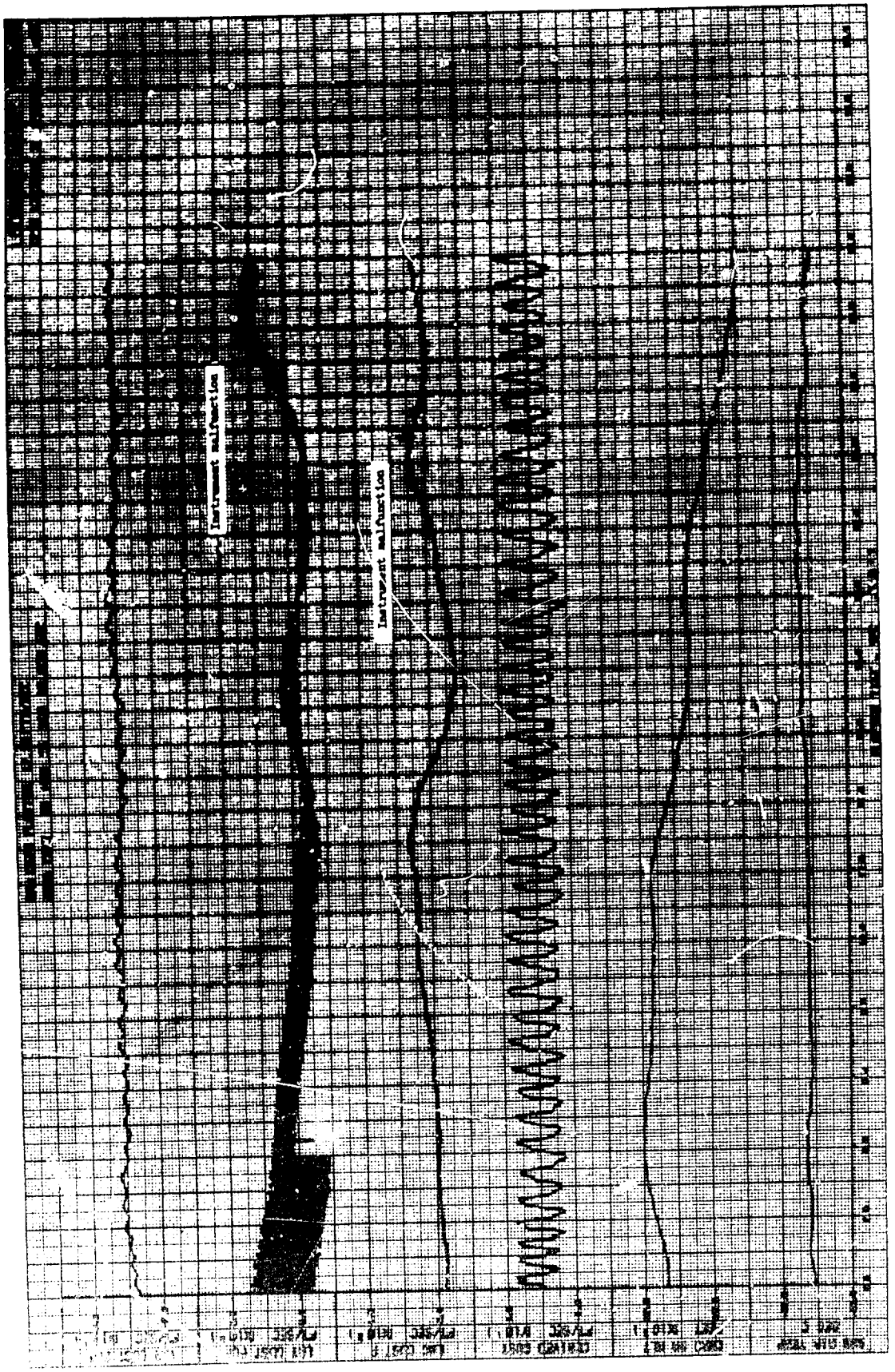

Figure 52A. Roller Coaster Maneuver Gust Velocity Time History - Test 172, Run 3

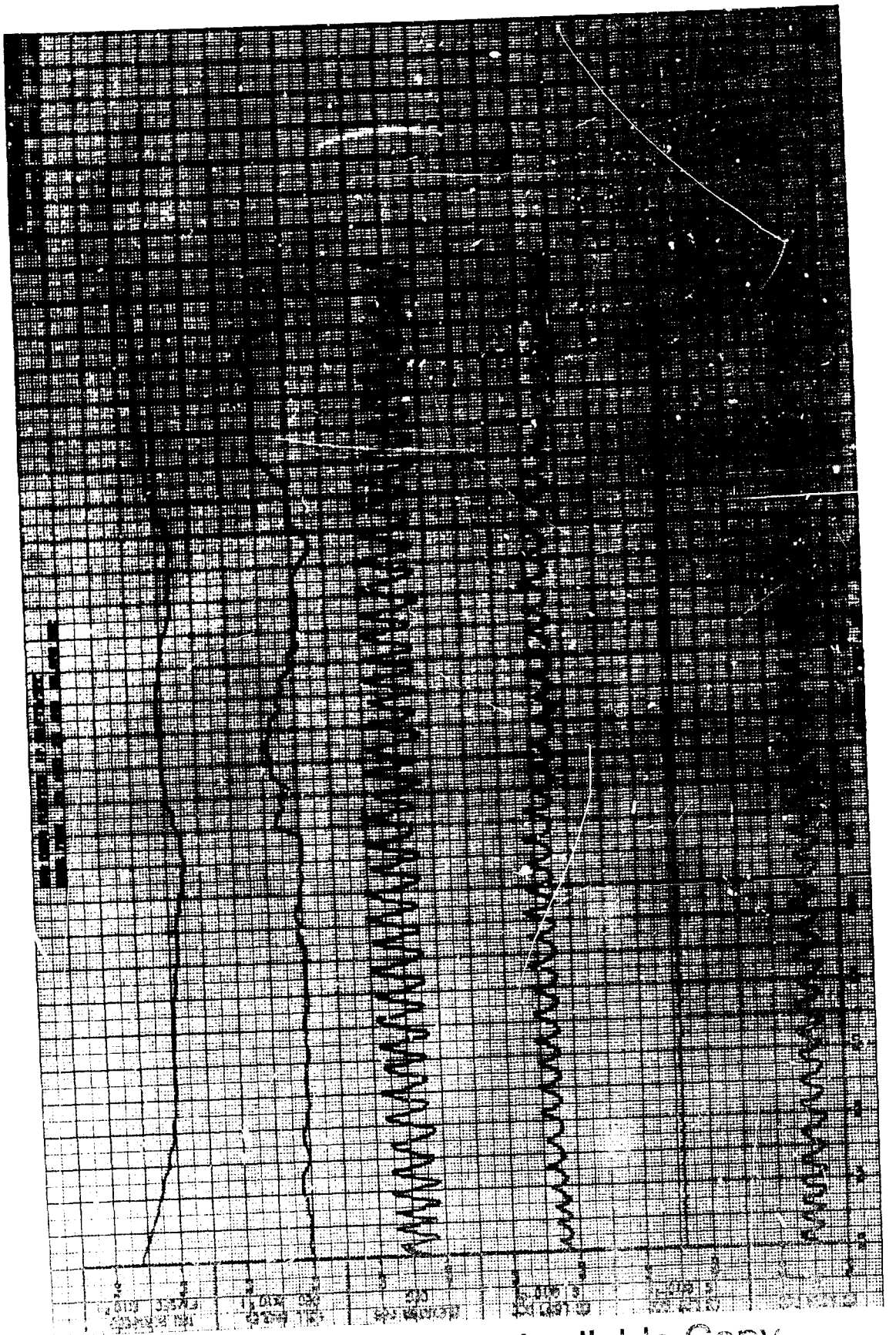

Figure 52B. Roller Coaster Maneuver Gust Velocity Time History - Test 172, Run 3

$$\Delta U_L = V_T \Delta\beta + V_T \Delta\psi - \Delta U_{PG_Y} \tag{2}$$

$$\Delta U_F = \Delta V_T - \Delta U_{PG_X} \tag{3}$$

If the instrumentation system is assumed to be perfectly accurate except for its resolving capability, then the only errors which can occur will be those attributable to this less than perfect resolution. Table VI in Appendix II lists the various measurements and their resolution in the PCM system.

By applying the following relationships from Reference 14, the resolution error may be evaluated for each gust velocity component.

$$y = F(x_1, x_2 \ldots . x_n)$$

$$\sigma_y^2 = \sum_{i=1}^{n} \left(\frac{\partial F}{\partial x_i}\right)^2 \sigma_i^2 \tag{4}$$

where σ_y^2 = variance of y

x_i = ith-numbered x term contributing an error

σ_i^2 = variance of the ith term.

To compute the vertical gust velocity resolution, an average value of V_T is assumed (V_T = 700 fps) and σ_i is considered to be ±1/2 the resolution of the appropriate measurements listed in Table VI in Appendix II. Expanding equation 4 for vertical gusts, let $\epsilon_i^2 = \left(\frac{\partial F}{\partial x_i}\right)^2 \sigma_i^2$.

where, $$\sigma_V^2 = \epsilon_{V1}^2 + \epsilon_{V2}^2 + \epsilon_{V3}^2$$

where ϵ_{V1} refers to the resolution error in the first term of the vertical gust velocity, ϵ_{V2} the second, etc.

then, $\epsilon_{V1}^2 = \left[700(\pm.01)/57.3\right]^2 = (\pm.122)^2 = 0.015$

$\epsilon_{V2}^2 = \left[700(\pm.015)57.3\right]^2 = (\pm.183)^2 = 0.033$

In order to evaluate the acceleration integral, it is assumed that the resulting velocity Δv_Z is the maximum value of an integrated sinusoidal acceleration response to a very long wavelength gust, in which case

$$\Delta v_Z = \Delta a_Z/\omega = \Delta a_Z \lambda/(2\pi V_T)$$

and if λ = 60,000 feet

$$\epsilon_{V3}^2 = \left[\frac{(\pm.0015)\ 32.2\ (60{,}000)}{2\pi(700)}\right]^2 = (\pm.660)^2 = 0.435$$

so that for the vertical gust velocity

$$\sigma_V = \sqrt{\epsilon_{V1}^2 + \epsilon_{V2}^2 + \epsilon_{V3}^2}$$

$$\sigma_V = \sqrt{0.015 + 0.033 + 0.435}$$

$$\sigma_V = \pm .70 \text{ ft/sec}$$

Note that if λ is assumed to be only 30,000 feet ϵ_{V3}^2 = .109 and

$$\sigma_V = \pm 0.40 \text{ ft/sec.}$$

In the case of the lateral gust velocity

$$\epsilon_{L1}^2 = \left[700(\pm.01)/57.3\right]^2 = (\pm.122)^2 = .015$$

$$\epsilon_{L2}^2 = \left[700(\pm.07)/57.3\right]^2 = (\pm.854)^2 = .730$$

and $\epsilon_{L3}^2 = 1.0$

so that for the lateral gust velocity

$$\sigma_L = \sqrt{0.015 + 0.730 + 0.435}$$

$$\sigma_L = \pm 1.32 \text{ ft/sec}$$

For the longitudinal gust velocity case it is necessary to consider the true airspeed fluctuations, ΔV_T, in terms of the differential pressure (approximated herein by the dynamic pressure, q) in order to determine ϵ_{F1}.

Thus $$q = \frac{V_T^2(\rho/\rho o)}{841}$$

and $$dq = \frac{2V_T(\rho/\rho o)\ dV_T}{841}$$

so that $$dV_T = \frac{841\ dq}{2V_T(\rho/\rho o)}$$

assuming an average altitude of 57,000 ft ($\rho/\rho o = .109$) so that

$$\epsilon_{F1}^2 = \left[\frac{841(\pm.001).144}{2(700)(.109)}\right]^2 = (\pm.795)^2 = .632$$

$$\epsilon_{F2}^2 = 1.0$$

which gives for the longitudinal gust velocity

$$\sigma_F = \sqrt{0.632 + 1.0} = \pm 1.28 \text{ ft/sec}$$

Summarizing, the approximate resolution of the gust components is as follows:

Vertical Gust Velocity:	$\pm$0.70 fps for λ = 60,000 ft $\pm$0.40 fps for λ = 30,000 ft
Lateral Gust Velocity:	$\pm$1.32 fps
Longitudinal Gust:	$\pm$1.28 fps

GUST VELOCITY MEASUREMENT ACCURACY

The measurement accuracy of each HICAT transducer appears in the final column of Table I, Appendix II. These are percentage rms values of the transducer measurements before they are filtered and digitized in the PCM system. The table indicates all the measurements which are used in the gust velocity equations to have basic accuracies of ±1.5 percent rms or better. Calibration inaccuracies will contribute another 0.5 to 1.0 percent to this figure.

The analog filters attenuate the measurement signals slightly, depending upon the frequency. This effect varies from filter to filter, but can be as much as two or three percent at 5 cps. At frequencies less than 1 cps, the average attenuation amounts to less than 0.5 percent of the input amplitude.

The PCM digitizing process introduces another very small error. This error is ±.05 percent ±1/2 of the least significant bit, which is equivalent to an accuracy capability of 0.1 percent.

It is therefore estimated that on the basis of the above considerations, the overall accuracy of the gust velocity determination is approximately ±3.2 percent rms at frequencies less than 1 cps. For higher frequencies, the amplitude error will be slightly greater because of the analog filters.

RECAPITULATION

The foregoing analysis of the results of the HICAT program shows that high altitude CAT generally occurs in relatively short, fairly thin patches which decrease in intensity with increasing altitude. The gust velocity power spectra when averaged appear to be roughly similar to lower-altitude spectra except that the vertical gust velocity components have significantly less slope and all components indicate a scale of turbulence, L, in excess of 6,000 ft. High altitude CAT appears to be isotropic only at the shortest wavelengths as well as statistically nonstationary overall. Although a few CAT spectra extend to 40,000 ft. wavelength, a dearth of very long wave CAT samples appears to limit the useful range of the spectra to between 10,000 and 20,000 ft. Measurement errors due to aliasing, instrumentation inaccuracies, and elevator control effects are shown to be insignificant.

SECTION VII

METEOROLOGICAL ASPECTS

GENERAL

One of the objectives of the HICAT program was to investigate the occurrence of clear air turbulence at high altitude in a variety of meteorological and geophysical conditions. The sampling sites selected for this purpose are listed and the reasons for their selection are explained. The CAT forecasting procedures used at each site are reviewed as well as the difficulties of forecast verification. In the section on analysis and interpretation, the effects of geographical location and terrain on intensity of turbulence are discussed and summarized in tables and graphs. A brief discussion of the probable influence of convection and the relationship between cloud forms and turbulence is included. Based on a preliminary analysis of all available meteorological and turbulence data and pilot reports, a possible mechanism for triggering CAT is suggested. A more detailed analysis of the meteorological data with particular emphasis upon the relationship between turbulence and specific meteorological parameters and derived indices is presently being conducted by Lockheed for the Flight Dynamics Laboratory. This analysis will be the subject of another report under a separate Air Force contract (Reference 3).

SAMPLING SITE SELECTION

Sampling sites were selected initially to provide combinations of latitude and season considered most favorable for the occurrence of high altitude turbulence. Consideration was also given to the investigation of the effects of wind flow and heating over four terrain categories, water, flat land, hills, and mountains. Final selection was based upon the requirements for a sequential schedule and for airfields compatible with U-2 flight operations. A brief description of each test site, of the potential high altitude CAT source, and the ideal season for operations is outlined below.

- Edwards AFB, California

  General area: Southwestern U.S.

  Terrain: Predominantly mountainous

  CAT source: Mid-latitude tropospheric jet combined with the effects of mountain waves and convections.

  Season: Fall, winter and early spring.

- Hickam AFB, Oahu Island, Hawaii

  General area: Hawaiian Islands

  Terrain: Predominantly water with isolated mountain peaks.

  CAT source: Southern edge of mid-latitude tropospheric jet combined with convective and frontal activity over relatively smooth water surface and isolated mountain peaks.

  Season: Spring

- Christchurch, New Zealand

  General area: New Zealand and surrounding ocean.

  Terrain: Mountain chain oriented perpendicular to prevailing wind.

  CAT source: Mid-latitude tropospheric jet crossing an abrupt mountain chain surrounded by a relatively smooth ocean surface.

  Season: Winter

- Laverton, Australia

  General area: Southeastern Australia

  Terrain: Mountain range with an extensive area of relatively flat land to the west and ocean to the east.

  CAT source: Mid-latitude tropospheric jet combined with effects of convection over the flat land and waves generated over the mountain range.

  Season: Winter

- Hanscom Field, Massachusetts

  General area: Eastern U.S., including adjoining portions of Canada and coastal waters.

  Terrain: Mostly hilly but including the Appalachian mountain range and relatively flat coastal plain.

  CAT source: A variety of regimes ranging from pure convection and frontal activity to strong jet streams over the four types of terrain, water, flat land, hilly land, and mountain range.

  Season: Late summer and early fall.

- Ramey AFB, Puerto Rico

  General area: Puerto Rico, Virgin Islands and windward island chain.

  Terrain: Predominantly water and small islands.

  CAT source: Convection, easterly waves, zones of converging winds aloft, troughs aloft, and frontal systems with or without jet streams over water and heated island surfaces.

  Season: Fall

- Elmendorf AFB, Alaska

  General area: All of Alaska including the eastern Aleutian chain and adjoining Gulf of Alaska coastal waters.

  Terrain: Mountain ranges with some hilly and level areas.

  CAT source: Very low tropospheric jet in absence of convection over the various types of terrain as well as the lower portion of the stratospheric circumpolar jet.

  Season: Winter

FORECASTING PROCEDURES

For economic reasons, the HICAT forecasting program had to rely upon the local forecasting personnel at each test site. As a consequence, there was considerable variation in the forecasting techniques at the various sites. In most cases, these local personnel had had little or no experience in forecasting high altitude CAT at levels above 40,000 feet. To compound the problem, at some sites there was little if any data routinely received via teletype or facsimile for altitudes above 40,000 feet. To help alleviate this situation, arrangements were made with the Air Force Global Weather Central, Offutt AFB, to supply CAT forecasts at Hanscom Field, and at Ramey and Elmendorf Air Force Bases.

The Global Weather Central (GWC) forecasts were based on the hypothesis that the gradient of shear is more critical than the shear itself. A parameter was developed which considered the combination of the Laplacian of the horizontal wind shear and the vertical gradient of the thermal wind shear. It was recognized that the vertical change in thermal wind shear is proportional to the horizontal gradient of static stability in the same way that the thermal wind shear is proportional to the horizontal gradient of temperature. The input data for the CAT computer forecasting program were the forecast height fields for six standard pressure levels including the 100 and 50 mb levels. The Laplacian term was computed from each of the height distributions on constant pressure surfaces and the thermal wind was computed from three pairs of temperature distributions. It was found that the Laplacian term was

normally about one order of magnitude larger than the other term. It was arbitrarily decided to increase the value of the thermal wind shear term by an order of magnitude and subtract it from the first term to give the final CAT parameter. The parameter used during the HICAT program was based on the following formula:

$$C = \nabla^2\left(\frac{\partial V}{\partial N}\right) - 10\left|\frac{\partial}{\partial z}\left(\frac{\partial V_g}{\partial z}\right)\right|$$

with turbulence intensities shown in the Table below.

Table of Turbulence Intensities

Value of C	Forecast turbulence intensity: Over Land	Forecast turbulence intensity: Over Water
-25	No turbulence	No turbulence
-25 to -35	Light	No turbulence
-35 to -55	Light-moderate	Light
-55 to -75	Moderate	Light-moderate
-75	Severe	Moderate

Shortcomings of the GWC method were the lack of vertical resolution in the forecasts due to the rather thick layers considered, the lack of consideration of mountain wave activity, and the dependence of turbulence forecasts upon the results of numerical predictions of pressure and temperature fields 24 to 36 hours ahead irrespective of prior CAT occurrence.

Local forecasters at Hanscom Field and at Ramey and Elmendorf Air Force Base found it necessary to supplement these forecasts with their own either because the GWC forecast defined too large an area or an area beyond the range of the aircraft.

In New Zealand, the turbulence forecasts were prepared by the Wellington office of the New Zealand Meteorological Service and transmitted to Christchurch where pilot briefings were provided by the regular meteorological personnel. In Australia, personnel of the Bureau of Meteorology, who were assigned specifically to the project, prepared the forecasts and conducted the pilot briefings and debriefings. This group was headed by Mr. F.A. Powell with scientific support from Mr. J.N. McRae and Mr. Kevin Spillane.

A brief review of the primary meteorological parameters considered in the forecasts made at each site is given below.

California

As these tests were conducted intermittently throughout the period November 1965 to January 1967, no single forecast method was used consistently. Various parameters considered were strong winds over the Sierra Nevada (Sierra Wave) and other mountain ranges, large vertical wind speed and wind direction shear, and an irregular-shape temperature sounding depicting alternating layers of sharply changing vertical temperature gradient, i.e., several significant levels in the temperature sounding.

Hawaii

Turbulence forecasts were based primarily upon position of the jet stream and especially when associated with 200 mb troughs and wind shift zones. Altitudes of turbulence were specified by the altitude interval through which wind speeds decreased markedly and wind direction shifted to easterly.

New Zealand

Turbulence forecasts were primarily based on the possibility of lee waves whenever a jet stream crossed the mountains. In addition, turbulence was forecast in the area of troughs aloft and over intensifying cyclonic depressions at the surface. Some consideration was also given to areas of temperature change or advection.

Australia

Turbulence parameters which were computed on a routine basis included Richardson number, Scorer parameters, and the index of the product of wind speed and wind direction shear. However, the Richardson number was found to be the most useful single derived index from a qualitative point of view, so that the turbulence forecasts were based primarily upon this parameter. Values of Richardson number were calculated for each layer having a significant change in lapse rate or wind shear. Charts were drawn delineating areas of low Richardson number for each layer. These charts were then used to highlight possible search areas. The radiosonde traces from stations near these areas were examined in detail in order to select the optimum height to search for turbulence. The heights selected were those which were situated in a comparatively stable layer overlying a layer for which the calculated Richardson number was low - generally less than 3. This procedure was based on the assumption that eddies generated in layers of low Richardson number would break down in the base of the upper stable layer into disturbances of a scale small enough to disturb the aircraft. The lowest Richardson numbers were usually found to be located on the north (equatorial) side of the 200 mb jet. In addition, lee waves and turbulence were forecast whenever a jet stream passed over the Great Dividing Range in eastern Australia.

Massachusetts

The forecasts were based primarily upon the Global Weather Central forecast. In addition, the local forecasters predicted CAT in areas of strong winds

(jet streams) and large horizontal shear as determined from the maximum wind speed charts. Turbulence was predicted at altitudes coinciding with inversion layers.

Puerto Rico

In addition to the Global Weather Central forecasts, the local forecasters considered strong winds aloft, horizontal convergence and frontal zones, troughs aloft, and cooling aloft which results in "overturning the air".

Alaska

In addition to the Global Weather Central turbulence forecasts, the local project personnel considered areas of apparent temperature advection, i.e., areas and altitudes where the isotherms crossed the height contours and hence crossed the flow, as suggested in Reference 15. The effects of the stratospheric circumpolar jet were not considered because it was found to be located at approximately 100,000 feet, well above available flight altitudes.

EVALUATION OF METHODS

The problem of forecast verification was complicated by lack of precise definition of the volume of air in which turbulence was anticipated and in particular the horizontal extent. The forecasts tended to be either too general by including an area of thousands of square miles or too specific by defining the coordinates of a point or a particular site where the upper air observations were made. In the former case, the question arose as to whether turbulence was expected to occur throughout the entire area or whether perhaps just a patch somewhere within the area. In the latter case, it is not known whether the designated point was supposed to define the center of a turbulence area and if so, the horizontal extent of the anticipated area was not given. Also, due to operating limitations, the aircraft was not always able to fly to the forecast area.

In any event, the number of turbulence forecasts utilizing a particular method are in most instances too small to make any valid and statistically significant comparisons as to the relative accuracy of the various forecasting techniques.

It should be noted that the rawinsonde and radiosonde data upon which the forecasts were based were usually 12 to 18 hours old, and in the case of Global Weather Central forecasts, 24 to 36 hours old by the time a test was well underway. Hence the various parameters had to be forecast well in advance and not just evaluated from recent observations. For some of the parameters, such as fronts, troughs aloft, and perhaps wind speeds, this was not difficult; for others, such as vertical wind speed and direction shear, isothermal advection patterns and Richardson number, the problem was much more difficult. Forecasting mountain waves is complicated by the fact that they do not always cause turbulence at flight altitudes. In several instances, photographs were obtained of wave cloud formations over mountains below but no turbulence was encountered at flight altitudes even though the winds at flight altitudes were flowing perpendicular to the mountain range.

METEOROLOGICAL DATA

All available radiosonde and rawinsonde data along the flight track for each test are given in Appendix X. In some cases, and especially for the tests in Puerto Rico and Alaska, the data were obtained from copies of the original teletype reports; hence a few reports are incomplete and some may contain coding errors and omissions.

In order to reduce the data to manageable proportions, only temperature and wind data at flight altitudes are given. These include all pressure levels, both standard and significant,(15) between 150 and 50 mb, corresponding to approximately 45,000 and 70,000 feet. In addition, the height of maximum wind is given along with the direction and speed based on the complete rawinsonde data at all available altitudes. In Alaska these altitudes included the stratospheric circumpolar jet centered around 100,000 feet.

ANALYSIS AND INTERPRETATION

Effect of Terrain on Intensity, Duration and Continuity of Turbulence

In order to analyze the effect of the terrain below on the intensity, duration and continuity of turbulence, a table was constructed using the turbulence data from the oscillograph records supplemented by information from the pilots' notes and debrief summaries. Four classifications of terrain were considered, mountains, hills, relatively flat land, and water surfaces. For each test, the intensity of turbulence was categorized according to whether it was very light, light, light to moderate, moderate, or severe. In addition, three categories describing the duration and continuity of turbulence were considered. Turbulence which persisted only for 10 seconds to five minutes was categorized as a patch, and if longer than five minutes, it was classified as either intermittent or continuous. These data are summarized for each test area in Table V.

In this type of turbulence classification, it should be recognized that there is but slight difference between a succession of patches and intermittent turbulence. The distinction was based upon whether the oscillograph record indicated a few minutes of smooth air between turbulence areas, or upon the pilot's description when no oscillograph record was available. The five-minute limitation for a patch of turbulence was partially based upon the pilot's debrief statements, which tended to refer to turbulent areas of lesser duration as a patch. In addition, it seems reasonable to presume that turbulent areas extending more than 30 miles may be more closely related to the large-scale meteorological situation than to the local terrain below. In each test the most intense turbulence and its duration category are listed for each terrain classification. When a less intense turbulence category was of longer duration or more continuous, this category was also entered.

---

[15] A level at which the temperature data indicate a change in gradient or lapse rate where temperatures are read to the nearest 0.1 degree.

TABLE V. TURBULENCE CLASSIFICATION ACCORDING TO TERRAIN

EDWARDS AFB, CALIF.

Test No.	Mountains*	Hills*	Flat*	Water*	Test No.	Mountains*	Hills*	Flat*	Water*
39	VL/P	-	VL/P	VL/P	54	M/P	-	L-M/P	-
40	L/I	-	L/P	L/P	55	L-M/P VL/C	-	0	-
41	VL/P	-	0	-	56	L/P	-	0	-
44	L/P	-	L/P	0	113	0	-	0	-
46	M/P	-	-	-	114	M/C	-	-	-
50	L/P	-	L/P	-	115	VL-M/C	-	0	-
51	L/P	-	0	-	116	VL/P	-	0	0
52	0	-	0	-	159	0	-	0	0
53	L/C M/P	-	0	-	160	M/C	-	L-M/C	-

HAWAII

Test No.	Mountains*	Hills*	Flat*	Water*	Test No.	Mountains*	Hills*	Flat*	Water*
58	0	0	-	0	69	0	L/P	-	L/P
59	0	VL/P	-	VL/P	70	0	L-M/P	-	L/C
60	0	L/C	-	M/P L/C	71	L/I	0	-	L/I
61	0	0	-	VL/C L/I	72	0	0	-	0
62	0	0	-	L/P	73	0	0	-	L/C
63	L-M/P L/C	L/C	-	L-M/P L/C	74	VL/C	VL/C	-	VL/C
64	0	0	-	0	75	0	0	-	M/C
65	L/I	L/I	-	L/I	76	M/P	M/P	-	M/C
66	L/P	L/P	-	L/P	77	L-M/C	L-M/C	-	L-M/C
67	L/P	L/P	-	M/P	78	L-M/C	L-M/C	-	M/C
68	0	0	-	M/P L/I	79	M/P	0	-	M/P
					83	0	0	-	L/P

TABLE V. TURBULENCE CLASSIFICATION ACCORDING TO TERRAIN (Continued)

CHRISTCHURCH, NEW ZEALAND

Test No.	Mountains*	Hills*	Flat*	Water*	Test No.	Mountains*	Hills*	Flat*	Water*
86	0	0	-	L-M/P	92	0	0	-	VL/P
87	0	0	-	M/C	93	M/C	M/P	-	M/P
88	M/P L/C	M/P L/C	-	L/C	94	VL/P	0	-	C
89	L/P	M/P	-	L/P	95	0	0	-	M/C
90	M/C	L/P	-	L/P	96	L-M/I VL/C	0	-	M/P L/C
91	inc	inc	-	inc	97	0	0	-	0

LAVERTON, AUSTRALIA

Test No.	Mountains*	Hills*	Flat*	Water*	Test No.	Mountains*	Hills*	Flat*	Water*
99	0	0	M/P	-	105	L/P	L/P	L/P	-
100	0	0	M/C	-	106	L/P	M/P	0	-
101	L-M/I	0	L-M/C	-	107	0	L-M/C	M/C	-
102	M/P L-M/C	M/P	L-M/P	M/C	108	L/P	L/P	L/C	VL/P
103	M/C	L-M/I	L-M/I	L-M/I	109	M/P L-M/I	0	L/P	0
104	L-M/C	0	0	L/P					

HANSCOM AFB, MASS.

Test No.	Mountains*	Hills*	Flat*	Water*	Test No.	Mountains*	Hills*	Flat*	Water*
121	0	L-M/P L/C	M/P L-M/I	L-M/P	131	M/P	VL/P	VL/P	-
122	0	VL/P	VL/C	0	132	-	VL/P	L/P	L/P
123	-	L/P	0	-	133	L-M/C	M-S/I L-M/C	0	-
124	0	VL/I L/P	L/P	0	134	VL/P	L/C	0	-
125	0	VL/P	VL/P	VL/P	135	VL/P	VL/P	VL/P	VL/P
126	M/P	M/I	-	M/P	136	L/P	L/P	L/P	L-M/C
130	VL/P	VL-M/I VL-L/C	VL-L/C	0	137	0	M/P	-	-

TABLE V. TURBULENCE CLASSIFICATION ACCORDING TO TERRAIN (Concluded)

RAMEY AFB, PUERTO RICO

Test No.	Mountains*	Hills*	Flat*	Water*	Test No.	Mountains*	Hills*	Flat*	Water*
140	-	0	-	L-M/C	148	-	-	-	VL/P
141	-	0	-	L-M/P L/C	149	-	-	-	VL/C
142	-	L/P	-	L/C	150	-	-	-	L/P
143	-	-	-	0	151	-	-	-	M/C
144	L/I	L/P	-	M/P L-M/C	152	-	-	-	L-M/I
145	-	-	-	0	153	-	L/C	-	VL/C
146	0	L-M/P	-	L-M/P L/C	154	-	L/C	-	L/P
147	-	-	-	M/C					

ELMENDORF AFB, ALASKA

Test No.	Mountains*	Hills*	Flat*	Water*	Test No.	Mountains*	Hills*	Flat*	Water*
163	VL/P	VL/C	VL/C	VL/C	171	0	0	0	0
164	L-M/C	0	0	L-M/C	172	L/P	L/I	L/P	0
165	0	L/C	L/C	VL/P	173	M/C	L-M/C	L-M/P	M/C
166	L/C	0	0	0	174	VL-L/C L/P	0	0	L-M/P
167	0	0	0	0	175	0	VL/P	0	0
168	inc.	inc.	inc.	inc.	176	0	0	0	0
169	VL/P	0	VL/C	VL/P	177	0	0	0	0
170	0	0	0	0	178	VL/P	0	0	0

Legend

0 - Smooth air
VL - Very Light
L - Light
M - Moderate
C - Continuous
P - Patchy
I - Intermittent

- No extensive areas of this terrain condition were flown over on this flight.

* Mountains - Over 2500 ft
Hills - 500 to 2500 ft
Flat - 0 to 500 ft
Water - Ocean or large bay

An examination of the data in the tables shows no consistent relationship from day to day between types of terrain and intensity, duration, and continuity of turbulence. On some days, the turbulence was more intense, more extensive, and more continuous over rougher terrain, but on other occasions, the reverse was true. It would appear that there exists some mechanism which produces turbulence that is quite independent of the type of terrain directly beneath. Examples of such mechanisms would be fronts and troughs which move across an area comprising all classifications of terrain. Moreover, turbulence associated with mountain waves usually extends from its source many miles downwind over terrain which may be relatively flat or entirely level, e.g., the ocean.

Turbulence Intensity as a Function of Geographical Location

In order to examine the relationship between turbulence intensity and terrain as a function of geographical location, the data from Table V are summarized in Figure 53, in which turbulence intensity is summarized in terms of percent of tests when it was encountered regardless of the duration or extent, i.e., whether just a patch, a long intermittent or continuous run. In addition, transition intensities are here categorized as the more intense, i.e., very light is classified light and light to moderate is classified as moderate. Terrain classifications which apply to only a relatively small percentage of the terrain beneath the flight tracks are not included. An exception might be Hawaii, but in this area the flight tracks were concentrated over the islands, and especially the large island of Hawaii.

Influence of Convection

The influence of pure convection on the absence of thunderstorms is difficult to assess, but comparing the turbulence categories over hilly terrain in the eastern U.S. during the early fall season with the corresponding figures for mountainous terrain in the southwestern U.S. representative mostly of the winter season, it is evident that the percentage frequencies of moderate turbulence are similar. However, the frequency of light turbulence in the east is about 50 percent greater than in the southwest. From these figures it is only possible to state that pure convection due to surface heating may cause an increase in light turbulence at flight altitudes. On at least four occasions, patches of very light to light turbulence were encountered over the Virgin Islands in an otherwise tranquil area. However, in the Hawaiian Islands, the turbulence was not always present over the islands and seemed to occur when a jet stream or trough aloft was present and hence cannot be attributed to pure convection. Moreover, the persistent cloudiness over the low-lying portions of the islands would tend to minimize surface heating since only the mountain peaks were exposed.

Meteorological Parameters as Related to Turbulence

It is well known that turbulence is frequently associated with a jet stream, but the data show that a jet stream centered in the altitude range 20,000 to 40,000 feet does not necessarily imply there will be turbulence at the higher altitudes. The strength of the jet stream is not closely correlated with the occurrence or the intensity of turbulence. In Australia, the jet stream speed

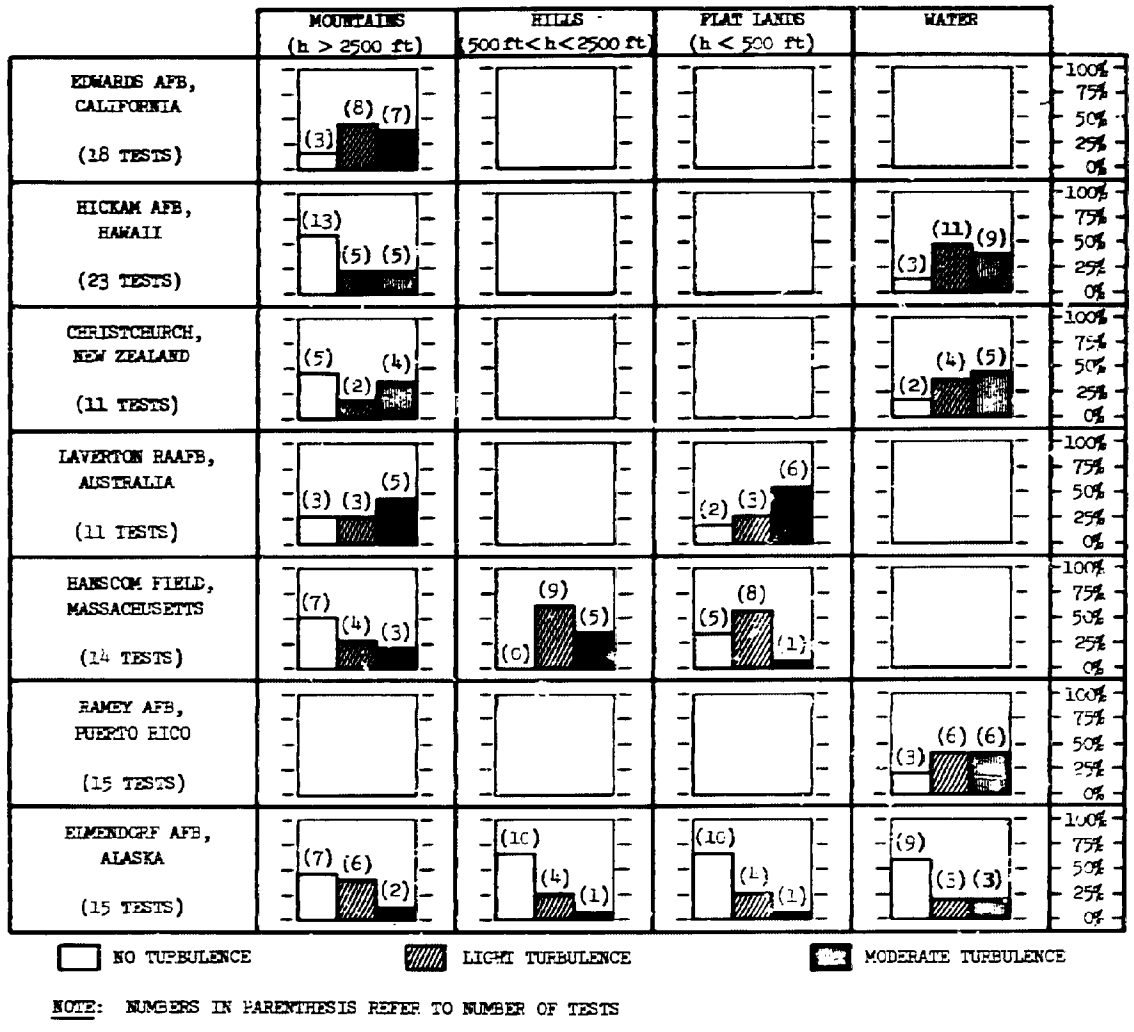

Figure 53. Terrain Classification of CAT Encounters

averaged around 150 knots and on at least one occasion reached 200 knots; yet the frequency of occurrence of turbulence was not much greater than in other areas where the jet stream speeds averaged much less. Since the magnitude of the horizontal and vertical speed shears are frequently closely related to the maximum speed of the jet, it is not surprising to find that these parameters do not always correlate well with the occurrence of turbulence. The same may be said of the Richardson number, although this includes the temperature gradient as well. Nevertheless, certain generalizations may be made from the available meteorological data, the turbulence data, and the pilot reports.

Since mountain wave turbulence is initiated by the vertical displacement of air streams, it might be assumed that turbulence over other types of terrain, which appears quite similar in nature and occurs at nearly the same frequency, might also be initiated by air streams being subjected to a vertical displacement. Converging or diverging air currents aloft and thermal advection patterns whereby the isotherms cross the streamlines or various combinations of these must be expected to be associated with vertical motion. For example, in the Puerto Rican area, turbulence was found to occur on one or more occasions in an area of converging or diverging wind currents, over frontal zones, or in an area of cooling aloft. On several occasions turbulence in the southwestern U.S. was associated with an isothermal advection pattern, and on at least one occasion, vertical wind direction shear (which according to the geostrophic thermal wind relationship implies an isothermal advection pattern) was used successfully to predict turbulence.

During some tests, the temperature in the turbulence area was found to be several (up to eight) degrees warmer or colder than the air on either side; this strongly suggests that the air had descended and warmed, or ascended and cooled adiabatically. In the eastern U.S. and in the Hawaiian area, a trough aloft was present on most of the days with turbulence. In the Alaskan area, where 150, 100, and 50 mb charts were prepared, the isothermal advection pattern proved very useful for prediction purposes - and correlated well with the occurrence of turbulence. The idea here is that the isotherms do not advect or move with the speed of the wind but appear at least in part as a consequence of vertical motion.

Cloud Forms as Related to Turbulence

While most of the clouds observed and photographed were well below flight altitudes, some interesting relationships between cloud forms and turbulence were noted.

- Turbulence is very likely to occur above an abrupt edge of a cirrus deck or above a large break in the cirrus deck. Such an abrupt break might well be produced by descending air.

- Photographs taken in smooth air of low lenticular clouds over mountain ranges indicate that mountain waves are not always associated with turbulence at flight altitudes. However, lenticular cirrus are more likely to be associated with turbulence and the higher the lenticulars the greater the probability of turbulence at flight altitude.

- Turbulence is very likely to occur in clear air above the tops and at some distance (up to 20 miles) horizontally from thunderstorms.

- Cirrus streaks or wisps and long streaming cumulo-nimbus anvils are indicative of the presence of a jet stream which sometimes is associated with turbulence. Frequently alto-cumulus (cotton balls) are oriented in parallel bands along the direction of the jet stream.

Flight Description

As an aid to further and more detailed HICAT analyses, a brief summary of the meteorological situation and pilot's debrief statements are included for each test in Appendix IX and appear on the page facing each flight track map.

When no pilot report was available - such as when a flight was aborted - no meteorological summary was prepared.

SECTION VIII

CONCLUSIONS

The HICAT measurements were obtained in U-2 test flights covering approximately 256,000 miles in seven geographical areas. The following conclusions are based upon an analysis of the clear air turbulence measured in these flights in the altitude band from 45,000 to 70,000 feet:

1. In the areas investigated, turbulence appears to occur most frequently in the altitude band from 50,000 to 55,000 feet.

2. In terms of physical extent, regions of continuous CAT vary considerably in length. Lengths measured by level traverses ranged from about 1000 feet to more than 125 miles. Roughly half the regions measured exceeded 14 miles in length, but only about 5 percent of the total were longer than 100 miles.

3. Based upon a very small number of high-rate climbs and descents, the thickness of CAT areas was found to vary from about 500 feet to more than 7000 feet. The thickness of most of the regions penetrated was less than 3000 feet.

4. A comparison of the turbulence measured in the HICAT program with that measured by VGH recorders in U-2 operational flights (Reference 2, NASA TN D-548) on the basis of frequency of exceedance of derived equivalent gust velocity indicates the following:

   a. Excluding from the TN D-548 data the operations over Japan — where, primarily as the result of two individual flights, the turbulence exposure was markedly more severe than over other areas of the world — turbulence was encountered about 4.5 times as frequently in the HICAT program as in the U-2 operational flights, but was comparable in intensity. The higher frequency of encounter in the HICAT flights is to be expected, since these flights were specifically directed toward locating and flying through turbulence.

   b. With the data obtained over Japan included in the TN D-548 results, the turbulence intensities reported in TN D-548 were significantly higher than measured in the HICAT program. The maximum U_{de} reported in TN D-548 was 20 fps; the highest measured in the redirected HICAT program was 12.6 fps, with a value of 16.7 fps reached in the earlier HICAT flights. Even

the highest of these is some 20 percent below the value ordinarily specified for structural design.

c. In both programs, turbulence in the 60,000 to 70,000-foot altitude band was less frequent and less severe than in the 40,000 to 60,000 foot band.

5. In the high CAT gust velocity power spectra, the measured power spectral densities are characterized, on the average, by slopes on the log-log plots of -1.5 to -1.7 for the horizontal components of turbulence and -1.25 to -1.4 for the vertical component.

The power spectral density curves, on the average, remain straight or very nearly straight on the log-log plots throughout the full range of wavelengths for which calculated, from 200 to 40,000 feet. The longer wavelength components indicate a scale of turbulence of at least 6000 to 8000 feet.(16)

6. A comparison of the gust velocity component power spectral densities indicates the horizontal components of turbulence to be about equal in severity on the average, to the vertical component at the highest measured frequencies (roughly 0.007 cycles per foot) but to be somewhat more severe at the lower frequencies. Rms gust velocities obtained by integrating the power spectral densities over the frequency range from 0.0005 to 0.007 cycles per foot indicate that the horizontal components exceed the vertical by 20 to 45 percent with the lower figure applicable to the higher turbulence intensities. At the longest wavelengths, there is some indication that this percentage increases, so that the turbulence becomes even more anisotropic.

7. The turbulence encountered in the HICAT flights seldom occurred in uniform patches of more than half-minute traverse time. Consequently, samples of several minutes' duration, and to an even greater extent, the few samples close to 16 minutes' duration, vary significantly in turbulence intensity throughout the sample. As a result, at least in part, of this lack of stationarity, the ratio of peak airplane acceleration or load measured during a HICAT turbulence traverse, to the measured rms value for the same sample, has been found to range from 1.25 to 2.25 times the ratio indicated by theory (Rice's equation) for a stationary Gaussian time history.

8. From the meteorological standpoint, the following observations are significant:

a. High altitude CAT occurs over all types of terrain.

---

16 Scale of turbulence here means the constant, L, in the Von Karman equation - or similar equations - defining gust power spectral density as a function of frequency.

b. High altitude CAT appears to be as prevalent in subtropical latitudes during transition seasons of spring and fall as in mid-latitudes during the winter seasons. However, there appears to be a definite decrease in occurrence of CAT in polar regions during winter when the polar front and major storm systems have migrated south to lower latitudes.

c. Potential high altitude CAT areas can sometimes be identified by the type and form of clouds below. No particular type of cloud could be identified which was always associated with CAT at flight altitude and, of course, turbulence can occur in a completely cloudless sky.

d. Of the many forecasting methods which were used to predict regions of CAT, few were very successful in defining specific areas of turbulence. Those most successful involved parameters such as troughs aloft, fronts, converging winds, and thermal advection or associated wind direction shear. All of these parameters may be associated with the same mechanism, namely ascending or descending air masses. In which case, the mechanism for producing turbulence would be the same as that for turbulence associated with mountain waves, thunderstorms, or other areas of intense convective activity.

9. A full time meteorologist is needed in the field in order to provide continuity to the forecasting program and regular, systematic verification of forecasts. (17)

[17] This improvement has already been effected in the new HICAT program (Reference 6).

APPENDIX I

HICAT TEST SUMMARY TABLE

This appendix consists of the HICAT Test Summary Table. For the most part, the entries are self-explanatory; however, some amplification is presented in the following paragraphs.

An "f" or "c" under the test number indicates ferry or check flight respectively. The symbols following the run numbers, L (level), T (turn), C (climb), and D (descent) are indicative of the aircraft flight path during the turbulence penetration. X and Y distances from the base are obtained from the inertial platform. Average altitude is obtained when possible from the high-altitude pressure sensor and has been corrected for position error. The aircraft heading angle is obtained from the inertial platform and can differ from the ground track angle depending upon atmospheric winds. The heading angle is measured from true north to the direction the aircraft is pointed. The average wind direction, following meteorological convention, is measured from true north to the direction from which the wind is blowing.

The intensity of the turbulence in each run is indicated in several ways. It is classified subjectively in accordance with the oscillogram editing notes as VL (very light), L (light), etc. It is described by the maximum and minimum incremental cg acceleration, the maximum and minimum derived equivalent gust velocity, the root mean square (rms) cg acceleration, and rms derived equivalent gust velocity. In addition, where true gust velocity components were computed, the CAT intensity is also indicated for qualifying gust runs by their truncated spectral rms values at 2000 feet wavelength and at the maximum standard wavelength, i.e., one of the following: 4000, 10,000, 20,000 or 40,000 feet. For some runs a considerable reduction in statistical reliability was accepted in order to obtain rms data up to the 40,000-foot wavelength. These cases are indicated by an asterisk.

Gaps in the table occur when the cg acceleration or U_{de} peak count data indicate the turbulence was of insufficient intensity or duration to warrant further processing to determine gust velocity time histories and power spectra. Gaps also result from instrument or equipment malfunctions.

BASE	DATE	TEST	RUN	START TIME (GMT)	RUN LENGTH	LOCATION (Start x,y) (End x,y)	ALTITUDE (Avg)	AIRSPEED (Avg True)	HEADING (Avg True)	WIND (Avg)	TEMP (Avg)	TERRAIN CLASS.	WIND CLASS.	ΔG (max)	U_{pk} (max)	RMS ΔG	RMS U_{pk}	RMS @ λ = 2000 ft U_y	RMS @ λ = 2000 ft U_L	RMS @ λ = 2000 ft U_p	RMS @ λ = λ_{max} U_y	RMS @ λ = λ_{max} U_L	RMS @ λ = λ_{max} U_p	λ_{max}
				hr:min:sec	sec	nmi	feet	knots	degrees	deg/kt	°C			g	fps	g	fps	fps	fps	fps	fps	fps	fps	ft
Edwards	11-16-65	39	2L	18:31:15	105		49,800					M	L	+ .19 / - .18	+ 2.9 / - 2.7	.063	0.66							
			3L	19:14:55	40		50,800					F	L											
			4L	19:17:00	30		49,900					M	L	+ .15 / - .11	+ 2.7 / - 1.6	.049	0.71							
			5L	19:19:20	60		49,000					M	L	+ .26 / - .15	+ 3.5 / - 2.1	.068	0.70							
			6L	19:21:25	40		48,300					F	L	+ .17 / - .16	+ 2.6 / - 2.6	.046	0.65							
			7L	19:58:30	55		48,900					M	L	+ .13 / - .20	+ 1.9 / - 2.8	.042	0.55							
			8L	20:00:40	255		49,400					M	L	+ .13 / - .17	+ 1.7 / - 2.2	.038	0.50							
Edwards	11-17-65	40	1L	18:21:25	35		60,600					M	L	+ .13 / - .15	+ 2.6 / - 2.9	.049	0.95							
			2L	18:25:00	25		60,400					M	L	+ .19 / - .16	+ 3.3 / - 2.8	.048	0.84							
			3L	18:26:35	70		61,000					M	LM	+ .24 / - .17	+ 4.8 / - 3.3	.056	1.10							
			4L	18:29:50	15		59,600					M	L	+ .19 / - .14	+ 3.1 / - 2.3	.058	0.97							
			5L	18:30:40	97		59,800					M	LM	+ .27 / - .33	+ 5.0 / - 6.1	.065	1.19							
			6L	18:42:10	1		56,500					M	M	+ .30 / - .27	+ 4.8 / - 3.3	.076	1.58							
			7L	18:42:55	15		56,900					M	L	+ .17 / - .11	+ 2.8 / - 1.8	.046	0.78							
			8L	18:47:40	45		51,000					M	L	+ .27 / - .30	+ 3.8 / - 4.1	.085	1.18							
			9L	18:55:20	50		43,400					M	L	+ .25 / - .13	+ 3.7 / - 1.9	.052	0.75							
			10L	18:57:35	65		43,400					M	L	+ .27 / - .22	+ 3.0 / - 3.1	.059	0.84							
			11L	18:59:55	130		43,400					M-W	LM	+ .22 / - .31	+ 3.3 / - 4.5	.064	0.99							
			12L	19:08:20	9		43,400					M	VL	+ .07 / - .08	+ 1.1 / - 1.3	.026	0.43							
			13L	19:09:05	90		43,400					M	L	+ .23 / - .15	+ 4.1 / - 3.1	.052	0.91							
			14L	19:38:40	80		52,500					M	M											
			15L	21:36:00	35		51,000					M	L											
			16L	21:36:50	35		51,000						LM											
			17L	19:30:20	25		48,400						L											
			18L	18:10:40	25		53,400						L											
Edwards	12-02-65	41	1L	19:16:05	10		54,000					M	VL											
			2L	19:30:40	20		54,200					M	VL											

(f) - Ferry Flight

Flight Path
L - Level C - Climb
T - Turn D - Descent

M - Mountains (h>2500 ft)
H - Hills (500 ft<h<2500 ft)
F - Flat Lands (h<500 ft)
W - Water

VL - Very Light
L - Light
LM - Light to Moderate
M - Moderate

* 500 Legs

BASE	DATE	TEST	RUN	TIME (GMT, hr:min:sec)	Δt sec	LOCATION (Start x,y) (End x,y) mil	ALTITUDE (Avg) feet	AIRSPEED (Avg) knots	HEADING (Avg °True) degrees	WIND (Avg) deg/kt	TEMP (Avg) °C	TERRAIN CLASS.	TURB CLASS.	ΔG (max) g	U_{DE} (max) fps	RMS ΔG g	RMS U_{DE} fps	RMS @ λ = 2000 ft σ_w fps	σ_L fps	σ_T fps	RMS @ λ = λ max σ_w fps	σ_L fps	σ_T fps	λ max k ft
Edwards	2-10-66	A4	2L	19:07:25	50							M	L											
			3L	19:11:40	85							M	L											
			4L	19:29:40	50							M	L											
			5L	20:09:00	135							M	L											
			6L	20:24:50	125							M	L											
			7L	20:31:45	60							F	L											
			8L	20:37:30	160							F	L											
Edwards	2-17-66	A6	2C	15:18:25	100		49,300					M	VL	+ .21	+ 3.3									
			3C	15:55:35	230		52,300	410			-56.5	M	L	+ .26 - .40	+ 4.4 - 6.9	.051	0.87							
			4L	19:01:30	240		47,700	415			-55.2	M	M	+ .41 - .30	+ 6.2 - 4.6	.068	1.02							
			5L	19:06:35	130		51,400	407			-55.4	M	DK	+ .35 - .22	+ 5.8 - 3.7	.068	1.13							
			6C	19:11:05	65		55,900					M	L	+ .37 - .27	+11.6 - 3.1	.041	0.74							
			7L	19:40:40	65		59,100					M	L	+ .10 - .13	+ 2.0 - 2.5	.039	0.75							
			8C	19:36:00	75		57,900					M	L	+ .15 - .14	+ 3.1 - 2.9	.044	0.90							
			9C	19:57:00	225		50,300					M	L	+ .19 - .26	+ 2.8 - 3.9	.041	0.61							
Edwards	3-22-66	A9	2L	19:32:30	25		55,600					M	L	+ .15 - .11	+ 2.2 - 1.6	.046	0.66							
			3C	20:01:05	20		58,000					M	L	+ .13 - .10	+ 2.0 - 1.5	.047	0.71							
			4L	20:26:55	40		53,200					F	L	+ .15 - .13	+ 2.4 - 1.6	.055	0.80							
			5L	20:15:15	140		54,100	419			-56.5	M	L	+ .32 - .45	+ 4.4 - 6.7	.078	1.15							
			6L	20:18:25	55		54,900					M	L	+ .22 - .24	+ 4.7 - 3.4	.063	0.91							
			7L	20:26:20	95		60,700					M	L	+ .16 - .17	+ 2.6 - 2.8	.051	0.84							
			8L	20:42:05	60		64,400					M	L	+ .19 - .11	+ 3.1 - 1.8	.051	0.84							
Edwards	3-31-66	A3	2C	15:30:50	50	12K 87R 14K 88R	45,800		098			M	L											
			3C	15:35:55	30	45K 94R 46K 96R	50,400		094			M	L	+ .14 - .14	+ 2.1 - 2.1	.051	0.77							
			4C	15:37:50	45	58K 98R 60K 101R	51,300		092			M	L											
			5L	15:39:30	55	71K 94R 78K 97R	51,000		084			M	L	+ .26 - .11	+ 3.6 - 1.5	.071	0.96							
			6L	19:21:55	115		54,400		285			M	VL											

(f) - Ferry Flight

Flight Path
L - Level C - Climb
T - Turn D - Descent

M - Mountains (h>2560 ft)
H - Hills (500 ft<h<2500 ft)
F - Flat Lands (h<500 ft)
W - Water

VL - Very Light
L - Light
LM - Light to Moderate
M - Moderate

* 500 Legs

RACE	DATE	TEST	RUN	START TIME (GMT)	RUN ABORT	LOCATION (Start x,y) (End x,y)	ALTITUDE (Avg)	AIRSPEED (Avg / Error)	HEADING (Avg / Error)	WIND (Avg)	TEMP (Avg)	TERRAIN CLASS.	TURB CLASS.	Δσ (max)	σ_{RMS} (max)	RMS Δσ	RMS σ_{RMS}	200 ≤ λ < 2000 ft σ_V	200 ≤ λ < 2000 ft σ_L	200 ≤ λ < 2000 ft σ_T	λ ≥ 2000 ft σ_V	λ ≥ 2000 ft σ_L	λ ≥ 2000 ft σ_T	λ min
				hr:min:sec	nmi	nmi	feet	knots	degrees	deg/sec	°C			g	fps	g	fps	fps	fps	fps	fps	fps	fps	λ ft
			170	20:36:25	120		57,600		329			M	VL											
			172	20:50:35	55		49,000		325			M	L	+ .09 / - .04	+ 0.5 / - 0.4	.013	0.17							
			173	21:04:40	45		51,200		324			M	L	+ .12 / - .15	+ 1.6 / - 2.1	.046	0.62							
			174	21:24:40	89		52,300		331			M	VL	+ .16 / - .09	+ 2.2 / - 1.2	.030	0.42							
			175	21:38:45	175		56,500		329			M	L											
			176	22:02:45	195		63,900	423	249		-65.7	M	L											
			177	22:16:20	75		53,600	423	252		-66.4	M	VL	+ .10 / - .11	+ 1.3 / - 1.5	.035	0.33							
			180	22:34:30	105		49,400		249			M	L											
			181	22:52:00	305		54,000		257			M	L											
			182	23:41:10	120		44,500					M	M											
			91	19:37:40	20		58,500		001			M	L	+ .12 / - .12	+ 1.9 / - 1.6	.032	0.51							
			92	21:15:20	204		54,700	396	252	321 / 46	-68.3	M	M	+ .29 / - .27	+ 4.4 / - 4.1	.056	0.84	1.44	2.03	1.79	1.64	2.49	1.98	4
			93	21:35:30	129		55,000	369	261	319 / 44	-67.7	F	L	+ .20 / - .21	+ 4.6 / - 3.3	.050	0.80	1.38	2.31	1.71	1.30	2.31	1.71	2
			95	21:52:50	19		54,200		230			F	L	+ .11 / - .09	+ 1.6 / - 1.2	.029	0.40							
			96	21:55:50	29		54,300		230			F	L	+ .16 / - .15	+ 2.1 / - 2.4	.037	0.49							
			97	21:40:31	59		54,800		252			M	L	+ .11 / - .26	+ 2.3 / - 3.4	.055	0.77							
			98	22:48:01	19		55,700		253			M	L	+ .16 / - .15	+ 2.1 / - 2.3	.045	0.67							
			99	23:09:03	39		54,600	430	262	336 / 49	-71.8	M	M	+ .24 / - .26	+ 3.7 / - 3.4	.047	0.60	0.88	1.12	1.26	0.88	1.12	1.26	2
			101	23:35:03	94		54,700		266			M	L	- .09 / - .12	+ 1.2 / - 1.6	.025	0.46							
			93	19:20:00	15		55,000		301			M	VL	+ .06 / - .14	+ 1.4 / - 1.9	.026	0.45							
			95	20:14:15	209		61,800	434	191	275 / 16	-62.2	M	-	+ .15 / - .15	+ 3.1 / - 3.1	.044	0.77	0.85	1.27	1.14	1.00	1.64	1.37	4
			97	20:33:00	14		61,700		193			M	L	+ .09 / - .15	+ 1.6 / - 2.7	.044	0.72							
			50	19:10:40	50		60,000		039			M	L	+ .17 / - .15	+ 2.5 / - 2.2	.057	0.88							
			41	23:37:35	42		46,700						L											

(f) - Ferry Flight

Flight Path
L - Level C - Climb
T - Turn D - Descent

M - Mountains (h>2500 ft)
H - Hills (500 ft<h<2500 ft)
F - Flat Lands (h<500 ft)
W - Water

VL - Very Light
L - Light
LM - Light to Moderate
M - Moderate

* 500 Legs

Appendix I

MSFC	DATE	TEST	RUN	START TIME (GMT)	RUN LENGTH	LOCATION (Start x,y) (End x,y)	ALTITUDE (Avg)	AIRSPEED (Avg)	HEADING (Avg)	WIND (Avg)	TEMP (Avg)	TERRAIN CLASS.	RUN CLASS.	ΔG (max)	V_{RMS} (max)	RMS ΔG	RMS V_{RMS}	RMS @ λ - 2000 ft			RMS @ λ - λ max			
																		$\bar{u}_V$	$\bar{u}_L$	$\bar{u}_T$	$\bar{u}_V$	$\bar{u}_L$	$\bar{u}_T$	λ max
				hr:min:sec	sec	nmf	feet	knots	degrees	deg/kt	$^{\circ}C$			g	fps	g	fps	fps	fps	fps	fps	fps	fps	k ft
Elchus	4-25-66	63	13L	22:27:00	30		60,700	431	053	055 / 21	-67.2	M	L	+.06 -.08	+1.8 -1.4	.081	0.34							
			14L	22:28:00	90		60,800	430	054	068 / 21	-67.3	M	L	+.09 -.11	+1.5 -1.8	.031	0.51							
			15L	22:29:55	90		60,800	430	054	071 / 22	-67.2	M	L	+.12 -.13	+1.6 -1.7	.086	0.43							
			16L	22:31:20	170		60,800	429	053	074 / 19	-67.2	M	L	+.08 -.11	+1.9 -1.8	.055	0.59		0.94	0.89		1.05	0.99	k
			17L	22:40:55	90		60,900	425	276	301 / 15	-66.7	M	L	+.12 -.16	+2.1 -2.8	.089	0.48							
			18L	22:42:45	50		60,700	433	270	313 / 13	-65.6	M	L	+.16 -.10	+2.5 -1.6	.035	0.56							
			19L	22:46:35	170		60,900	428	272	312 / 14	-66.6	M	L	+.08 -.09	+1.4 -1.5	.025	0.41		0.67	0.85		0.80	0.99	k
			20L	22:52:10	45		60,900	426	142	135 / 12	-66.6	M	L	+.14 -.08	+2.4 -1.5	.035	0.58							
			21L	22:56:25	10		60,700	431	144	181 / 24	-67.6	M	L	+.11 -.07	+1.7 -1.1	.034	0.54							
			22L	23:00:15	20		60,700	436	143	154 / 27	-67.7	M	L	+.11 -.13	+1.7 -2.0	.046	0.73							
			23L	23:18:55	60		60,700	431	321	060 / 8	-68.0	M	L	+.12 -.12	+1.9 -2.0	.036	0.56							
			24L	23:24:10	20		60,800	428	322	039 / 20	-67.0	M	L	+.09 -.10	+1.5 -1.6	.036	0.58							
			25L	23:26:45	35		60,700	429	326	089 / 16	-66.1	M	L	+.08 -.08	+1.3 -1.3	.027	0.43							
			26L	23:57:55	50		60,700	430	270	326 / 21	-68.1	M	L	+.13 -.13	+2.1 -2.0	.035	0.53							
			27L	00:39:55	110		60,800	425	273	333 / 14	-66.3	M	LM	+.20 -.16	+3.1 -2.5	.051	0.78							
			28L	00:15:50	5		61,100	419	270	343 / 40	-66.2	M	L	+.11 -.17	+1.8 -2.7	.047	0.75							
			29L	00:23:30	170		60,700	430	097	102 / 21	-66.3	M	L	+.17 -.20	+2.6 -1.9	.039	0.59		0.65	0.71		1.23	1.13	10
			30L	00:34:00	16		60,500	430	092	130 / 26	-67.2	M	L	+.12 -.08	+1.8 -1.2	.054	0.79							
			31L	00:39:40	285		60,700	429	001	016 / 17	-65.7	M	L	+.15 -.19	+2.1 -2.8	.042	0.62		0.83	0.85		1.16	1.04	k
Elchus	4-27-66	65	2L	22:34:45	69		53,700		002			M	L	+.06 -.09	+1.2 -1.4	.018	0.27							
			3L	22:39:20	83		53,700	417	000	274 / 31	-73.1	M	VL	+.08 -.04	+1.2 -0.6	.020	0.28							
			4L	22:51:00	30		53,800		002			M	L	+.11 -.08	+1.6 -1.1	.024	0.36							
			5L	23:38:30	30		53,500		273			M	L	+.08 -.12	+1.2 -1.8	.029	0.41							
Elchus	4-29-66	67	3D	22:36:30	55		50,200		088			M	L											
			4L	23:15:35	115		50,500		169			M	L	+.09 -.11	+1.3 -1.6	.023	0.32							
			5L	00:00:10	20		50,500		314			M	L	+.09 -.08	+1.1 -1.0	.036	0.43							
			6L	00:58:35	25		45,100		293			M	M	+.04 -.09	+0.6 -0.3	.011	0.15							

(f) - Ferry Flight

Flight Path
L - Level C - Climb
T - Turn D - Descent

M - Mountains (h>2500 ft)
H - Hills (500 ft<h<2500 ft)
F - Flat Lands (h<500 ft)
W - Water

VL - Very Light
L - Light
LM - Light to Moderate
M - Moderate

* 500 Laps

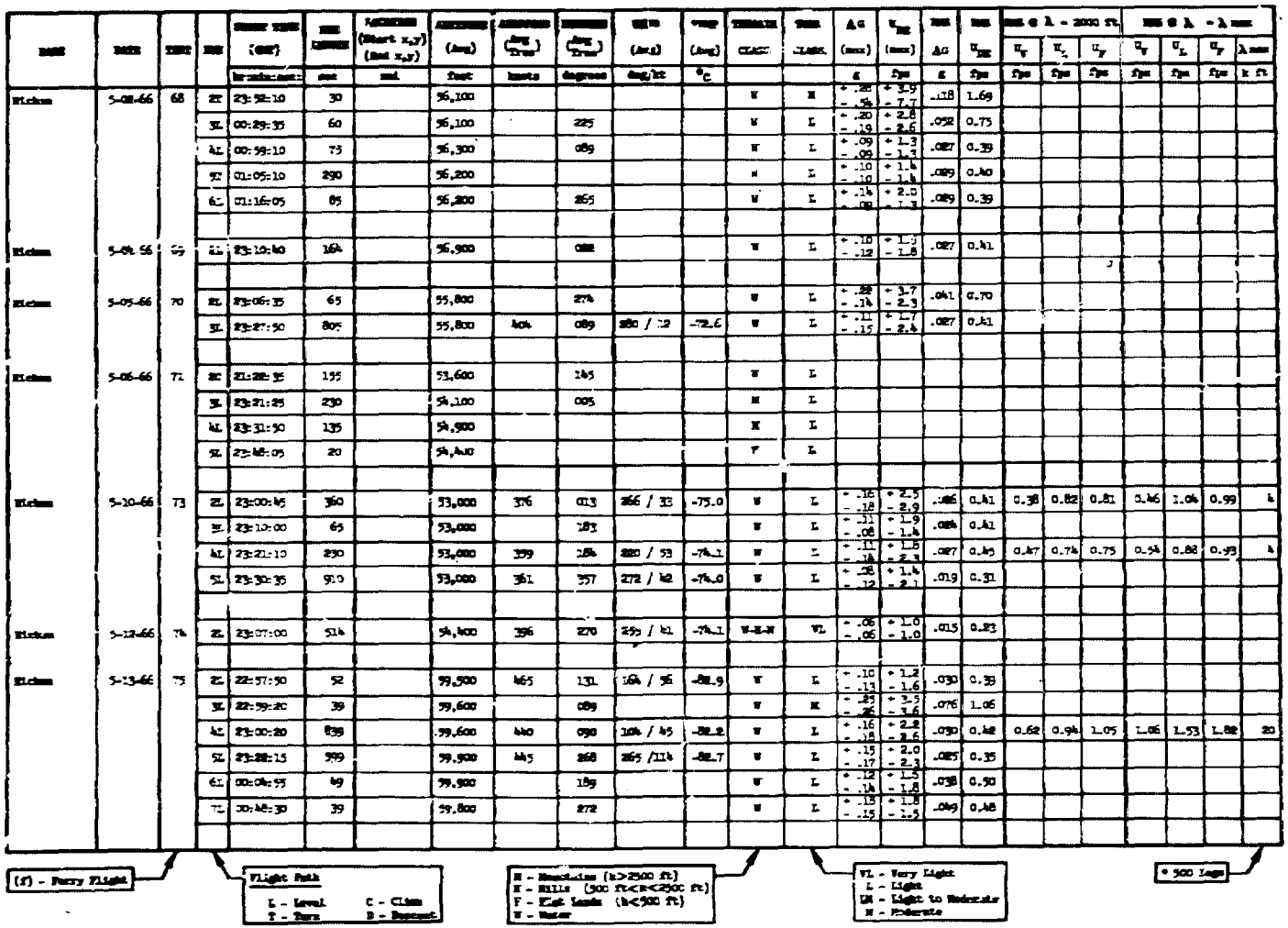

Event	Date	Time	Run	Event time (GMT)	Run distance	Acceleration (Start x,y) (End x,y)	Acceleration (kts)	Acceleration (avg Time)	Acceleration (avg Time)	Wind (kts)	Temp (deg)	Terrain class	Turb. class	ΔG (max)	U_{de} (max)	Run ΔG	Run U_{de}	Run @ h - 2000 ft U_V	Run @ h - 2000 ft U_L	Run @ h - 2000 ft U_T	Run @ h - h max U_V	Run @ h - h max U_L	Run @ h - h max U_T	Run @ h - h max h max ft
				hr:min:sec	nmi	mi.	feet	knots	degrees	deg/kt	°C			g	fps	g	fps	fps	fps	fps	fps	fps	fps	ft
Hickam	5-08-66	68	2L	23:52:10	30		56,100					M	M	+ .28 - .54	+ 3.9 - 7.7	.18	1.69							
			3L	00:29:35	60		56,100		225			M	L	+ .20 - .19	+ 2.8 - 2.6	.052	0.75							
			4L	00:59:10	75		56,300		089			M	L	+ .09 - .09	+ 1.3 - 1.3	.027	0.39							
			5L	01:05:10	290		56,200					M	L	+ .10 - .10	+ 1.4 - 1.4	.029	0.40							
			6L	01:16:05	85		56,200		265			M	L	+ .14 - .09	+ 2.0 - 1.3	.029	0.39							
Hickam	5-04-66	69	2L	23:10:40	164		56,900		088			M	L	+ .10 - .12	+ 1.5 - 1.8	.027	0.41							
Hickam	5-05-66	70	2L	23:06:35	65		55,800		274			M	L	+ .28 - .14	+ 3.7 - 2.3	.041	0.70							
			3L	23:27:50	805		55,800	404	089	280 / 12	-72.6	M	L	+ .11 - .15	+ 1.7 - 2.4	.027	0.41							
Hickam	5-06-66	71	2L	21:28:35	155		53,600		145			M	L											
			3L	23:21:25	230		54,100		005			M	L											
			4L	23:31:50	135		54,900					M	L											
			5L	23:48:05	20		54,400					F	L											
Hickam	5-10-66	73	2L	23:00:45	360		53,000	376	013	266 / 33	-75.0	M	L	+ .16 - .18	+ 2.5 - 2.9	.086	0.41	0.38	0.82	0.81	0.46	1.04	0.99	4
			3L	23:10:00	65		53,000		183			M	L	+ .11 - .08	+ 1.9 - 1.4	.084	0.41							
			4L	23:21:10	290		53,000	359	184	280 / 53	-74.1	M	L	+ .11 - .14	+ 1.8 - 2.3	.087	0.45	0.47	0.74	0.75	0.54	0.88	0.93	4
			5L	23:30:35	910		53,000	361	357	272 / 42	-74.0	M	L	+ .08 - .12	+ 1.4 - 2.1	.019	0.31							
Hickam	5-12-66	74	2L	23:07:00	514		54,400	396	270	295 / 41	-74.1	M-H-M	VL	+ .06 - .06	+ 1.0 - 1.0	.015	0.23							
Hickam	5-13-66	75	2L	22:57:50	52		59,500	465	131	164 / 36	-82.9	M	L	+ .10 - .13	+ 1.2 - 1.6	.030	0.39							
			3L	22:59:20	39		59,600		089			M	M	+ .29 - .26	+ 3.5 - 3.6	.076	1.06							
			4L	23:00:20	838		59,600	440	098	104 / 45	-82.2	M	L	+ .16 - .18	+ 2.2 - 2.6	.030	0.48	0.62	0.94	1.05	1.06	1.53	1.88	20
			5L	23:28:15	999		59,900	445	268	265 /114	-82.7	M	L	+ .15 - .17	+ 2.0 - 2.3	.085	0.35							
			6L	00:04:55	49		59,900		189			M	L	+ .12 - .14	+ 1.5 - 1.8	.038	0.50							
			7L	00:48:30	39		59,800		272			M	L	+ .13 - .15	+ 1.8 - 2.5	.049	0.48							

(f) - Ferry Flight

Flight Path
L - Level C - Climb
T - Turn D - Descent

M - Mountains (h>2500 ft)
H - Hills (500 ft<h<2500 ft)
F - Flat Lands (h<500 ft)
W - Water

VL - Very Light
L - Light
LM - Light to Moderate
M - Moderate

* 500 Legs

RACE	DATE	FLT	RUN	START TIME (GMT)	RUN LENGTH	LOCATION (Start x_0,y_0) (End x_0,y_0)	ALTITUDE (Avg)	AIRSPEED (Avg True)	HEADING (Avg True)	WIND (Avg)	TEMP (Avg)	TERRAIN CLASS.	TURB CLASS.	ΔS (max)	σ_{SIG} (max)	SIG ΔG	SIG σ_{SIG}	SIG @ λ = 3000 ft. σ_V	SIG @ λ = 3000 ft. σ_L	SIG @ λ = 3000 ft. σ_T	SIG @ λ = λ max. σ_V	SIG @ λ = λ max. σ_L	SIG @ λ = λ max. σ_T	λ max.
				hr:min:sec	sec	feet	knots	degrees	deg/kt	°C			g	fps	g	fps	fps	fps	fps	fps	fps	fps	kft
Hicks	5-16-66	76	2L	22:24:55	299		58,300	428	064	139 / 19	-66.1	W	L	+ .14 - .---	+ 2.2 - 2.1	.086	0.43							
			3L	23:09:15	51		58,000		280			M	M	+ .13 - .21	+ 2.1 - 3.3	.039	0.52							
			4L	23:16:45	134		58,100	434	281	282 / 8	-66.6	W	M	+ .30 - .36	+ 4.8 - 5.4	.051	0.79	0.87	0.91	1.12	1.20	1.23	1.52	4
			5L	23:29:40	84		58,400	428	102	073 / 3	-66.8	W	L	+ .41 - .13	+ 6.5 - 2.1	.044	0.70	0.85	0.96	1.15	0.85	0.96	1.15	2
			6L	23:33:05	239		58,200	435	272	120 / 6	-66.7	W	M	+ .21 - .19	+ 3.3 - 3.0	.047	0.72	0.88	1.01	1.13	1.14	1.23	1.64	4
			7L	23:52:55	54		52,100	434	010	011 / 15	-67.1	M	M	+ .15 - .14	+ 2.3 - 2.2	.046	0.69							
			8L	00:14:15	41		58,000		192			W	L	+ .10 - .11	+ 1.5 - 1.6	.052	0.48							
			9L	00:24:50	19		58,100		009			W	L	+ .11 - .16	+ 1.7 - 2.3	.040	0.60							
			10L	00:36:25	277		58,100		010			W	L	+ .15 - .12	+ 2.2 - 1.6	.084	0.96							
Hicks	5-17-66	77	2L	21:48:45	244		58,200	430	210	196 / 12	-68.5	W	L	+ .19 - .18	+ 3.1 - 2.9	.055	0.97							
			3L	21:59:05	69		58,400		209			W	L	+ .14 - .19	+ 2.3 - 3.1	.050	0.82							
			5L	22:09:00	85		58,100	435	299	260 / 15	-70.0	W-M-M	L	+ .11 - .20	+ 1.- - 3.2	.027	0.42							
			6L	22:16:10	459		58,100		269			W	L	+ .15 - .12	+ 2.2 - 1.8	.036	0.55							
			7L	00:01:30	84		58,100		119			W	L	+ .15 - .08	+ 2.1 - 1.1	.032	0.45							
			8L	00:25:05	74		58,200		265			W	L	+ .16 - .16	+ 2.2 - 2.3	.047	0.67							
			9L	00:32:40	409		58,200	430	085	269 / 5	-68.2	M-M-W	L	+ .16 - .20	+ 2.2 - 2.8	.028	0.40							
Hicks	5-19-66	78	2L	22:47:45	240							W	M											
			3L	22:51:55	15							W	M											
			4L	23:23:30	960							W	M											
			5L	23:36:00	190							W-M-M	M											
			6L	23:48:15	905							M-M-M	DM											
			7L	00:09:50	875							W-M-M	DM											
			9L	00:30:35	80							W	M											
Hicks	5-20-66	79	2L	22:44:40	114	78E 53S 91E 58S	54,500	404	091	180 / 19	-73.8	W	L	+ .13 - .17	+ 1.9 - 2.6	.043	0.66	0.68	1.13	1.03	0.63	1.13	1.03	2
			3L	23:24:00	239	98E 41S 73E 39S	54,500	401	271	269 / 36	-73.0	M-M-M	M	+ .25 - .21	+ 3.8 - 3.1	.060	0.60	0.75	1.07	1.15	0.87	1.28	1.45	4
			4L	00:14:50	64	121E 35S 121E 27S	54,400		359			W	L	+ .13 - .10	+ 1.9 - 1.4	.028	0.40							
			7L	00:31:45	264	102E 6S 80E 2S	49,500	390	266		-74.8	W	M	+ .45 - .49	+ 6.1 - 6.5	.074	0.98	1.27	1.46	1.53	1.67	2.25	2.07	4

(f) - Ferry Flight

Flight Path
L - Level C - Climb
T - Turn D - Descent

M - Mountains (h>2500 ft)
H - Hills (500 ft<h<2500 ft)
F - Flat Lands (h<500 ft)
W - Water

VL - Very Light
L - Light
LM - Light to Moderate
M - Moderate

* 500 Legs

BASE	DATE	TEST	RUN	START TIME (GMT)	RUN LENGTH	LOCATION (Start x,y) (End x,y)	ALTITUDE (Avg)	AIRSPEED (Avg True)	HEADING (Avg True)	WIND (Avg)	TEMP (Avg)	TURBULENCE CLASS.	GUST CLASS.	ΔG (max)	U_{DE} (max)	RMS ΔG	RMS U_{DE}	rms @ λ = 2000 ft			rms @ λ = λ max			
																		U_V	U_L	U_T	U_V	U_L	U_T	λ max
				hr:min:sec	sec	nmi	feet	knots	degrees	deg/kt	°C			g	fps	g	fps	fps	fps	fps	fps	fps	fps	ft
Eielson	5-22-66	80 (f)	2L	19:27:10	94	105E 20N 117E 17N	55,900		084				L	+.19 -.14	+3.4 -2.6	.038	0.70							
			3L	21:11:25	634	805E 258N 878E 291N	54,400		072				L	+.14 -.18	+2.1 -2.8	.034	0.37							
Edwards	6-02-66	81 (e)	2L	23:25:55	144		60,100		176				M	+.61 -.33	+12.3 -6.2	.100	2.00							
			3L	23:29:25	59		60,300						M	+.53 -.44	+8.3 -7.0	.134	2.11							
			4L	23:31:30	184		60,300		174				M	+.37 -.36	-6.3 -6.1	.064	1.08							
Eielson	6-08-66	83	2L	23:24:00	94	19W 676N 14E 673N	46,100		089			W	L	+.13 -.13	+2.5 -2.5	.038	0.72							
			3L	00:40:05	14	74W 302N 72W 299N	53,500		000			W	L	+.12 -.08	+1.6 -1.1	.036	0.68							
			4L	00:42:30	89	74W 284N 74W 277N	53,500		001			W	L	+.13 -.13	+1.7 -1.7	.038	0.50							
Christchurch	6-17-66	87	2L	02:06:13	34		64,000		335			W	L	+.14 -.11		.035								
			3L	02:17:13	79		63,600		241			W	L	+.13 -.18		.040								
			4L	02:23:03	944		63,500		202			W	M	+.42 -.41		.060								
			5L	02:40:58	224		64,000		330			W	L	+.23 -.21		.050								
			6L	04:10:23	59		63,800		092			W	L	+.15 -.12		.037								
			7L	04:20:53	308		62,700		337			W	IM	+.48 -.39		.058								
			8L	04:30:08	164		63,600		316			W	L	+.15 -.20		.032								
			9L	04:32:58	68		63,000		316			W	L	+.20 -.19		.043								
			10L	04:42:03	83		62,600		175			W	L	+.23 -.20		.049								
Christchurch	7-29-66	88	2L	23:39:13	34	447E 35N 448E 42N	50,100		324			W	L	+.11 -.12	+1.7 -1.8	.039	0.63							
			3L	23:49:28	44		50,200		324			W	L	+.10 -.11	+1.5 -1.7	.029	0.45							
			4L	23:56:38	202	524W 184N 529W 130N	50,300		198			W	L	+.15 -.10	+2.5 -1.7	.027	0.45							
			5L	23:58:38	74	533W 160N 530W 134N	50,200					W	L	+.12 -.12	+2.0 -2.0	.035	0.43							
			6L	01:18:08	203	162W 229N 134W 286N	52,100	442	141	271 / 38	-55.8	W	L	+.12 -.13	+1.7 -1.8	.035	0.41	0.55	1.09	0.85	0.68	1.30	1.00	4
			7L	02:09:12	913	87W 29N 15E 112N	52,100	431	142	285 / 19	-56.3	M-W	VL	+.43 -.27	+6.1 -4.0	.034	0.48							
			8L	02:37:38	794	12E 67N 42W 30N	52,000	435	383	262 / 27	-56.7	W-M-W	L	+.16 -.13	+2.4 -1.7	.027	0.37	0.90	0.96	0.64	0.88 .38	1.95 2.43	1.63 2.58	80 440

(f) - Ferry Flight

Flight Path
L - Level C - Climb
T - Turn D - Descent

M - Mountains (h>2500 ft)
H - Hills (500 ft<h<2500 ft)
F - Flat Lands (h<500 ft)
W - Water

VL - Very Light
L - Light
LM - Light to Moderate
M - Moderate

* 500 Legs

Appendix I

BASE	DATE	TEST	RUN	START TIME (GMT)	RUN LENGTH	LOCATION (Start x,y) (End x,y)	ALTITUDE (Avg)	AIRSPEED (Avg, True)	HEADING (Avg, True)	WIND (Avg)	TEMP (Avg)	TERRAIN CLASS	TURB CLASS	Δσ (max)	U_{DE} (max)	RMS Δσ	RMS U_{DE}	RMS @ λ = 5000 ft U_V	U_L	U_T	RMS @ λ = λ max U_V	U_L	U_T	λ max
				hr:min:sec	sec	nmi	feet	knots	degrees	deg/kt	°C			g	fps	g	fps	fps	fps	fps	fps	fps	fps	k ft
Christchurch	7-29-66	88	9L	02:54:58	113		52,000	440	169	264 / 33	-58.4	M	M	+ .38 - .31	+ 5.2 - 4.3	.064	0.87	1.63	1.90	2.00	1.69	1.90	2.00	2
			10L	03:01:28	214	40E 11N / 54E 21N	52,600	450	319	285 / 43	-55.0	M	M	+ .44 - .42	+ 5.7 - 5.5	.072	0.94	0.96	1.31	1.39	1.44	1.68	1.35	4
			11L	03:11:58	395	63E 19N / 33E 9N	52,200	368	139	241 / 20	-55.7	M-H	L	+ .20 - .15	+ 3.5 - 2.6	.039	0.68							
			12L	03:24:28	38	6E 4N / 10E 3N	48,100		066			H-W	M	+ .34 - .24	+ 4.7 - 3.2	.067	0.92							
Christchurch	6-22-66	89	2L	23:14:15	40		50,700					M	L											
			3L	23:17:55	19	273E 314N / 281E 315N	51,300		303			M	L	+ .14 - .13	+ 2.0 - 1.7	.044	0.61							
			4L	23:19:05	19	216E 316N / 214E 319N	51,500		302			H	M	+ .32 - .33	+ 6.1 - 4.9	.090	1.34							
			6L	00:16:35	54	37E 272N / 36E 271N	52,000		190			W	L	+ .21 - .21	+ 2.9 - 2.8	.047	0.64							
			7L	00:19:05	39	35E 246N / 33E 238N	51,800		205			W	L	+ .13 - .17	+ 1.5 - 2.4	.035	0.49							
			8L	00:56:50	84	29E 186N / 31E 189N	51,900		020			W	L	+ .11 - .09	+ 1.5 - 1.1	.037	0.48							
Christchurch	6-24-66	90	2F	22:07:02	34	52E 81N / 54E 84N	54,000					M	L	+ .21 - .18	+ 4.4 - 3.7	.070	1.45							
			3C	22:13:57	229	76E 120N / 92E 142N	53,000	411	034	293 / 27	-54.6	W	L	+ .13 - .16	+ 2.6 - 3.0	.038	0.75							
			4L	22:24:57	484	119E 183N / 146E 231N	60,800	410	027	314 / 24	-57.7	W-H-M	L	+ .13 - .09	+ 2.3 - 2.1	.026	0.63							
			5L	22:33:47	304	149E 234N / 165E 253N	58,700	414	027	234 / 33	-57.6	M	L	+ .17 - .21	+ 3.6 - 4.5	.048	1.08	1.11	1.01	0.79	2.03	2.07	1.25	10
			6D	22:41:20	285				027			M	L											
			7L	22:46:17	334	180E 310N / 185E 347N	55,800	416	004	310 / 30	-56.6	M	M	+ .29 - .30	+ 5.7 - 5.2	.063	1.25							
			8L	23:32:27	36	192E 265N / 188E 264N	60,000		272			M	L	+ .13 - .19	+ 2.7 - 3.9	.048	1.01							
			9L	23:40:07	349	145E 267N / 106E 269N	59,900	422	272	257 / 27	-55.0	M	M	+ .29 - .33	+ 5.9 - 6.8	.064	1.30	1.54	1.82	2.05	2.42	2.89	3.45	10
			10L	00:04:12	79	82E 257N / 92E 266N	60,200		092			F	L	+ .10 - .18	+ 1.5 - 3.3	.058	1.06							
			11L	00:07:02	349	103E 266N / 142E 264N	59,700	445	092	027 / 5	-55.3	M	L	+ .26 - .21	+ 4.7 - 3.8	.050	0.92	1.30	1.20	1.36	2.40	2.07	2.40	10
			12L	00:39:07	304	116E 311N / 119E 275N	59,600	448	180	230 / 37	-53.9	M	M	+ .29 - .34	+ 5.0 - 5.9	.069	1.21	1.89	2.67	2.19	2.49	4.16	3.19	10
			13F	00:54:57	113	114E 208N / 111E 200N	60,000	428			-53.0	M	L	+ .20 - .22	+ 3.7 - 4.1	.059	1.11							
			14L	01:00:22	83	120E 218N / 120E 289N	59,700		359			M	L	+ .20 - .17	+ 3.3 - 2.9	.045	0.76							
Christchurch	6-27-66	91	2D	23:04:05	145		56,900						L											
			3L	23:19:40	364		60,400						LM	+ .32 - .23	+ 5.8 - 5.4	.071	1.32							

(f) - Ferry Flight

Flight Path
L - Level C - Climb
T - Turn D - Descent

M - Mountains (h>2500 ft)
H - Hills (500 ft<h<2500 ft)
F - Flat Lands (h<500 ft)
W - Water

VL - Very Light
L - Light
LM - Light to Moderate
M - Moderate

* 500 Lags

Base	Date	Sheet	Run	Time (GMT)	Run Length	Location (Start x,y) (End x,y)	Altitude (Avg)	Airspeed (Avg / Type)	Heading (Avg / Error)	Wind (Avg)	Temp (Avg)	Terrain Class.	Cond Class.	Δσ (max)	U_{RMS} (max)	Rec Δσ	Rec U_{RMS}	PSD @ λ = 2000 ft U_x	PSD @ λ = 2000 ft U_z	PSD @ λ = 2000 ft U_y	PSD @ λ = λ max U_x	PSD @ λ = λ max U_z	PSD @ λ = λ max U_y	PSD @ λ = λ max λ max
				hr:min:sec	sec	ft	Knots	Knots	degrees	deg/kt	°C			g	fps	g	fps	fps	fps	fps	fps	fps	fps	λ ft
Christchurch	6-30-66	93	1L	07:03:00	979	[illegible]	51,900	401	094	204 / 27	-55.1	M	L	+ .20 / - .15	+ 3.4 / - 2.5	.086	0.43							
			2L	00:15:24	74	[illegible]	51,900					M	M	+ .25 / - .25	+ 3.8 / - 3.8	.064	0.94							
			3L	00:21:29	182	[illegible]	51,700		358			M	M	+ .15 / - .25	+ 2.2 / - 3.7	.033	0.89							
			4L	00:26:39	222	[illegible]	51,700	406	357	302 / 27	-55.2	M	M	+ .17 / - .16	+ 2.7 / - 2.5	.039	0.60							
			5L	00:40:49	89	[illegible]	51,900		186			M	M	+ .12 / - .32	+ 1.7 / - 4.7	.052	0.78							
			6L	00:41:59	374	[illegible]	51,800	428	184	226 / 30	-55.3	M	M	+ .16 / - .18	+ 2.2 / - 2.6	.056	0.51							
			7L	00:56:34	19	[illegible]	52,000		184			M	M	+ .17 / - .13	+ 2.9 / - 2.1	.042	0.70							
			100	01:38:00	40							M												
Christchurch	7-08-66	95	1L	03:17:00	53	[illegible]	45,700		272			M	L	+ .12 / - .08	+ 1.8 / - 1.2	.027	0.42							
			2L	03:45:45	307	[illegible]	51,300		272			M	M	+ .24 / - .25	+ 3.2 / - 3.4	.036	0.69							
			3L	03:52:50	18	[illegible]	51,300		271			M	L	+ .12 / - .12	+ 1.6 / - 1.7	.031	0.83							
			4T	04:26:45	68	[illegible]	51,300					M	L	+ .14 / - .19	+ 1.8 / - 2.4	.049	0.64							
			5L	04:25:45	88	[illegible]	51,300		231			M	L	+ .13 / - .13	+ 1.7 / - 1.7	.029	0.38							
			6L	04:29:50	168	[illegible]	51,300		289			M	M	+ .15 / - .28	+ 2.2 / - 3.4	.043	0.83							
			7T	04:36:15	88	[illegible]	51,800					M	L	+ .19 / - .25	+ 2.5 / - 3.4	.058	0.77							
			8L	04:37:40	317	[illegible]	51,400		350			M	L	+ .16 / - .17	+ 1.8 / - 2.4	.032	0.44							
			9L	05:15:50	83	[illegible]	51,300		184			M	L	+ .21 / - .16	+ 2.5 / - 1.9	.035	0.44							
Christchurch	7-11-66	96	2S	22:56:49	19	[illegible]	60,200		085			M	L											
			3T	23:12:28	90	[illegible]	50,500	446	335	282 / 61	-55.9	M	L											
			4T	23:16:23	186	[illegible]	49,800	449			-54.5	M	M											
			5L	23:41:48	199	[illegible]	51,000	468	271	280 / 67	-55.4	M	M	+ .44 / - .30	+ 5.6 / - 3.8	.057	0.71							
			6T	23:55:03	481	[illegible]	50,000	458			-56.2	M	L	+ .27 / - .34	+ 3.4 / - 4.3	.070	0.87							
			7L	00:01:35	180							M	L											
			8L	00:13:23	353	[illegible]	50,300	460	087	290 / 48	-55.2	M	L	+ .21 / - .12	+ 2.6 / - 1.5	.089	0.35	0.51	0.72	0.80	0.57	0.85	0.97	4
			9T	00:53:08	163	[illegible]	50,400	463			-53.8	M	L	+ .10 / - .17	+ 1.2 / - 2.0	.027	0.31							
			10L	00:58:58	841	[illegible]	50,400	463	353	274 / 63	-55.1	M	L	+ .20 / - .15	+ 2.3 / - 2.0	.027	0.31	0.38	0.74	0.54	0.45	0.95	0.64	4
			11L	01:19:12	170	[illegible]	50,800	458	305	292 / 72	-57.9	M	L	+ .14 / - .26	+ 1.6 / - 2.7	.032	0.35	0.49	0.74	0.66	0.39	0.74	0.60	2
			12L	01:58:38	734	[illegible]	67,380	431	210	235 / 26	-60.2	H	VL	+ .16 / - .13	+ 2.7 / - 2.1	.022	0.38		1.02	0.95		1.65	1.53	14

(f) - Ferry Flight

Flight Path
L - Level C - Climb
T - Turn D - Descent

H - Mountains (h>2500 ft)
M - Hills (500 ft<h<2500 ft)
F - Flat Lands (h<500 ft)
W - Water

VL - Very Light
L - Light
LM - Light to Moderate
M - Moderate

* SCC Logs

Base	Date	Test	Run	Start Time (GMT)	Run Length	Location (Start x,y) (End x,y)	Altitude (Avg)	Airspeed (Avg True)	Heading (Avg True)	Wind (Avg)	Temp (Avg °C)	Terrain Class.	Wx Class.	Δσ (mean)	u_{RMS} (mean)	RMS Δσ	RMS u_{RMS}	RMS @ λ = 2000 ft u_x	RMS @ λ = 2000 ft u_y	RMS @ λ = 2000 ft u_z	RMS @ λ = λ max u_x	RMS @ λ = λ max u_y	RMS @ λ = λ max u_z	λ max
				hr:min:sec	sec	nmi	feet	knots	degrees	deg/kt	°C			fps	fps	fps	fps	fps	fps	fps	fps	fps	fps	ft
Christchurch	7-11-66	96	1St	08:18:38	289	80E 109N 66E 80N	62,300	435	221	246 / 33	-54.2	W	M	+ .18 - .27	+ 3.2 - 4.8	.043	0.75							
Laverton	7-19-66	99	2L	02:14:37	83		50,300		275			F	L	+ .16 - .13	+ 2.8 - 2.3	.044	0.75							
			3T	03:46:22	44		55,300					F	M	+ .21 - .27	+ 3.8 - 4.8	.069	1.23							
Laverton	7-21-66	100	2L	01:11:29	897	72E 39N 70E 44N	50,400	402	351	298 / 52	-66.0	F	VL	+ .19 - .22	+ 3.3 - 3.9	.031	0.54							
			3L	01:42:34	89	72E 42N 72E 43N	50,500	400	191	286 / 73	-66.4	F	M	+ .23 - .31	+ 4.1 - 5.8	.051	0.90	0.94	1.54	1.39	0.54	1.54	1.39	2
			4L	01:52:03	461	71E 39N 70E 39N	50,600	404	189	286 / 63	-65.4	F	L	+ .22 - .22	+ 3.9 - 3.8	.035	0.61							
			5L	02:09:03	264	101E 38N 76E 39N	50,400	401	277	252 / 60	-65.8	F	L	+ .19 - .14	+ 3.2 - 2.4	.036	0.61	0.96	1.07	0.98	0.61	1.23	1.14	4
			6L	02:15:39	543	65E 37N 14E 37N	50,400	402	270	259 / 58	-65.4	F	M	+ .38 - .42	+ 6.6 - 7.1	.049	0.83	0.84	1.35	1.36	1.1	2.3[illegible]	[illegible].31	10
			7L	02:31:29	899	15E 39N 123E 39N	50,700	404	269	250 / 26	-65.7	F	IM	+ .33 - .24	+ 4.9 - 3.6	.039	0.65	0.72	1.05	1.10	1.00 - .19	1.53 1.22	1.77 2.30	88 0 in
Laverton	7-26-66	101	7L	01:29:19	103	221W 45N 226W 46N	59,500		326			F	M	+ .26 - .20	+ 4.9 - 3.7	.063	1.20							
			3L	01:38:55	119	278W 51N 258W 52N	61,800		325			F	IM	+ .25 - .20	+ 5.2 - 4.2	.052	1.10							
			4L	01:55:15	179	259W 51N 264W 49N	60,600		153			F	L	+ .13 - .13	+ 2.6 - 2.7	.040	0.80							
			5L	02:25:33	54	31E 41N 31E 40N	49,400		198			F	L	+ .11 - .20	+ 1.8 - 3.2	.066	1.05							
			6C	02:33:07	25	28E 36N 27E 36N	51,000		737			F	M	+ .35 - .26	+ 5.7 - 4.0	.078	1.22							
			7T	03:07:59	260	16E 12N 13E 9N	54,900		187			F	L	+ .26 - .20	+ 3.9 - 3.1	.049	0.74							
Laverton	7-28-66	102	2L	02:51:37	239	44E 61N 46E 59N	59,600	407	126	075 / 13	-62.2	H	M	+ .33 - .31	+ 6.7 - 6.4	.087	1.79	2.04	2.48	2.36	2.52	3.64	2.81	4
			3L	02:16:37	169	46E 59N 48E 58N	59,800	407	124	091 / 16	-63.8	W	M	+ .40 - .25	+ 8.2 - 5.2	.072	1.48	1.62	1.75	1.68	2.17	2.27	2.13	4
			4D	01:13:32	69	50E 57N 50E 57N	60,200		303			W	M	+ .29 - .22	+ 5.9 - 4.3	.058	1.16							
			5L	03:15:17	629	49E 58N 44E 61N	60,200	398	296	263 / 37	-64.4	W	M	+ .31 - .44	+ 6.5 - 9.3	.068	1.42	1.66	2.09	1.91	2.68	4.98	3.06	10
			6L	03:33:35	124	44E 61N 42E 57N	59,800	392	176	216 / 25	-63.4	H	VL	+ .16 - .13	+ 3.1 - 2.7	.038	0.81	1.16	1.38	1.23	1.16	1.38	1.23	2
			7T	03:35:17	114	42E 57N 43E 56N	59,700					H	L	+ .20 - .19	+ 4.3 - 4.1	.041	0.89							
			8L	03:39:47	353	44E 57N 45E 61N	60,700	410	018	316 / 25	-63.6	W	M	+ .40 - .34	+ 7.9 - 6.7	.075	1.48	1.77	2.01	2.07	2.19	2.55	2.73	4
			9L	04:03:37	274	46E 61N 43E 52N	60,200	398	198	296 / 17	-64.2	W-H	M	+ .46 - .47	+ 9.3 - 9.6	.062	1.24	1.35	1.76	1.74	2.23 2.48	3.23 3.53	1.28 4.09	10 40
			10T	04:20:42	128	43E 50N 42E 49N	58,700		193			H	M	+ .38 - .41	+ 7.1 - 7.7	.095	1.76							
			11T	04:25:47	53	42E 47N 42E 46N	54,200		197			H	L	+ .23 - .20	+ 4.1 - 3.5	.052	0.91							
			12L	04:39:57	648	40E 38N 35E 30N	63,400	428	210	236 / 33	-59.1	H	M	+ .45 - .43	+ 8.4 - 8.3	.059	1.13	1.30	1.57	1.47	2.39	3.57	2.83	10

(f) - Ferry Flight

Flight Path
L - Level C - Climb
T - Turn D - Descent

M - Mountains (h>2500 ft)
H - Hills (500 ft<h<2500 ft)
F - Flat Lands (h<500 ft)
W - Water

VL - Very Light
L - Light
LM - Light to Moderate
M - Moderate

* 500 knots

BASE	DATE	TEST	RUN	START TIME (GMT)	RUN LENGTH	LOCATION (Start x,y) (End x,y)	ALTITUDE (Avg)	AIRSPEED (Avg True)	HEADING (Avg True)	WIND (Avg)	TEMP (Avg)	TERRAIN CLASS	TURB CLASS	ΔG (max)	U_{DE} (max)	RMS ΔG	RMS U_{DE}	RMS @ λ = 2000 ft U_V	U_L	U_P	RMS @ λ = λ max U_V	U_L	U_P	λ max
				hr:min:sec	sec	nmi	feet	knots	degrees	deg/kt	°C			g	fps	g	fps	fps	fps	fps	fps	fps	fps	k ft
Laverton	7-28-66	102	13L	05:02:37	149	326E 256N 319E 242N	66,300	431	209	240 / 34	-61.9	F	L	+ .20 - .17	+ 4.0 - 3.4	.050	0.98	1.25	1.61	1.44	2.21	3.07	2.39	10
			14L	05:07:12	71	313E 229N 310E 222N	66,000	416	209	270 / 36	-60.1	F	LM	+ .29 - .23	+ 5.9 - 4.7	.058	1.16	1.32	1.74	1.60	1.82	1.74	1.66	2
			15L	05:15:42	524	276E 190N 233E 149N	65,100	430	228	275 / 28	-58.4	M	L	+ .21 - .25	+ 4.1 - 4.7	.046	0.92	0.97	1.29	1.23	1.35	1.77	1.62	4
			16L	05:28:12	109	215E 130N 209E 123N	65,000	425	236	279 / 34	-57.9	M	M	+ .34 - .48	+ 7.0 - 9.3	.118	2.27	2.36	2.38	2.42	3.86	3.37	3.17	4
Laverton	7-29-66	103	2C	00:21:00	119	193E 84N 207E 88N	62,500	449	073	060 / 23	-64.6	M	L	+ .15 - .18	+ 3.3 - 3.9	.044	0.94							
			3L	00:33:25	64	274E 115N 279E 122N	62,200		033			M	L	+ .14 - .14	+ 3.3 - 3.4	.046	1.08							
			4L	01:28:20	999	410E 455N 430E 564N	58,600	425	008	337 / 29	-67.6	M	M	+ .49 - .59	+ 9.8 - 11.8	.072	1.41							
			5L	01:54:15	979	424E 585N 412E 480N	58,300	421	159	219 / 31	-67.1	M	M											
			6L	02:33:55	419	410E 494N 454E 485N	58,300	419	106	098 / 14	-67.7	M-H-F-M	M	+ .35 - .32	+ 6.9 - 6.2	.054	1.03							
			7L	02:51:55	529	459E 490N 408E 507N	58,200	416	246	280 / 46	-67.7	H	LM	+ .29 - .30	+ 5.5 - 5.7	.059	1.12							
			8C	03:11:40	74	422E 494N 430E 494N	60,400		118			H	L	+ .22 - .22	+ 3.9 - 4.0	.060	1.09							
			9D	04:43:55	59	90E 37N 84E 33N	54,500		237			M	M	+ .23 - .24	+ 3.4 - 3.6	.066	0.97							
Laverton	8-02-66	104	2L	04:06:32	809	228E 87N 138E 46N	55,800		245			M	M	+ .38 - .37	+ 6.3 - 6.0	.050	0.84							
			4C	04:33:37	45	61E 12N 56E 10N	47,500		254			M	VL	+ .13 - .09	+ 1.6 - 1.2	.034	0.46							
Laverton	8-03-66	105	2L	00:11:20	84	192E 63N 203E 71N	57,200		034			M	L	+ .14 - .13	+ 2.6 - 2.7	.045	0.82							
			3L	00:43:00	189	269E 159N 284E 172N	53,700		038			M	L	+ .18 - .16	+ 3.1 - 2.7	.033	0.56							
			4L	02:55:50	89	14E 302N 4E 291N	50,700		191			H	L	+ .09 - .12	+ 1.3 - 1.8	.030	0.45							
Laverton	8-05-66	106	2L	02:48:12	17	6E 353N 6E 351N	51,700		187			H	M	+ .21 - .24	+ 3.6 - 4.0	.064	1.10							
			3C	04:11:27	17		53,800		243			M	VL	+ .05 - .06	+ 0.8 - 1.0	.023	0.37							
Laverton	8-08-66	107	2C	23:44:15	49	24E 50N 26E 56N	48,200		004			H	M	+ .40 - .27	+ 8.0 - 5.4	.088	1.77							
			3L	23:45:10	359	26E 57N 27E 96N	49,300	376	356	243 / 45	-58.9	F	LM	+ .23 - .19	+ 4.7 - 3.9	.037	0.76	0.76	1.05	0.99	0.86	1.25	1.19	4
			4L	00:04:40	110	29E 185N 30E 197N	49,300	384	357	241 / 51	-59.0	F	LM	+ .24 - .21	+ 4.7 - 4.2	.047	0.93	1.00	1.62	1.14	1.00	1.62	1.14	2
			5L	00:20:45	54	29E 210N 30E 205N	49,500		185			F	L	+ .13 - .13	+ 2.4 - 2.6	.036	0.74							
			6L	00:29:25	959	28E 156N 20E 61N	49,300	382	187	245 / 52	-58.3	F	LM	+ .40 - .36	+ 7.6 - 6.8	.050	0.95	0.98	1.24	1.06	1.86 1.35	1.66 2.08	1.69 1.82	20 *40
			7L	00:50:00	529	43E 54N 92E 95N	49,800	394	050	224 / 46	-59.2	H	LM	+ .29 - .26	+ 5.4 - 4.8	.047	0.86	0.84	1.99	0.90	1.11	3.03	1.37	10

(f) - Ferry Flight

Flight Path
L - Level, T - Turn, C - Climb, D - Descent

M - Mountains (h>2500 ft)
H - Hills (500 ft<h<2500 ft)
F - Flat Lands (h<500 ft)
W - Water

VL - Very Light
L - Light
LM - Light to Moderate
M - Moderate

* 500 Legs

BASE	DATE	TEST	RUN	START TIME (GMT)	RUN LENGTH	LOCATION (Start x_E,y_N) (End x_E,y_N)	ALTITUDE (Avg)	AIRSPEED (Avg True)	HEADING (Avg True)	WIND (Avg)	TEMP (Avg)	TURBULENCE CLASS.	TYPE CLASS.	ΔG (max)	Σ_{RMS} (max)	RMS ΔG	RMS Σ_{RMS}	RMS @ λ - 2000 ft Σ_y	Σ_L	Σ_y	RMS @ λ - λ_{max} Σ_y	Σ_L	Σ_y	λ_{max}
				hr-min-sec	sec	feet	feet	knots	degrees	deg/kt	°C			g	rms	g	rms	rms	rms	rms	rms	rms	rms	λ ft.
Laverton	8-08-66	107	8L	01:01:10	959	68E 104N 4E 104S	49,200	387	270	258 / 49	-58.9	F	M	+ .48 - .48	+ 7.8 - 9.0	.061	1.14	1.07	1.63	1.30	1.44	2.64	2.17	44
			9L	01:17:15	484	68E 104N 20E 104S	50,000	386	267	253 / 69	-58.7	F	M	+ .34 - .34	+ 6.2 - 6.3	.056	1.08	1.08	1.42	1.51	1.40	2.09	2.67	11
			10L	01:31:30	489	68E 104N 4E 104S	49,200	388	094	254 / 59	-58.1	F	M	+ .37 - .39	+ 5.5 - 7.4	.055	1.00	1.10	1.58	1.33	1.45	2.41	2.19	11
			11L	01:45:05	879	52E 104N 16E 104S	49,400	389	092	261 / 43	-59.1	M	M	+ .37 - .23	+ 6.5 - 4.0	.045	0.79	0.89	1.40	1.00	1.08	1.99	1.35	22
			12C	08:01:55	29	177E 100N 180E 100S	52,300		102			M	L	+ .25 - .16	+ 5.0 - 2.8	.062	1.08							
			13L	08:32:00	629	18E 104N 20E 104S	53,100	410	270	264 / 47	-58.3	F	L	+ .29 - .22	+ 4.7 - 3.7	.040	0.66	0.63	0.96	0.87	0.98	1.37	1.35	10
			14L	08:49:15	670	44E 104N 46E 104S	51,800	408	089	274 / 45	-59.2	F	LM	+ .38 - .37	+ 6.2 - 5.2	.044	0.74	0.74	1.06	0.83	1.08	1.56	1.35	10
			15L	03:17:10	349	27E 136N 27E 163N	51,800	412	355	245 / 44	-60.3	F	L	+ .18 - .14	+ 2.8 - 2.3	.029	0.62	0.60	0.89	0.74	0.69	1.07	0.91	1
			16L	03:24:40	339	28E 179N 28E 216N	51,800	404	357	227 / 50	-60.0	F	VL	+ .21 - .21	+ 3.5 - 3.4	.041	0.67	0.55	0.87	0.73	0.65	1.12	0.91	1
			17L	03:57:40	484	28E 197N 28E 150S	51,800	403	188	269 / 56	-59.1	F	M	+ .55 - .55	+ 6.7 - 7.1	.058	0.91	0.97	1.35	1.11	1.30	1.56	1.68	10
			18L	04:07:00	989	24E 241N 24E 38N	51,500	407	189	273 / 64	-58.1	F	L	+ .23 - .24	+ 3.5 - 3.9	.038	0.59	0.66	1.13	0.95	0.89 0.90	1.72 1.87	1.43 1.96	22 880
Laverton	8-09-66	108	2L	03:23:10	65	190E 118N 190E 115N	50,500		285			M	L	+ .15 - .14	+ 2.2 - 2.1	.041	0.62							
			3L	03:40:50	9	101E [illegible] 98E 146N	50,400		287			M	L	+ .18 - .12	+ 2.8 - 1.9	.038	0.59							
			4L	04:01:35	679	6W 174N 66W 165N	50,300		260			F	L	+ .14 - .15	+ 2.1 - 2.3	.033	0.50							
Laverton	8-11-66	109	2L	00:29:45	40		52,400					M	LM											
			3L	00:58:00	740		52,200					M	LM											
			4L	01:20:20	55		53,400					M	L											
			5L	01:40:30	60		50,400					M	L											
			6L	01:49:50	190		57,400					M	L											
			7L	02:05:30	120		58,600					M	M											
			8L	03:22:00	180		50,400					F	L											
			9L	03:28:00	180		54,600					F	L											
Laverton	8-13-66	110 (f)	2L	23:31:55	23	215E 197N 214E 198N	58,700		068				M	+ .16 - .12	+ 3.3 - 3.6	.058	1.19							
Edwards	8-29-66	114	2L	17:45:55	84	59W 157N 50W 160N	55,800		064			M	VL	+ .12 - .11	+ 2.3 - 2.0	.038	0.64							
			3L	17:48:10	874	39W 165N 10W 181N	54,700	416	063	188 / 28	-57.6	M	M	+ .43 - .28	+ 7.9 - 4.5	.045	0.85							
			4C	17:55:30	64	1W 197N 2E 207S	54,600					M	L	- .14 - .16	+ 2.6 - 3.0	.046	0.85							

(f) - Ferry Flight

Flight Path
L - Level C - Climb
T - Turn D - Descent

M - Mountains (h>2500 ft)
H - Hills (500 ft<h<2500 ft)
F - Flat Lands (h<500 ft)
W - Water

VL - Very Light
L - Light
LM - Light to Moderate
M - Moderate

* 500 Legs

BASE	DATE	TEST	RUN	START TIME (GMT)	RUN LENGTH	LOCATION (Start x,y) (End x,y)	ALTITUDE (Avg)	AIRSPEED (Avg True)	HEADING (Avg True)	WIND (Avg)	TEMP (Avg)	TERRAIN CLASS.	TURB CLASS.	ΔG (max)	U_{DE} (max)	RMS ΔG	RMS U_{DE}	RMS @ λ = 2000 ft U_T	RMS @ λ = 2000 ft U_L	RMS @ λ = 2000 ft U_V	RMS @ λ = λ max U_T	RMS @ λ = λ max U_L	RMS @ λ = λ max U_V	RMS @ λ = λ max λ max
				hr:min:sec	sec	nmi	feet	knots	degrees	deg/kt	°C			g	fps	g	fps	fps	fps	fps	fps	fps	fps	ft
Edwards	8-29-66	114	5L	18:00:55	439	[illegible]	54,600	415	242	203 / 11	-58.3	M	IM	+ .26 - .25	+ 4.7 - 4.6	.046	0.84							
			6L	18:11:40	389	[illegible]	54,900	~32	027	230 / 20	-59.0	M	IM	+ .24 - .27	+10.1 - 5.0	.049	0.92							
			7L	18:23:05	464	[illegible]	55,100	420	272	243 / 19	-58.3	M	IM	+ .14 - .38	+ 7.9 -10.5	.049	0.88							
			8L	18:36:20	519	[illegible]	54,800	420	347	211 / 22	-57.8	M	IM	+ .28 - .33	+ 5.6 - 9.4	.051	0.91							
			9L	18:48:40	69	[illegible]	56,800		015			M	L	+ .33 - .12	+ 6.0 - 3.4	.066	1.20							
			10L	18:53:00	839	[illegible]	56,800	425	271	237 / 22	-57.7	M	IM	+ .22 - .27	+ 5.0 - 4.6	.050	0.88	0.67 1.78	1.01 3.11	0.61 2.39	1.59 1.78	2.30 3.11	1.68 2.39	20 est.
			11L	19:12:00	704	[illegible]	56,700	428	347	239 / 26	-57.7	M	L	+ .22 - .22	+ 3.8 - 3.9	.045	0.78	0.63	1.01	0.63	1.18	1.81	1.36	10
			12L	19:27:25	174	[illegible]	56,700	413	151	239 / 25	-57.8	M	L	+ .29 - .17	+ 5.1 - 3.1	.053	0.94	0.83	1.34	0.69	1.17	1.61	0.91	4
			13L	19:36:20	339	[illegible]	56,660	430	260	239 / 23	-57.6	M	IM	+ .33 - .33	+ 5.6 - 5.6	.060	1.07	0.81	1.11	0.68	1.17	1.60	0.96	4
			14L	19:55:00	599	[illegible]	56,700	429	359	212 / 10	-57.8	M	IM	+ .28 - .33	+ 4.6 - 5.6	.045	0.75	0.64	0.83	0.57	2.04	1.88	1.37	10
			15L	20:27:45	479	[illegible]	53,300	395	152	212 / 26	-59.5	M	M	+ .29 - .26	+ 4.9 - 4.5	.066	1.13							
			16L	20:42:20	99	[illegible]	52,900		147			M	M	+ .28 - .26	+ 4.7 - 4.4	.078	1.31							
			17L	20:45:20	119	[illegible]	54,100	403	149	225 / 18	-60.1	M	M	+ .20 - .26	+ 3.4 - 4.3	.051	0.85							
			18L	20:52:00	69	[illegible]	54,200		239			M	L	+ .18 - .12	+ 3.1 - 2.0	.052	0.88							
			20L	21:03:50	69	[illegible]	49,200		269			M	M	+ .30 - .28	+ 5.1 - 4.8	.077	1.33							
Edwards	8-31-66	115	2L	17:31:00	160							M	M											
			3L	17:39:15	75							M	L											
			4L	17:50:05	65							M	L											
			5L	18:25:10	335							M	L											
			6L	18:59:15	110							M	L											
			7L	19:57:50	70							M	L											
			9L	20:40:30	615							M	L											
Edwards	8-31-66	116	2L	17:59:47	194	[illegible]	49,800		339			M	L	+ .12 - .12	+ 2.4 - 2.0	.085	0.98							
Edwards	9-19-66	120 (f)	2L	16:37:15	419	[illegible]	48,500		084				IM											
			3L	16:40:40	699	[illegible]	49,100		084				IM											
			4L	16:56:10	264	[illegible]	48,900		083				L											
			5T	19:59:10	285								IM											

(f) - Ferry Flight

Flight Path
L - Level C - Climb
T - Turn D - Descent

M - Mountains (h>2500 ft)
H - Hills (500 ft<h<2500 ft)
F - Flat Lands (h<500 ft)
W - Water

VL - Very Light
L - Light
LM - Light to Moderate
M - Moderate

* 500 Legs

Appendix I

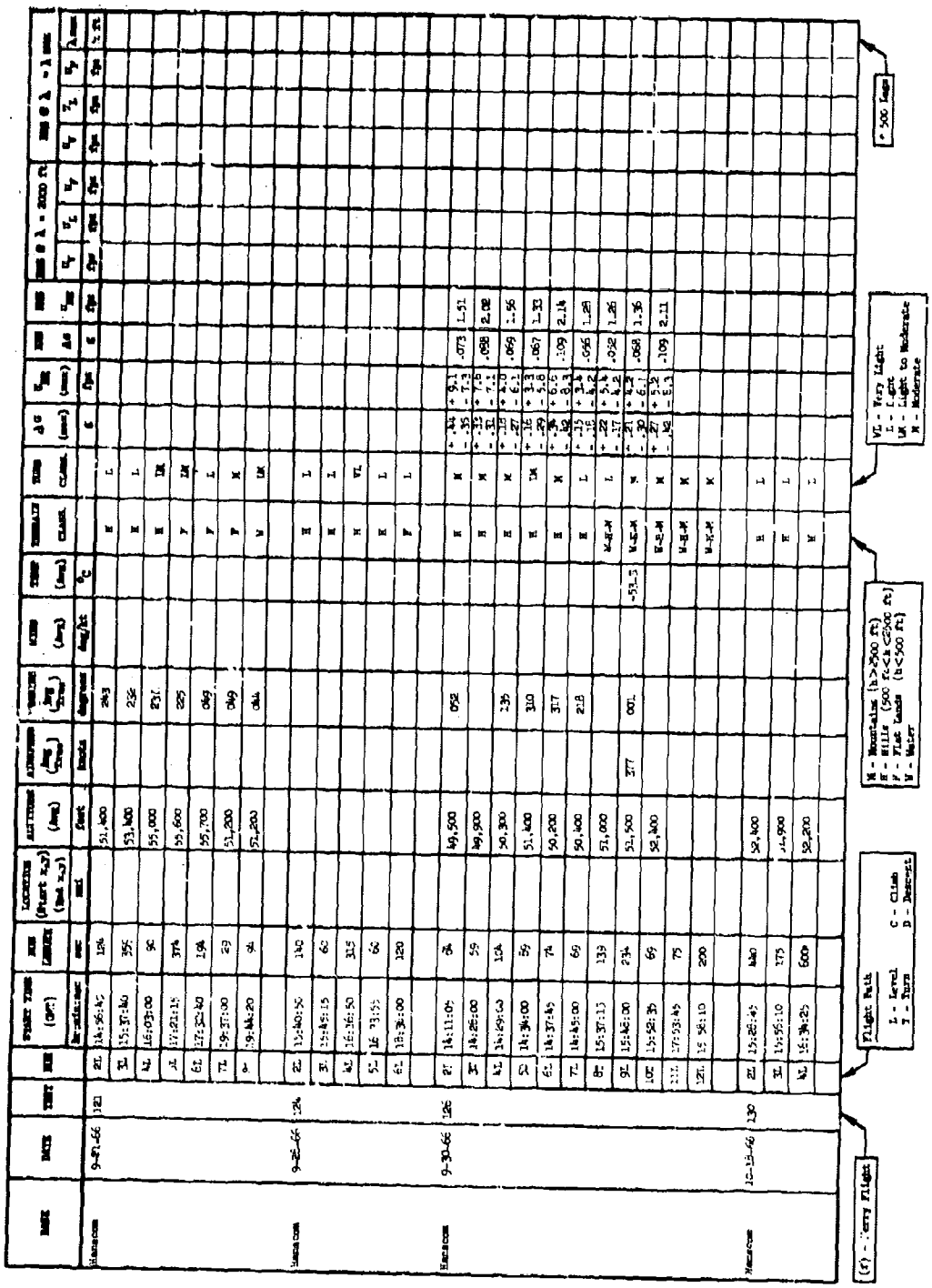

MAKE	DATE	TEST	RUN	START TIME (GMT)	RUN LENGTH	LOCATION (Start x_s,y) (End x_e,y)	ALTITUDE (msl)	AIRSPEED (Avg True)	HEADING (Avg True)	WIND (Avg)	TEMP (Avg)	TERRAIN CLASS.	TURB CLASS.	ΔG (max)	U_{DE} (max)	RMS ΔG	RMS U_{DE}	RMS @ λ - 2000 ft: U_V	U_L	U_T	RMS @ λ - λ_{max}: U_V	U_L	U_T	λ max
				hr:min:sec	sec	nmi	feet	knots	degrees	deg/kt	°C			g	fps	g	fps	fps	fps	fps	fps	fps	fps	ft
Hanscom	10-20-66	131	2C	14:51:50	55							H	L											
			3L	15:25:10	135		56,900					M	LM											
			4T	19:15:40	230		58,900					M	LM											
Hanscom	10-21-66	132	2L	14:31:20	239		59,600		214			W	L	+ .14 - .15	+ 2.4 - 2.7	.038	0.68							
			3L	15:16:50	133		51,600		221			P	L	+ .23 - .31	+ 4.1 - 5.4	.058	1.02							
Hanscom	10-24-66	133	2L	14:40:20	139	7W 19N / 88W 19N	55,600		269			M	M	+ .30 - .26	+ 7.9 - 6.9	.085	2.27							
			3L	14:44:50	514	100W 19N / 90W 33N	54,300	398	303		-67.9	M	L	+ .15 - .20	+ 3.9 - 5.3	.050	1.37							
			4L	15:12:10	484	3W 68N / 42W 108N	54,200	417	298	296 / 61	-62.4	M	L	+ .16 - .20	+ 4.6 - 5.1	.044	1.09							
			5L	15:25:00	724	39W 88N / 15W 14N	54,200	429	169	197 / 45	-61.9	M	LM	+ .31 - .35	+ 7.2 - 8.3	.045	1.46							
			6L	15:47:45	139	19W 128N / 24W 27N	54,400		339			M	LM	+ .14 - .18	+ 3.2 - 4.3	.050	1.16							
			7L	15:56:25	164	55W 63N / 40W 80N	54,100		336			M	LM	+ .25 - .19	+ 5.7 - 4.5	.054	1.24							
			8L	16:01:50	64	45W 96N / 17W 103N	54,100		333			M	L	+ .10 - .15	+ 2.4 - 3.6	.038	0.87							
			9L	16:09:35	269	21W 100N / 5W 94N	54,800	428	117	154 / 54	-64.7	M	L	+ .31 - .17	+ 7.1 - 3.9	.062	0.98							
			10L	16:17:10	119	81W 63N / 26W 73N	54,200		163			M	L	+ .12 - .18	+ 2.8 - 4.1	.038	0.87							
			11L	16:24:35	179	11W 55N / 4W 48N	54,200		247			M	L	+ .19 - .20	+ 3.0 - 4.5	.036	0.83							
			12L	16:37:40	174	56W 30N / 17W 27N	54,200		254			M	VL											
Hanscom	10-25-66	134	2L	14:08:22	99	16W 33N / 16W 44N	57,100		000			M	L	+ .16 - .19	+ 3.1 - 3.6	.058	1.00							
			3L	14:21:25	125		58,600		007			M	L	+ .16 - .18	+ 3.2 - 3.6	.057	1.13							
Hanscom	10-27-66	136	2L	14:27:10	670		52,400					W	VL											
			3L	15:26:10	145		52,400					W	L											
			4L	15:39:45	170		53,400					W	L											
Hanscom	10-28-66	137	2L	15:54:50	19	18W 156N / 18W 158N	52,400		348			M	M	+ .13 - .19	+ 1.7 - 2.5	.049	0.64							
			3L	16:05:15	59	105W 174N / 106W 176N	52,200		179			M	M	+ .22 - .19	+ 2.8 - 2.4	.066	0.83							
Hanscom	10-31-66	138 (C)	2L	16:04:20	124		54,500		218				VL	+ .16 - .12	+ 3.0 - 2.7	.085	0.54							

(f) - Ferry Flight

Flight Path
L - Level C - Climb
T - Turn D - Descent

M - Mountains (h>2500 ft)
H - Hills (500 ft<h<2500 ft)
F - Flat Lands (h<300 ft)
W - Water

VL - Very Light
L - Light
LM - Light to Moderate
M - Moderate

* 500 Legs

Appendix I

BASE	DATE	TEST	RUN	START TIME (GMT)	RUN LENGTH	LOCATION (Start x,y) (End x,y)	ALTITUDE (Avg)	AIRSPEED (Avg True)	HEADING (Avg True)	WIND (Avg)	TEMP (Avg)	TERRAIN CLASS.	TURB CLASS.	Δ (max)	u_{RE} (max)	RMS Δa	RMS u_{RE}	RMS @ λ = 2000 ft u_V	u_L	u_T	RMS @ λ = λ max u_V	u_L	u_T	λ max
				hr:min:sec	sec	nmi	feet	knots	degrees	deg/kt	°C			g	fps	g	fps	fps	fps	fps	fps	fps	fps	k ft
Hanscom	10-31-66	138 (f)	3L	16:23:40	99		58,000		286				L	+ .11 / - .11	+ 2.1 / - 2.2	.088	0.56							
			4T	18:31:40	89		53,800						L	- .37 / - ...	1.8 / - 2.2	.049	0.86							
			5L	18:37:50	689		54,100		075				LM	+ .27 / - .23	+ 4.7 / - 4.0	.032	0.56							
			6T	18:51:40	44		55,900						M	+ .21 / - .21	+ 3.6 / - 3.7	.054	0.98							
			7L	18:55:35	719		54,800		252				LM	+ .16 / - .24	+ 2.8 / - 4.1	.027	0.47							
Ramey	11-01-66	140	2L	16:18:35	66	590E 84N / 576E 28N	50,700		313			W	LM	+ .22 / - .22	+ 5.6 / - 5.6									
			3L	16:22:00	60	559E 43N / 525E 46N	50,900		355			W	L	+ .14 / - .14	+ 3.4 / - 3.4									
			4L	16:23:35	420	530E 50N / 520E 91N	50,900	384	353	272 / 30	-72.7	W	LM	+ .13 / - .22	+ 3.2 / - 5.2									
			5L	16:35:15	239	580E 118N / 525E 141N	51,300	384	353	237 / 29	-71.8	W	LM	+ .22 / - .38	+ 5.4 / - 9.3									
			6L	16:47:20	214	538E 136N / 532E 111N	50,900	316	184		-71.6	W	L	+ .16 / - .17	+ 4.0 / - 4.1									
			7L	16:56:00	499	533E 74N / 533E 17N	50,800	313	186	341 / 11	-71.9	W	LM	+ .16 / - .28	+ 3.9 / - 6.9									
			8L	17:06:45	584	523E 12N / 491E 58N	51,000	312	121	178 / 35	-72.1	W	L	+ .14 / - .15	+ 3.4 / - 3.6									
			9L	17:36:00	119	557E 93N / 571E 95N	59,200		086			W	L	+ .12 / - .11	+ 3.0 / - 2.8									
			10L	17:48:35	164	579E 91N / 564E 88N	51,100		267			W	LM	+ .18 / - .17	+ 4.4 / - 4.1									
Ramey	11-07-66	141	2L	18:59:15	90		49,000					W	L											
			3L	19:12:45	125		49,200					W	LM											
Ramey	11-08-66	142	2L	16:18:55	54	589E 106N / 525E 102N	51,300		220			W	L	+ .13 / - .13	+ 2.3 / - 2.3	.035	0.64							
			3L	17:08:35	330	460E 113N / 458E 98N	50,200	372	186	304 / 29	-73.0	W	L	+ .16 / - .14	+ 2.8 / - 2.5	.031	0.55	0.68	1.02	0.39	0.74	1.24	0.48	4
			4L	17:11:25	225	457E 76N / 457E 52N	50,000	376	184	321 / 29	-73.1	W	L	+ .21 / - .30	+ 3.6 / - 5.3	.042	0.74	0.79	1.05	0.41	0.87	1.27	0.55	4
Ramey	11-10-66	144	2L	14:53:35	64	361E 121N / 308E 121N	56,700		090			W	M	+ .27 / - .37	+ 4.4 / - 5.9	.084	1.35							
			3L	15:17:40	239	395E 124N / 360E 123N	56,800	420	272	298 / 55	-73.3	W	L	+ .20 / - .24	+ 3.2 / - 4.0	.044	0.72	0.80	1.11	0.56	1.05	1.47	0.67	1
			4L	15:22:35	39	354E 122N / 346E 122N	57,000		272			W	L	+ .18 / - .13	+ 2.9 / - 2.	.042	0.69							
			5L	15:33:40	29	357E 88N / 360E 86N	57,600		045			W	L	+ .15 / - .15	+ 2.3 / - 2.4	.040	0.63							
			6L	15:38:00	64	373E 86N / 374E 36N	57,000		180			W	L	+ .16 / - .21	+ 2.9 / - 3.4	.047	0.76							
			7L	15:40:50	94	374E 105N / 386E 116N	56,800		182			W	L	+ .14 / - .19	+ 2.3 / - 3.1	.035	0.56							
			8L	15:46:20	44	375E 143N / 375E 148N	57,000		182			W	L	+ .15 / - .14	+ 2.8 / - 2.2	.036	0.57							

(f) - Ferry Flight

Flight Path

L - Level C - Climb
T - Turn D - Descent

M - Mountains (h>2500 ft)
H - Hills (500 ft<h<2500 ft)
F - Flat Lands (h<500 ft)
W - Water

VL - Very Light
L - Light
LM - Light to Moderate
M - Moderate

* 500 Lags

RUN	DATE	TEST	RUN	START TIME (GMT)	RUN LENGTH	LOCATION (Start x_E,y_E) (End x_E,y_E)	ALTITUDE (Avg)	AIRSPEED (Avg True)	HEADING (Avg True)	WIND (Avg)	TEMP (Avg)	TERRAIN CLASS.	TURB CLASS.	ΔG (max)	U_{DE} (max)	RMS ΔG	RMS U_{DE}	RMS @ λ = 2000 ft: U_T	U_L	U_F	RMS @ λ = λ_{max}: U_T	U_L	U_F	λ_{max}
				hr:min:sec	sec	nmi	feet	knots	degrees	deg/kt	°C			g	fps	g	fps	fps	fps	fps	fps	fps	fps	k ft
Runway	11-10-66	144	9L	16:05:20	643	375E 125N 364E 97N	57,400	410	356	332 / 29	-72.1	W	L	+ .19 - .18	+ 3.0 - 2.9	.030	0.47							
			10L	16:21:35	124	373E 96N 372E 86N	57,900	406	179	189 / 25	-74.0	W	L	+ .17 - .20	+ 2.6 - 3.1	.038	0.60							
			11L	16:51:40	29	376E 57N 375E 53N	57,900					W	M	+ .25 - .40	+ 3.9 - 6.2	.096	1.50							
Runway	11-15-66	146	2L	15:20:57	79	318E 188N 316E 154N	49,800		164			W	L	+ .15 - .14	+ 2.6 - 2.3	.037	0.63							
			3L	16:20:42	359	366E 254N 366E 221N	51,700	368	357	080 / 6	-81.3	W	L	+ .20 - .22	+ 3.3 - 3.6	.036	0.61							
			4L	16:28:52	94	366E 209N 365E 195N	51,700		357			W	L	+ .13 - .12	+ 2.1 - 3.0	.033	0.56							
			5C	16:32:17	64	365E 189N 365E 177N	52,400		357			W	L	+ .09 - .16	+ 1.5 - 3.0	.031	0.52							
			6L	16:45:12	139	366E 189N 366E 255N	51,600	357	182	353 / 9	-80.9	W	L	+ .25 - .17	+ 4.1 - 3.0	.037	0.63							
			7L	17:02:57	214	371E 204N 357E 231N	52,000		315			W-E	DR	+ .26 - .36	+ 4.0 - 5.0	.045	0.77							
			8L	17:25:37	383	401E 213N 346E 213N	51,600	357	086	048 / 29	-80.2	W	VL	+ .13 - .16	+ 2.1 - 2.6	.031	0.52							
			9L	17:51:32	428	401E 204N 362E 221N	51,500	357	269	201 / 27	-77.1	W	DR	+ .45 - .33	+ 7.3 - 5.4	.043	0.71							
			10L	17:57:40	75								L											
Runway	12-16-66	147	2C	15:13:15	740	14[illegible] 211N 147E 236N	48,100	362	011		-66.4	W	L	+ .29 - .27	+ 5.5 - 5.1	.051	0.98							
			3L	15:17:15	325	137E 236N 127E 217N	48,700	356	010	220 / 73	-65.5	W	M	+ .49 - .53	+ 7.8 - 9.8	.094	1.75	1.44		0.62	1.57		0.76	4
			4L	15:38:10	255	111E 205N 100E 181N	48,800	346	198	298 / 92	-67.6	W	M	+ .42 - .36	+ 7.9 - 7.3	.100	1.90	1.68		0.68	1.79		0.89	4
			5L	15:48:15	230	99E 178N 107E 165N	48,800	350	287	194 / 23	-67.2	W	M	+ .46 - .35	+ 9.1 - 6.4	.093	1.71	1.66		0.71	1.78		0.81	4
			6L	15:58:27	43	121E 165N 125E 165N	48,500		292			W	M	+ .62 - .53	+ 12.2 - 10.4	.150	2.90							
			7L	16:01:20	140	129E 167N 119E 167N	48,500	333	115	[illegible]	-67.2	W	M	+ .36 - .28	+ 6.3 - 5.6	.081	1.59	1.70		0.85	1.91		1.07	4
			8L	15:11:35	297	100N 264E 100N 276E	45,600	389	250		-69.3	W	M	+ .28 - .29	+ 5.6 - 5.7	.066	1.36	1.42		0.64	1.60		0.76	4
Runway	11-21-66	144	1C	16:01:57	83	286E 70N 286E 71N	55,500		011			W	VL	+ .05 - .05	+ 0.8 - 0.8	.018	0.27							
			3L	16:10:07	89	279E 72N 278E 72N	50,900		296			W	L	+ .12 - .11	+ 1.7 - 1.7	.038	0.59							
			4L	16:18:37	364	252E 77N 210E 77N	56,500		253			W	VL											
Runway	11-23-66	151	3L	15:37:35	52		54,000					W	M	+ .53 - .20	+ 9.1 - 3.4	.090	1.37							
			4L	15:57:17	224		53,900	417			-74.0	W	M	+ .47 - .45	+ 8.2 - 7.8	.088	1.46							
			5L	15:26:45	144		53,900	421			-72.3	W	L	+ .29 - .25	+ 4.9 - 4.3	.073	1.28							
			6L	15:35:75	34		53,700	480			-74.3	W	VL	+ .36 - .09	+ 1.4 - 1.6	.089	0.36							

(f) - Every Flight

C - Climb
D - Descent

M - Mountains (h>2500 ft)
H - Hills (500 ft<h<=2500 ft)
F - Flat Land. (h<500 ft)
W - Water

VL - Very Light
L - Light
DR - Light to Moderate
M - Moderate

* 500 Legs

RUN	DATE	TEST	RUN	START TIME (GMT)	RUN LENGTH	LOCATION (Start x,y) (End x,y)	ALTITUDE (Avg)	AIRSPEED (Avg True)	HEADING (Avg True)	WIND (Avg)	TEMP (Avg)	TURBULENCE CLASS.	TURB CLASS.	Δz (max)	U_{RMS} (rms)	RMS $\Delta\Omega$	RMS V_{RMS}	RMS @ λ = 2000 ft			RMS @ λ = λ_{max}			
																		σ_V	σ_L	σ_T	σ_V	σ_L	σ_T	λ_{max}
				hr:min:sec	sec	nmi	feet	knots	degrees	deg/kt	°C			g	fps	g	fps	fps	fps	fps	fps	fps	fps	k ft
Kenny	11-23-66	157	7L	15:59:55	419		54,300	418			-70.7	V	M	+ .50 - .24	+8.4 - 9.0	.111	1.85							
			8L	16:07:20	359		54,100	418			-74.8	V	M	+ .61 - .36	+10.1 - 6.4	.091	1.51							
			9L	16:27:25	624		54,100	408			-77.0	V	M	+ .43 - .41	+ 7.2 - 7.0	.082	1.39							
			10L	16:51:30	124		59,400	456			-72.8	V	LM	+ .36 - .33	+ 3.8 - 5.7	.063	1.08							
			11L	17:01:25	74		59,400					V	M	+ .30 - .27	+ 4.9 - 4.4	.075	1.28							
			12L	17:06:40	134		60,600	460			-73.8	V	VL	+ .20 - .38	+ 3.2 - 6.0	.058	0.90							
Kenny	11-24-66	159	2L	14:27:00	930		57,100					V	L	+ .12 - .17	+ 2.4 - 3.3	.064	0.54							
			3L	14:54:00	500		54,900					V	VL	+ .08 - .09	+ 1.3 - 1.3	.033	0.52							
			4L	15:07:55	75		53,800					V	L	+ .36 - .20	+ 3.7 - 3.0	.053	0.81							
			5L	17:22:25	125		53,100					V	VL											
Kenny	12-01-66	155 (f)	2L	13:05:47	105		53,900						M	+ .60 - .52	+12.6 -10.9	.105	2.19							
			3L	13:23:52	105		49,500						LM	+ .31 - .27	+ 4.9 - 4.2	.087	1.35							
			4L	13:35:57	303		55,200	477			-80.5		LM	+ .29 - .23	+ 4.5 - 3.7	.058	0.90							
			5L	13:52:17	103		55,500	477			-81.1		L	+ .21 - .28	+ 3.2 - 4.3	.064	0.99							
			6L	14:03:35	300		55,200						M	+ .28 - .36	+ 4.2 - 5.3	.077	1.19							
Patrick	12-02-66	156 (f)	2L	17:50:45	114		60,900						VL	+ .18 - .17	+ 2.0 - 2.0	.057	0.55							
			3L	18:06:45	26		62,200						VL	+ .08 - .09	+ 0.9 - 1.4	.036	0.41							
			4L	18:12:35	149		61,300						VL	+ .17 - .26	+ 3.5 - 3.0	.051	0.61							
			5L	18:21:35	599		62,300						L	+ .26 - .29	+ 2.9 - 3.4	.056	0.63							
			6L	18:38:20	519		62,300						LM	+ .26 - .27	+ 3.1 - 4.1	.053	0.56							
Edwards	1-04-67	160	2L	21:44:40	360							F	LM											
Eisendorf	1-15-67	164	2L	23:06:35	169	37N6 22E5 36N4 23E6	51,900		160			W	VL	+ .15 - .08	+ 1.7 - 2.1	.038	0.66							
			3L	23:13:05	354	35N4 23E6 35N1 23E8	50,600	404	190		-47.8	W	L	+ .24 - .30	+ 4.3 - 5.1	.057	1.02							
			4L	23:20:20	214	35N4 23E7 35N6 23E5	51,200	375	193	260 / 30	-48.0	M	M	+ .29 - .37	+ 5.8 - 7.4	.070	1.42	1.44	1.96	1.48	1.62	2.50	1.78	4
			5L	23:29:55	319	35N6 23E5 36N 23E6	51,100	401	000	260 / 44	-47.8	M	LM	+ .23 - .28	+ 4.3 - 5.1	.053	0.95	0.93	1.48	1.06	1.16	1.82	1.32	4

(f) - Ferry Flight

Flight Path
L - Level C - Climb
T - Turn D - Descent

M - Mountains (h>2500 ft)
H - Hills (500 ft<h<2500 ft)
F - Flat Lands (h<500 ft)
W - Water

VL - Very Light
L - Light
LM - Light to Moderate
M - Moderate

* 500 Legs

RACE	DATE	TEST	RUN	START TIME (GMT)	RUN LENGTH	LOCATION (Start x,y) (End x,y)	ALTITUDE (Avg)	AIRSPEED (Avg True)	HEADING (Avg True)	WIND (Avg)	TEMP (Avg)	TERRAIN CLASS.	TURB CLASS.	ΔG (max)	U_{DE} (max)	RMS ΔG	RMS U_{DE}	RMS @ λ = 2000 ft U_V	RMS @ λ = 2000 ft U_L	RMS @ λ = 2000 ft U_F	RMS @ λ = λ max U_V	RMS @ λ = λ max U_L	RMS @ λ = λ max U_F	RMS @ λ = λ max λ max
				hr:min:sec	sec	nmi	feet	knots	degrees	deg/sec	°C			g	fps	g	fps	fps	fps	fps	fps	fps	fps	λ ft
Elsenhorf	1-18-67	184	6L	23:54:15	509	339W 268S 333W 298S	51,200	408	094		-47.4	M	M	+ .31 - .39	+ 8.2 - 6.8	.061	1.05	0.72	0.92	0.76	1.10	1.34	1.26	10
			7L	00:10:10	439	352W 297S 329W 254S	51,200	413	269	221 / 41	-46.7	M	DR	+ .25 - .28	+ 8.1 - 4.6	.057	0.53	0.72	1.06	0.80	1.03	1.44	1.23	10
			8C	00:19:00	59	405W 288S 394W 288S	51,300		097			M	L	+ .23 - .23	+ 6.2 - 4.0	.063	1.41							
			9L	00:33:45	309	309W 268S 280W 246S	55,300	424	043	316 / 38	-49.3	M	VL	+ .20 - .21	+ 11.1 - 3.6	.044	0.74							
Elsenhorf	2-04-67	172	2L	20:22:55	25	189E 44S 192E 49S	59,200		105			F	VL	+ .10 - .25	+ 1.3 - 3.5	.091	1.24							
Elsenhorf	2-06-67	173	2D	20:25:05	120		55,600					F	DR											
			3D	20:35:00	300		53,400					M	DR											
			4D	20:4[illegible]:00	300		52,400					M	DR											
			5L	20:56:05	275		52,400					M	DR											
			6L	21:41:00	60		63,400					F	L											
			7L	22:07:35	85		60,400					M	DR											
			8L	22:21:55	440		54,400					M	M											
			9L	22:38:25	420		52,700					M	M											
Elsenhorf	2-07-67	174	2L	20:56:35	155		56,200					M	L											
			3L	21:23:35	150		57,200					M	VL											
			4L	21:43:30	20		57,000					M	DR											
			5L	22:06:00	115		57,000					M	VL											
			6L	22:18:15	85		57 100					M	L											
Elsenhorf	2-08-67	175	2D	23:45:35	135		60,900					M	VL											

(f) - Ferry Flight

Flight Path
L - Level C - Climb
T - Turn D - Descent

M - Mountains (h>2500 ft)
H - Hills (500 ft<h<2500 ft)
F - Flat Lands (h<500 ft)
W - Water

VL - Very Light
L - Light
DR - Light to Moderate
M - Moderate

* 500 Legs

Appendix II

APPENDIX II

INSTRUMENTATION SYSTEM

GENERAL DESCRIPTION

The airborne data acquisition system is a digital system employing Pulse Code Modulation (PCM) techniques. The system accepts data signals from various sources and processes them into a digital format which is supplied to a magnetic tape recorder for storage. The data signals are also recorded concurrently on an oscillograph for purposes of quick-look analysis and data sensor performance evaluation after flight. The basic HICAT instrumentation list is given in Table

Analog data signals are routed to the PCM system from a variety of sensors. A specially-designed gust probe provides measurement of airspeed and gust forces. An inertial navigation system provides information on aircraft attitudes, longitudinal and transverse displacement and velocity, and vertical acceleration. Additional acceleration, temperature, angular rates, altitude, and control surface position information is supplied from strategically located sensors throughout the test aircraft. Through the use of appropriate conditioning equipment, these signals are standardized to a 0- to +5-volt excursion domain prior to entry into the PCM system. The PCM system also accommodates five channels of external digital information which is generated by thumbwheel switches located on the pilot's instrumentation control panel and by other switches external to the system.

The magnetic tape generated in the airborne system must be processed through a PCM ground station. This equipment first decommutates the time-multiplexed data into its component data signals. Monitoring equipment in the station provides for direct visual display and digital-to-analog conversion for a limited number of selectable channels. Concurrently, the decommutated data is made available to a buffer-formatter which assembles the data into a preprogrammed computer-compatible format. Under control of the formatter, an output tape deck generates a gapped-format magnetic tape which can then be processed directly through computing equipment for the final automatic data processing.

FUNCTIONAL DESCRIPTION OF AIRBORNE EQUIPMENT

The instrumentation system major components are mounted just behind the pilot in the aircraft Q-bay with the exception of some signal conditioning units, sensors, and control panels which are of necessity located throughout the aircraft. Locations of instrumentation system components are shown in Figure 54. Most of the equipment housed in the Q-bay can be seen in Figures 55, 56, and 57.

TABLE VI. HICAT INSTRUMENTATION LIST AND SENSOR CHARACTERISTICS

Measurement	Inst Type	Ship Location	Mfr	Model No.	Natural Freq (Hz)	Damping Ratio (% CRIT)	Inst Range	Meas Range	System Resolution	Accuracy(1) (% RNG)
α-Vane Force	Vane	Probe FS 56	Lockheed	PT 3809	155	0.4	±12 lb	±2 lb	.004 lb(2)	±1.5(5)
β-Vane Force	Vane	"	"	"	155	0.4	±12 lb	±2 lb	.004 lb(2)	±1.5(5)
Probe Norm Acc	Acc	"	United Controls	PAL-5655	300	70	-2, +4g	-2, +4g	.006g	±0.9
Probe Lat Acc	Acc	"	"	"	300	70	±3g	±3g	.006g	±0.9
Cg Norm Acc	Acc	FS 408	"	"	300	70	-.5, +2.5g	-.5, +2.5g	.003g	±0.8
Cg Lat Acc	Acc	FS 408	"	"	300	70	±.5g	±.5g	.001g	±0.8
Cg Long Acc	Acc	"	"	"	300	70	±.5g	±.5g	.001g	±0.8
L Wing Nod Acc	Acc	WS 175	"	"	300	70	-.5, +2.5g	-.5, +2.5g	.003g	±0.9
R Wing Nod Acc	Acc	"	"	"	300	70	-.5, +2.5g	-.5, +2.5g	.003g	±0.9
Ind Airspeed	ΔPress.	Probe	Statham	PL 283 TC	3600	-	0-1 psid	0-200 kt	.20 kt(3)	±1.5(5)
Coarse Alt	Press.	A/C Nose	"	P 9CD	-	-	0-15 psi	0-75 krt	28-620 ft	±2.2(5)
Fine Alt(4)	Press.	"	Rosemount	830 G1	-	-	0-2 psi	46-75 krt	20-83 ft	±0.8
Vernier Alt(4)	ΔPress.	"	"	830 G1 & 521A	-	-	.125 psi	Inac 46-75 krt	1.2-5.2 ft	±0.8
Total Temp	Temp.	"	"	102	-	-	0,-80°C	0,-80°C	.08°C	(9)
Pitch Rate	Gyro	"	H.C. Allen	F2880-045	15	70	±10°/Sec	±10°/Sec	.02°/Sec	±0.8
Roll Rate	Gyro	"	"	"	15	70	±10°/Sec	±10°/Sec	.02°/Sec	±0.8
Yaw Rate	Gyro	"	"	"	15	70	±10°/Sec	±10°/Sec	.02°/Sec	±0.8
L Aileron Pos	Pot	L Wing	Giannini	851725-93	-	-	360°	±15°	.03°	±2.2(5)
Elevator Pos	Pot	Tail	"	"	-	-	360°	-15° +30°	.03°	±2.2(5)
Rudder Pos	Pot	"	"	"	-	-	360°	±10°	.02°	±2.2(5)
Fuel Counter	Ctr	Fus	BOEING	-	-	-	Full Load	Full Load	.5 Gal	(10)
Pitch Angle	Stable Platform	G-Bay FS 288	Litton	LN-3-2A	-	-	±90°	±15°	.03°	±0.51(6)
Roll Angle	"	"	"	"	-	-	±90°	±15°	.03°	±0.51(6)
Heading Sine	"	"	"	"	-	-	±1.0	±.707	.11°-.16°	±0.52(7)
Heading Cosine	"	"	"	"	-	-	±1.0	±.707	.11°-.16°	±0.52(7)
Vert Accel	"	"	"	"	-	-	1 ±8g	0, +8g	.008g	±0.7(5)
X Velocity	"	"	"	"	-	-	±2000 fps	±1000 fps	2 fps	±1.1(5)
Y Velocity	"	"	"	"	-	-	±2000 fps	±1000 fps	2 fps	±1.1(5)
X Distance	"	"	"	"	-	-	Pole-to-Pole ±1500 nmi	±300 nmi	1.0 nmi	±1.7(8)
Y Distance	"	"	"	"	-	-	Pole-to-Pole ±1500 nmi	±300 nmi	1.0 nmi	±1.7(8)
AL Rad Count	Geiger-Müller	"	See Text	-	-	-	-	-	1024 Counts	-
BI Rad Count	Geiger-Müller	"	"	-	-	-	-	-	1024 Counts	-
TK Rad Count	Geiger-Müller	"	"	-	-	-	-	-	64 Counts	-

NOTES: (1) Accuracy figures include such factors as linearity, hysteresis, gain stability, zero stability, and temperature coefficients.

(2) Approximately equal to 0.00 degrees

(3) At 150 knots

(4) Stability is 0.1% FS per 6 months

(5) Includes effects of CEC 1-361-0001 dc amplifier

(6) Includes effects of Natel D5006-763-08-400-26-A Demodulator

(7) Includes effects of Natel D5006-761-08-400-26-A Demodulator

(8) Includes effects of Litton RC18 Potentiometer and CEC 1-361-0001 dc amplifier

(9) Not rigorously definable; errors considered negligible

(10) Driven from ship's fuel conservation instrumentation

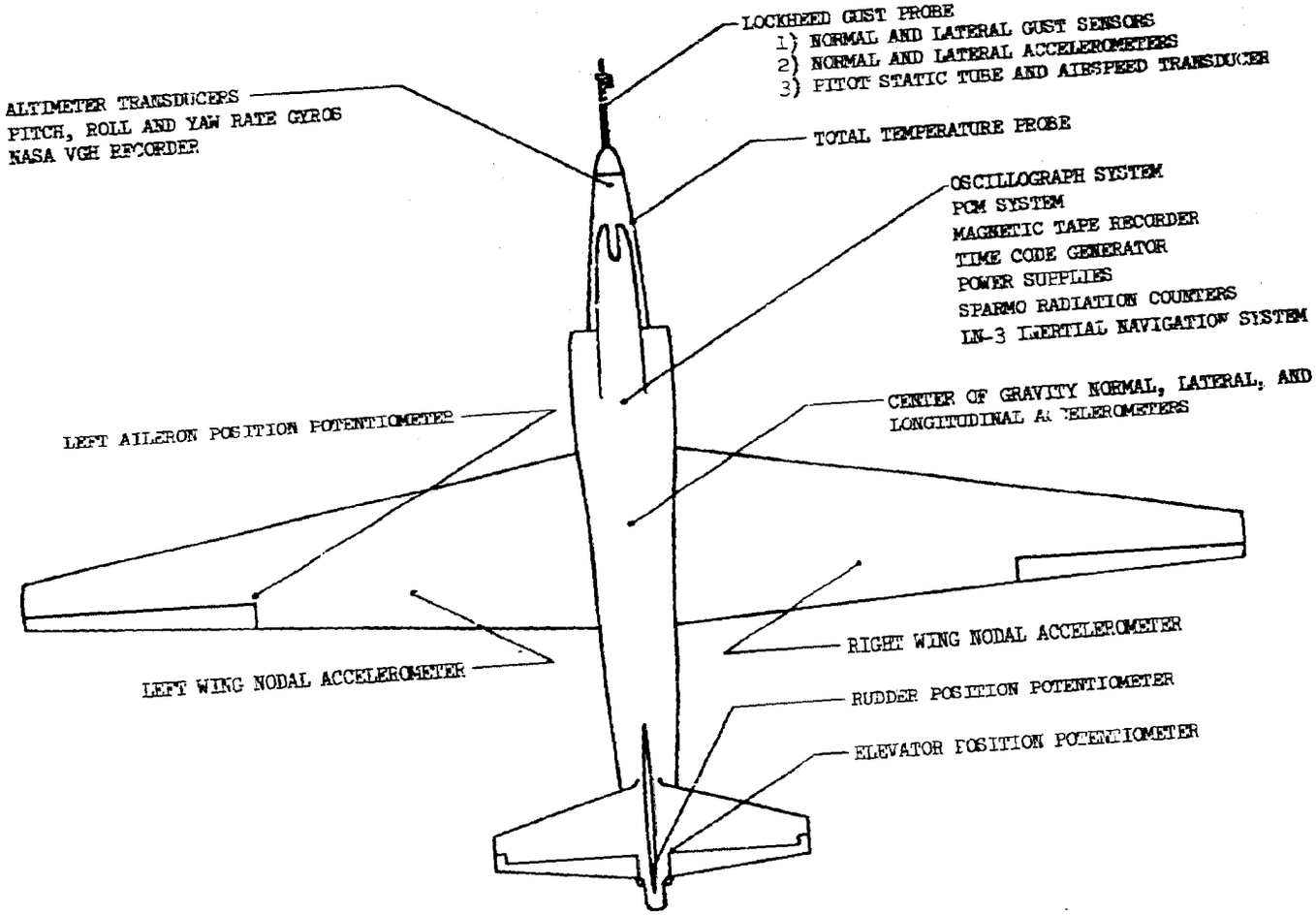

Figure 54. Aircraft Instrumentation Location Diagram

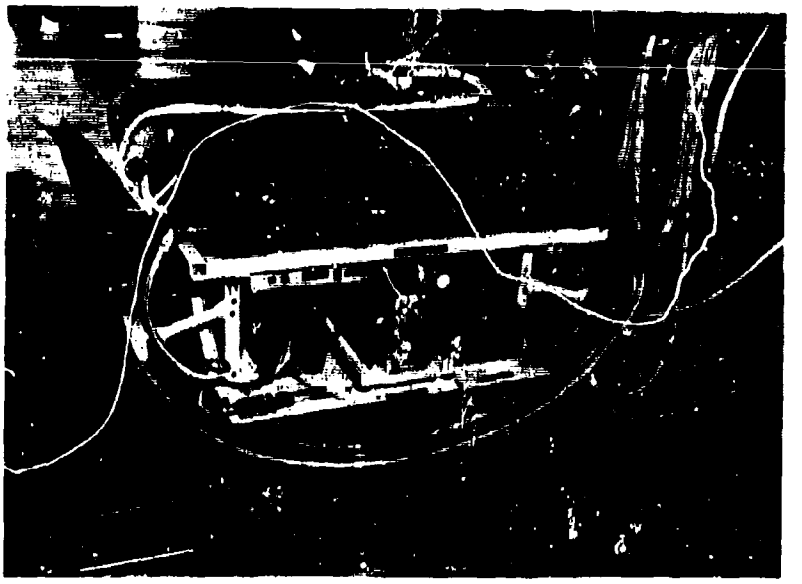

Figure 55. Instrumentation Hatch. Note PCM package and instrumentation J-Box on top shelf. Time code generator, LN-3 computer, and LN-3 adapter are on lower shelf.

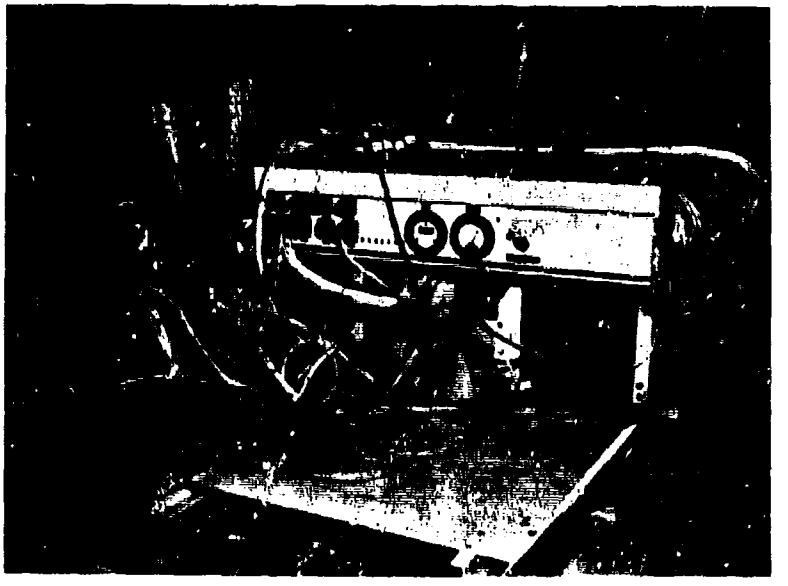

Figure 56. Aft View of Instrumentation J-Box

Appendix II

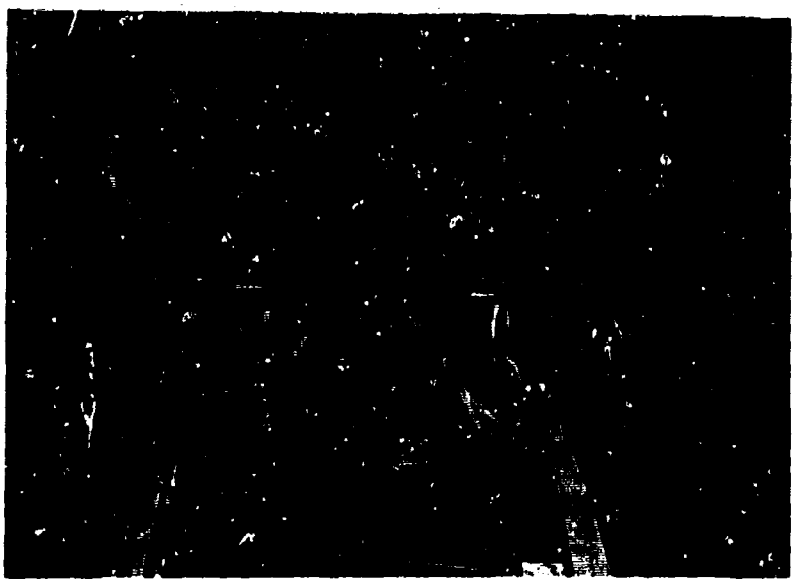

Figure 57. View of Magnetic Tape Recorder, LN-3 Stable Platform and SPARMO Radiation Instrumentation (Lower Left).

PCM SYSTEM

The PCM system was designed and manufactured to Project HICAT specifications by Dynatronics, Incorporated, of Orlando, Florida. In general, it is a 10-bit digital system with a corresponding channel resolution of one part in 1024 and an accuracy capability of 0.1 percent.

Exclusive of transducers and recorders, the airborne PCM system is housed in three packages: The PCM package, the time code generator, and the system control panel. The PCM system package is contained within a maximum envelope of 7 inches high by 34.75 inches long by 13.2 inches wide; the package weighs 143 pounds. The time code generator is confined to 5.0 inches wide by 10.5 inches high by 20.5 inches deep and weighs 26 pounds. The system is designed to operate over a temperature range of -10°C to +80°C, at altitudes from sea level to 50,000 feet, and to withstand a range of temperatures from -55°C to +125°C in a nonoperating condition. The system is also designed to withstand vibration levels of 0.08 inches double amplitude, 10 to 50 Hz, and of up to 10g random, 50 to 2000 Hz and 3 axis shocks to 30g for up to 11 milliseconds, as well as relative humidity up to 100 percent with sand and dust conditions as encountered in desert areas

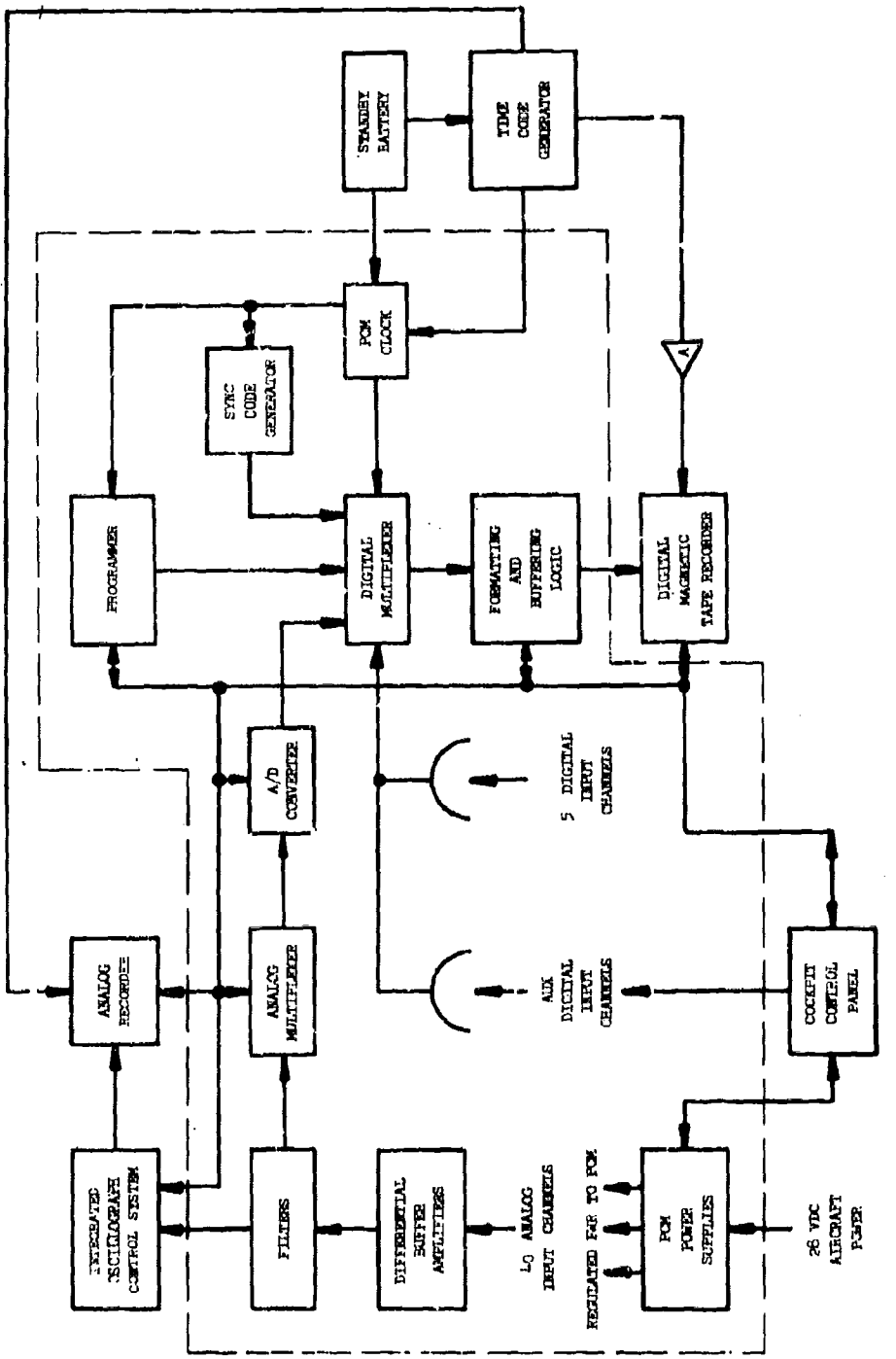

Figure 58. HICAT Digital Instrumentation System

Appendix II

PCM system functions are described in the following paragraphs and depicted in block form in Figure 58. Photographs of the components are given in Figures 59, 60, 61, and 62.

The PCM system contains main power supplies, digital timing and control, PCM format generation, analog amplifiers, multiplexing, and digitizing circuitry. These circuits employ both integrated and discrete component logic elements. Prime system timing is derived externally in the time code generator package. The PCM system is best described in terms of its analog and digital subsystems.

Analog Subsystem

The function of this subsystem is to accept 40 analog inputs, sample and store these signals, and convert them to equivalent 10-bit binary codes. All analog samples are acquired within a maximum period of one millisecond.

The front end of the subsystem is a differential buffer amplifier for each channel which accepts a 0- to +5-volt data signal. The main function of the amplifier is to provide impedance buffering between the analog signal source and the data filter which follows. Input impedance of this amplifier is nominally 200 kilohms. Secondary functions of this amplifier include limited gain control, common mode voltage rejection control, and differential overvoltage protection against input voltages of up to 35-vdc.

Following the buffer amplifier, the data signal is applied to a passive low-pass filter. The filter is a 3-terminal, 8-pole Butterworth network with a passband (-3 db point) of zero to 7 Hz and a rolloff rate of -48 db per octave. It is a constant amplitude device with an attendant lagging phase shift whose slope is constant to about 4 Hz. Transfer function of a typical filter is given in Figures 63 and 64. The power spectra in Figures 65 through 82 illustrate the attenuation effect of the low pass filters on the critical gust velocity measurements. Note the absence of significant power at frequencies above 12.5 Hz (an indication that aliasing effects are negligible, see Aliasing Errors discussion in Section VI).

After the data has been subjected to filtering, the signal is applied to a sample-and-hold network. The function of this network is to provide an analog store from which data can be read out at the proper time. The 40 sample gates are triggered simultaneously, and all 40 channels are sampled sequentially within a maximum period of one millisecond. Further buffering takes place in this stage in order to provide galvanometer drive capability for the analog oscillograph monitor system.

The output of the sample-and-hold networks is fed to a 40-channel high level multiplexer. Command pulses to the multiplexer are derived in the digital subsystem, with the sequence rate controlled by a front panel switch. Available scan rates are 20, 25, 40, and 50 frames per second. Output of the multiplexer is a serial PAM (Pulse Amplitude Modulation) pulse train.

The multiplexer output is then applied to the analog-to-digital conversion circuitry. Conversion is performed by half-split successive approximations in which the PAM signal is compared with precision voltages generated within the converter, and registers are set until the sum of the precision voltage segments equals the input PAM magnitude. The 10-bit binary output from the registers is then made available to digital multiplexing circuitry to enable the binary code to be entered into the data format.

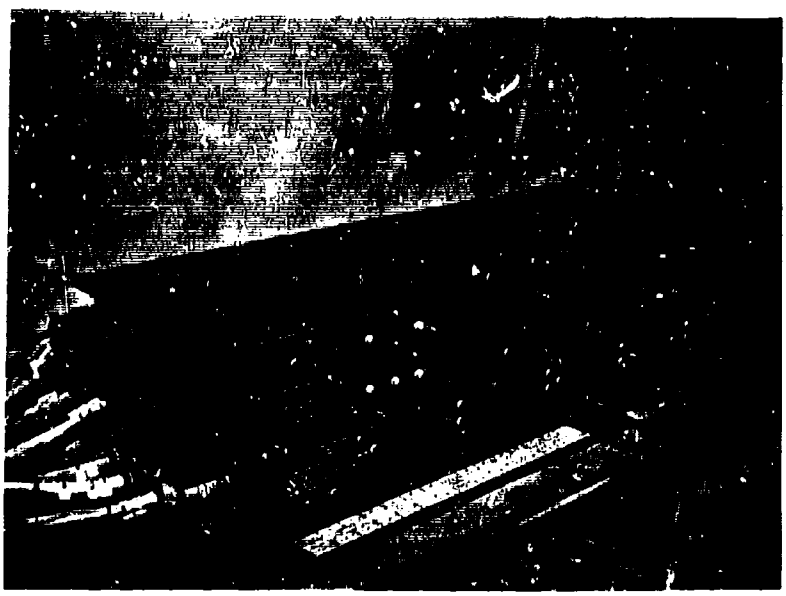

Figure 59. PCM Package

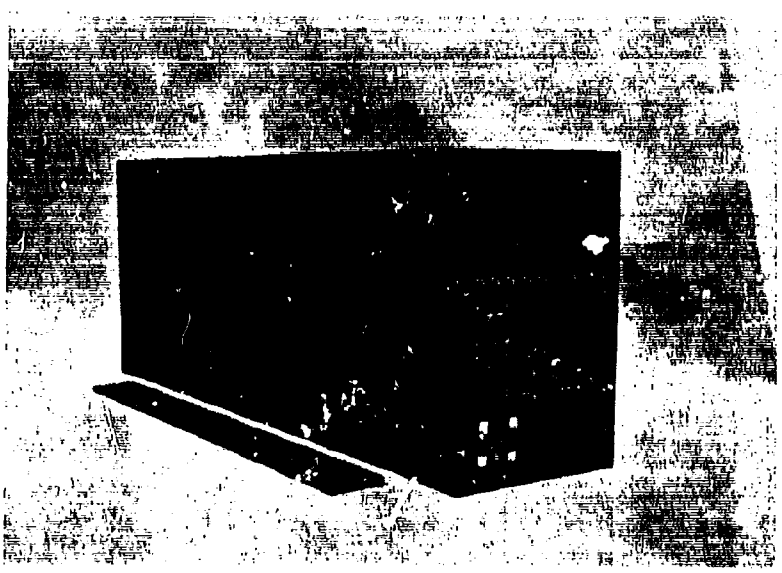

Figure 60. Time Code Generator

Appendix II

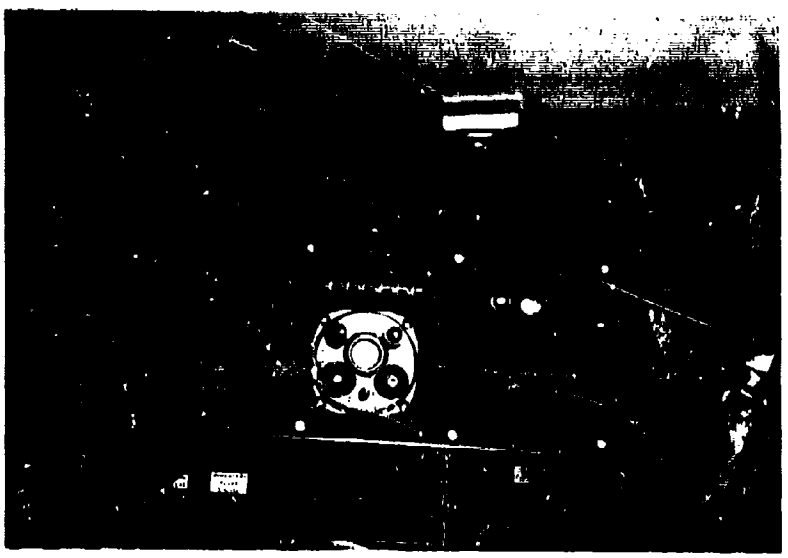

Figure 61. Instrumentation Control Panels in Cockpit

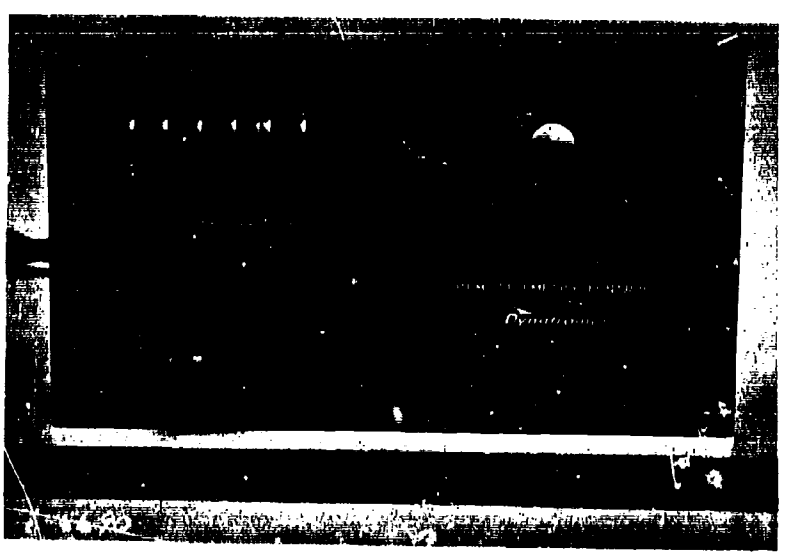

Figure 62. PCM Control Panel

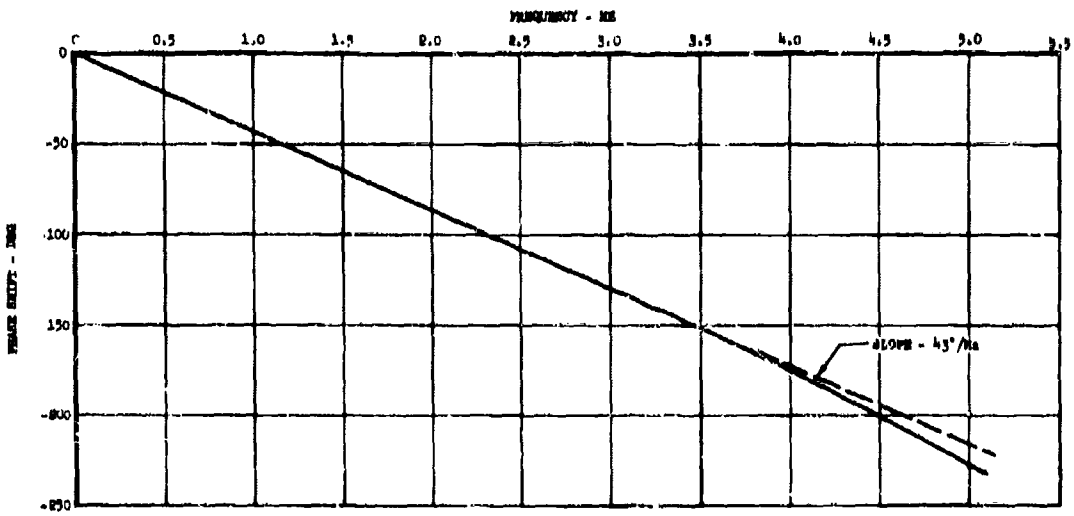

Figure 63. Phase Response of HICAT Passive Low Pass Filter at Room Temperature

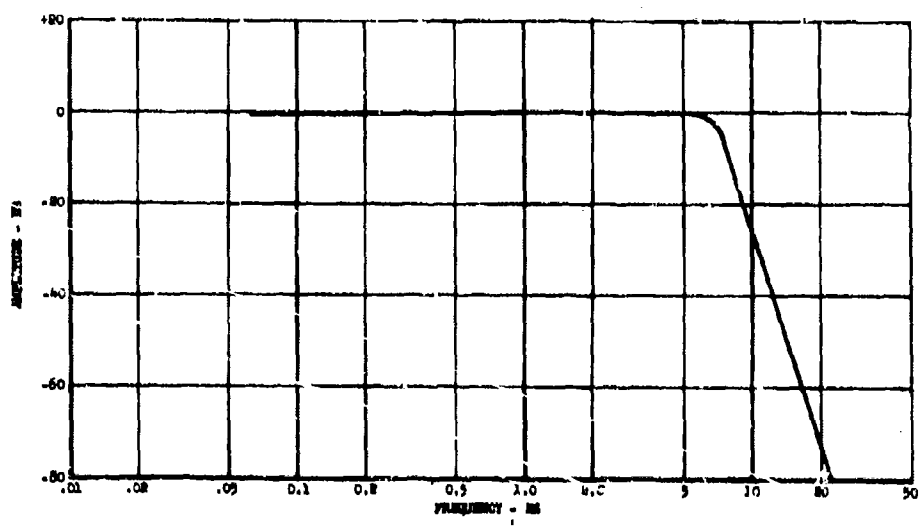

Figure 64. Amplitude Response of HICAT Passive Low Pass Filter at Room Temperature

Appendix II

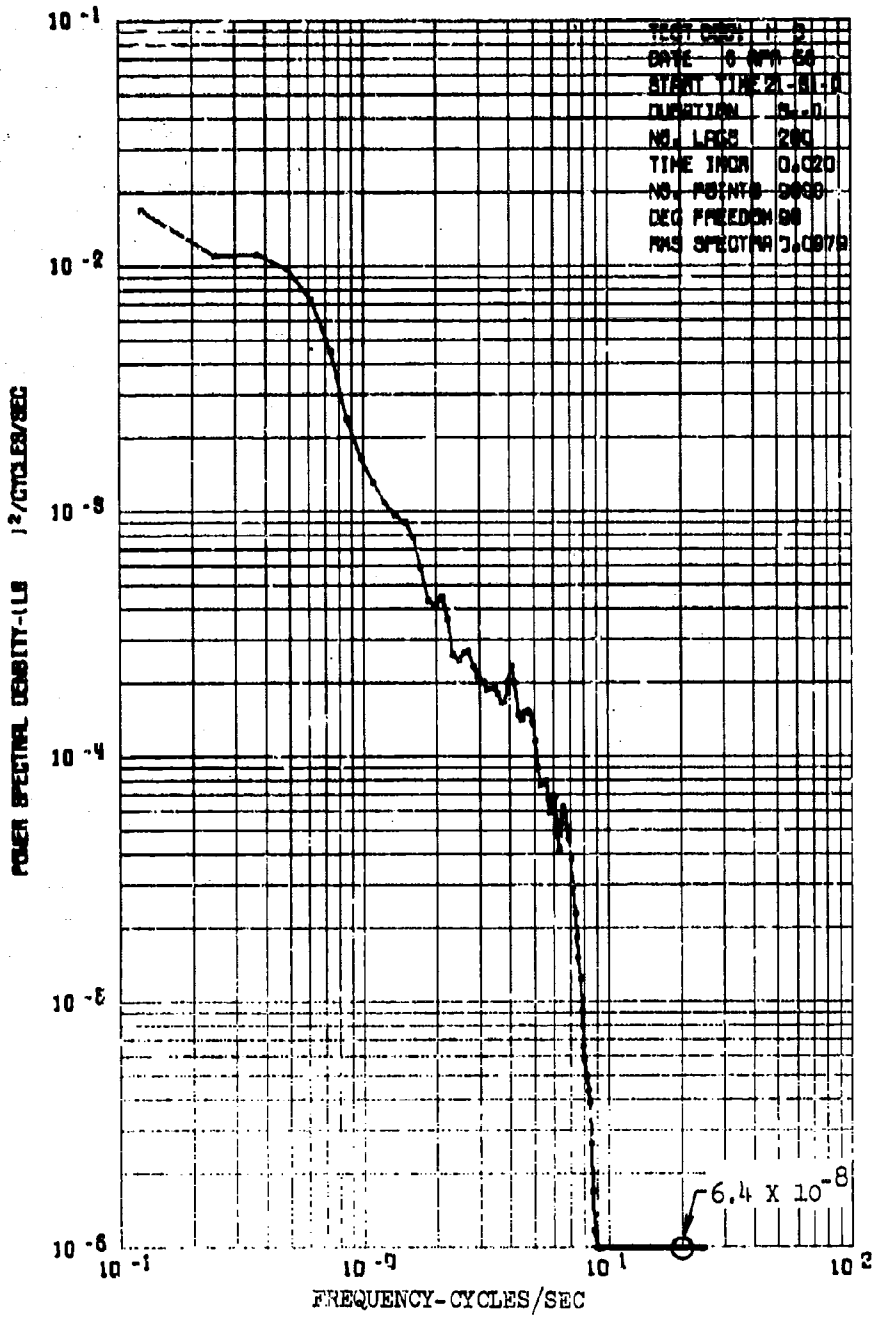

Figure 65. Power Spectrum of Alpha-Vane Force

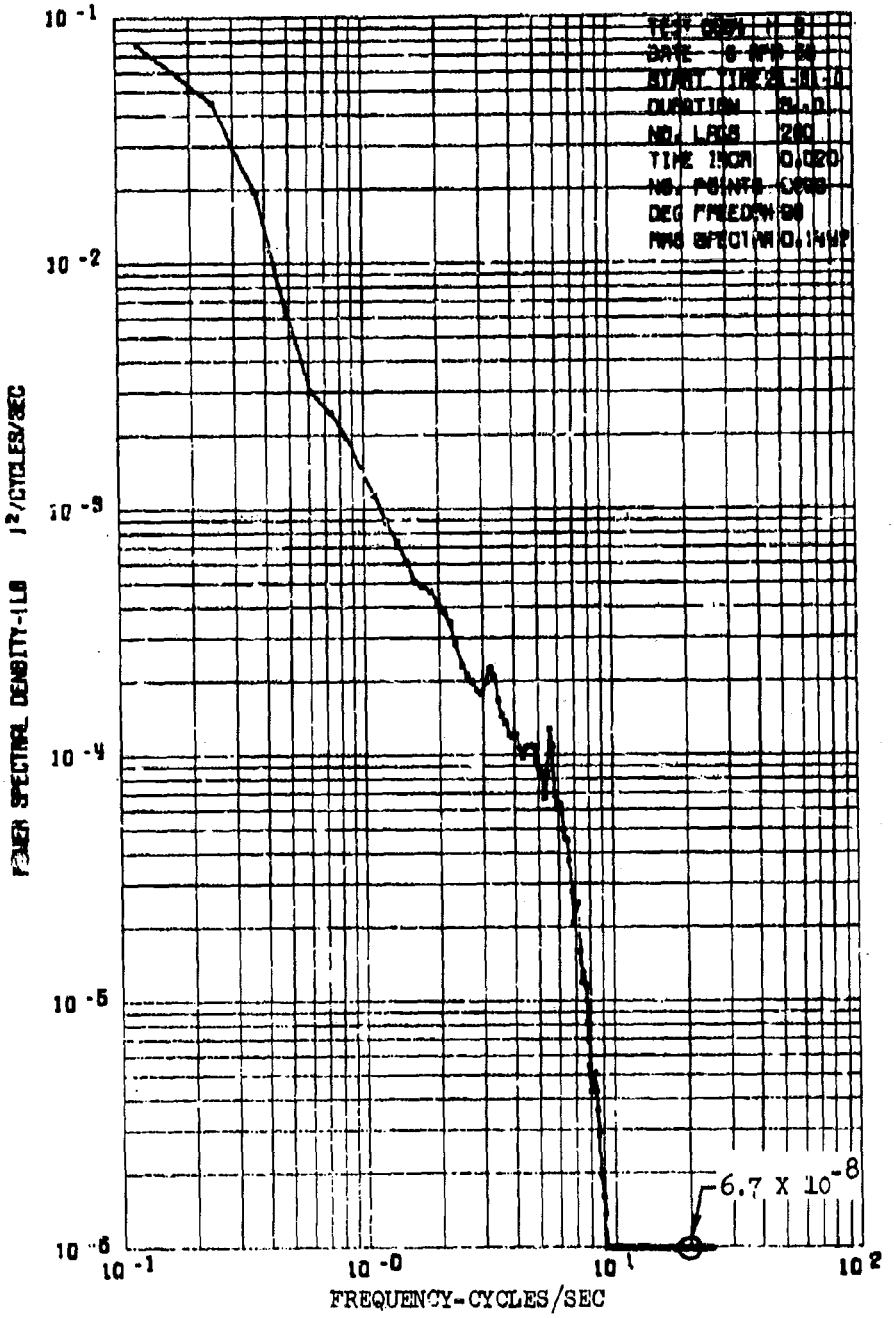

Figure 66. Power Spectrum of Beta-Vane Force

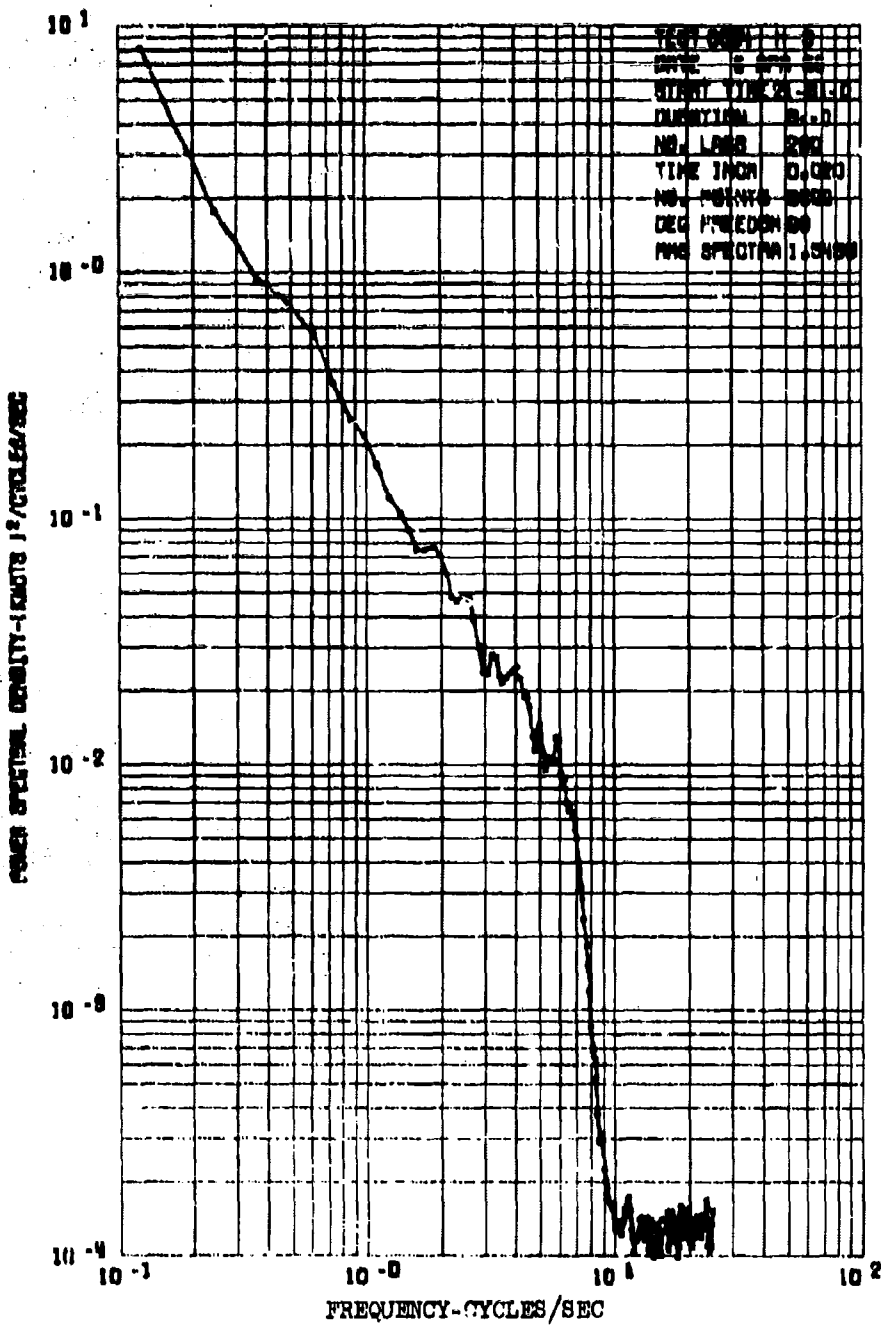

Figure 67. Power Spectrum of Indicated Airspeed

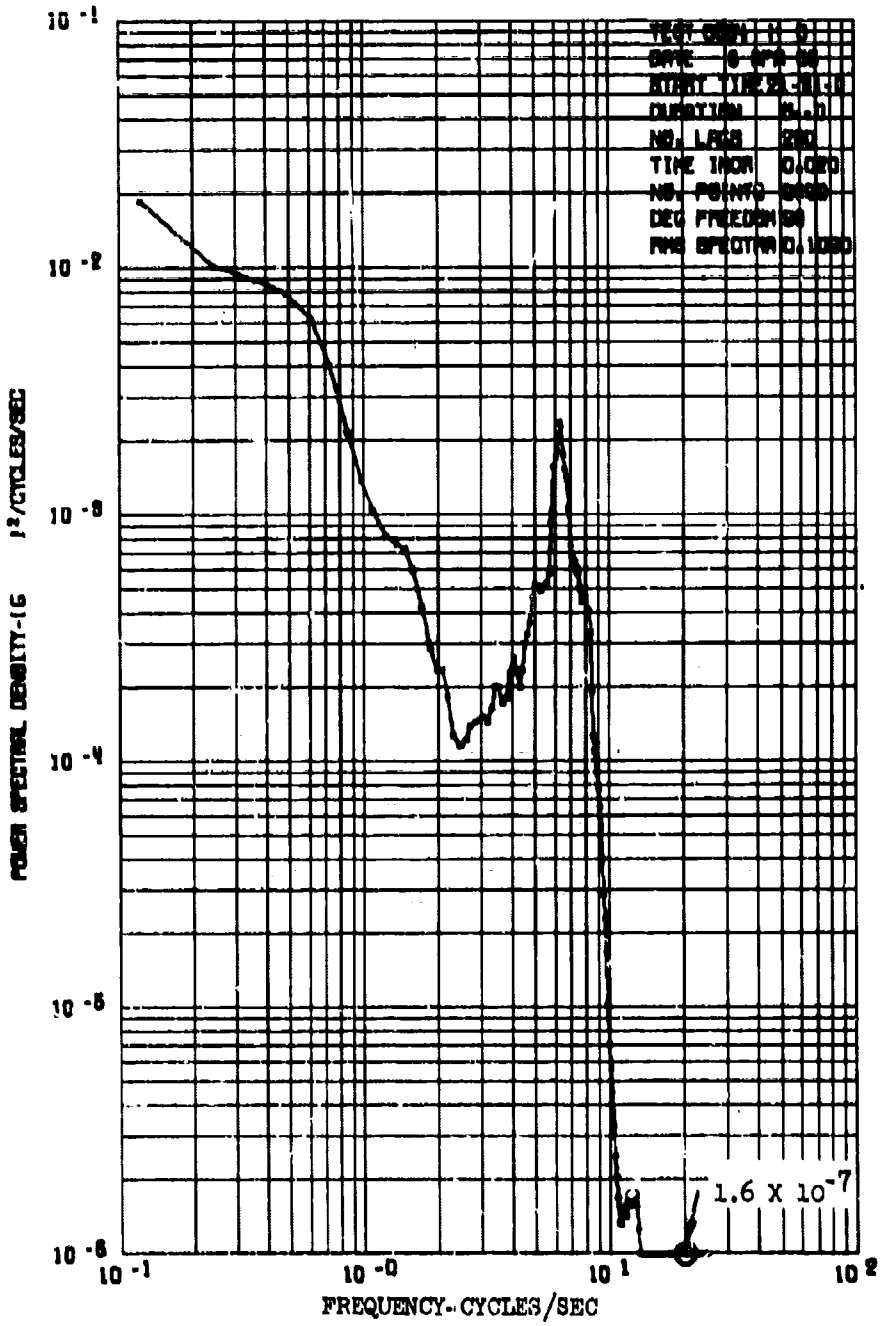

Figure 68. Power Spectrum of Gust Probe Normal Acceleration

Appendix II

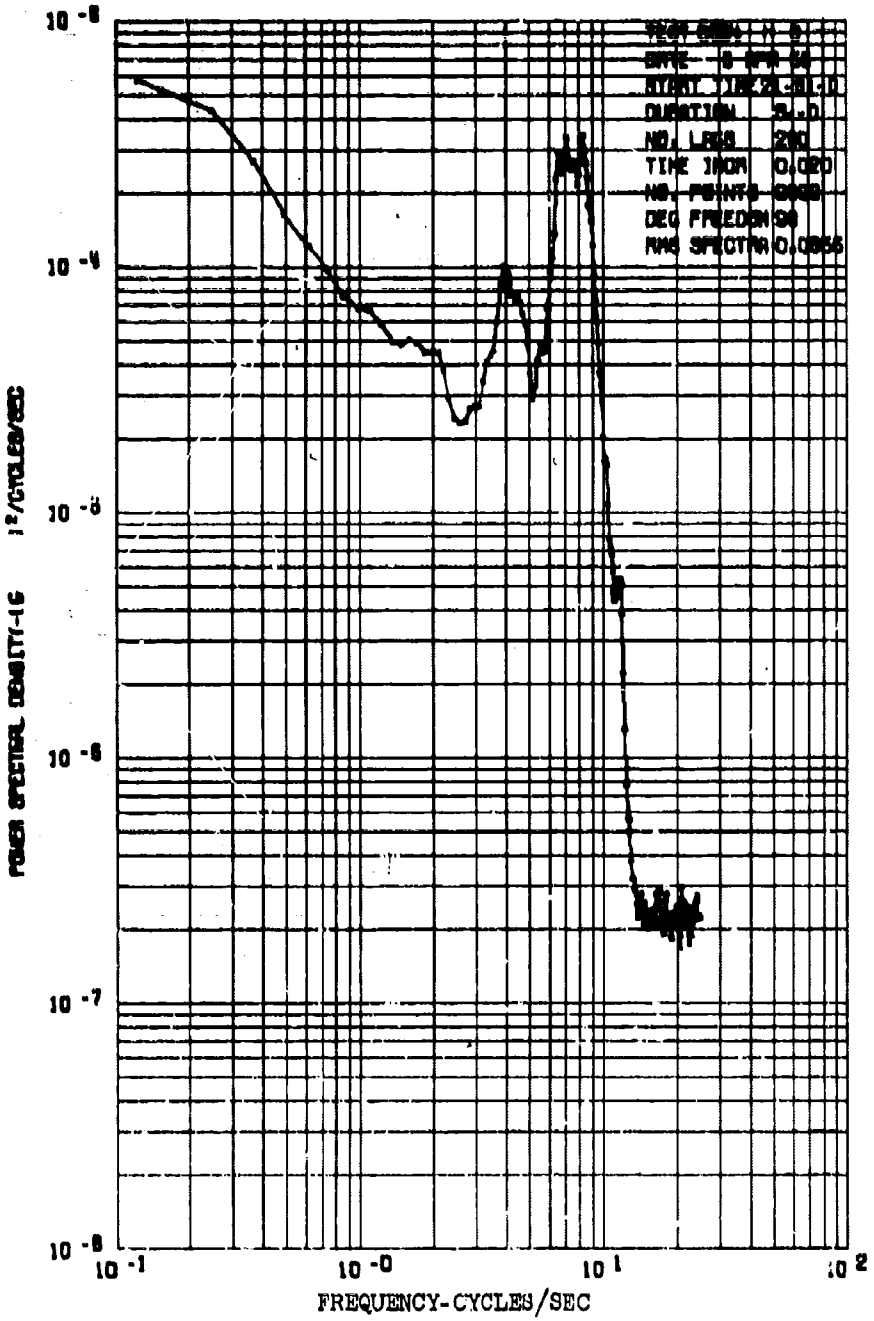

Figure 69. Power Spectrum of Gust Probe Lateral Acceleration

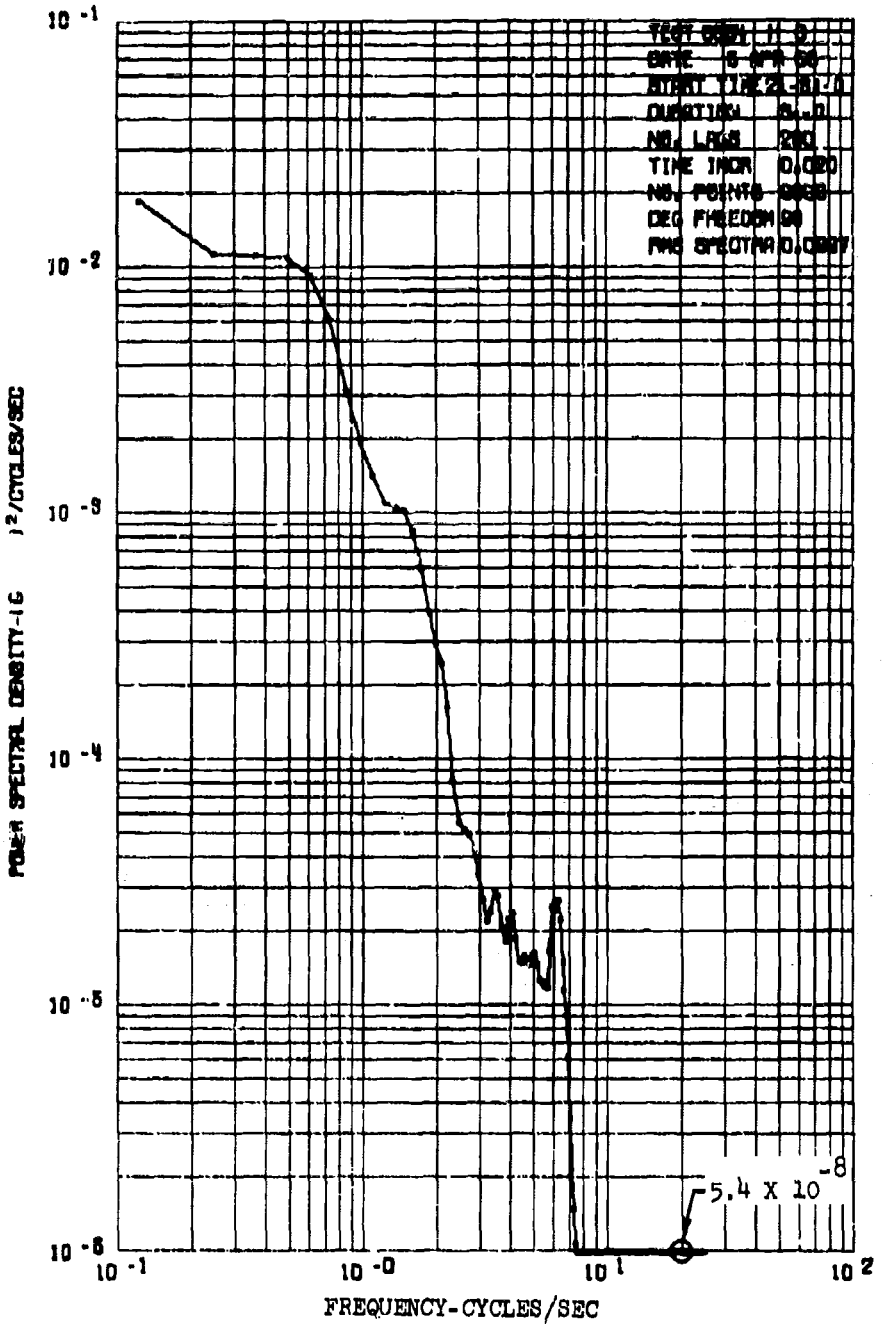

Figure 70. Power Spectrum of Vertical Acceleration

Appendix II

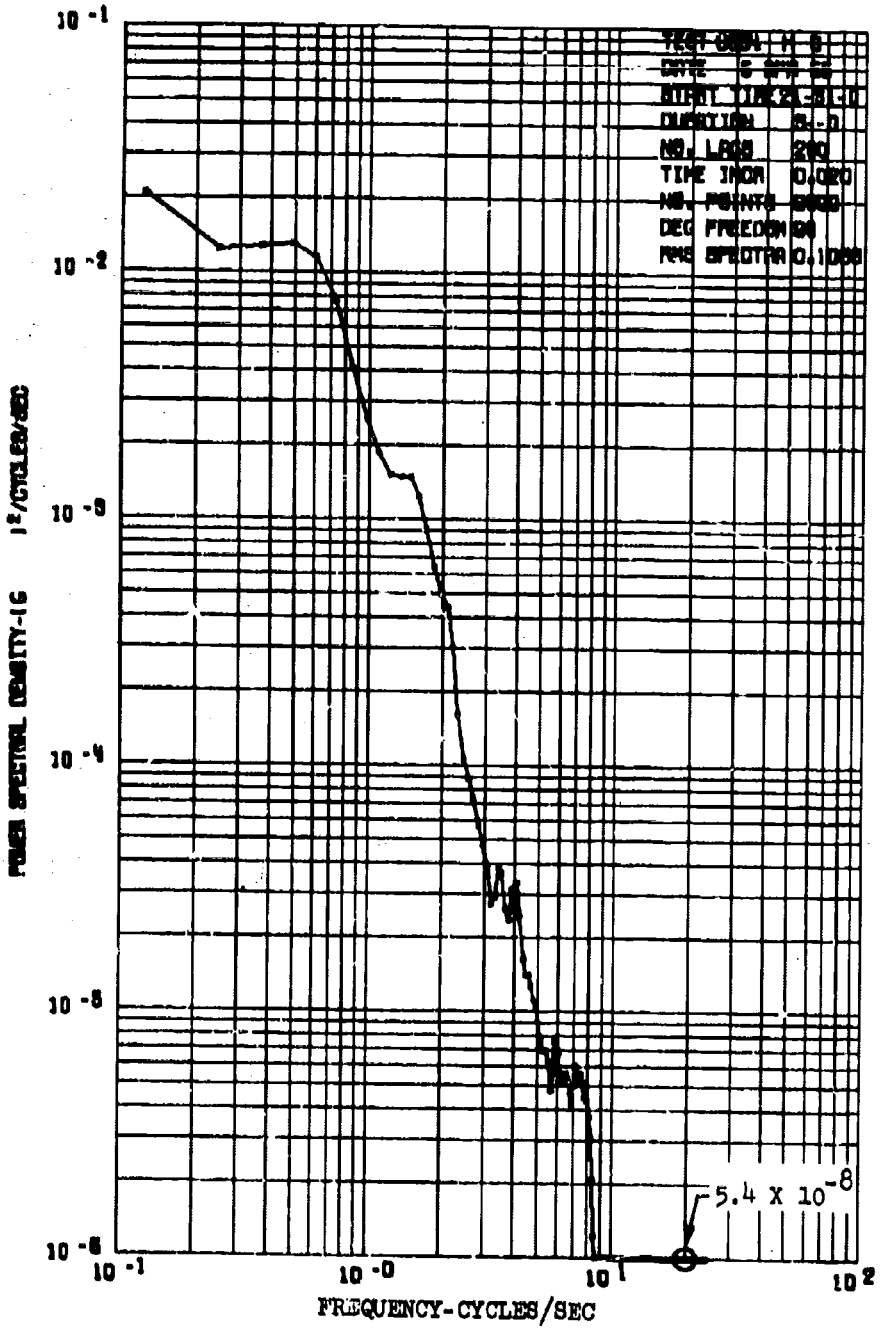

Figure 71. Power Spectrum of CG Normal Acceleration

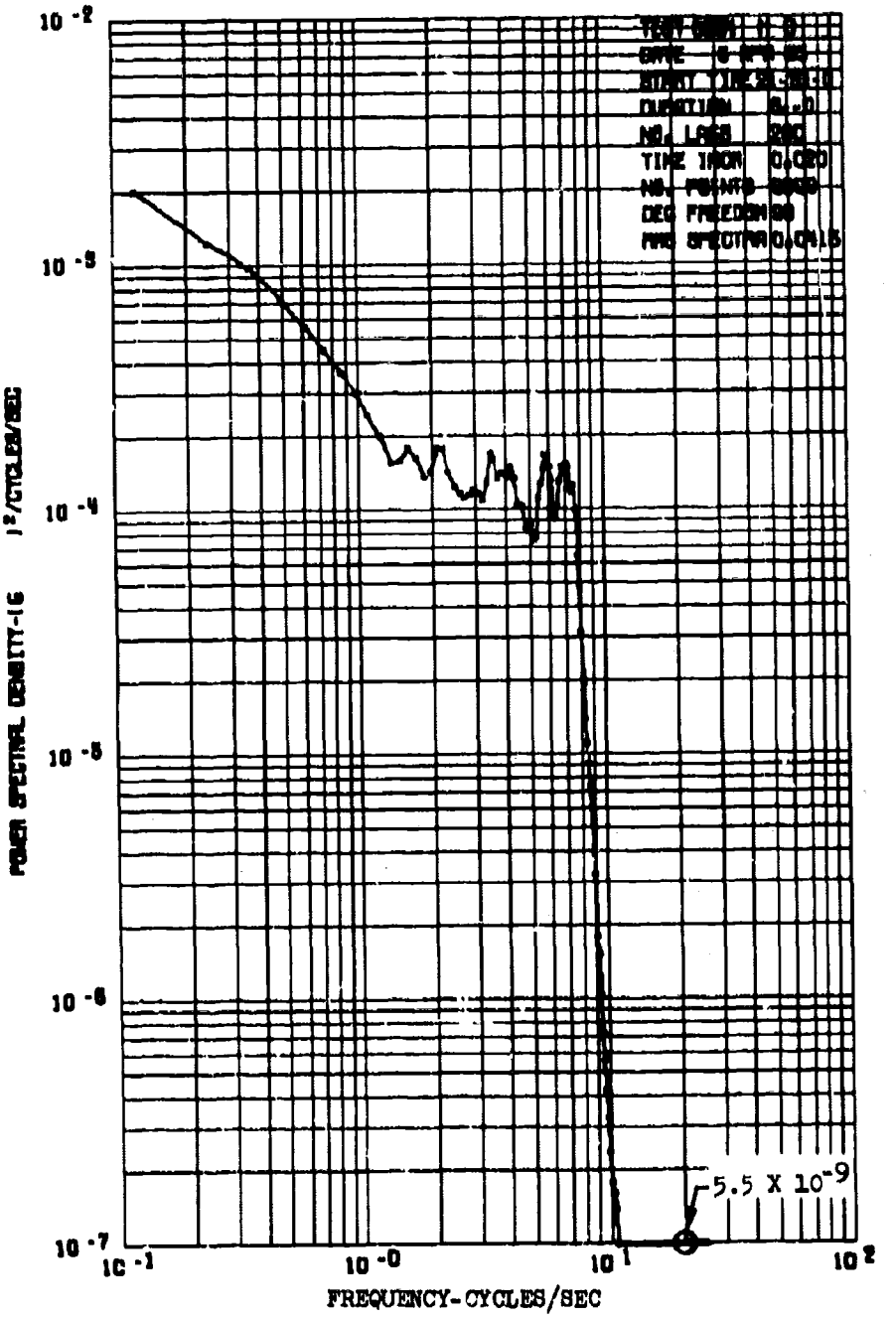

Figure 72. Power Spectrum of CG Lateral Acceleration

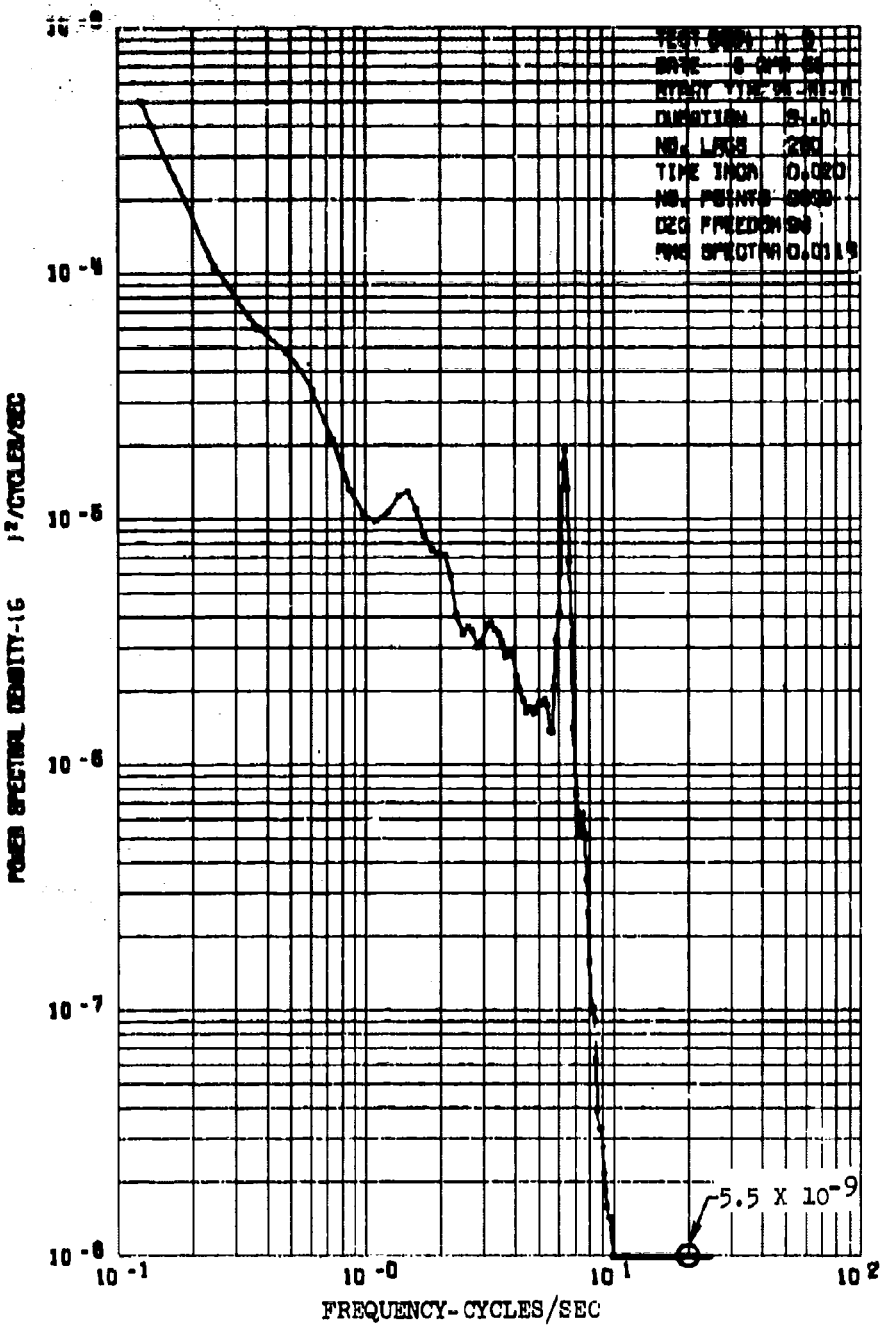

Figure 73. Power Spectrum of CG Longitudinal Acceleration

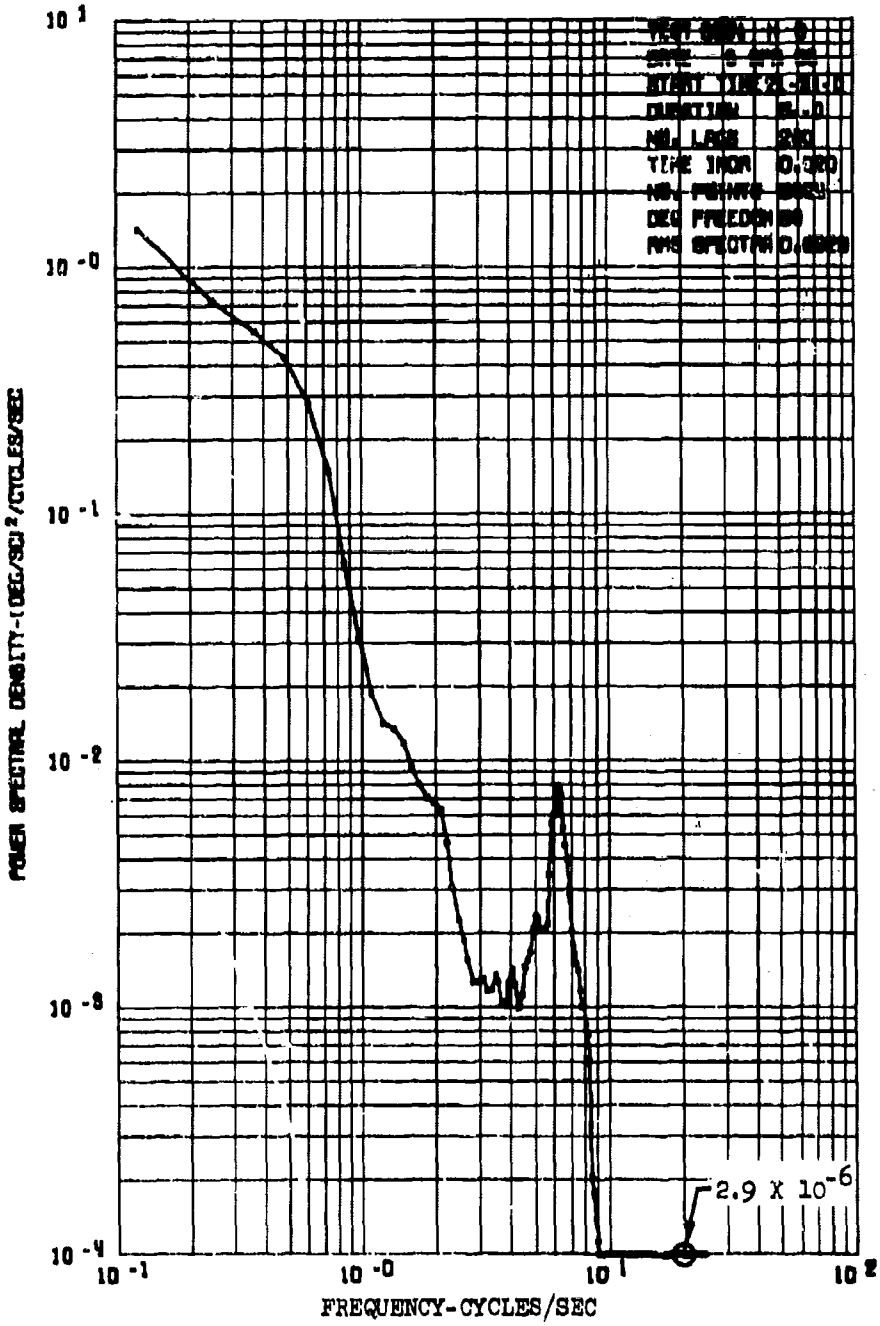

Figure 74. Power Spectrum of Pitch Rate

Appendix II

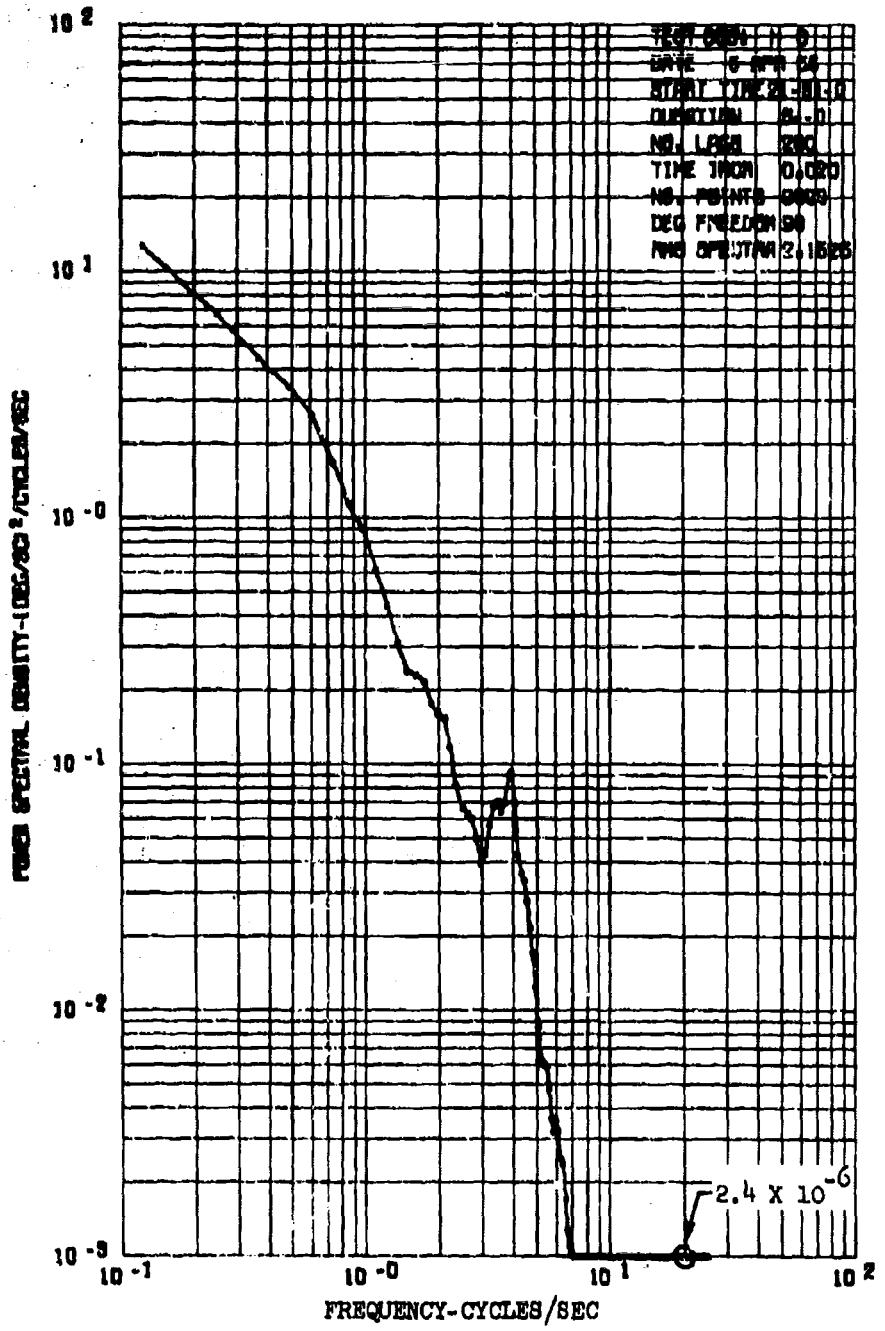

Figure 75. Power Spectrum of Roll Rate

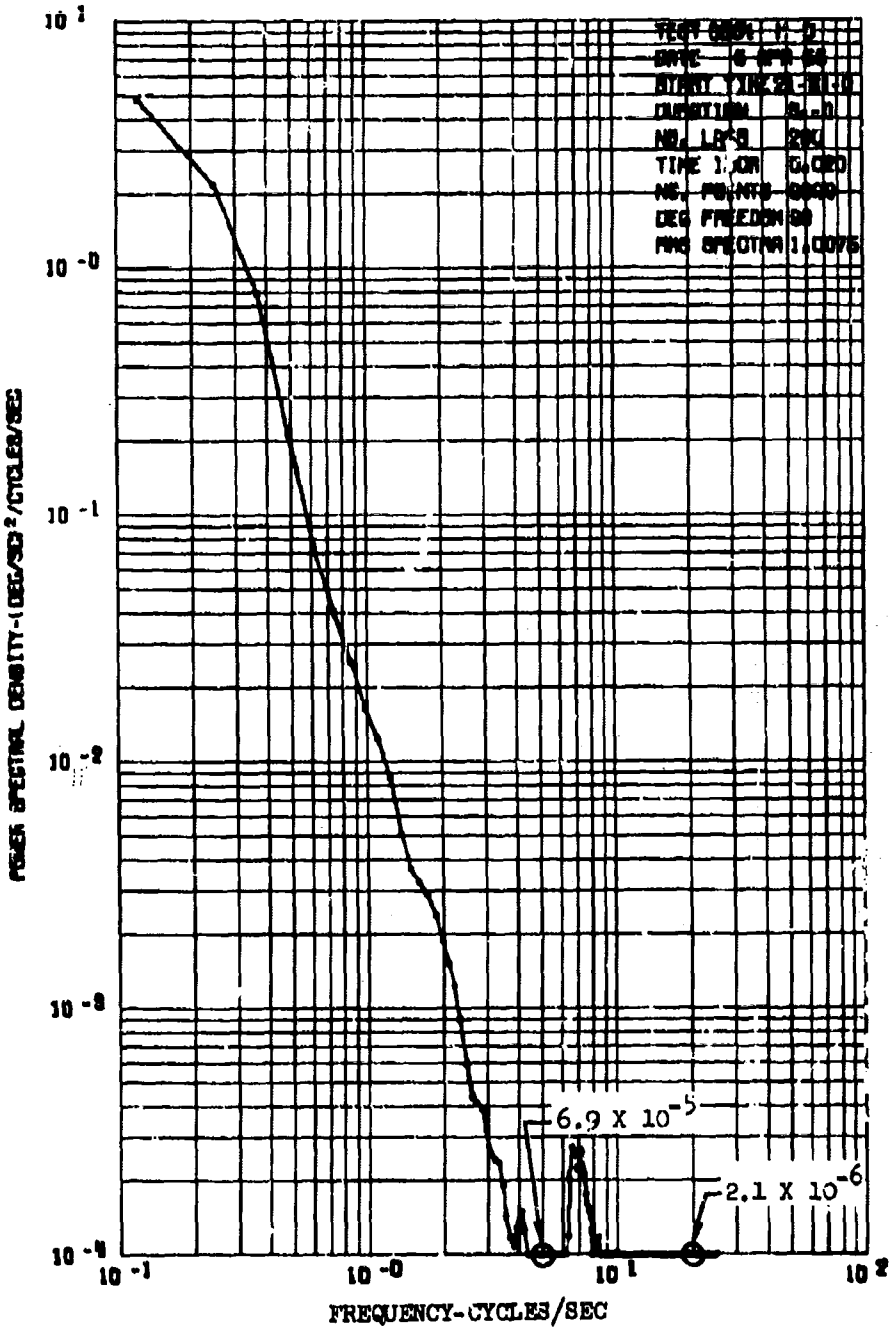

Figure 76. Power Spectrum of Yaw Rate

Appendix II

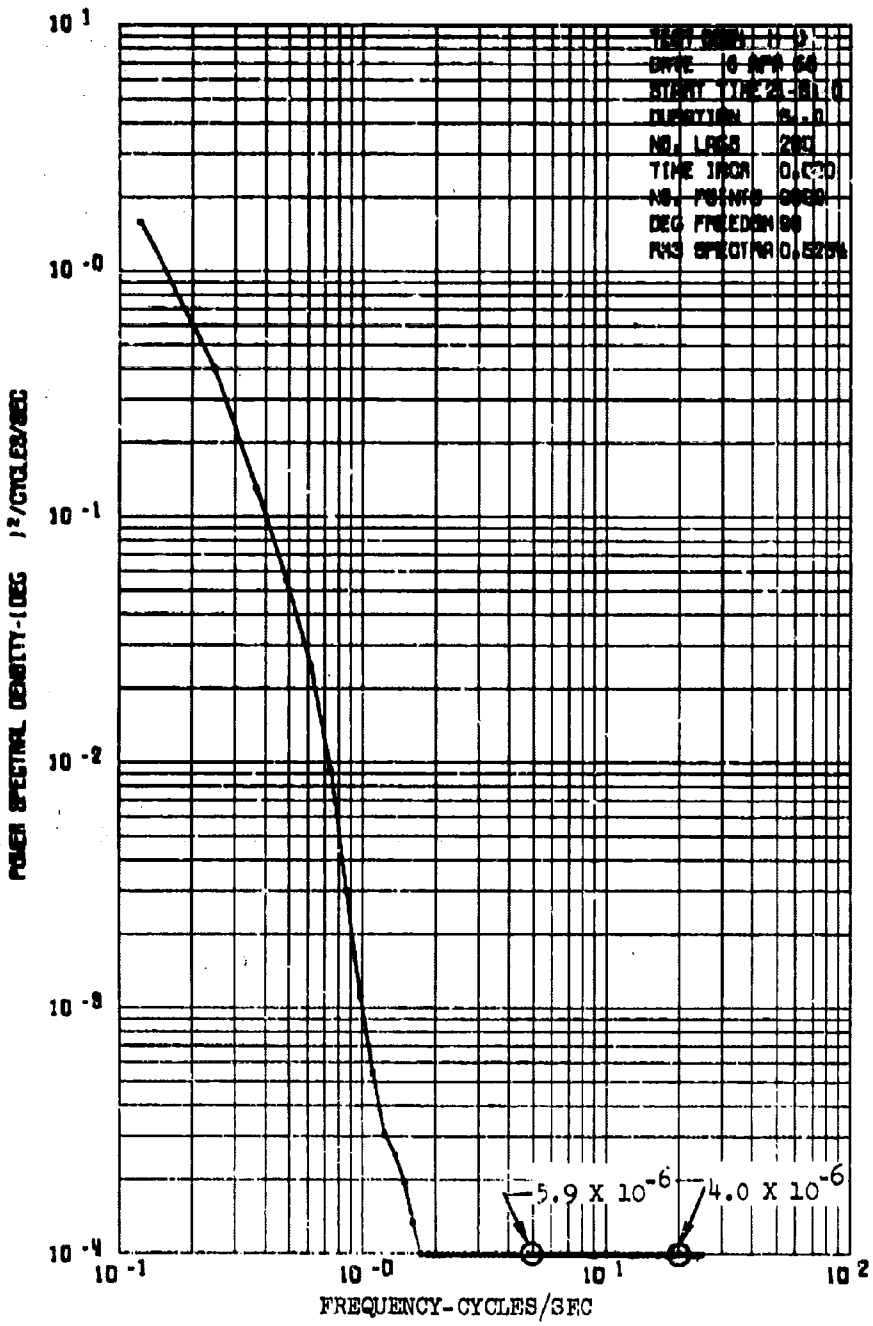

Figure 77. Power Spectrum of Pitch Angle

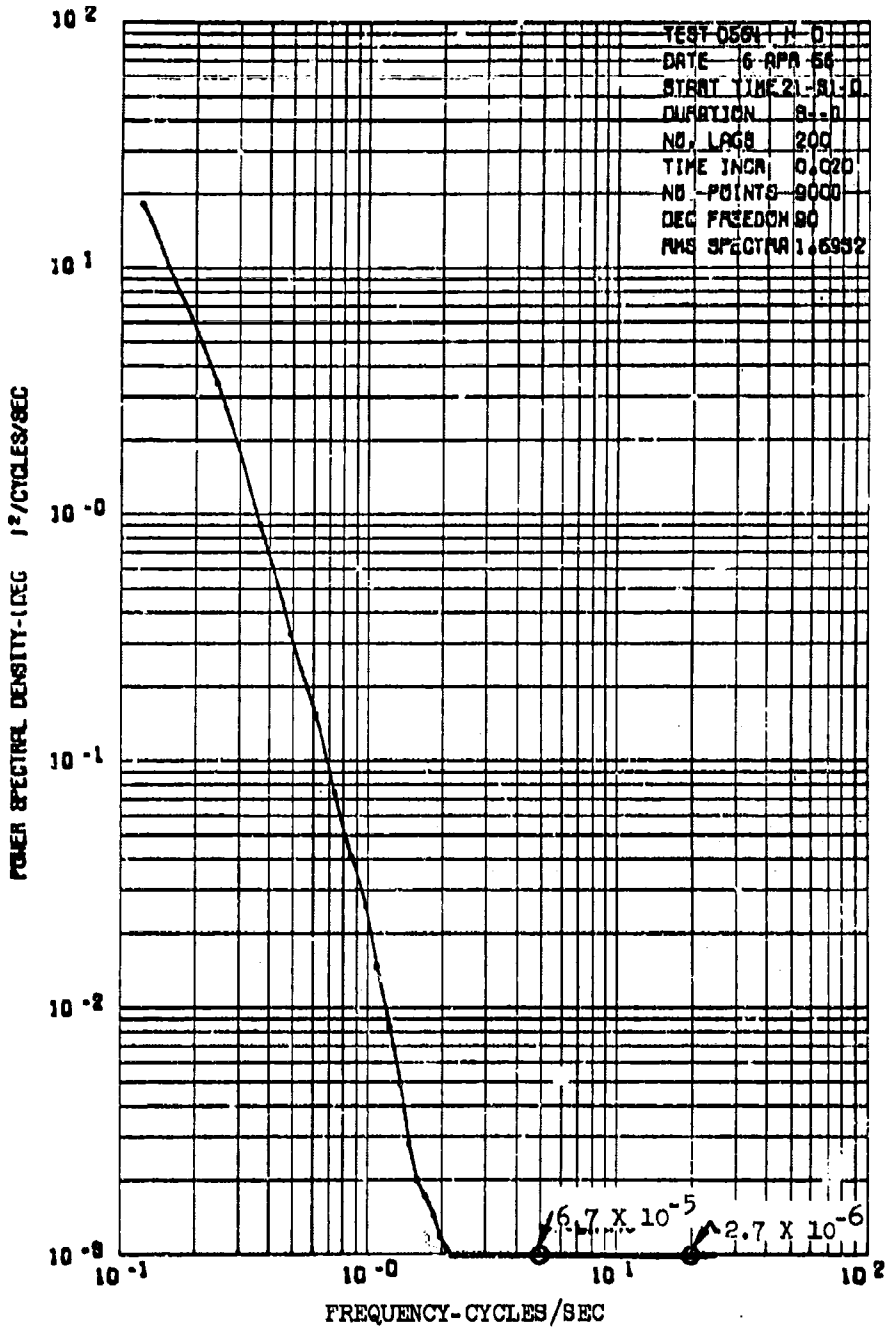

Figure 78. Power Spectrum of Roll Angle

Appendix II

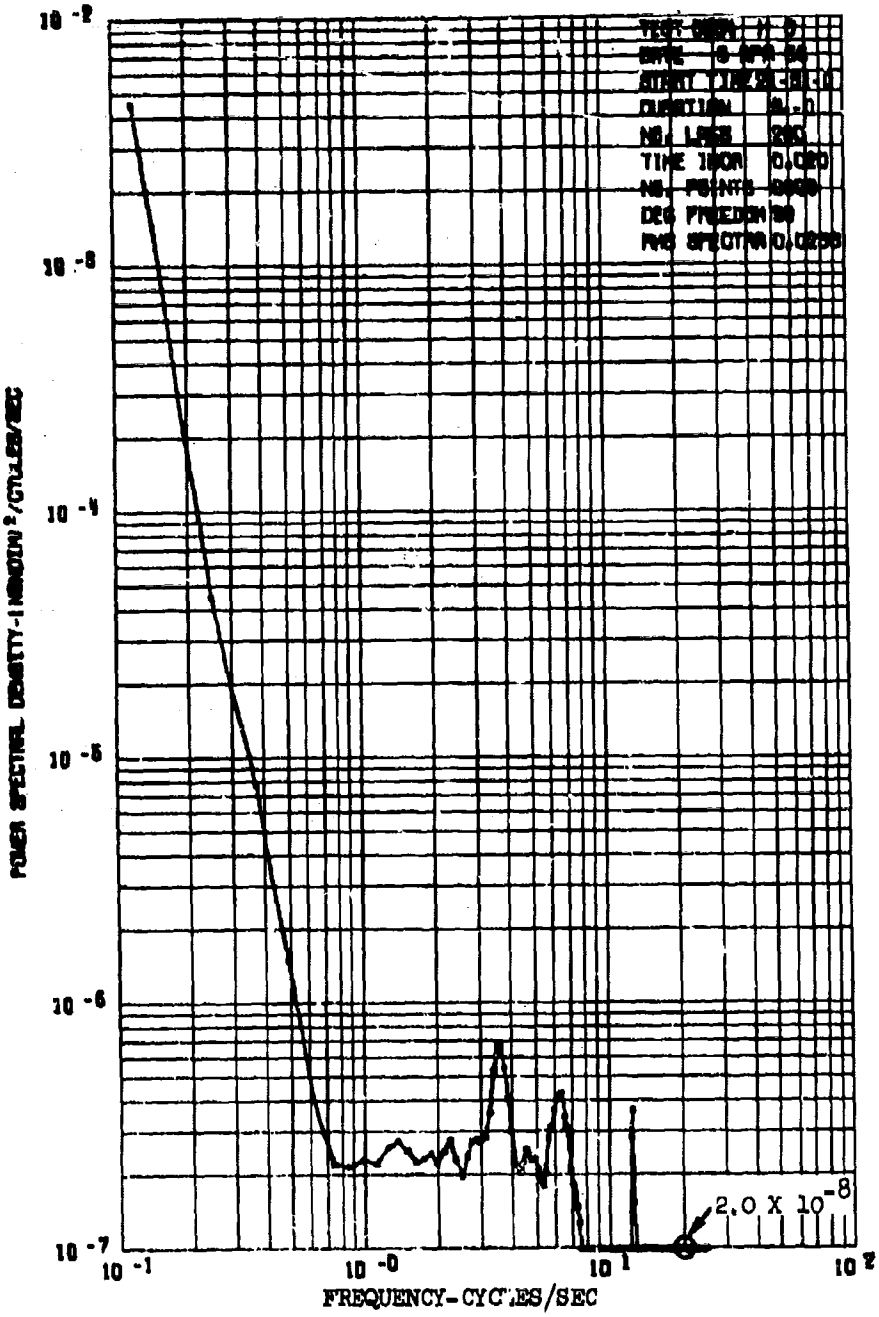

Figure 79. Power Spectrum of Heading Sine

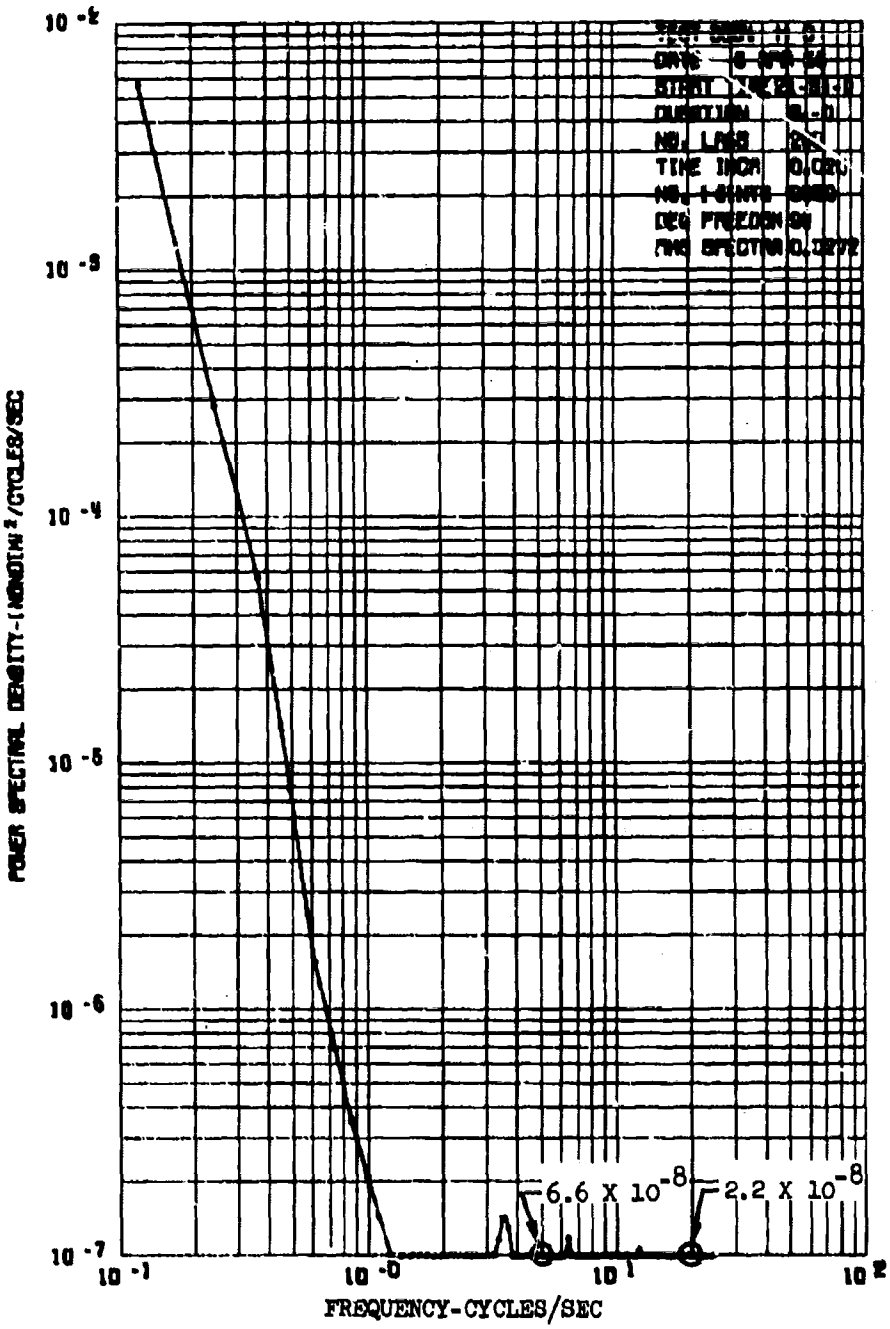

Figure 80. Power Spectrum of Heading Cosine

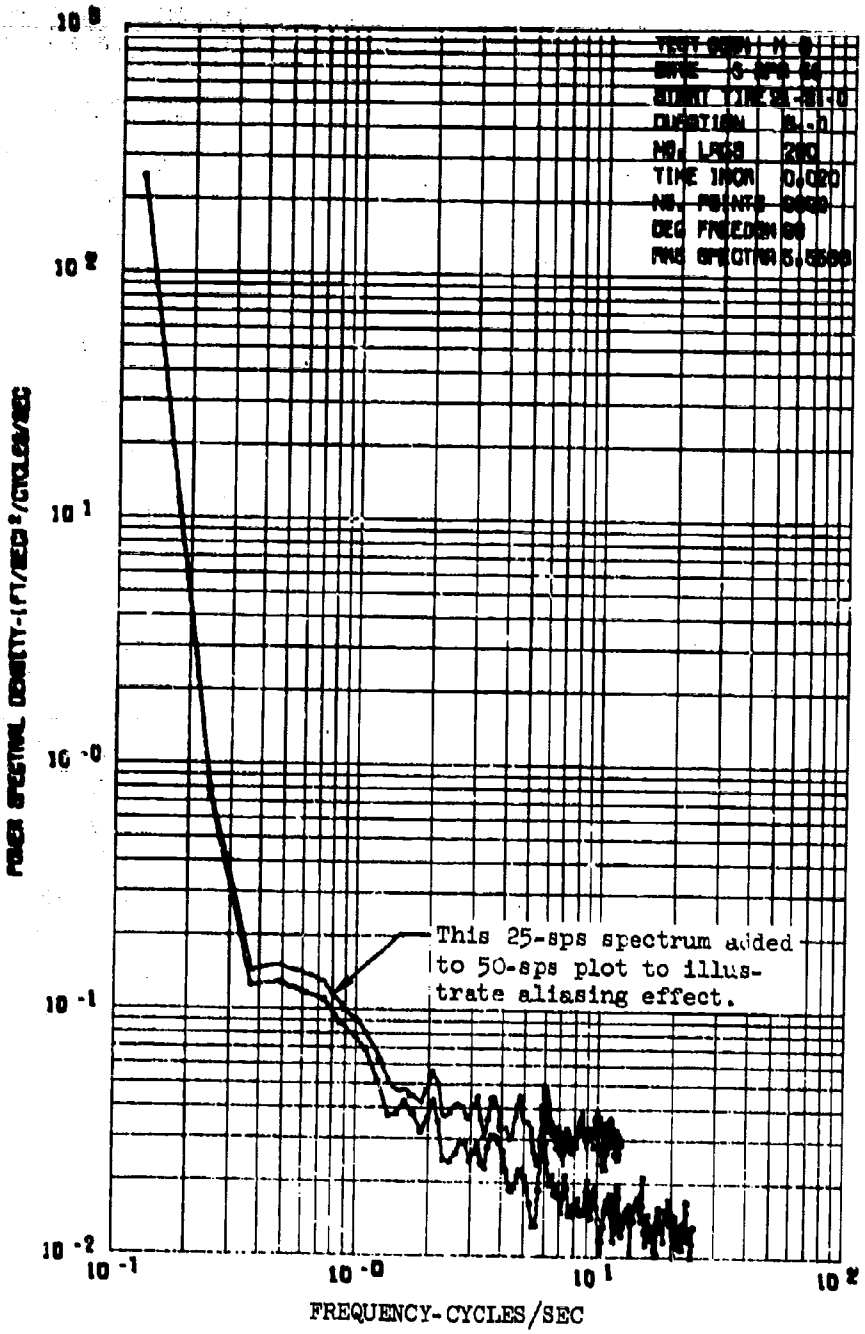

Figure 81. Power Spectrum of X Velocity

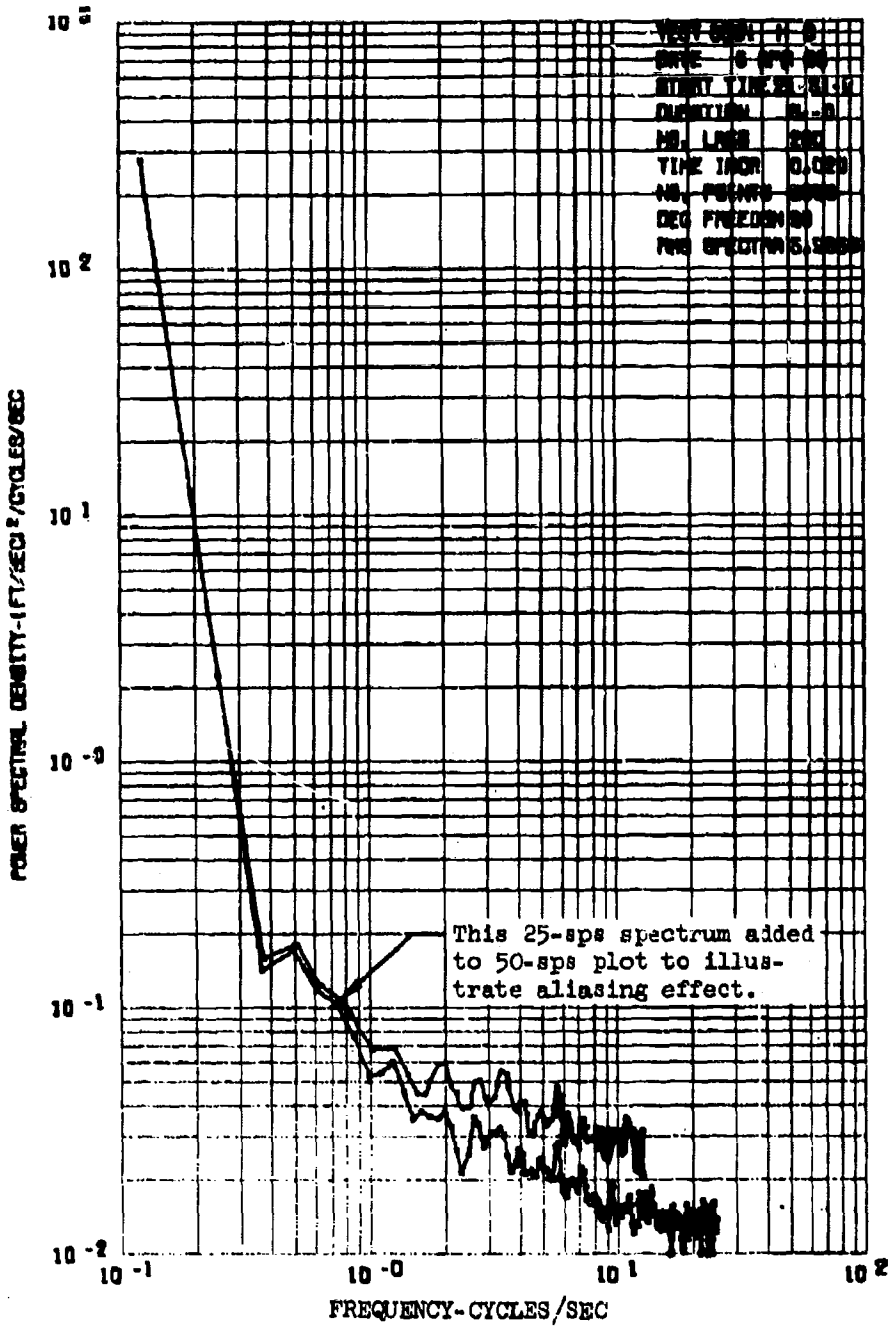

Figure 82. Power Spectrum of Y Velocity

Appendix II

For calibration and maintenance purposes, the data signal flow may be interrupted between the analog multiplexer and the analog-to-digital (A/D) converter with a circuit card which permits calibrate signals to be applied directly to the A/D converter from a remote source such as the field checkout unit.

Digital Subsystem

This subsystem develops all system timing from a 10 kilohertz source in the time code generator, accepts and processes digital input data, generates a binary time-of-day code, develops a parity bit, establishes a data format sequence, develops control signals for the analog subsystem (sample-and-hold, multiplexer, and A/D converter) and drives the record heads of the system tape recorder.

A 20-bit frame synchronization code is developed on a removable program card which can be wired for any desired pattern of bits. This code is presented to the system as two 10-bit words. A 27-bit binary time-of-day code is developed and, coupled with three forced-zero bits, presented to the system as three 10-bit words. The remaining five 10-bit digital input channels are derived from external switch contact closures. Twenty-four of these 50 bits are developed within the system control panel from six decimal (0-9) thumbwheel switches, and the remaining 26 bits are developed from external contact closures within aircraft systems.

Each of ten digital multiplexers accepts a 10-bit parallel digital word (frame sync, time of day, etc.) on 10 lines. An eleventh multiplexer accepts a 10-bit word from the output lines of the A/D converter in the analog subsystem. The outputs of all multiplexer common data bit lines are bussed together and then processed through a parity generator. This network develops on odd parity bit such that there is always present an odd number of logic ONE bits in each 11-bit data word (10 data bits plus parity).

The combined 11 data bits from the digital multiplexer array and the parity generator are gated into record amplifier storage flip-flops. From this storage, data enters the record amplifiers which develop NRZ-MARK drive currents for the digital record head of the system tape recorder. Concurrently, synchronizing clock pulses at the selected system word rate are processed through a twelfth record amplifier and on to the tape deck. The airborne data frame format is shown in Figure 83.

TIME CODE GENERATOR

The PCM system operates in conjunction with an Astrodata, Incorporated, Model 5100 time code generator. The precision frequency standard of the 5100 is a 1 megahertz crystal oscillator which operates in a temperature-stable oven. Stability of the oscillator is 5 parts in 10^9 per day with a corresponding equivalent accuracy of 0.25 milliseconds drift per day.

A standby battery is contained within the time code generator package to maintain accurate time accumulation through any primary power interruption. The

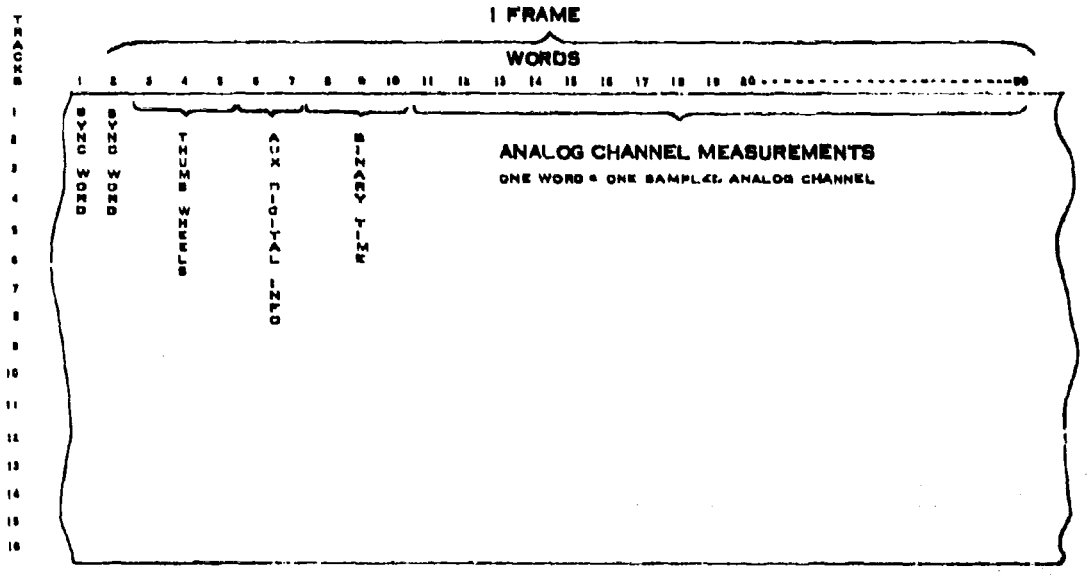

Figure 83. Airborne Data Frame and Tape Format

standby system contains integral charging circuitry from primary system power as well as power-interrupt sensors. The battery has capacity to operate the time code generator for approximately 30 minutes.

This unit develops timing information in various modes for several functions of the instrumentation system. IRIG C time-of-year code is used to modulate a 100 Hz carrier, and this modulated carrier is supplied both to a magnetic tape analog record amplifier and to the airborne oscillograph for recording. This same code in dc level shift form is provided to the PCM package and can be monitored at the PCM checkout unit. A 10-kilohertz square wave is provided to the PCM system from which all PCM timing is derived through counters internal to the PCM. Further, 1 pps and 1 ppm timing signals are provided to the PCM system for use in certain monitor functions associated with the PCM field checkout unit; and power is provided from the standby battery to maintain time accumulation in the binary time generator in the event of primary power interruption to the PCM.

Three rotary thumbwheel switches on the front panel of the time code generator are used to insert the HICAT test number in coded form into the IRIG C time code.

Appendix II

AIRBORNE SENSORS

Turbulence Instrumentation

Gust Probe. The determination of the gust velocity components of atmospheric turbulence from an aircraft flying through it generally requires the measurement of two quantities:

1. Motion of the aircraft relative to the ground.

2. Motion of the air disturbance or gusts relative to the aircraft.

The first measurement is obtained in the HICAT program by recording aircraft motion with respect to inertial or gravity references carried aboard the vehicle. The second measurement is obtained by detecting component changes in flow direction and flow velocity.

The measurement of Item 2 above at altitudes above 50,000 feet from a vehicle operating at high subsonic speeds requires a sensor designed to restrictive specifications. It must operate in temperatures ranging from -100°F to 130°F and atmospheric pressures from 0.5 psi to 14.7 psi without significant change in its zero reference or sensititivity. The instrument must be able to detect atmospheric gusts with velocities as small as 1/2 ft/sec over a frequency range from near zero to 5 Hz. In practice this requires an ability to resolve angular changes in flow direction of the order of 1/20 of a degree.

The fixed vane sensor developed by Lockheed meets these requirements. The sensor consists of a lightweight wedge-shaped vane (4-inch span and 2-inch chord) attached to a specially constructed strain gage beam. The slotted construction of the beam allows the wedge to deflect parallel to itself under load. Figure 84 shows how this deflection takes place without change of angle-of-incidence. Note that this would not be the case if the wedge were mounted on a simple beam as shown in Figure 85. Here the aerodynamic lift load bends the beam and causes the vane to rotate, changing the angle of incidence by a small but undesired amount ($\Delta\alpha$).

By measuring the lift load in terms of shear instead of bending moment, considerations of moment arm changes due to center-of-pressure shifts on the vane can be entirely eliminated. Figure 84 shows the strain gage installation used to accomplish the measurement of the vane vertical shear or lift. The shear is a function of the difference in the bending strains between the forward and aft gage stations. The Wheatstone Bridge circuit arrangement of the strain gages produces an electrical signal directly proportional to this difference. At the same time, the bridge circuit cancels out all unwanted responses. That is, there is no electrical response due to twisting of the vane about its longitudinal axis, no response due to sideways loading of the vane, and no response due to fore-and-aft loading of the vane.

The gust sensor is strong and very stiff. It will withstand without damage airloads as large as ±12 lb distributed over the surface of the vane and has a natural bending frequency of 155 Hz as mounted. This frequency is so much

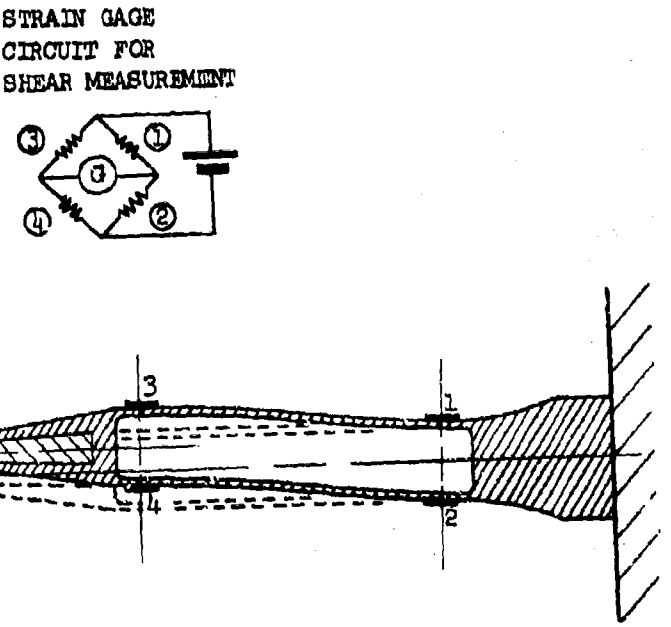

Figure 84. Double Beam Sensor with Strain Gage Installation for Shear Measurement (Sensor Shown Deflected Due to Airload)

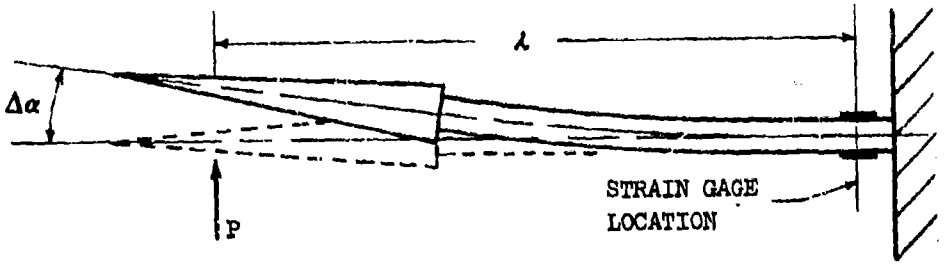

Figure 85. Angular Deflection of Simple Sensor

greater than the turbulence frequencies of interest that maximum amplitude distortion in the measurement is less than 1 percent for frequencies below 10 Hz.

Despite its rugged construction, the gust sensor is extremely sensitive, with an output of 12 mv/v per pound of lift or about 0.15 mv/v for a 1 ft/sec gust at 60,000 feet. This relatively large output is achieved through the use of semiconductor strain gages rather than the usual wire or foil gages.

The HICAT gust probe consists of one vertical sensor (the alpha vane) and one lateral gust sensor (the beta vane) grouped about a central pitot-static tube and mounted on a long stiff boom. The boom supports the sensors sufficiently foward of the aircraft nose so that they will be relatively unaffected by the aircraft flow field. The boom and the sensors can be seen in Figures 86 and 87. Static and dynamic pressures at the boom are determined by a Statham strain gage type airspeed transducer. The boom also houses the United Controls accelerometers to determine normal and lateral accelerations of the boom. In these accelerometers, the seismic mass is loosely suspended and retained in position by a force electromagnetically developed from the position error of the mass. The restoration force, electrically measured, provides a signal proportional to acceleration. The resolution and accuracy of these units are sufficient to eliminate the need for dual range or redundant instruments.

Aircraft Accelerometers. Aircraft cg normal, lateral, and longitudinal accelerations and wing nodal accelerations are recorded in order to define the response of the aircraft. Accelerometers for these applications are United Controls force balance types described in the preceding paragraph. A typical installation is shown in Figure 88.

Total Temperature. Outside air temperature is sensed with a Rosemount Engineering Model 102 total temperature probe mounted in the aircraft nose. Within the altitude-airspeed envelope of the HICAT test aircraft, this instrument has a frequency response that is flat within 1 percent to about 5.7 Hz and flat within 5 percent to 10 Hz. The instrument recovery error, which increases with Mach number, has a maximum value of about 0.12°C and is therefore considered negligible. The self-heating error is also negligible. This instrument can be seen in Figure 89.

Altitude. Aircraft altitude is determined in three presentations. Coarse altitude information is provided by a Statham strain gage pressure transducer with full scale output over the range 0 to 75,000 feet. A second system, manufactured to HICAT specifications by Rosemount Engineering, provides two outputs of high-resolution information. The first is a full scale output (0 to +5 volts) for the overall range of 2 psi which corresponds approximately to an altitude range of 46,400 feet to above 100,000 feet. The second output, derived from the same pressure transducer, provides full scale output (0 to +5 volts) in each of 16 bands over the same altitude range. Switching between adjacent bands is accomplished automatically; and the operating band is automatically defined by 4 switches whose action is entered in binary-coded-decimal form into the PCM digital multiplexer. The Rosemount system is enclosed in a temperature-controlled environment to achieve an overall error in the transducer of less than 0.002 psi. The system can be seen in Figure 90.

Figure 86. HICAT Gust Probe and Boom Installation on Nose of U-2

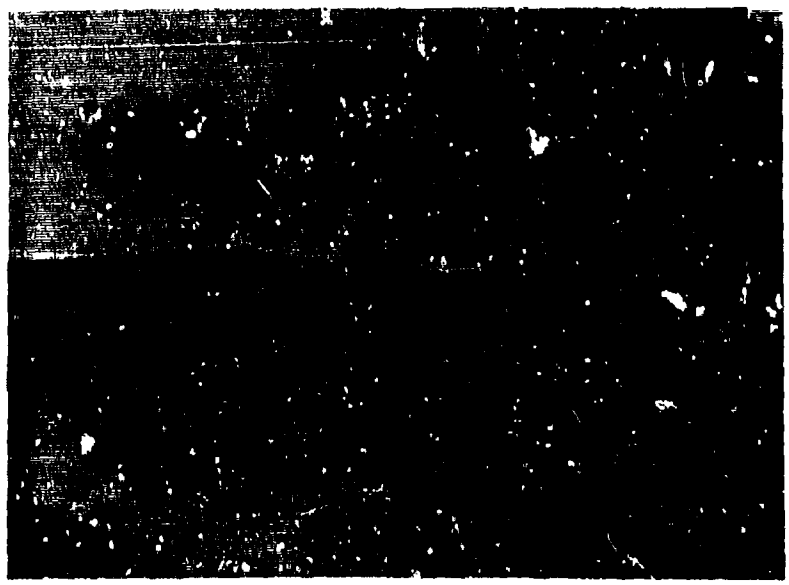

Figure 87. HICAT Gust Sensors - Alpha Vane (bottom) and Beta Vane (right side)

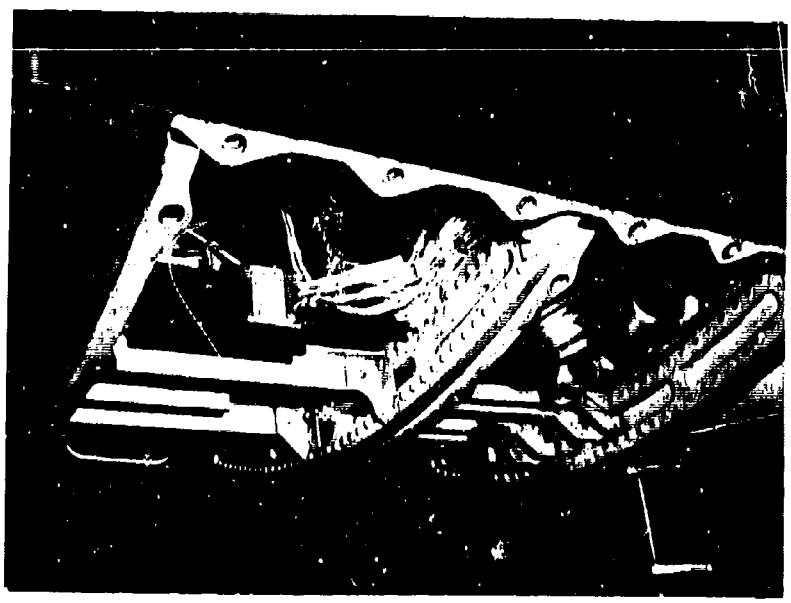

Figure 88. Typical CG Accelerometer Installation

Figure 89. Rosemount Total Temperature Probe

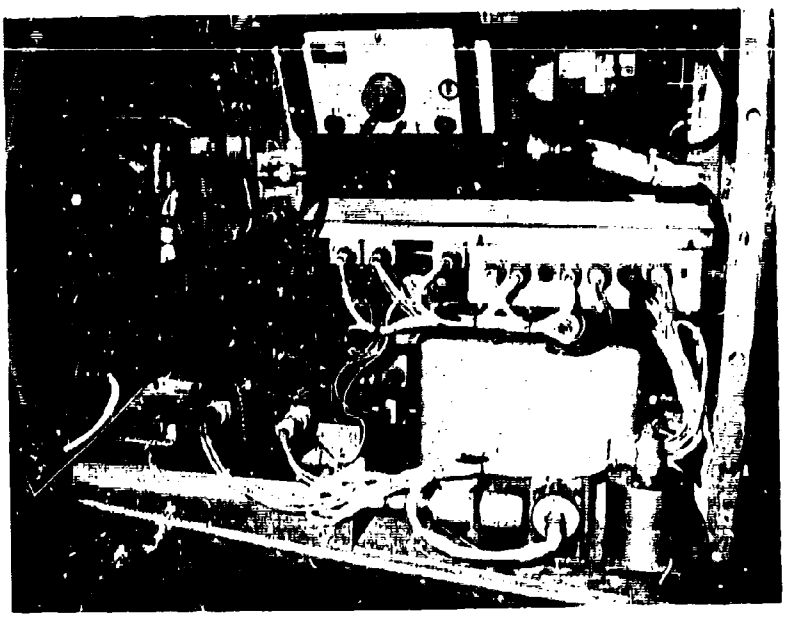

Figure 90. Instrumentation in Aircraft Nose Compartment (Rosemount Altitude System, Rate Gyros, and VGH Recorder)

Attitude Rates. Rate gyros manufactured by R. C. Allen provide a direct measure of aircraft pitch, roll and yaw rates. Gyro output is an ac signal from a microsyn which is demodulated and standardized to a 0 to +5 volt dc signal prior to entry into the PCM system. These instruments are shown in Figure 90 also.

Control Surface Position. Surface position measurements are made by high resolution Giannini potentiometers linked directly to aircraft rudder, aileron, and elevator control surfaces.

Auxiliary Sensors. Aircraft functions such as gear and flap operation, fuel consumption and flight characteristics which are quasi-static or infrequently changing can be monitored by remote switch closure and entered into the PCM data format as single-bit information. This procedure is described in the PCM discussion.

Auxiliary data recorded by this method uses only a portion of the PCM system capability. The vernier altitude system uses four bit positions to depict, in binary-coded-decimal (BCD) form, the specific 1 of 16 altitude bands in which the aircraft is operating at any given time. Two bit positions are used to indicate two pilot signal functions, and another two are used to indicate navigation system fault and no-go. One bit is used to indicate a count in the fuel consumption instrumentation.

Appendix II

A chart showing bit usage of all 10 PCM digital channels is given in Table VII.

Inertial Navigation System (LN-3). Motion of the test aircraft with respect to Earth is monitored by a Litton Industries LN-3 inertial navigation system carried aboard the aircraft. This system can be seen in Figures 55 and 57.

The key element in the LN-3 system is the inertial platform, which isolates the inertial elements from the aircraft through a four-axis gimbal. The configuration permits unrestricted angular maneuverability of the aircraft and prevents platform "gimbal-lock" even if the aircraft were to pitch through the vertical.

Two identical, floated, two-degree-of-freedom gyroscopes provide platform stabilization signals to platform servos which maintain three identical mutually perpendicular accelerometers in a fixed orientation. The platform thus provides simultaneous measurement of aircraft acceleration along the three axes. The platform aligns itself by gyrocompassing to a unique grid north and is maintained at local level by appropriately precessing the gyros. The platform is contained in an environmentally controlled package.

The sensitive element of the accelerometers is a floated pendulum mounted on jewel-and-pivot bearings and equipped with a sensitive pickoff and precision torquer. At operating temperature, the pendulum mass is adjusted to neutral buoyancy in the flotation fluid which completely fills the instrument. An acceleration along the sensitive axis produces a pickoff signal which is amplified and returned to the torquer to restore the pendulum to its null position. The torquer current is a precise measurement of the sensed acceleration, and this quantity forms the basis for determination of aircraft acceleration, velocity and position. These computations are performed by an earth reference computer which is integral with the system.

The gyroscopes in the stabilized platform utilize an independently floated gimbal ring and a spherical, sealed-float assembly for maximum symmetry and rigidity. Precision torquers operating in permanent magnetic fields torque the gyros to maintain the platform locally level. Sensitive pickoffs moving in high-frequency, alternating magnetic fields detect displacements of the platform about each gyro axis.

An adapter unit in the LN-3 system contains a heading servo system and the servo followups which provide outputs of pitch, roll and heading angles.

For the HICAT program, nine data quantities are derived from the precision LN-3 system. These are: vertical acceleration, pitch angle, roll angle, heading sine, heading cosine, North-South velocity, North-South distance, East-West velocity, and East-West distance.

Pertinent performance data on all HICAT sensors is given in Table VI.

TABLE VII. BIT USAGE OF 10 PCM SYSTEM DIGITAL CHANNELS

CH NO	FUNCTION	BIT 10	9	8	7	6	5	4	3	2	1
01	SYNC WORD 1	1	1	1	0	0	1	0	1	0	0
02	SYNC WORD 2	1	1	0	1	0	1	0	1	1	1
03	THUMBSW, RB	A8	A4	A2	A1	B8	B4	B2	B1	RB1	RB2
04	THUMBSW, RB	C8	C4	C2	C1	D8	D4	D2	B1	RB3	RB4
05	THUMBSW, RB	E8	E4	E2	E1	F8	F4	F2	F1	RB5	RB6
06	RB	07	08	09	10	11	12	13	14	15	16
07	RB	17	18	19	20	21	22	23	24	25	26
08	TIME MS DAY	0	0	0	MSB ———						
09	TIME MS DAY	———									
10	TIME MS DAY	———									LSB

THUMBSWITCH FUNCTIONS AND SIGNIFICANCE

A	NOT USED	D	TEST NUMBER HUNDREDS
B	NOT USED	E	TEST NUMBER TENS
C	NOT USED	F	TEST NUMBER UNITS

REMOTE BIT SIGNIFICANCE

RB NO	FUNCTION	RB NO	FUNCTION
01		14	NAV SYSTEM FAULT
02		15	
03		16	FUEL REMAINING 0.5
04		17	
05		18	
06		19	
07	ALTITUDE RANGE 8	20	
08	ALTITUDE RANGE 4	21	
09	ALTITUDE RANGE 2	22	
10	ALTITUDE RANGE 1	23	
11	PILOT SIGNAL STEADY	24	
12	PILOT SIGNAL MOMENTARY	25	
13	NAV SYSTEM NO-GO	26	

Appendix II

Pilot's Instrumentation

Basic instrumentation power functions are controlled from the cockpit. Remote switches provide on/off control of the PCM system, the magnetic tape recorder, and the oscillograph. Start/Stop and Fast Forward controls and a "Tape Remaining" visual indicator are provided for the tape recorder as well as Start/Stop and calibrate control for the oscillograph. These can be seen in Figures 61 and 62.

Inertial navigation information is provided to the pilot independent of the instrumentation system. The aircraft ground speed is presented and allows the pilot to make accurate determinations of winds aloft as well as easing his navigation effort. The aircraft position, in nautical miles along the X and Y grid system from his point of origin, is also displayed. This permits the pilot to make an accurate return to a point in space in the event he encounters turbulence in a small area. It also enables him to navigate over water where no fixes exist. Thus, on an over-water mission, the pilot can fly to a predetermined X and Y position.

The pilot may enter information into the instrumentation system in several ways. The PCM control panel contains six thumbwheel switches previously described, and another panel provides a dual-mode pilot signal toggle switch.

Thumbwheel switches, A, B, and C are currently unused. Switches D, E, and F are used to enter HICAT test number in hundreds, tens and units, respectively. This entry is generally made by the HICAT field team rather than by the pilot. The dual-mode pilot signal toggle switch provides either a steady or momentary event signal. These signals are entered into the PCM digital multiplexer as remote bits 11 and 12, respectively, and are recorded concurrently on the airborne oscillograph.

Installed in the cockpit are a mechanical accelerometer and an outside air temperature indicator.

The pilot carries with him a 35-mm Kodak Motormatic camera to take still photographs of weather formations which are used in the evaluation of turbulence data.

SPARMO Radiation Counter.

A three-channel radiation detector is carried aboard the HICAT test aircraft to collect auxiliary data not peculiar to present HICAT investigations. The SPARMO unit in use was developed as a balloon-borne device to detect ionizing radiation at high altitudes and is an outgrowth of a sonde that has been in operation for several years at Max-Planck-Institut fur Aeronomie, Institut fur Stratospharen-Physik, Lindau/Harz, Germany. Development of the present unit was done in cooperation with Laboratoire Cosmique, Meudon, France and Fa. A. Sprenger KG., St. Andreasberg, Germany. The unit was supplied to the HICAT Project by the French Cosmic Physics Laboratory through the French Embassy in Washington, D.C. A block diagram of the system is given in Figure 91, and the installation in the aircraft can be seen in Figure 57.

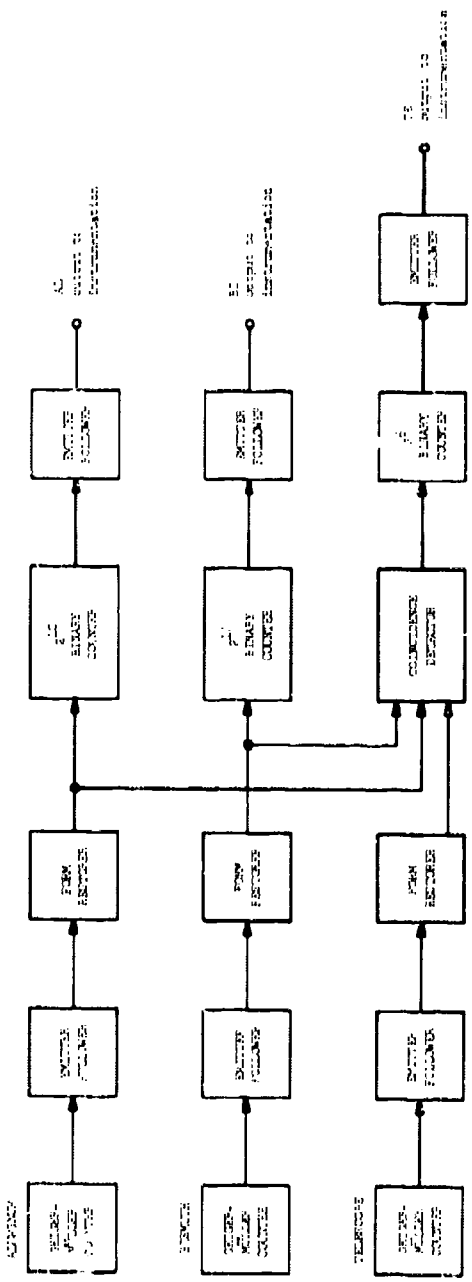

Figure 91. Block Diagram of SPARMO Radiation Counter

Appendix II

The detector consists of three Geiger-Muller counters mounted horizontally and stacked vertically to form a "telescope" aimed toward the zenith. One of the counters uses an aluminum diaphragm of 30 milligrams/square centimeter of thickness, and a second has a bismuth diaphragm of 135 milligrams/square centimeter. Efficiencies of the two counters are different with respect to photons of energies below 1 mev, and this difference can be used to approximate the average energy of photons which can reach the detector at HICAT altitudes. Discrimination between photons and charged particles is made by coincidences with the telescope which is uniquely sensitive to charged particles. This is achieved through the vertical stacking such that a particle approaching from the zenith must pass through the aluminum and bismuth counters in order to be counted by the telescope counter.

Each of the counters is followed by an emitter follower and a form restorer or pulse shaping network to provide calibrated pulses. These pulses are used to drive a 2^{10} binary counter whose final stage drives an emitter follower for data output. Between two identical output states (1 or 0) the number of particles having ionized the radiation counter is 1024. If the data pulse train is recorded with a time base, the value of the computation or count as a function of time can be determined by measuring the time interval between two successive states of the binary counter output stage. This is illustrated in the following sketch.

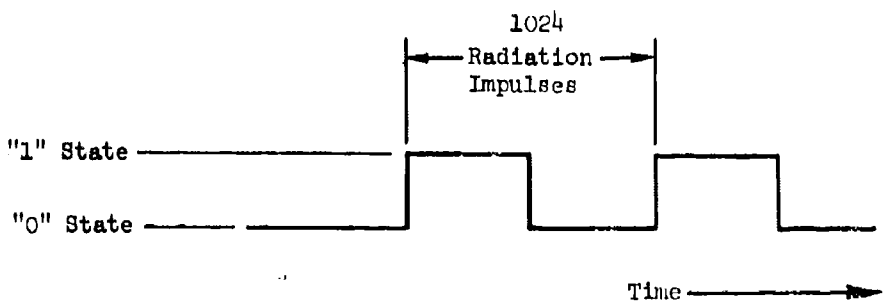

For the telescope circuit, the output of the form restorer of each radiation counter is entered into a selector circuit which delivers an impulse at triple coincidence (a logic AND gate). This results in a single pulse when the three radiation counters are ionized simultaneously. The selector circuit drives a 2^{6} binary counter whose output is identical to the 2^{10} counters except that its period represents 64 radiation counts rather than 1024. The voltage level of the "0" state is 0 volts and the level of the "1" state is +5-vdc. The three outputs are entered directly into three analog channels of the PCM system and into the oscillograph.

RECORDERS

Magnetic Tape

The airborne magnetic tape recorder is an Ampex, Inc., Model AR 216 equipped with a 16-track digital record head stack. The PCM system output is 12 lines (10 data lines, 1 parity character line, and 1 synchronizing clock pulse line) of NRZ-MARK record head drive currents which are tailored to drive the Ampex heads directly without further buffering. The PCM data is recorded, then, in a 12-bit parallel format.

Three Ampex analog direct record amplifiers are available for recording auxiliary information. Two of these are used to record IRIG C time in carrier-modulated form for tape search and control purposes during ground station processes. Original plans to record pilot's voice annotation on the third analog channel were never consummated because the retrieval of such information proved to be too costly. Three heads in the digital stack are used to record the analog signals, and satisfactory record levels are achieved. Recorder track assignments are shown below.

Track No.	Data
1	Bit 2^0 (LSB)
2	Bit 2^1
3	Bit 2^2
4	Bit 2^3
5	Bit 2^4
6	Bit 2^5
7	Bit 2^6
8	Bit 2^7
9	Bit 2^8
10	Bit 2^9 (MSB)
11	Parity Bit
12	Clock Bit
13	Not Used
14	IRIG C Coded Time
15	Not Used
16	IRIG C Coded Time

The recorder has the capacity for recording data for a continuous period of eight hours at a tape speed of 1-7/8 ips using 4600 feet of 1.0 mil, thin oxide magnetic tape. Optimum recording parameters for HICAT evolved into a tape speed routine of 1-7/8 ips and a PCM scan rate of 25 frames per second. This results in a bit packing density on the tape of 667 bits per inch.

This machine measures 27 x 12 x 8 inches and weighs 65 pounds. The recorder analog electronics cabinet measures 16 x 8 x 4 inches and weighs 9 pounds. The installation in the aircraft can be seen in Figure 57.

Oscillograph

A Lockheed-owned 48-channel Midwestern Model 591 oscillograph is included in the airborne system to provide quick-look data for the field team after each flight. These quick-look records are also used for editing purposes prior to ground station processing of the magnetic tapes and then become a permanent part of the HICAT data files. A portable oscillogram processor which is carried as part of the ground support equipment enables the field team at the test site to develop and view the records immediately following each flight.

Data signals to the oscillograph are provided from the PCM package following presampling filtering as described in the PCM section of this report. The signals are isolated and conditioned to a suitable galvanometer recording level at the oscillograph integrated control system. This control system also has provisions for interrupting data signal flow to the oscillograph and substituting a precision calibrate voltage in each channel. The calibrate cycle is initiated by a cockpit switch and sequencing is accomplished automatically within the control box. All data channels shown in Table VIII as well as IRIG C time and pilot event signals are recorded on the airborne oscillograph. The oscillograph measures 15 x 18 x 40 inches and weighs 150 pounds. Its installation in the aircraft is shown in Figure 92.

VGH Recorder

A NASA VGH recorder is carried aboard the HICAT test aircraft for purposes of obtaining additional time history records of the aircraft's airspeed, altitude and normal acceleration. Installation in the aircraft can be seen in Figure 90.

The NASA instrument contains two pressure-sensitive elements for measuring airspeed and altitude, a galvanometer element for measuring the output of the remotely located acceleration transmitter, and a timing mechanism. Each element causes rotation of a mirror which in turn moves a reflected lamp image across the recording medium. Recording is effected on a 200-foot roll of 70-mm photographic paper. A removable recording drum advances the paper at a rate of approximately 20 feet per hour with a resulting recording time of approximately 10 hours.

POWER SUPPLY

A Bendix 3-phase rotary inverter provides the 400-Hz power required to operate the LN-3 system. This inverter also provides heater power to the Rosemount altitude system and power to operate the PCM checkout unit during preflight operations. The oscillograph and PCM systems operate directly from the +28-vdc ship's power. The inverter installation in the aircraft is shown in Figure 93.

TABLE VIII. TYPICAL PCM ANALOG CHANNEL USAGE

PCM CHANNEL	MEASUREMENT
11	Zero volts
12	Four volts
13	α-vane force
14	β-vane force
15	Indicated airspeed
16	Vertical acceleration (LN-3)
17	Gust probe normal acceleration
18	Gust probe lateral acceleration
19	Vernier altitude
20	Total temperature
21	"Aluminum" Radiation count
22	Roll rate
23	Yaw rate
24	CG normal acceleration
25	CG lateral acceleration
26	CG longitudinal acceleration
27	Elevator position
28	Left aileron position
29	Rudder position
30	Coarse altitude
31	"Bismuth" Radiation count
32	Left wing nodal acceleration
33	Right wing nodal acceleration
35	Pitch angle (LN-3)
36	Roll angle (LN-3)
37	Heading sine (LN-3)
38	Heading cosine (LN-3)
39	X-velocity (LN-3)
40	Y-velocity (LN-3)
41	Telescope Radiation count
42	Y-distance (LN-3)
43	Pitch rate
44	Fine altitude
45	X-distance (LN-3)

Note: Minor variations occurred in this setup during some early HICAT tests.

Appendix II

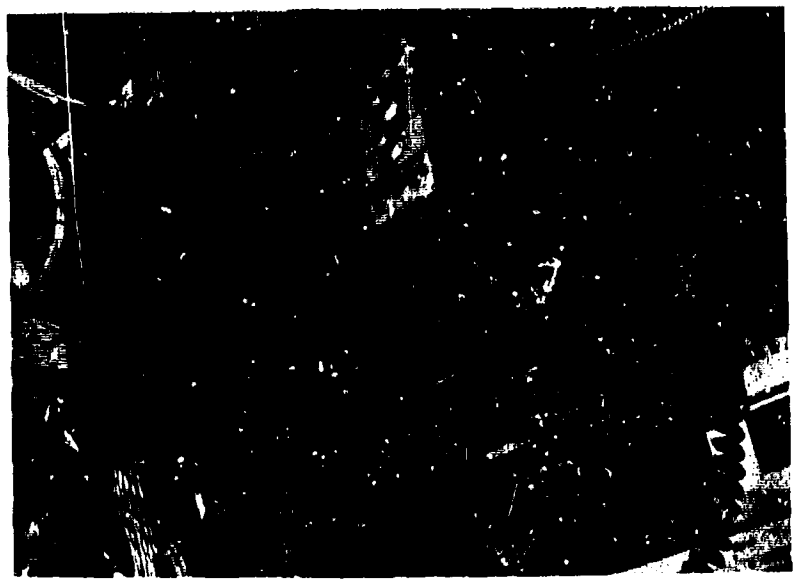

Figure 92. Oscillograph Installation in Q-Bay

Figure 93. Instrumentation Inverter in Q-Bay

Appendix II

FUNCTIONAL DESCRIPTION OF GROUND EQUIPMENT

FIELD TEST EQUIPMENT

The basic maintenance and checkout equipment for the PCM system is a field checkout unit which was designed and manufactured as a part of the overall PCM system; it is shown in Figure 94. The unit is best described in terms of its analog simulation and digital subsystems.

Analog Simulation Subsystem

The analog source simulation circuitry provides both discrete and continuously variable precision voltages which can be applied as a differential input to any combination of analog channels simultaneously. Front panel switches select 0, 1, 2, 3, 4, or 5 volts, internal variable, or externally applied voltages. Front panel test points are provided for monitoring the selected calibrate voltage, and front panel jacks are provided for inserting external voltages. The simulation circuitry also provides a selectable source impedance, balanced or unbalanced, which consists of a precision rheostat in each output leg of the simulated source. Each of these rheostats can be varied from zero to 10 kilohms in 10-ohm steps, and each is controlled from the front panel. Front panel jacks accommodate external inputs for simulating common mode voltages and overvoltages.

Digital Subsystem

The digital timing and data display section provides for testing the digital portion of the PCM system for correct operation. A binary light display is incorporated for visual display of all 12 data bits in any of the 50 words in the PCM format, with word selection accomplished by front panel switches. Input circuitry to this display is driven by the NRZ-MARK waveforms which normally drive the tape recorder heads. Test points are mounted on the front panel so that an oscilloscope can be used to examine each word in the format.

Inputs into the digital input channels can be simulated by use of ten toggle switches which insert either a logic ONE or logic ZERO in any bit position of the five available digital words.

All dc voltages, both regulated and unregulated, used in the PCM system can be monitored in the checkout unit by means of a voltmeter and selector switch which are mounted on the front panel. In addition, two meter terminals are brought out on test points so that these voltages can be measured with an external voltmeter.

Front panel switches provide for inserting a precision voltage into the A/D converter for calibration, as described in the PCM discussion. Another front panel switch exercises the analog multiplexer, with test points for observing the PAM pulse train.

Appendix II

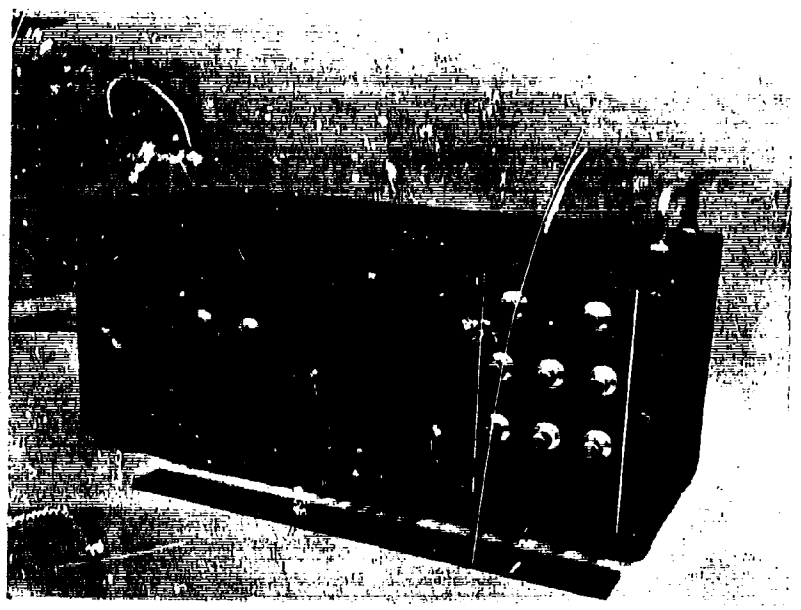

Figure 94. PCM Field Checkout Unit

Other front panel test points provide monitor capability for the following PCM functions and checkout aids:

10-kilohertz clock

Scan rate clocks

Analog multiplexer drive lines

Sample-and-hold gate trigger

Binary time of day stop (read) trigger

Frame rate

IRIG C code in dc level shift form

1 pps wavetrain

Checkout unit internal voltages

Sync pulse for external oscilloscope.

Oscillogram Processor. A Consolidated Electrodynamics Corporation Type 23-109B-P4 portable oscillogram processor accompanies the field team as part of the ground support equipment. This equipment is a completely self-contained motorized unit which develops and dries oscillograms. No external water circulating system is required, and the processor can be operated in a normally illuminated room without danger of fogging the most sensitive recording papers.

Gyro Bias Test Set. The gyro bias test set allows accurate bias adjustments on the LN-3 gyros in the field to eliminate drift. It has controls for placing the LN-3 system in the open-loop mode and recorders for analyzing the drift rates of the three gyros. In the open-loop mode the gyros are free to drift and a bias torque can be applied to eliminate the drift. The test set indicates the amount of bias to be used. It also contains a test point panel where system performance can be evaluated by use of voltmeters. This instrument is shown in Figure 95.

Miscellaneous Test Equipment. A Hilger and Watts Clinometer is carried with the field team for use in calibration and checkout of instrumentation accelerometers and gust sensors. A John Fluke voltmeter and a Hewlett-Packard dual-trace oscilloscope are also included in the ground equipment to aid in calibration and troubleshooting.

PCM GROUND STATION

The complete HICAT data processing ground station with all peripheral equipment consists of the following items:

CEC Model VR-2600 input magnetic tape reproducer

Astrodata Model 5220-100 IRIG time code translator

Astrodata Model 5224-100 tape search and control unit

LEC Model PCD 101A PCM telemetry decommutation and computer tape buffer-formatter system

CEC Model 5-133 direct print oscillograph recorder (Lockheed-owned)

IBM Model 729 V magnetic tape recorder (Leased from IBM)

The airborne data, which is recorded digitally on magnetic tape at 1-7/8 inches per second using parallel format PCM techniques, is reproduced on the CEC Model VR-2600 magnetic tape reproducer at 30 inches per second and input to the ground station, permitting data conversion at 16 times the real-time recording speed. The HICAT digital input format is a parallel 12-bit format with a 10-bit data word, a lateral parity bit and a synchronizing clock bit. Additionally, IRIG C time code is recorded on two of the remaining four tracks using analog techniques.

Appendix II

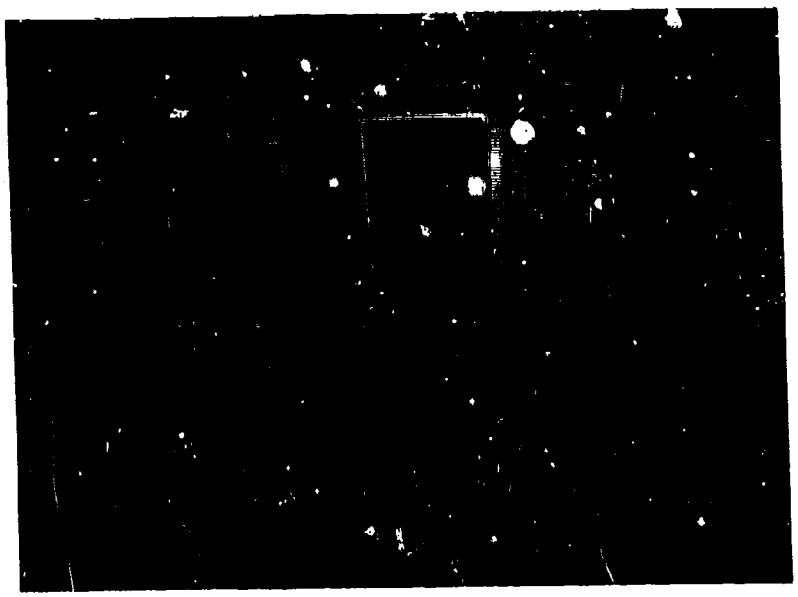

Figure 95. Gyro Bias Test Set Used With LN-3 System

The HICAT recorded frame length is 50 words, including 2 Barker Code words for synchronization, 5 words for reference data, 3 words for time-of-day code and 40 words available for analog data.

The system will accept the parallel data inputs at a word rate of 36,000 words per second for an 11-bit word. The input format, including the input coding, word length, frame length and frame synchronization is programmable on a removable patch board. The system is capable of handling serial or parallel data in NRZ-MARK or RZ format. The word length is programmable from 4 to 16 bits. Prime frame length is programmable from 2 to 399 words. The frame sync word is programmable from 4 to 32 bits in the search mode. In check and lock modes, the frame sync is programmable as one, two, or three consecutive words.

The VR-2600 tape reproducer is controlled by the Astrodata tape search and control unit and the time code translator. By means of thumbwheel switches, the start and stop times from the IRIG C code for the selected data to be processed through the ground station may be manually set into the control unit. The data to be processed through the ground station is visually selected from the airborne-recorded oscillograph record. IRIG C time is recorded on the oscillograph record to provide the start/stop time inputs to the control unit. The IRIG C time code recorded by analog techniques on a separate track on the tape is input to the time code translator where it is translated to a parallel BCD time code which is input to the tape search and control unit. A visual

display presents the translated time from the input tape in days, hours, minutes, and seconds for monitoring purposes. When the search mode is put into operation, the tape time, as received from the time code translator, is constantly compared with the run start time set in by the thumbwheel switch on the tape search and control unit. When equivalent time is achieved in the parallel comparator, a start pulse initiates the transfer of data from the input tape to the level shifting amplifiers on the ground station. Data is read into the ground station until the time comparison logic detects equivalence between tape time and run end time as manually inserted with the thumbwheel switches. A stop pulse is then generated to stop the transfer of data from the input tape.

Parallel data from the input tape is amplified and then input to a shift register where a 500 kHz clock shifts the parallel data bits out of the register in serial fashion.

The serial word-bit patterns, both sync and data, are clocked into the decommutator. The frame synchronization pattern preceding the data words is compared to a patched sync code. The input serial data train is converted to continuously available parallel output data. These data words are gated to the decommutator output subsystems by the decommutator control logic which is dependent upon the patched word, sync, and frame formats.

Three output subsystems provide analog, visual, and digital outputs simultaneously: The digital-to-analog conversion subsystem, the decimal display output subsystem, and the buffer formatter subsystem.

Fourteen storage registers and fourteen D/A converters simultaneously provide 14 dc analog outputs selected from any of the digital data words by means of thumbwheel switches on the control unit. The analog signals are input to a CEC direct-write oscillograph recorder for immediate and simultaneous analog display of up to 14 data channels plus IRIG C time. This analog record provides a means of monitoring playback of the data, for analysis and editing, and for troubleshooting. The eight most significant bits from the decommutator output (MSB) bus are parallel-connected to each of the 14 independent D/A converters.

The decimal display provides a visual digital monitoring of any two channels simultaneously. Two four-decade decimal displays are provided which simultaneously convert the 13 most significant bits of any pair of words from binary to decimal. Display modes are "Read Continuous" and "Read Hold". "Read Continuous" is automatically updated; "Read Hold" may be manually updated. Channels are selectable by means of thumbwheel switches on the control unit.

The buffer-formatter receives words programmable from 4 to 14 bits from the decommutator output MSB bus. In addition, there are 24 bits input to the buffer-formatter for run identification information which are inserted manually by means of thumbwheel switches on the control unit. The run identification data is entered before the first data character in each record.

Appendix II

The core memory has a capacity of 4096 seven-bit characters. Data is gated into memory in six-bit groups with each group becoming one memory character. Each character is accompanied by a parity bit (odd parity) during entry into memory which is generated at the input data gate and monitored during the memory read-cycle at the output register. Data is loaded into the "input side" of memory until the number of six-bit words that are stored is equivalent in number to the selected record length. Record lengths of up to 2048 six-bit characters may be selected by means of octal switches at the rear of the control panel. The HICAT record length is 1446 characters.

When a full record length is achieved in the input storage register, the output storage register dumps the stored record. The record in the input storage register is transferred to the output storage register and new data is loaded into the input storage register to complete the cycle. Memory cycle time is 2.0 microseconds.

Data records are fed to the IBM 729 V tape recorder under automatic control of the buffer-formatter control logic. The control logic further provides a reset-to-zero for decommutator parity errors and stops further formatter operation if an error is detected in core memory operation. Data is stored on seven-track magnetic tape in computer-compatible format at a recording density of 800 bits per inch per track at a tape speed of 75 ips. The format consists of parallel six-bit characters with lateral and longitudinal parity, a 3/4-inch inter-record gap and an end-of-file mark and gap. Each 10-bit PCM data word plus two dummy bits is formatted into two parallel, six-bit characters.

The ground station is shown in block form in Figure 96 and photographically in Figure 97. Ground station Operation and Maintenance manuals are listed as Reference 16.

OPERATIONAL PROCEDURES

Documentation of field operation data is prepared as shown in Figure 98. Instrumentation procedures attendant to a HICAT flight are best described in terms of a check list, as noted below:

PREFLIGHT

Tape Recorder

1. Clean record heads
2. Load with unrecorded tape
3. Check tape speed LO-HI range switch is set to LO (1-7/8 in. per sec).
4. Check function of tape recorder using cockpit controls. Recording lamp will flash during normal operation.

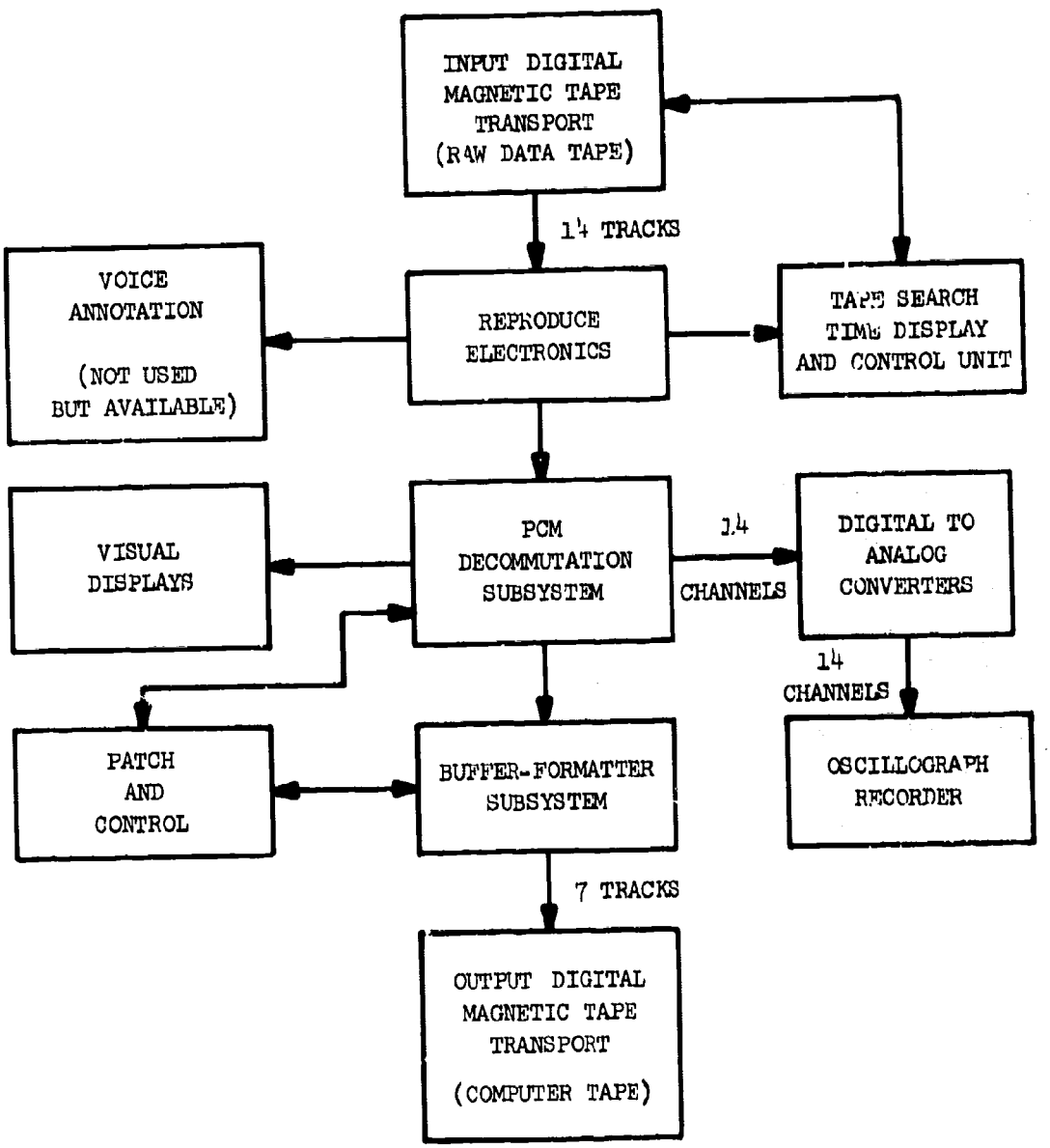

Figure 96. HICAT Data Processing Ground Station

Appendix II

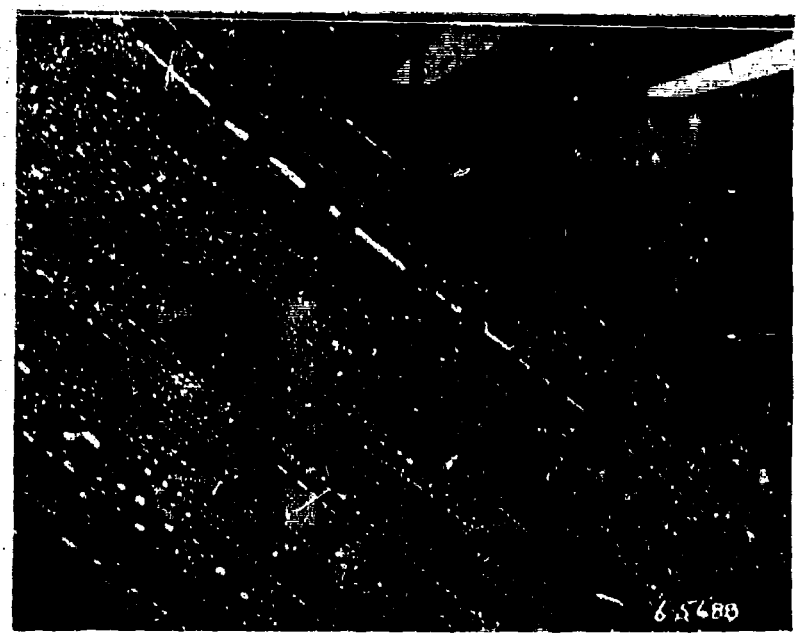

Figure 97. PCM Ground Station

Oscillograph and Calibrator

1. Load magazine and install on recorder

2. Check speed selector switch set to position 1. (0.162 in. per sec).

3. Press lamp test and check illumination of standby lamps.

4. Note NO RECORD lamps are out while recorder is running with loaded magazine fitted.

5. Check recorder operation using cockpit control.

6. Check operation of calibrator. A calibration cycle takes 60 seconds to complete.

PCM and Time Code Generator

1. Connect PCM test set and carry out a function check of each analog channel. Remove tester after checks complete.

2. Set up time of day on time code generator and PCM, for some convenient time ahead, and at that time synchronize with the cockpit stopwatch.

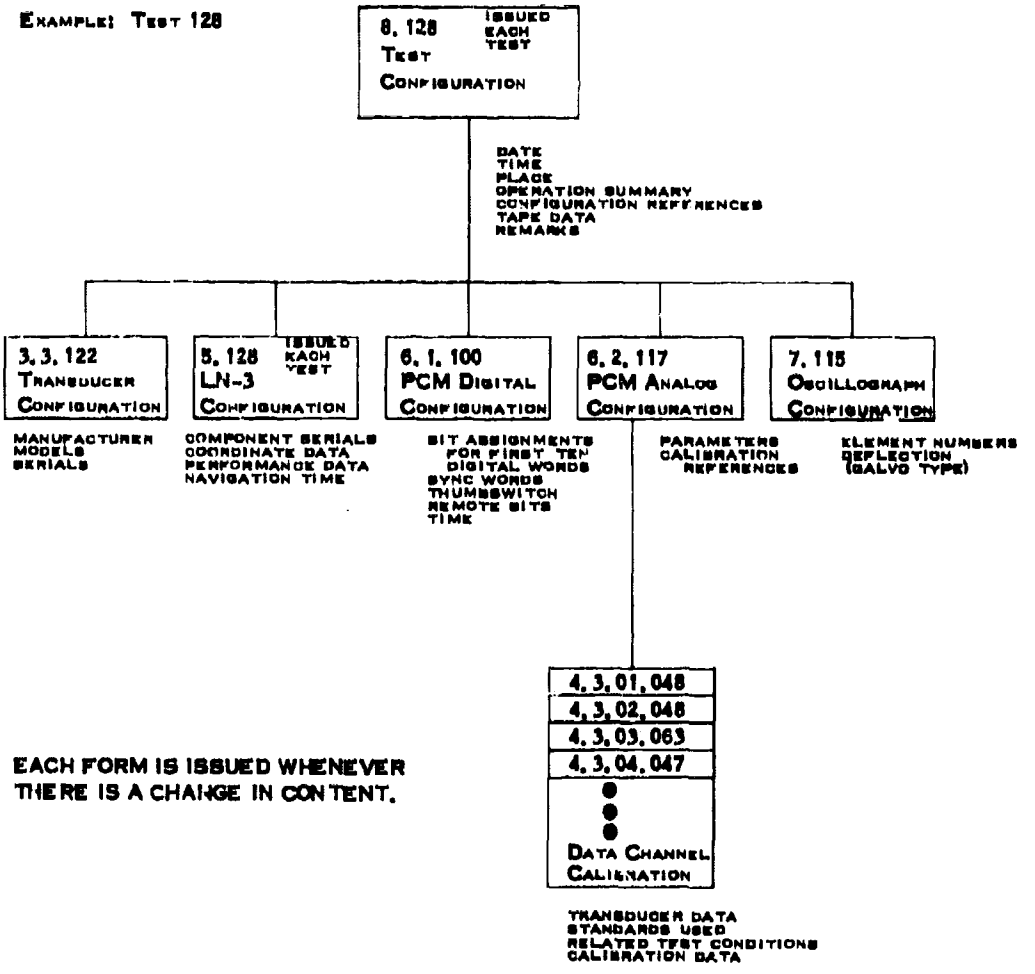

Figure 98. Organization of Field Operation Data

3. Set test number on time code generator and on thumbwheel switches in cockpit.

LN-3 Inertial Platform

1. Set up the alignment coordinates either on base or off base as required.

2. Set aircraft true heading (magnetic heading ± magnetic variation) on the heading dial.

3. Turn on the system in the following order:

a. Selector switch to STANDBY. This allows the platform and computer to heat to operating temperature. The heating period is 10-15 minutes from a cold start, depending on ambient temperature. During the heating period, the heat lamp will be on until the platform reaches its operating temperature. When the heat lamp goes out the selector switch may be turned to ALIGN.

b. Selector Switch to ALIGN. This causes the platform to progress through 3 modes, coarse align, fine align, and gyro compassing. As soon as the platform goes into the gyro compass mode, the mode light comes on steady; and when the gyro compass cycle is complete, the mode light blinks and the alignment is complete.

c. Selector Switch to NAV. As soon as the mode light begins blinking, the platform is ready to navigate and the NAV position may be selected.

4. After the platform has aligned, set the cockpit X and Y counters to 000.0 and the hatch X and Y counters to 500.0.

PRESTART CHECK

1. Turn on tape recorder. Check record light blinking.

2. Turn on oscillograph. Check record light on.

3. Check PCM switch on and light on.

4. Check LN-3 selected to NAV.

5. Press calibrate button. Check light on for 60 seconds.

POSTFLIGHT

Tape Recorder

1. Rewind tape and remove recorded tape from recorder.

2. Check switches off.

Oscillograph

1. Remove magazine.
2. Check switches off.
3. Process record.

PCM and Time Code Generator.

Check PCM switch OFF.

Note: It is important that this switch is in the OFF position when there is no external power connected to the aircraft. Otherwise the time code generator will switch automatically to its internal battery which will completely discharge in 30 minutes.

LN-3 Inertial Platform

1. Check selector switch to OFF.
2. Note terminal error on hatch X and Y coordinates.

CALIBRATION PROCEDURES

Calibration of the instrumentation system components can be accomplished in any of several ways. Routine procedures require that all sensors be calibrated in the laboratory prior to installation in the test aircraft. This laboratory calibration provides a direct measure of the linearity, sensitivity and repeatability of the sensing system and can be accomplished using certified primary laboratory standards which are directly traceable to the National Bureau of Standards. The response of the PCM system and the complementary oscillograph recording systems can be determined analytically with the sole restriction that proper impedance matching take place between the sensor and the remainder of the system. Once the instrumentation system with its sensors is installed in the aircraft, however, periodic check calibrations are required to maintain the data precision necessary to the HICAT project.

A calibration performed in the field is generally a direct end-to-end calibration of the sensor and all other elements in its recording channel. It is performed by subjecting the sensing device to a direct physical stimulus while monitoring the output of the recording system. In the HICAT field operation, system output is readily monitored on the field checkout unit. Field calibrations are thoroughly documented on the form shown in Figure 99.

PCM SYSTEM

In general, three procedures are available for calibrating the PCM system analog channels (with the exception of channels 1 and 2, which are permanently patched to 0 and 4 volts, respectively, for purposes of performance monitoring of the analog-to-digital converter).

Appendix II

LOCKHEED-CALIFORNIA COMPANY
HICAT PROJECT FIELD OPERATION DATA 4.3. . .1

DATA CHANNEL CALIBRATION PERFORMED BY

CHANNEL

FIRST USED ON TEST IS/IS NOT APPLICABLE TO EARLIER TESTS.

TRANSDUCER DATA: (IF NO ENTRIES, SEE 4.3. . .1.)

VENDOR:
MODEL NO: SERIAL NO.
INSTRUMENT RANGE: TO IN
IF AUXILIARY CIRCUITRY USED, SEE 3.2.

CALIBRATION DATE: 196 . TIME: START:
REASON: FINISH:

CALIBRATION STANDARDS USED:

RELATED TEST CONDITIONS:

TAPE IDENTIFICATION IF USED: IRIG C TIME IF RECORDED:

CONTAINER: - - START:
BASE MARKING: FINISH:

CAL STIMULUS PT UNITS NO.	IRIG C TIME DAY H M S	PCM LAMP OCTAL	PCM DEC COUNT	EQUIV VOLT LEVEL	THEO DEC COUNT
01				.	
02				.	
03				.	
04				.	
05				.	

Figure 99. Sample Field Calibration Data Sheet

Procedure I

Procedure I involves the removal of the PCM package cover, which is not a normally recommended field procedure. It does, however, enable the adjustment of the individual channel modules to achieve full system resolution while accommodating transducer impedances as large as 10,000 ohms

1. Determine the analog channel source (sensor/signal conditioner) impedance.

2. Using the field checkout unit (FCU), simulate the channel source impedance by inserting one-half the impedance in each input line.

3. Vary the FCU analog source voltage, and while monitoring the channel output on the binary display, adjust the particular channel input buffer amplifier module gain and offset potentiometers for zero offset at 0 volts and full scale at 5 volts. These adjustments are accessible with the package cover removed.

Note: To compensate for interaction, it may be necessary to readjust these controls several times.

4. Connect the sensor to the system, apply proper known stimulus, and observe the channel binary output. Make any necessary gain and zero adjustments in signal conditioning circuitry for final zero and full scale output.

5. Repeat application of known stimulus values. Observe and record final channel calibration data.

Procedure II

Procedure II is recommended for use when sensor stimulus is available in the desired accuracy tolerance for the particular measurement to be recorded and when some degradation of system resolution can be tolerated in the case of high impedance sources.

1. Connect the sensor to the system, apply proper known stimulus, and observe the channel binary output. Make any necessary gain and zero adjustments in signal conditioning circuitry for final zero and full-scale channel output.

2. Repeat application of known stimulus values. Observe and record final channel calibration data.

Procedure III

Procedure III is recommended for use when a sensor and associated laboratory calibration are used without an end-to-end system calibration. Examples are accelerometers, certain high-accuracy pressure sensors, and rate gyros. This procedure is often necessary to avoid transporting laboratory standards and other high-accuracy stimulus monitoring equipment to remote field locations.

Appendix II

1. Determine the analog channel source (sensor/signal conditioner) impedance from lab calibration data sheet.

2. Using the FCU, simulate the channel source impedance by inserting one-half the impedance in each input line.

3. Connect an accurate voltmeter, such as a Fluke, to the FCU analog source monitor. Vary the voltage applied through the simulated source impedance over the range shown on the lab calibration while monitoring the channel binary output.

4. Record the binary output for the values of sensor open circuit voltage applied through the simulated source impedance for the final channel calibration data.

Calibrations are performed periodically, when a sensor or other channel module is changed, or when test data looks questionable. Apart from sensor integrity, which can be determined with the sensor removed from the rest of the system, other system parameters (such as offset, gain, linearity, cross talk, over-voltage protection, common mode voltage rejection, A/D converter, and filter performance) can be evaluated with the FCU. Detailed procedures for obtaining this data are provided in the PCM system Operation and Maintenance Manuals and in the system Acceptance Test Procedure. These documents are shown as References 17 and 18 to this report.

LN-3/PCM SYSTEM

The LN-3 system is calibrated in conjunction with the PCM by performing operations as outlined below:

Vertical Acceleration

1. Align LN-3 system to local coordinates.

2. Using a Kearfott precision angle indicator (PAI), determine pitch and roll angles of the inertial platform.

3. Place LN-3 in NAV mode.

4. Torque azimuth gimbal to 180 degrees.

5. Torque pitch and roll gimbals to angles determined in step 2.

6. Read PCM output (count) on vertical acceleration channel. This is a +1.00000g condition.

7. Torque the roll gimbal in 10 degree steps, maintaining a constant pitch angle, and read the PCM count at each step. Acceleration in g is the cosine of the roll angle.

Pitch Angle

1. Align LN-3 to local coordinates and then switch to NAV.

2. Torque azimuth gimbal to 180 degrees as measured on PAI.

3. Torque the pitch gimbal to 0 degrees as measured on PAI and read PCM count. This is a level flight condition.

4. Torque the pitch gimbal in 3 degree steps to both count limits of the PCM, reading the count at each step.

Roll Angle

1. Align LN-3 to local coordinates and then switch to NAV.

2. Torque azimuth gimbal to 180 degrees as measured on PAI.

3. Torque the roll gimbal to 0 degrees as measured on PAI and read the PCM count. This is a zero-degree roll angle.

4. Torque the roll gimbal in 3 degree steps to both count limits of the PCM, reading the count at each step.

Heading Angle (Sine and Cosine)

1. Align LN-3 to local coordinates and then switch to NAV.

2. Torque azimuth gimbal to 180 degrees, as measured on PAI.

3. Open Schuler loop.

4. Read PCM count for both sine and cosine channels (PAI reading is displaced 180 degrees from actual heading).

5. Torque the azimuth gimbal in 10 degree increments and read PCM count for heading sine and cosine channels at each step.

X Velocity

Simulated velocity voltages are obtained from the LN-3 computer by slewing the inertial platform off level. Thus, an acceleration results and the computer will produce an increasing velocity. To stop or slow the rate at which the velocity voltage is changing, the platform must be releveled.

1. Align LN-3 to local coordinates and then switch to NAV.

2. Torque azimuth gimbal to 180 degrees as measured on PAI.

3. With the PAI, measure the platform pitch and roll angles so the platform can be slewed back to level if desired.

4. Slew platform off level in roll about four degrees. Using a precision voltmeter, observe the voltage at appropriate test point; as the voltage approaches the desired value, slew the platform back to level. Read the PCM count for each voltage level selected as a calibration point. Scale factor is 200 ft/sec = 1.333 volts. Velocity in the opposite direction is obtained by slewing the platform in the opposite direction, and voltage polarity at the test point will be negative.

Y Velocity

Y Velocity calibration is performed in the same manner as X velocity except that the platform is slewed in pitch rather than in roll.

X Distance

1. Set the X counter on the instrumentation interface unit to 500 and read the PCM count. This represents zero miles on the instrumentation.

2. Increase the X distance from 500 in steps of 100 miles and read the PCM count at each point.

3. Decrease the X distance from 500 in steps of 100 miles and read the PCM count at each point.

Y Distance

Y distance is calibrated in the same manner as X distance except that the Y counter is incremented rather than the X counter.

Further details on LN-3 system calibration may be found in Reference 19.

APPENDIX III

DATA PROCESSING

COMPUTING METHODS

NUMERICAL FILTERING

Numerical filters were applied to basic measurements to remove frequency components outside the range of interest. The filtering process consisted of applying selected sets of numerical filtering weights designed to pass only the useful frequency response range of each measurement. Four low-pass filters of the type developed by Martin and Graham were considered adequate (Ref. 20 and 21).

Ideally, the Martin-Graham filter will (1) pass unaffected all frequency components up to a certain cutoff value f_c, (2) progressively attenuate frequencies from f_c down to zero gain at a termination frequency f_t, and (3) reject all frequencies greater than f_t. The definition of this filter is given in the frequency domain by the transfer function H(f).

$$H(f) = \begin{cases} 1 & |f| \leq f_c \\ 0 & |f| \geq f_t \\ \frac{1}{2}\left[\cos \pi \left(\frac{f + f_c}{f_t - f_c}\right) + 1\right] & -f_t \leq f \leq -f_c \\ \frac{1}{2}\left[\cos \pi \left(\frac{f - f_c}{f_t - f_c}\right) + 1\right] & f_c \leq f \leq f_t \end{cases}$$

The time domain weighting function h(t) is obtained by performing an inverse Fourier transformation of H(f).

$$h(t) = \int_{-\infty}^{\infty} H(f)\, e^{2\pi i f t}\, df$$

$$= \frac{\sin 2\pi f_t t + \sin 2\pi f_c t}{2\pi t\left[1 - 4(f_t - f_c)^2 t^2\right]}$$

Appendix III

A time function x(t) is then filtered by applying the weighting function h(t) such that

$$\hat{x}(t) = \int_{-\infty}^{\infty} h(\tau)\, x(t+\tau)\, d\tau$$

where $\hat{x}(t)$ is the filtered output function.

However for the finite time case of discrete equispaced data, numerical approximations must be introduced. The technique here is to evaluate the weighting function at the data sampling interval Δt for the $(2N + 1)$ weights desired, thus

$$h_n = h(n\Delta t) \qquad n = \pm 1, \pm 2, \ldots \pm N$$

and

$$h_o = f_c + f_t$$

by L'Hospital's rule.

The numerical filtering weights w_n are determined by

$$w_n = \frac{h_n \Delta t}{\sum_{p=-N}^{N} h_p \Delta t} \qquad n = 0, \pm 1, \ldots \pm N$$

where the summation term effectively normalizes the weights to force the transfer function to unity gain at f = 0.

The numerical filtering operation is then given by

$$\hat{x}_i = \sum_{n=-N}^{N} w_n\, x_{i+n}$$

To evaluate the effectiveness of the numerical approximations on the transfer function of the original filter design, the transfer function of the filtering weights, $H^*(f)$, is computed by the cosine series transformation

$$H^*(f) = \sum_{n=-N}^{N} W_n \cos 2\pi f n \Delta t$$

Figure 100 graphically presents $H^*(f)$ for the four low-pass filters designed for this program. Table IX shows which filter was applied to each basic measurement.

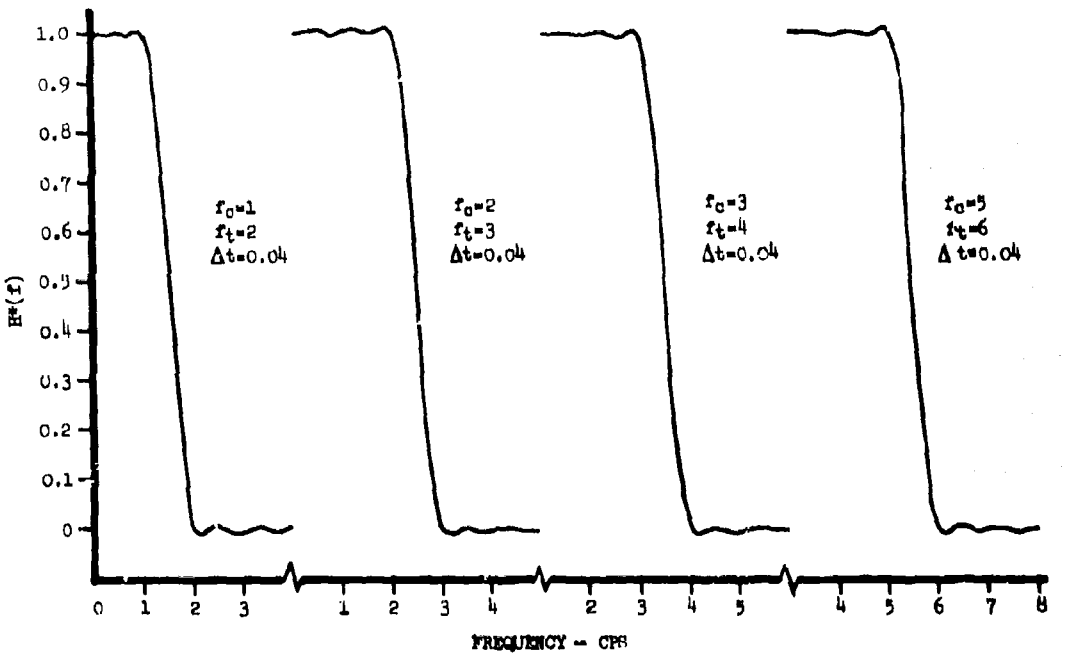

Figure 100. Numerical Filtering Transfer Functions

Appendix III

TABLE IX. LOW-PASS NUMERICAL FILTERING CUTOFF FREQUENCIES OF BASIC MEASUREMENTS

Assigned Number	Basic Measurement	Cutoff Freq, cps
3	Alpha-vane force	5
4	Beta-vane force	5
5	Indicated airspeed	5
6	Platform vertical acc	3
7	Gust probe normal acc	5
8	Gust probe lateral acc	5
9	Vernier altitude	3
10	Total temperature	5
11	Pitch rate	3
12	Roll rate	3
13	Yaw rate	3
14	CG normal acc	3
15	CG lateral acc	2
16	CG longitudinal acc	2
20	Coarse altitude	1
21	Fine altitude	2
22	Left wing nodal acc	5
23	Right wing nodal acc	5
25	Pitch angle	2
26	Roll angle	2
27	Heading sine	1
28	Heading cosine	1
29	Grid X velocity	1
30	Grid Y velocity	1

NUMERICAL INTEGRATION

Simpson's one-third rule was used for numerically integrating rate gyro measurements and acceleration terms required for gust velocity computations.

Simpson's integration of a time function x(t) sampled with frequency $f_s = 1/\Delta t$ is given by

$$\int_{t_n}^{t_n+2\,\Delta t} x(t)\,dt = \frac{\Delta t}{3}\left[x(t_n) + 4x(t_n + \Delta t) + x(t_n + 2\,\Delta t)\right]$$

Simpson's rule was selected for both its ideal phase and excellent amplitude characteristics. To illustrate this, a comparison is made with the trapezoidal rule. Since both rules have ideal phase, a complete comparison is afforded by the amplitude ratio of their transfer functions to that of the ideal integrator. The ratios are

$$\frac{W_s(f)}{W_I(f)} = \frac{2\pi f \Delta t}{3}\left(\frac{2 + \cos 2\pi f \Delta t}{\sin 2\pi f \Delta t}\right)$$

for Simpson's one-third rule, and

$$\frac{W_T(f)}{W_I(f)} = \pi f \Delta t(\cot \pi f \Delta t)$$

for the trapezoidal rule.

The superiority of Simpson's rule is shown in Figure 101 where the amplitude ratios were evaluated at the basic data sampling interval of 0.04 seconds. The maximum error is expected at the numerical filtering cutoff frequency of 5 cps. At this frequency, Figure 101 shows an error of 1.7 percent for Simpson's one-third rule and -13.5 percent for the trapezoidal rule.

AERODYNAMIC CALCULATIONS

Position error corrections and aerodynamic variables are determined in the gust velocity program prior to computation of the gust velocity components. The following calculations require H_{pn} selected from either coarse, fine, or vernier altitude transducer, V_{in} from the pitot static tube and t_t from the total temperature probe

(a) Static Pressure

if $H_{pn} \leq 36089$ ft.

$$P_s = 2116.22(1 - 6.87535 \cdot 10^{-6} H_{pn})^{5.2561}$$

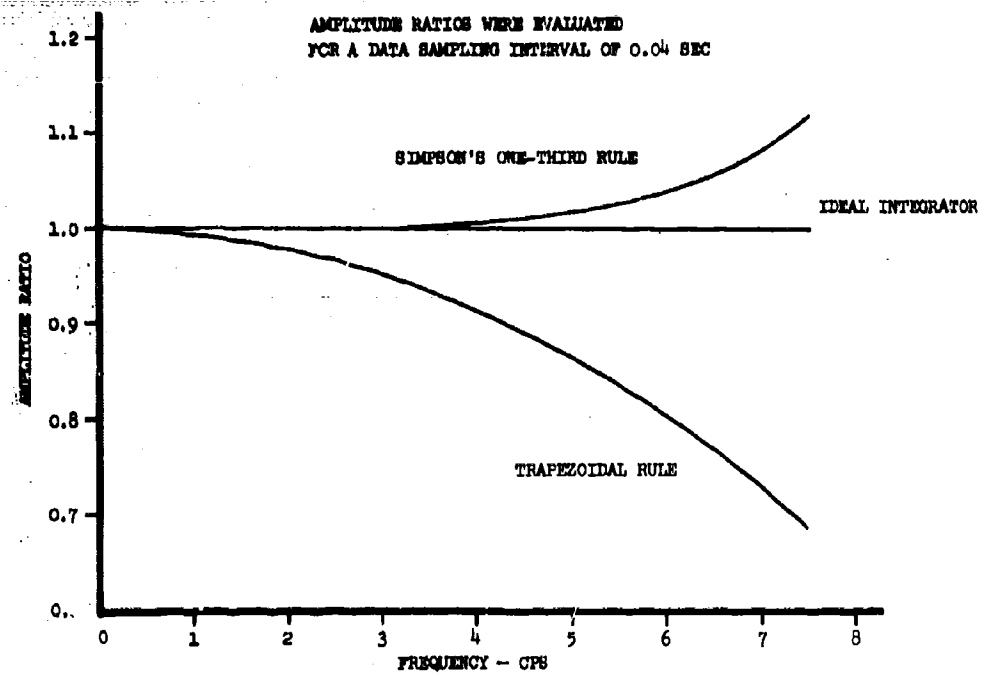

Figure 101. Amplitude Ratio Comparison of Simpson's One-Third Rule and Trapezoidal Integrations

if $H_{pn} > 36089$ ft.

$$P_s = 472.675\, e^{-4.80634 \cdot 10^{-5}(H_{pn} - 36089)}$$

(b) Differential pressure

$$q_c = 2116.22 \left[\left(1 + 7.72821 \cdot 10^{-7} V_{in}^2\right)^{3.5} - 1 \right]$$

(c) Indicated Mach No.

$$M_i = \sqrt{5\left[\left(\frac{q_c}{P_s} + 1\right)^{2/7} - 1\right]}$$

(d) The Mach number static position error correction, δM, is determined from the M_i versus δM relationship.

(e) True Mach No.

$$M_T = M_i + \delta M$$

(f) The altitude static position error correction, δH_p, is determined from the M_i versus δH_p relationship.

(g) Corrected pressure attitude

$$H_{pc} = H_{pn} + \delta H_p$$

(h) Ambient temperature

$$t_a = \frac{t_t + 273.16}{1 + 0.2M_T^2} - 273.16$$

(i) True airspeed

$$V_T = 65.769 M_T \sqrt{t_a + 273.16}$$

(j) Ambient pressure

if $H_{pc} \leq 36089$ ft.

$$P_a = 2116.22(1 - 6.87535 \cdot 10^{-6} H_{pc})^{5.2561}$$

if $H_{pc} > 36089$ ft.

$$P_a = 47\ 675\ e^{-4.80634 \cdot 10^{-5}(H_{pc} - 36089)}$$

(k) Air density ratio

$$\sigma = \frac{681.14\ P_a}{t_a + 273.16}$$

Appendix III

(l) Equivalent airspeed

$$V_e = V_T \sigma^{1/2}$$

(m) Air density

$$\rho = \frac{1.619\, P_a}{t_a + 273.16}$$

GUST VELOCITY

The three incremental gust velocity components (i.e., vertical ΔU_V, lateral ΔU_L and longitudinal ΔU_F) were computed as follows:

$$\Delta U_V = (V_T \Delta\alpha) + (V_T \Delta\beta)\, \Delta\phi - V_T \Delta\theta + \int \Delta a_v\, dt + L_x \Delta\dot{\theta}$$

$$\Delta U_L = (V_T \Delta\beta) - (V_T \Delta\alpha)\, \Delta\phi + V_T \Delta\psi - \Delta V_{X_1} \cos\bar{\Lambda} + \Delta V_{Y_1} \sin\bar{\Lambda} + L_x \Delta\dot{\psi}$$

$$\Delta U_F = \Delta V_T - \Delta V_{X_1} \sin\bar{\Lambda} - \Delta V_{Y_1} \cos\bar{\Lambda}$$

where

$$V_T \Delta\alpha = 2 \frac{\Delta F_{N_{M\alpha}} + m\Delta a_N}{C_{N\alpha}\, \rho\, V_T\, S_v}$$

$$V_T \Delta\beta = 2 \frac{\Delta F_{N_{M\beta}} + m\Delta a_L}{C_{N\beta}\, \rho\, V_T\, S_v}$$

As indicated by these equations, the incremental velocity components of the aircraft relative to the ground are normally computed from inertial platform measurements provided for this purpose. However, alternate methods have been

programmed for determining the ΔU_{PG} L, vector components based on cg or gust probe acceleration measurements corrected for aircraft attitude.

$$\Delta U_V = (V_T \Delta \alpha) + (V_T \Delta \beta)\ \Delta \phi - V_T \Delta \theta + \int (\Delta a_N - \Delta a_L \Delta \phi)\ dt + L_x \Delta \dot{\theta}$$

$$\Delta U_L = (V_T \Delta \beta) - (V_T \Delta \alpha)\ \Delta \phi + V_T \Delta \psi + \int (\Delta a_L + \Delta a_N \Delta \phi)\ dt + L_x \Delta \dot{\psi}$$

$$\Delta U_F = \Delta V_T - \int (\Delta a_F - \Delta a_N \Delta \theta)\ dt$$

Incremental angles of pitch and roll were computed from platform attitude measurements corrected for fuselage bending by

$$\Delta \theta = \Delta \theta_M + k_b \Delta a_N$$

$$\Delta \phi = \Delta \phi_M + k_b \Delta a_L$$

or from integration of the rate gyro measurements

$$\Delta \theta = \int \Delta \dot{\theta}\ dt$$

$$\Delta \phi = \int \Delta \dot{\phi}\ dt$$

Incremental yaw angles were obtained from platform true heading measurements

$$\Delta \psi = \Delta \Lambda$$

or from integration of the yaw rate gyro.

$$\Delta \psi = \int \Delta \dot{\psi}\ dt$$

Appendix III

After Simpson's one-third rule was employed for evaluating the integral terms, the gust velocities were computed at 12.5 samples per second (sps), half the basic sampling data frequency. Since low-pass numerical filters effectively terminated all frequency components beyond 6 cps, no aliasing of any significance was introduced by reducing the sampling frequency. This significantly reduced the processing effort involved with the gust velocities, yet retained the accuracy associated with Simpson's integration at 25 sps.

The derived equivalent gust velocity was computed as follows.

$$U_{de} = \frac{2 \Delta a_N W}{C_{L_\alpha} \rho_o K_g V_e S}$$

WIND VELOCITY

The average wind velocity, $\overline{U}_{AG}$, was determined from the average true airspeed and inertial platform measurements. The wind velocity components with respect to the aircraft are

$$\overline{U}_{AP_{X'}} = -\overline{V}_T \sin \overline{\Lambda}$$

$$\overline{U}_{AP_{Y'}} = -\overline{V}_T \cos \overline{\Lambda}$$

hence with respect to the ground

$$\overline{U}_{AG_{X'}} = -\overline{V}_T \sin \overline{\Lambda} + \overline{V}_{x'}$$

$$\overline{U}_{AG_{Y'}} = -\overline{V}_T \cos \overline{\Lambda} + \overline{V}_{y'}$$

The magnitude and direction, $\overline{\eta}$, of the average wind velocity vector are therefore computed by

$$\overline{U}_{AG} = \sqrt{\overline{U}^2_{AG_{X'}} + \overline{U}^2_{AG_{Y'}}}$$

$$\overline{\eta} = \tan^{-1}\left(\frac{\overline{U}_{AG_{X'}}}{\overline{U}_{AG_{Y'}}}\right)$$

POWER SPECTRA

The power spectrum of a stationary random function $x(t)$ is defined by

$$\Phi(f) = 4 \int_0^\infty R(\tau) \cos 2\pi f \tau \, d\tau$$

where $R(\tau)$, the autocorrelation function, is given by

$$R(\tau) = \lim_{T \to \infty} \frac{1}{T} \int_{-T/2}^{T/2} x(t) \, x(t + \tau) \, dt$$

To estimate the spectrum for discrete equispaced data, the Tukey method was employed (Ref. 22 and 23). The numerical approximations involved in this method for a discrete function x_q of $(n+1)$ evenly spaced samples from 0 to $n\Delta t$ seconds are presented in the following steps.

Prewhitening - To minimize the possible distortion from the relatively high power anticipated at the low frequencies, a prewhitening filter is applied to the data. This high-pass filter is defined by the transformation

$$\hat{x}_q = x_q - x_{q-1} \qquad q = 1, 2, \ldots n$$

Autocorrelating - The autocorrelation function of the prewhitened data is computed for $(m+1)$ time lags from 0 to $m\Delta t$.

$$\hat{R}_p = \frac{1}{n - p} \sum_{q=1}^{n-p} \hat{x}_q \, \hat{x}_{q+p} \qquad p = 0, 1, \ldots m$$

Estimating the Raw Power - The raw estimates of power are computed by numerically evaluating the cosine series transform of the autocorrelation function

$$\hat{L}_h = 4\Delta t \sum_{p=0}^{m} a_p \, \hat{R}_p \cos \frac{hp\pi}{m} \qquad h = 0, 1, \ldots m$$

where

$$a_p = 0.5 \qquad p = 0, m$$

$$a_p = 1 \qquad 0 < p < m$$

Smoothing the Raw Estimates - The raw estimates are refined by a smoothing technique called hanning.

$$\hat{\Phi}_h = 0.25\hat{L}_{h-1} + 0.5\hat{L}_h + 0.25\hat{L}_{h+1} \qquad h = 1, 2, \ldots m-1$$

$$\hat{\Phi}_m = 0.5\hat{L}_{m-1} + 0.5\hat{L}_m$$

Postdarkening - The final power spectral estimates are obtained after the smoothed estimates are compensated for the effect of the prewhitening transformation performed in the first step, thus

$$\Phi_h = \frac{\hat{\Phi}_h}{2 - 2\cos\frac{\pi h}{m}} \qquad h = 1, 2, \ldots m$$

where

$$\Phi_h = \Phi\left(f_h = \frac{h}{2m\Delta t}\right)$$

and represent the power average over the frequency band in cycles per second defined by

$$\frac{h}{2m\Delta t} \pm \frac{1}{m\Delta t}$$

In analyzing turbulence data, it is desirable to interpret their power spectra as a function of inverse wavelength in cycles per foot. The average true airspeed in feet per second is used for converting the spectral estimates.

$$\Phi(1/\lambda_h) = \frac{\Phi(f_h)}{V_T}$$

The number of spectral estimates m is normally selected so that the data will stay within certain confidence limits. The degrees of freedom k of a run of n samples is a measure of the stability of the spectral estimates and is given by

$$k = \frac{2n}{m}$$

Standard rms deviations are determined by numerically integrating the spectral estimates for standard wavelengths, thus

$$\sigma_s = \left[\int_{1/\lambda_1}^{1/\lambda_2} \Phi(1/\lambda)\, d(1/\lambda) \right]^{1/2}$$

where λ_2 is the wavelength corresponding to the 5 cps numerical filtering cutoff frequency and λ_1 is a standard wavelength. Rms deviations are computed for wavelengths of 1000, 2000, 4000, 10,000, 20,000 and 40,000 feet.

STATISTICAL COUNTING METHODS

Two statistical counting methods were employed to define the distribution characteristics of selected acceleration and velocity data. In both methods, the characteristic points are counted and classified into preestablished positive and negative intervals constructed about the mean. The two methods have different criteria for determining a count.

In the peak count method, the characteristic points (peaks) are defined as the maximum or minimum value between successive crossings of a narrow band about the mean. The purpose of the narrow band, called the threshold, is to eliminate the counting of peaks resulting from insignificant fluctuations in the data. Figure 102 shows how peaks are determined, classified, and counted. Note that the threshold in the example has been expanded for purposes of clarity; it is normally plus and minus 10 percent of the counting interval.

In the level-crossing count method, a count is made each time the trace of the discrete data intersects an interval level with a positive slope in the region above the mean and with a negative slope in the region below the mean. An example of the level-crossing count method is shown in Figure 103.

After a data run has been processed by one of the counting methods, the following statistical parameters are determined.

Frequency of Occurrence - In the peak count method the counts are summed within corresponding positive and negative intervals. The accumulated counts for interval levels y_i and y_{-i} are indicated by $g(y_i)$, the frequency of occurrence.

Appendix III

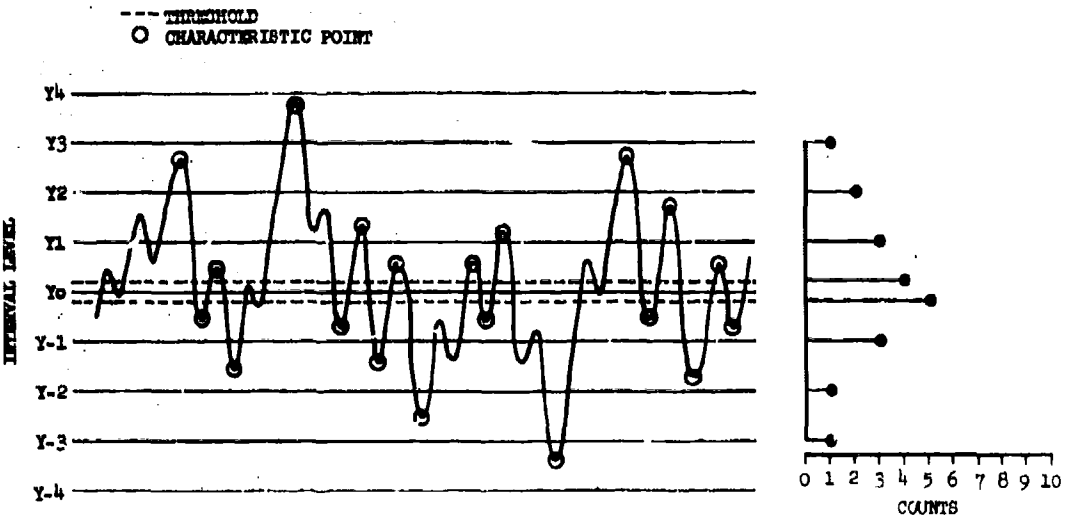

Figure 102. Example of Peak Count Method

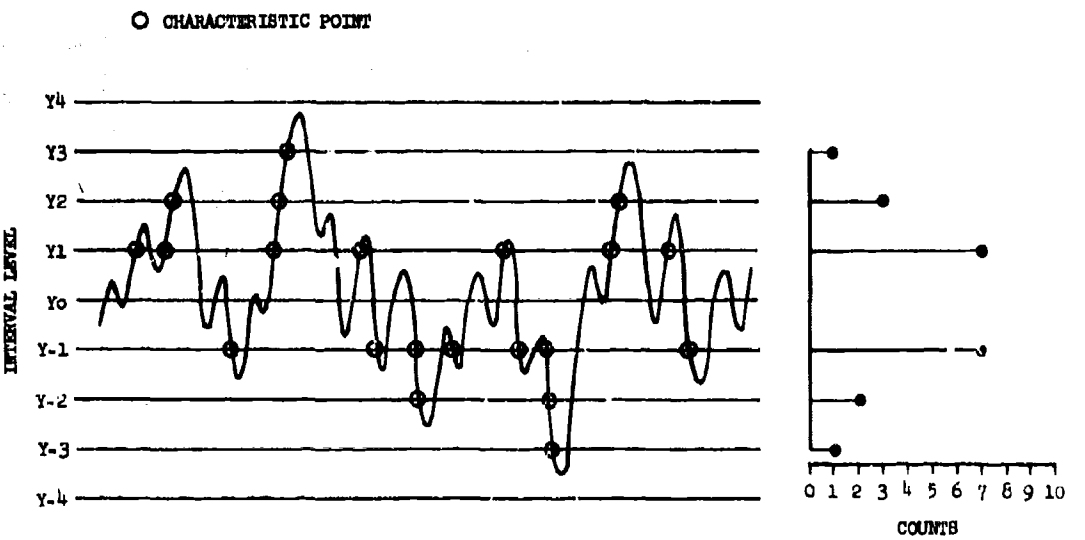

Figure 103. Example of Level-Crossing Count Method

Frequency of Exceedance - For peak counts, the frequency of exceedance, $G(y_i)$, is determined for each level. If N is the index of the maximum level for which a count was detected, then

$$G(y_0) = \sum_{i=0}^{N} g(y_i)$$

$$G(y_i) = G(y_{i-1}) - g(y_i) \qquad i = 1, 2, \ldots N$$

For the level crossing count method, the frequency of occurrence is the frequency of exceedance, hence

$$G(y_i) \equiv g(y_i)$$

Exceedance per Mile - If the frequency of exceedance is divided by the number of miles in a data run, the distribution becomes an estimate of the frequency of exceeding a given velocity or acceleration level per mile of flight. The exceedance per mile was computed by

$$\frac{G(y_i)}{V_T \, T_N}$$

where T_N is the elapsed time of the data run in seconds.

Probability Distribution Function - The probability distribution function indicated by $F(y_i)$, represents the probability of exceeding a given level. For level y_i,

$$F(y_i) = \frac{G(y_i)}{G(y_0)}$$

COMPUTER PROGRAMS

HICAT BASIC DATA PROGRAM

General

The HICAT basic data program is the first of five digital computer programs designed to reduce and display pulse code modulated (PCM) data previously processed to a computer compatible format in the HICAT ground station.

Appendix III

The purpose of the program in its normal production mode is to read the ground station tape on Lockheed-California Company's IBM System/360 Computer installation and perform the following sequential operations:

- Unpack the airborne-recorded data
- Monitor frames for constant time interval
- Calibrate to engineering units
- Detect and correct sporadic data errors
- Apply sets of numerical filtering weights
- Compute means and standard deviations
- Record the results on tape and list in tabular form.

The following programs in the HICAT series are designed to accept the tape generated in this program as their input data source:

- HICAT gust velocity program
- HICAT power spectral analysis program
- HICAT statistical analysis program
- HICAT plotting program

Input Requirements

The primary input to the program is a ground station tape containing edited runs of flight-recorded data. A complete description of the format structure of this tape is given in Figure 104. Each time step or frame contains 5 digital channels of switching information, 3 time channels, and 40 analog channels reserved for basic measurements. The packed data of 15 frames are assembled in logical records and the records are grouped by files. Each file contains the data for one edited run.

The following additional information is input to the program to control the reading, processing and reduction of the tape data.

- Test parameters identifying the test and defining test conditions including the status of the data acquisition system
- Analog channel assignments defining the configuration of the basic measurements in the analog channels.
- Calibration data defining the method of calibrating each measurement.
- Run parameters providing the identifications and conditions required for initiating the reduction of a data run.
- Status codes defining the logical path each measurement will follow through the error search and numerical filtering functions of the program

FILE FORMAT

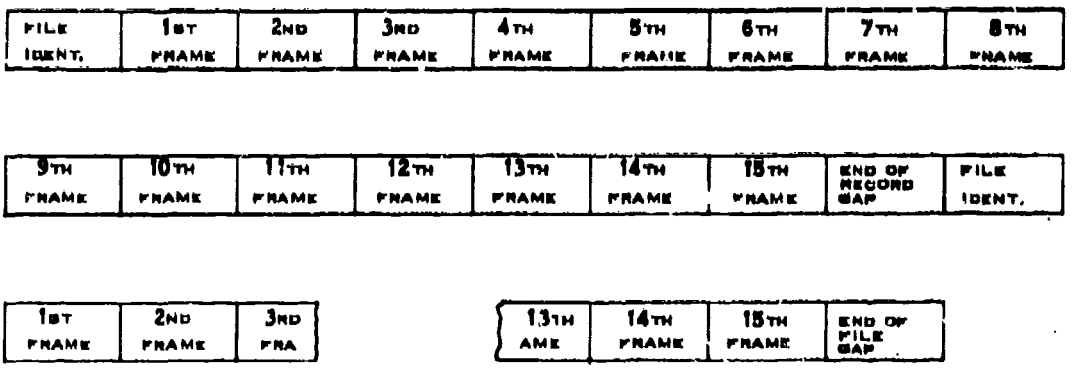

FRAME FORMAT

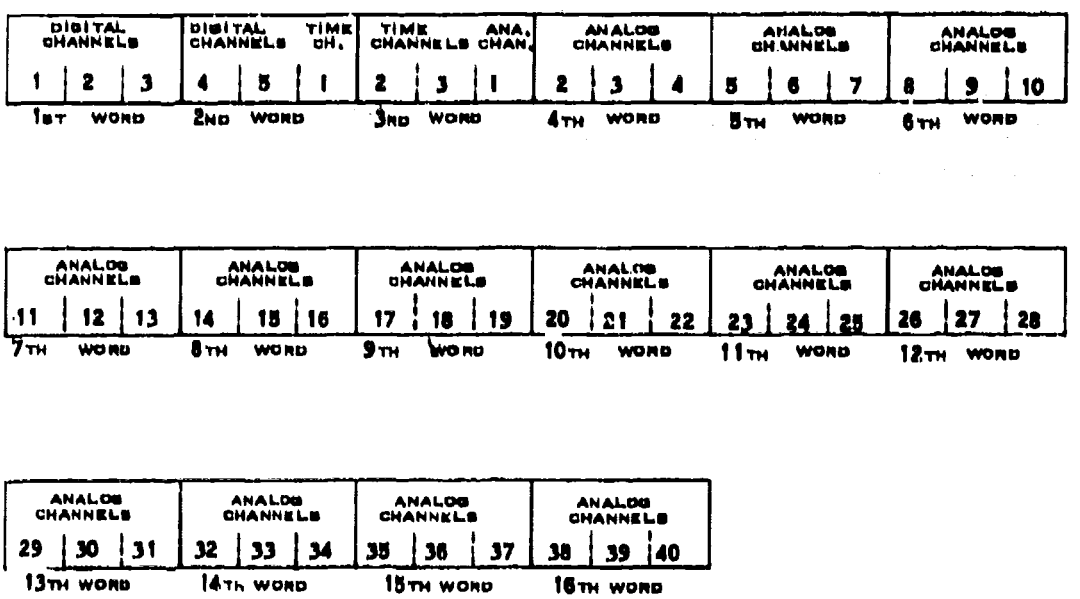

Figure 104A. Ground Station Tape Format - Part 1

Appendix III

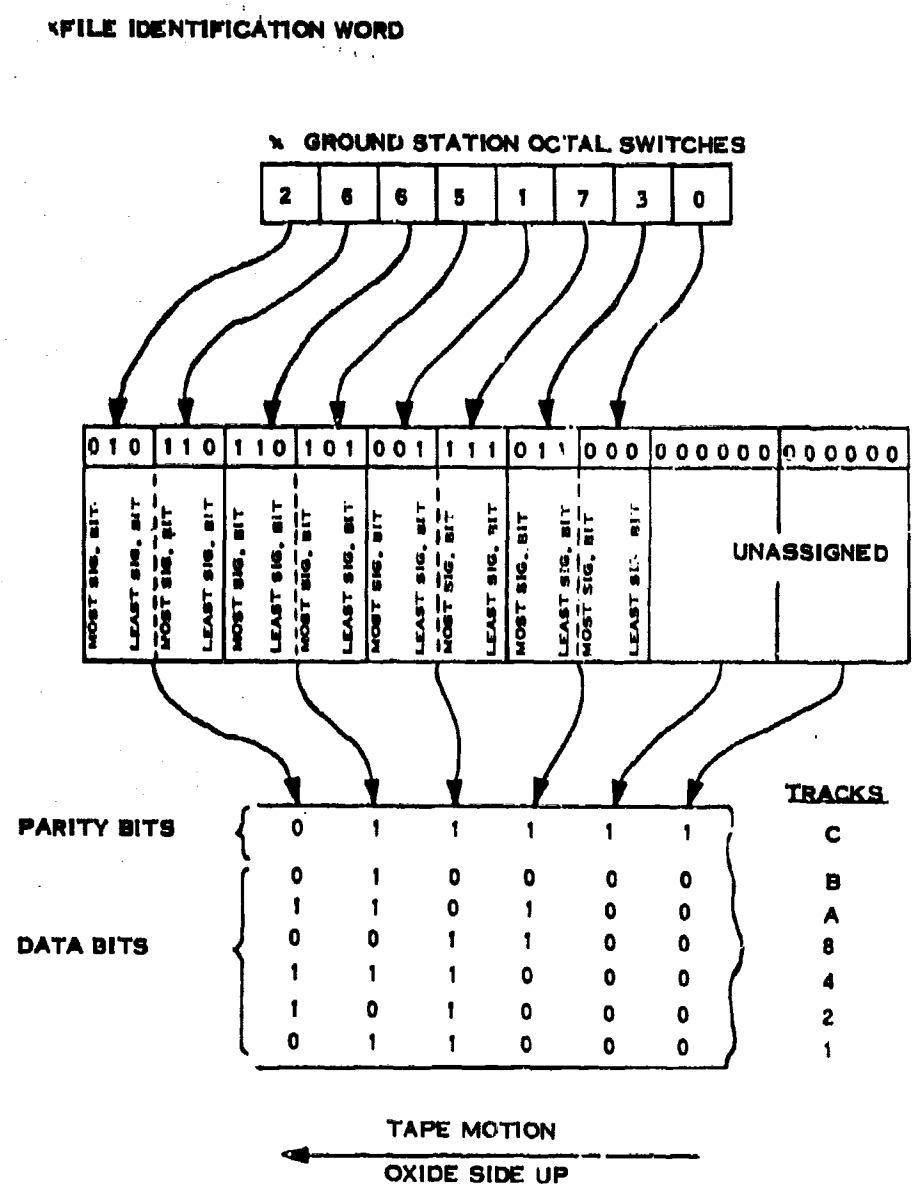

Figure 104B. Ground Station Tape Format - Part 2

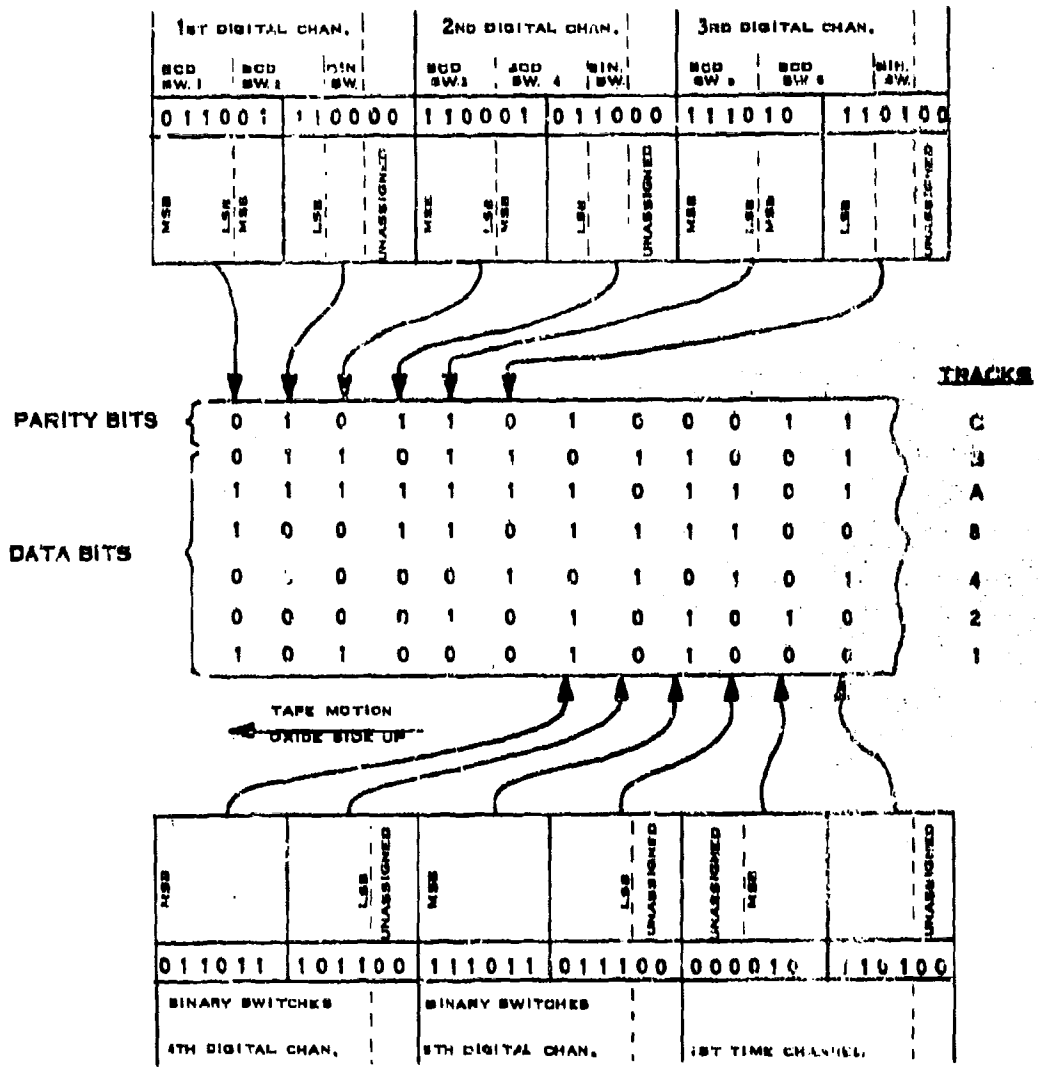

Figure 104C. Ground Station Tape Format - Part 3

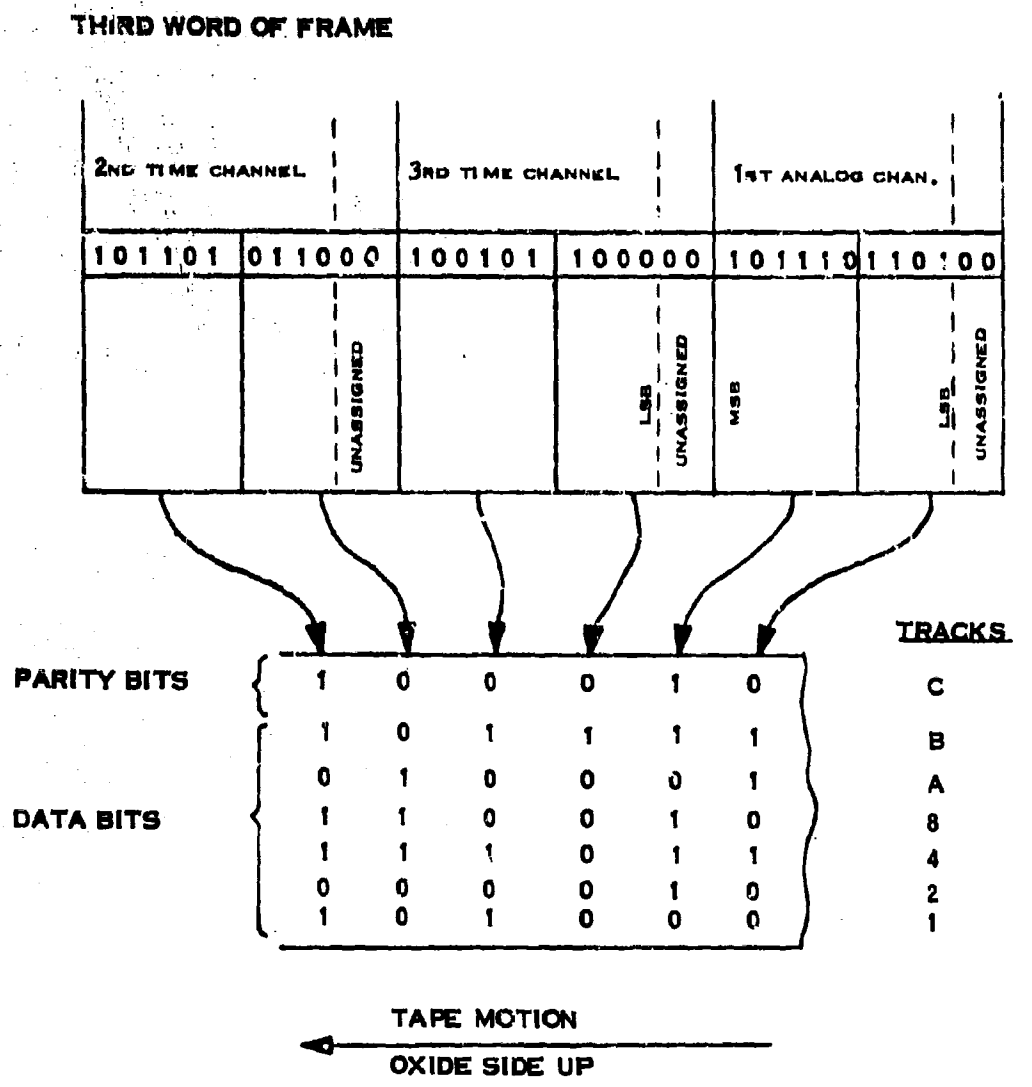

Figure 104D. Ground Station Tape Format - Part 4

FOURTH WORD OF FRAME

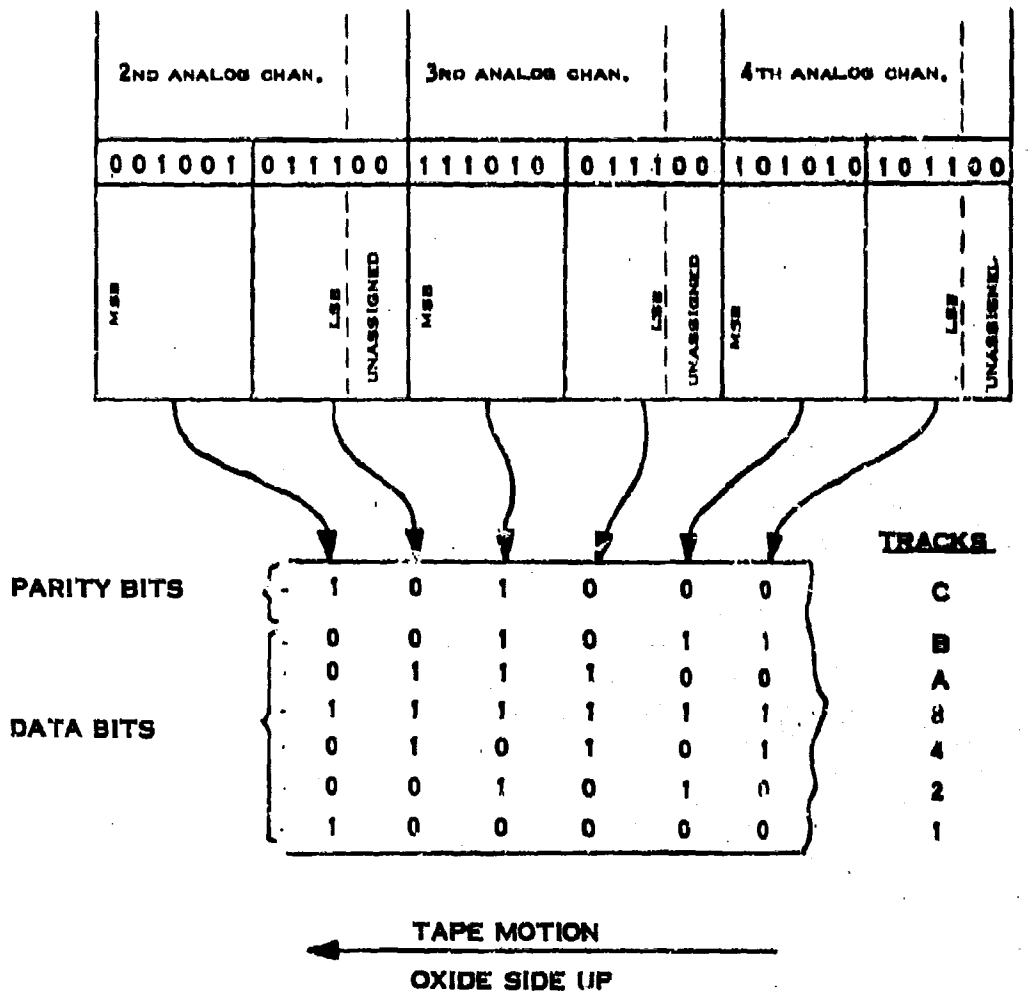

NOTE: THE FIFTH THROUGH SIXTEENTH WORDS OF A FRAME ARE RECORDED WITH THE SAME BIT CONFIGURATION AS THE FOURTH WORD

Figure 104E. Ground Station Tape Format - Part 5

Appendix III

Unpacking and Reformatting

After the ground station tape data has been read into a temporary buffer, an unpacking routine is employed to disassemble and translate the data channels into working data tables as shown in Figure 105. Then, the three time channels are merged to construct the time of day in milliseconds. Next, the switching information in the five digital channels is isolated and then combined in the proper sequence to form one word of binary switching information and one word of BCD switching information. Finally, analog channels containing measurement data are directed to their assigned position in the table.

Editing

Although the data runs are formed as a result of editing information obtained from the airborne-recorded data, additional information uncovered after the ground station tapes are generated may warrant further editing. For this purpose the program permits a start time and stop time to be input to limit the processing of data to frames within the previously selected times. This capability also enables a data run to be divided into several smaller runs. Each of these may then be processed individually.

Correcting Time Errors

The time error routine ensures a constant time interval of the data frames consistent with the sampling frequency of the data acquisition system. The times associated with contiguous frames are interrogated to determine if the proper time interval is maintained. Whenever an error is detected, a search is effected until the proper sequence is established. If the number of frames in the disturbed region is not equal to the number of time steps required to maintain the correct time interval, the frames are sorted into sequence in the data tables. The data associated with disturbed frames are then labeled for corrective action in the sporadic error correcting routine which follows. An error criterion may be input which limits each error search to a preestablished number of consecutive frames. If no solution is detected within the prescribed limits, further processing is terminated and the results are summarized and output for analysis.

Calibrating

Programming options are available for defining how each basic measurement shall be calibrated. Figure 106 shows the pertinent functions of the data acquisition process associated with the analog channel calibrations produced in the data reduction phase.

As shown in Figure 106, the conversion of the raw data counts into engineering units requires two calibration steps. The first step employs the calibration of the PCM system. This calibration curve is entered with the count reading and the corresponding voltage reading is obtained by linear interpolation. The second step employs the sensor calibrations to convert the data to engineering units. Options are available for utilizing either polynomial curve fits or table look-ups for these calibrations.

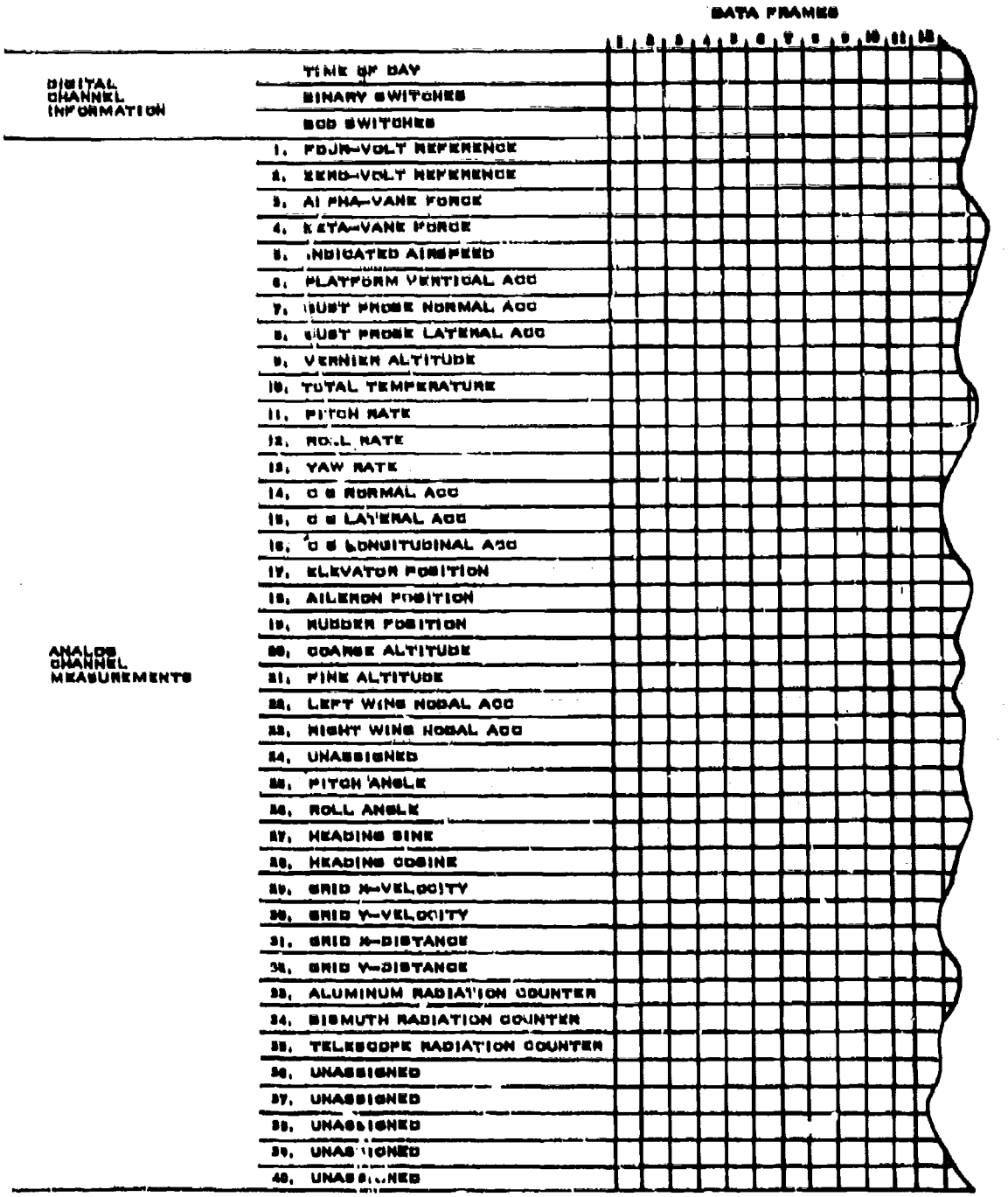

Figure 105. Basic Data Tables

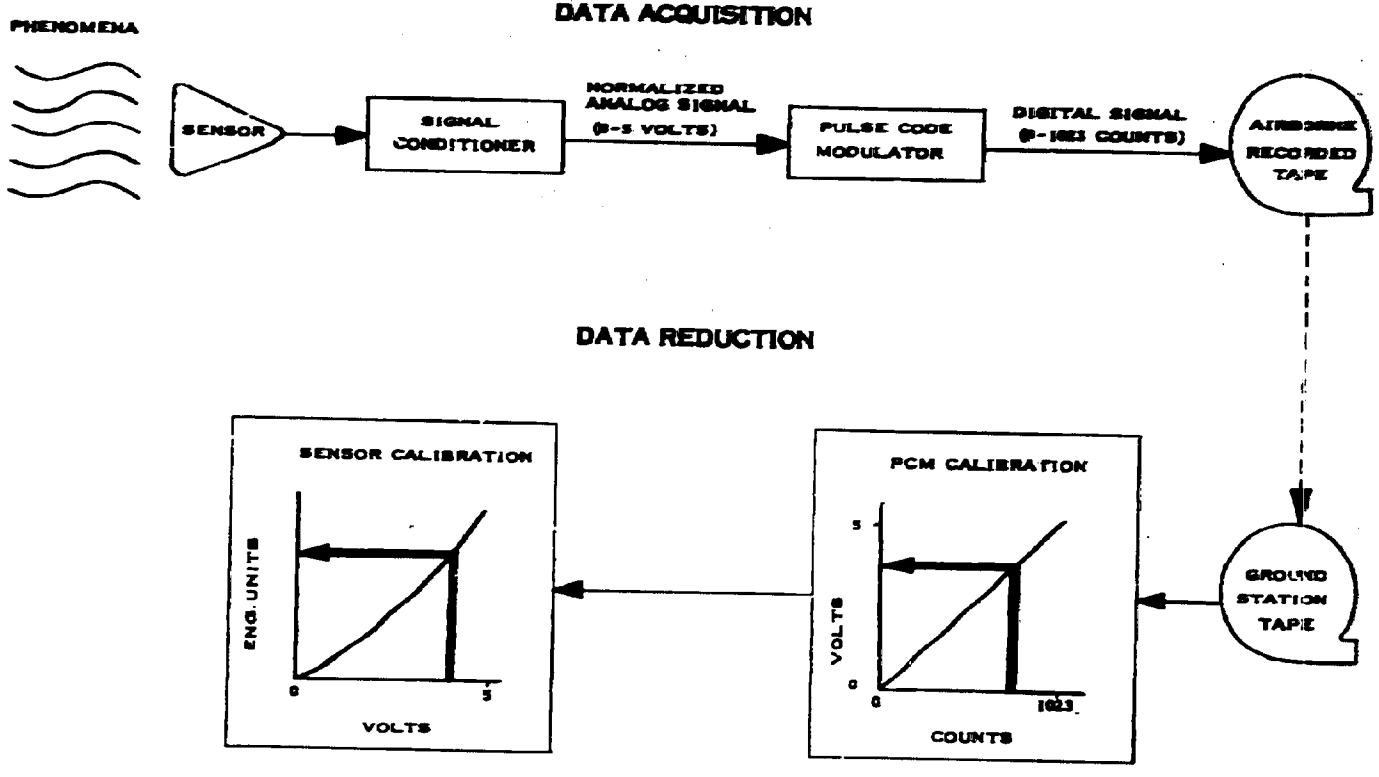

Figure 106. Data Acquisition and Reduction of Analog Channel Measurements

Additional options are available for bypassing all calibrations if raw data counts are desired or limiting the conversion process to just the first step if only volts are desired. These provisions were added to facilitate the checkout of the data acquisition system and to permit special data presentations.

Correcting Sporadic Data Errors

Sporadic data errors are defined as wild or accidental data samples outside the range normally associated with systematic or random errors. Sporadic errors are detected by comparing the first order differences of the data samples with preestablished limits. Limits were assigned to each measurement based on the data sampling interval. The detected errors are corrected by interpolating a linear fit constructed from data samples immediately preceding and following the disturbed area. Gaps in the table resulting from the inclusion of time errors are similarly corrected. All sporadic data errors and their corresponding corrections are summarized and tabulated in separate listings for review.

In addition, an error criteria may be established which limits the quantity and type of error occurrences and restricts the processing of the bad test data.

Numerical Filtering

The requirements for low-pass filtering are provided through the application of four sets of numerical filtering weights internally defined in the program. The transfer functions of the filtering weights are shown in Figure 100. One of the four weight sets may be selected for each basic measurement depending on what frequency response is desired.

The numerical weights were determined by the method developed by Martin and Graham (References 20 and 21). Application of the numerical filters is given by the operation

$$\hat{x}_i = \sum_{n=-N}^{N} w_n x_{i+n}$$

where w_n are the (2N+1) filtering weights, x_i are the input data samples and $\hat{x}_i$ are the corresponding filtered data samples.

Computing Means and Standard Deviations

The means and standard deviation are computed for each measurement in the basic data tables and printed on the tabular listings at the end of each run.

Appendix III

HICAT GUST VELOCITY PROGRAM

General

The HICAT gust velocity program was designed to compute aerodynamic variables, gust velocity components, and the derived equivalent gust velocity from the measurements reduced in the HICAT basic data program. Programming options are available for computing the vertical, lateral, and longitudinal gust velocity components using various combinations of the basic measurements.

The computed quantities are output on tape for use in the HICAT spectral analysis program and the HICAT statistical analysis program.

Input Requirements

The primary input to the gust velocity program is the output tape from the basic data program. Figure 105 lists the various measurements stored on tape. Accompanying the input tape is a group of cards specifying operational and computing information. The information appearing on the card input is as follows:

- Input and output tape identification
- Location of data on input tape, start and end time of selected data sample, averages of airplane response data, input tape sampling rate.
- Computation control codes, integration initialization values, output print sampling rate.
- Parameter adjustments, reference and general functions.

While a complete block of input is being read into the computer, initialization is performed. Commands positioning the input and output tapes are executed and all computing control information is stored.

Operational Checks

To insure that the proper data tapes were loaded, the data appearing in the status control block on the input tape is read and compared against the card input specifications. If any discrepancy occurs at this time, the program is immediately terminated and the reasons for termination are printed out to facilitate corrective action. The operational checks include tape loading, tape positioning, tape identification, and data sample selection. If no error is sensed while performing the operational checks the input tape is then positioned at the specified start time of the selected data sample.

Preliminary Calculations and Tabulations

A specified amount of data is read from the input tape, parameter adjustments applied, and gust entrance conditions and reference heading angle are computed.

The results of these calculations along with the input computing information are tabulated.

General Processing Method

The general processing scheme was to read data from tape into an input calculation table. Data in this table was used in the subsequent calculations and stored in an output buffer. This method eliminated all data sample length restrictions since the input data was processed in table-sized bites. The procedure was to perform input tape reads at the specified input sampling rate until the calculation table was full or until the end time or data sample end was reached. Then all specified parameter adjustments were applied to this table. If the end of the selected data was sensed an appropriate flag was set. Computing continued in this manner, selecting data from the input table, performing specified computations, and storing the answer in the output buffer. As the buffers were alternately exhausted or filled, input reads or sampled output writes into and from the appropriate buffers were executed. This process continued until the end of the selected data sample was sensed. When this occurred, a final output buffer write was performed and wind velocities calculated and output. If more input data was available, the program returned to the read input position. If no more input was available, all data tapes were rewound and unloaded and the computer run was terminated.

Computations

The methods used in computing aerodynamic variables, gust velocity components, and wind velocity are described earlier in this appendix under Computing Methods.

Appendix XII

HICAT SPECTRAL ANALYSIS PROGRAM

General

The HICAT spectral analysis program was designed to compute the statistical characteristics of turbulence data in the frequency domain. Power spectral techniques were programmed for application to basic measurements, aerodynamic variables, and gust velocity components recorded on magnetic tape by HICAT data reduction programs.

Basically, the program may be implemented to compute the following functions of the HICAT equispaced time series data

- Auto correlation
- Power spectrum

The numerical procedures used in evaluating these functions are essentially the same as those presented in Reference 22.

Input Requirements

The input data source may either be (1) the basic measurements recorded on the tape generated by the HICAT basic data program or (2) the aerodynamic variables and gust velocity components recorded on the tape generated by the HICAT gust velocity program. As data frames recorded on the input tape are read, the samples required for computing the first spectrum are directed to a table in core memory and the remaining data specified for processing are transferred to random access magnetic disk storage. Spectra are then computed until the data on disk is exhausted; whereupon the input tape is repositioned and the next case initiated.

The following information is input for identification purposes and to control the logical path through decision-making events in the program:

- Test parameters providing the necessary identification of test conditions
- Spectral parameters defining the many options available for computing spectra
- Run parameters defining the conditions under which each run is to be processed
- Data parameters defining the variables for which a spectrum is desired

Statistical Adjustment of the Data

After all samples for a run have been positioned in the data table, two statistical adjustments may be applied to the data prior to spectral computations. First, the linear trend is removed by subtracting from each sample, the corresponding time points along the least squares linear fit of the data. Second, the data may be prewhitened by executing the transformation

$$\hat{x}_q = x_q - x_{q-1}$$

However, due to the distorting effect of this prewhitening, the resulting spectrum must be compensated by postdarkening.

Power Spectra

The following mathematical operations are provided for the computation of power spectra. Let the samples in the data table be denoted by

$$x_q = x(q\Delta t) \quad q = 1, 2, \ldots n$$

where Δt is the sampling interval in seconds and n is the number of data samples in the table.

The autocorrelation function is computed for (m+1) lags of time from 0 to $m\Delta t$ seconds by

$$R_p = \frac{1}{n-p} \sum_{q=1}^{n-p} x_q x_{q+p} \qquad p = 0, 1, \ldots m$$

The raw estimates of power are computed by evaluating the cosine series transform of the autocorrelation function

$$L_h = 4\Delta t \sum_{p=0}^{m} a_p R_p \cos \frac{hp\pi}{m} \qquad h = 0, 1, \ldots m$$

where

$$a_p = 0.5 \qquad p = 0, m$$

$$a_p = 1 \qquad 0 < p < m$$

A programming option is available for refining the raw estimates by hanning or hamming, i.e.,

$$\Phi_0 = w_c (L_0 + L_1)$$

$$\Phi_h = w_c L_h + \left(\frac{1 - w_c}{2}\right)(L_{h-1} + L_{h+1}) \qquad h = 1, 2, \ldots m-1$$

$$\Phi_m = w_c (L_{m-1} + L_m)$$

where w_c, the central smoothing weight, is 0.5 for hanning and 0.54 for hamming.

If the estimates were based on prewhitened data, $\hat{x}_q$, the desired power spectrum is obtained by postdarkening the estimates by

$$\Phi_h = \frac{\hat{\Phi}_h}{2 - 2\cos\frac{\pi h}{m}} \qquad h = 1, 2 \ldots m$$

The power spectral estimates thus computed are a function of frequency in cycles per second defined by

$$\Phi_h = \Phi\left(f_h = \frac{h}{2m\Delta t}\right)$$

If the power spectral estimates are required as a function of angular frequency, ω, in radians per second or inverse wavelength, $1/\lambda$, in cycles per foot, the estimates are converted by

$$\Phi(\omega) = \frac{\Phi(f)}{2\pi} \quad \text{or} \quad \Phi(1/\lambda) = \frac{\Phi(f)}{\bar{V}_T}$$

respectively, where $\bar{V}_T$ is average true airspeed in feet per second.

The degrees of freedom and standard rms values are determined for each power spectral case. The number of degrees of freedom is a measure of the stability of the spectral estimates and is given by

$$k = \frac{2n}{m}$$

If the power spectrum is requested as a function of inverse wavelength, standard rms deviations are determined by numerically integrating the spectral estimates for various standard wavelengths, thus

$$\sigma_s = \left[\int_{1/\lambda_1}^{1/\lambda_2} \Phi(1/\lambda)\, d(1/\lambda)\right]^{1/2}$$

where λ_2 is the wavelength corresponding to the cutoff frequency of the numerical filter applied to the time series data and λ_1 is a standard wavelength.

Appendix III

STATISTICAL ANALYSIS PROGRAM

General

The statistical analysis program provides capabilities for determining distribution characteristics of time series data. Two separate and distinct methods are available. (See Figures 102 and 103.)

The first method is commonly referred to as the peak count method. A peak is defined as the maximum data excursion between two successive crossings of a specified reference line. This reference may be designated to be the mean of the data or, where drift may be present, to be the linear least squares fit of the data. Allowances for the "noise level" and reading resolution of the data may be made by the specification of a threshold value. This threshold value determines a bandwidth on each side of the reference line. The only data considered in the peak determination is that data that occurs outside of this threshold. Peak occurrences are determined, classified within intervals, and then counted. Any interval width may be specified.

The second method, the level crossing count, is concerned with the interval levels intersected if one were to connect the discrete points of the data time history. A threshold is not used in this method but the definition of the reference and interval width is maintained exactly as in the peak count method. In the region above the reference line, only level-crossings with positive slopes are counted. Similarly, in the region below the reference line, only level crossings with negative slopes are counted.

The frequency of occurrence, frequency of exceedance, and the distribution function of the count data are computed. Other statistical quantities such as the mean of the data, the rms of the data, and the rms of the peaks are also calculated and tabulated.

The statistical analysis program will accept either the basic data output tape or the gust velocity output tape. The basic data tape is used as input primarily to take advantage of an available option to calculate and count derived equivalent gust velocity. The analysis of this output is useful in determining the turbulence intensity.

Input Requirements

The data to be processed is supplied on magnetic tape. Operational and computing information is specified on card input. Information appearing on the card input is as follows:

Appendix III

- Input tape identification
- Location of data on tape, start and end time of selected data sample, parameter selection
- Threshold and interval specifications
- Computation control codes, reference information

Operational Checks

During the input phase, the functions of program initialization, tape positioning, tape read format specification, and computing control definition are performed. Following this phase and prior to any computations, an operational check is performed to ensure that the proper data will be processed. This is accomplished by reading the information appearing in the status control block preceding the selected data sample on tape and comparing it with the data and tape requests as specified on the card input. If any inconsistencies occur, error comments are printed and the run terminated. If not, the input tape is positioned at the time specified to be the data sample origin.

General Processing Method

To minimize tape manipulations and reduce card input requirements, all data parameters selected for processing are read from the input tape at one pass. The first data parameter requested is moved directly to a calculation table. Any remaining parameters are stored on random access magnetic disk storage. As each parameter is processed through the statistical analysis program and the results printed, another parameter is moved from disk storage into the calculation table. This process continues until all the selected data is processed. If more card input is available, the program returns to the read input position. If not, the input tape is rewound and the computer run is terminated.

Counting Reference Determination

The reference to be used in the counting methods may be defined in any of three various methods. The mean or a linear least squares fit of the data may be calculated for use, or the coefficients of any linear fit may be input. Once the reference line is determined, data deviations from this line are calculated. The counts are performed on the adjusted data array.

Calculations

The rms of the fitted data as well as the rms of the peaks are computed. The time between the first and last reference crossing and total number of peak occurrences are also determined. A time series tabulation of all peak occurrences is also formed. The counts are summed for corresponding positive and negative interval levels. The counts are also summed for corresponding absolute interval levels to provide frequency of occurrence. The frequency of exceedance is determined for each level. The frequency of exceedance is defined as the number of times that an absolute interval level is exceeded. The probability

distribution function, the probability of exceeding a given level, is computed by dividing by the total number of peaks or counts. The optional derived equivalent gust velocity, U_{de}, was computed using average values as indicated in the following equation:

$$U_{de} = \frac{2\Delta a_N W}{\bar{C}_{L_\alpha} \rho_o \bar{K}_g \bar{V}_e S}$$

APPENDIX IV

DERIVATION OF GUST VELOCITY EQUATIONS

HICAT GUST VELOCITY MEASUREMENTS

The determination of the gust velocity components of atmospheric turbulence from an aircraft flying through turbulence requires the measurement of two quantities:

1) Motion of the air disturbances relative to the aircraft.

2) Motion of the aircraft with respect to the ground.

In the HICAT instrumentation system, the air disturbances relative to the aircraft are measured with a gust probe; the aircraft motion with respect to the ground is determined by an inertial platform.

The following vector equation for gust velocity measurement may be written:

$$\underline{U}_{AG} = \underline{U}_{AP} + \underline{U}_{PG} \qquad (1)$$

where:

$\underline{U}_{AG}$ = velocity of the air (A) relative to the ground (G).

$\underline{U}_{AP}$ = velocity of air (A) relative to the airplane or gust probe (P).

$\underline{U}_{PG}$ = velocity of the airplane or probe (P) relative to the ground (G).

The three gust velocity components are defined as follows:

U_{AG_Z} = Vertical gust component in earth reference axes measured perpendicular to the horizontal plane along the flight track (positive upwards).

U_{AG_Y} = Lateral gust component in earth reference axes measured in the horizontal plane perpendicular to the average grid heading of the aircraft over the duration of the run (positive to aircraft left).

U_{AG_X} = Longitudinal gust component in earth reference axes measured in the horizontal plane parallel to the average grid heading of the aircraft over the duration of the run (positive aft).

Gust Probe Measurements

The primary gust sensor is the HICAT gust probe. The probe senses vertical and lateral gust velocities by the changes in normal force that are produced on small, fixed, wedge-shaped vanes. Longitudinal gust velocities are sensed by the differential pressures produced on a very sensitive pitot-static system. The principle of the fixed-vane measurement of gust velocity is illustrated below for a vane aligned parallel to the average air flow:

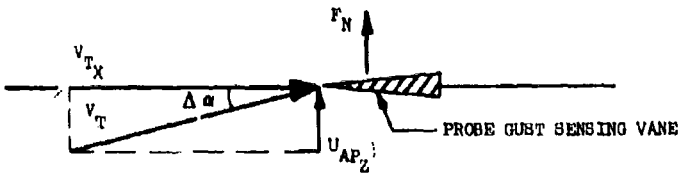

where

V_{T_X} = aircraft true velocity (ft/sec.)

U_{AP_Z} = vertical gust component sensed by probe (ft/sec.)

V_T = resultant instantaneous relative wind due to vertical gust velocity component and aircraft velocity (ft/sec.)

$\Delta\alpha$ = instantaneous vane angle-of-attack (rad)

F_N = vane normal force (lb)

hence

$$U_{AP_Z} = V_{T_X} \tan \Delta\alpha$$

and

$$F_N = C_{N_\alpha} \Delta\alpha \, q \, S_V \qquad (2)$$

where

C_{N_α} = vane normal force coefficient per radian angle-of-attack

Appendix IV

q = dynamic pressure (lb/ft^2)

S_V = vane area (ft^2)

Since $\Delta\alpha$ is always very small ($<10°$)

$$U_{AP_Z} = V_{T_X} \Delta\alpha$$

substituting for $\Delta\alpha$ from equation (2)

$$U_{AP_Z} = V_{T_X} \left(\frac{F_N}{C_{N_\alpha} q S_V} \right) \qquad (3)$$

Ordinarily the probe and the vane will be subjected to oscillatory accelerations caused by the turbulence so that the vane normal force measurement, $F_{N_{M\alpha}}$, will include some small vane inertia force. The actual aerodynamic force, F_N, due to the gust may be obtained free of vane inertia force effects by computing the vane inertia force and removing it from the vane force measurement. Based upon the incremental acceleration measurements at the gust probe the vane inertia force, F_I, is

$$F_I = -m \Delta a_N$$

where

m = vane mass $\left(\frac{lb\ sec^2}{ft} \right)$

Δa_N = incremental vane normal acceleration (ft/sec^2)

The minus sign indicates that the inertia force is in the opposite direction from the acceleration. Then

$$F_{N_{M\alpha}} = F_N + F_I$$

and

$$F_N = F_{N_{M\alpha}} - F_I$$

substituting:

$$F_N = F_{N_{M\alpha}} + m \Delta a_N$$

thus equation (3) becomes

$$U_{AP_Z} = V_{T_X} \Delta\alpha = V_{T_X} \left(\frac{F_{N_{M\alpha}} + m \Delta a_N}{C_{N_\alpha} q S_V} \right)$$

This equation may be expressed entirely in terms of velocity by substituting for q

where

$$q = \frac{\rho V_{T_X}^2}{2}$$

ρ = air density (lb sec^2/ft^4)

$$U_{AP_X} = V_{T_X} \Delta\alpha = \frac{2 \left(F_{N_{M\alpha}} + m \Delta a_N \right)}{C_{N_\alpha} \rho V_{T_X} S_V} \qquad (4)$$

The lateral component may be derived by similar means so that

$$U_{AP_X} = V_{T_X} \Delta\beta = \frac{2 \left(F_{N_{M\beta}} + m \Delta a_L \right)}{C_{N_\beta} \rho V_{T_X} S_V} \qquad (5)$$

when Δa_L = incremental vane lateral acceleration (ft/sec^2).

Aircraft Ground Velocity from LN-3 Platform Components

The platform grid axes are X'-Y' in the diagram. Airplane axes are X-Y.* V_Y, and V_X, are the platform velocity components comprising U_{PG} in the horizontal plane. The airplane reference heading angle is $\bar{\Lambda}$.

*For a true north heading, $\bar{\Lambda}$ = 0, the platform Y' axis corresponds to the airplane X axis.

Hence in airplane axes in the X direction

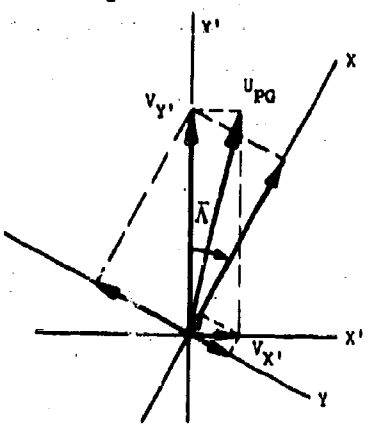

$$U_{PG_X} = V_{X'} \sin\bar{\lambda} + V_{Y'} \cos\bar{\lambda} \qquad (6)$$

$$U_{PG_Y} = V_{X'} \cos\bar{\lambda} - V_{Y'} \sin\bar{\lambda} \qquad (7)$$

GUST VELOCITY EQUATIONS

Vertical Gust Velocity Equation

In the diagram the probe is shown at a positive pitch attitude angle, θ, with respect to the horizontal and with an instantaneous angle-of-attack, α. The inclination with respect to the horizontal of the instantaneous relative wind is γ.

The gust equation in the vertical plane is:

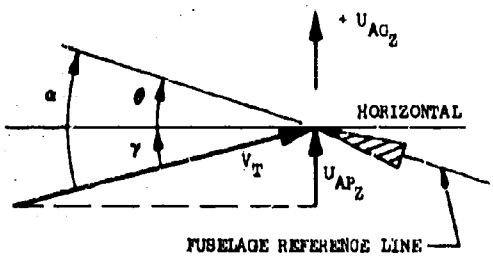

$$U_{AG_Z} = U_{AP_Z} + U_{PG_Z} \qquad (8)$$

$$U_{AP_Z} = V_T \sin\gamma \qquad (9)$$

$$\alpha = \gamma + \theta$$

$$U_{AP_Z} = V_T \sin(\alpha - \theta)$$

$$U_{PG_Z} = \int_0^t (a_Z - g)\, dt + L_X \dot{\theta} \qquad (10)$$

where the integral of the vertical acceleration minus the acceleration of gravity is the aircraft vertical velocity at the accelerometer location and $L_X \dot{\theta}$ is the vertical velocity increment at the probe due to aircraft pitching velocity.

Substituting (9) and (10) in (8)

$$U_{AG_Z} = V_T \sin(\alpha - \theta) + \int_o^t (a_Z - g)\, dt + L_X \dot{\theta}$$

$$= V_T (\sin\alpha \cos\theta - \cos\alpha \sin\theta) + \int_o^t (a_Z - g)\, dt + L_X \dot{\theta}$$

which for small α and θ becomes:

$$U_{AG_Z} = V_T \alpha - V_T \theta + \int_o^t (a_Z - g)\, dt + L_X \dot{\theta} \qquad (11)$$

In this equation θ and a_Z normally come from the platform and hence are always measured in the vertical plane in earth reference axes. However α is measured by the probe as described above by equation (4) and is measured in vertical airplane axes.

For an accurate measurement of U_{AG_Z}, α should be measured in vertical earth axes instead of airplane axes. Hence an α_Z proportional to the normal vane force F_{N_Z} is required and the roll angle, ϕ, must be taken into account.

Adding together the components sensed by each vane:

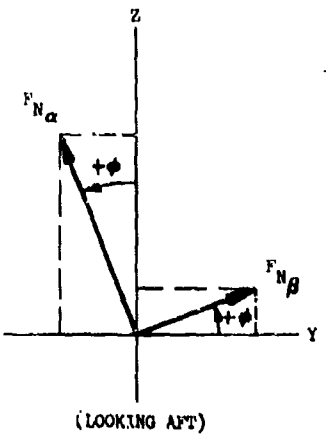

$$F_{N_Z} = F_{N_\alpha} \cos\phi + F_{N_\beta} \sin\phi \qquad (12)$$

where

$$F_{N_Z} = C_{N_\alpha}\, \alpha_Z\, q\, S_V$$

$$F_{N_\beta} = C_{N_\beta}\, \beta\, q\, S_V$$

$$C_{N_\alpha} = C_{N_\beta}$$

Appendix IV

dividing (12)by C_{N_α} q $S_v$gives:

$$a_Z = \alpha \cos \phi + \beta \sin \phi$$

assuming ϕ is small

$$a_Z = \alpha + \beta \phi$$

so that equation (11) becomes:

$$U_{AG_Z} = V_T \alpha + V_T \beta \phi - V_T \theta + \int_o^t (a_Z - g)\, dt + L_X \dot{\theta}$$

If zero mean data is used such that $\Delta\alpha = \alpha - \bar{\alpha}$, $\Delta\theta = \theta - \bar{\theta}$ etc., then

$$U_{AG_Z} = V_T \Delta\alpha + V_T \Delta\beta \Delta\phi - V_T \Delta\theta + \int_o^t \Delta a_Z\, dt + L_X \Delta\dot{\theta} \qquad (13)$$

Note that $L_X = 0$ if the gust probe accelerometer is used in place of platform acceleration.

If platform acceleration is unavailable it may be approximated as follows:

$$a_Z = a_V \cos \theta$$

where

a_V = vertical acceleration in airplane axes.

The vertical acceleration components under rolling conditions may be computed in a similar way to the vane vertical lift (equation 12). Thus

$$a_Z = (a_N \cos \phi - a_L \sin \phi) \cos \theta$$

when

a_N = airplane cg normal acceleration (ft/sec^2)

a_L = airplane cg lateral acceleration (ft/sec^2)

and for ϕ and θ are small

$$a_Z = a_N - a_L \phi$$

which for zero mean data is approximately

$$\Delta a_Z = \Delta a_N - \Delta a_L \Delta\phi$$

The yaw angle corrections have been assumed to be negligible for this analysis.

Lateral Gust Velocity Equation

The equation for lateral gust measurement in the horizontal plane is

$$U_{AG_Y} = U_{AP_Y} + U_{PG_Y} \tag{14}$$

The diagram shows the probe with a positive instantaneous heading angle and a positive reference heading angle with respect to LN-3 grid axis Y'-Y'. Yaw angle, ψ, and sideslip angle, β, are also positive as is the instantaneous lateral gust velocity.

$$U_{AP_Y} = V_T \sin(\beta + \psi) \tag{15}$$

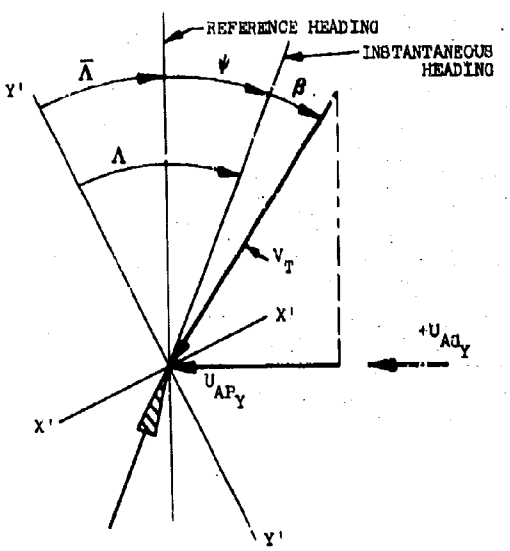

The diagram indicates a positive gust should produce a leftward aircraft velocity relative to the ground. This velocity must be positive so that in the gust velocity equation

$$U_{PG_Y} = -(V_{X'} \cos\bar{\Lambda} - V_{Y'} \sin\bar{\Lambda})$$

U_{PG_Y} is determined from the LN-3 platform velocity components $V_{X'}$ and $V_{Y'}$ as indicated in equation (7). Therefore

$$U_{PG_Y} = -V_{X'} \cos\bar{\Lambda} + V_{Y'} \sin\bar{\Lambda} + L_X \dot{\psi} \tag{16}$$

where L_X is the yawing moment arm between the platform and the probe so that $L_X \dot{\psi}$ is the lateral velocity increment at the probe due to the aircraft yawing velocity. Substituting (15) and (16) into (14)

$$U_{AG_Y} = V_T \sin(\beta + \psi) - V_{X'} \cos \bar{\Lambda} + V_{Y'} \sin \bar{\Lambda} + L_X \dot{\psi}$$

$$= V_T (\sin \beta \cos \psi + \cos \beta \sin \psi) - V_{X'} \cos \bar{\Lambda} + V_{Y'} \sin \bar{\Lambda} + L_X \dot{\psi}$$

which for small angles becomes

$$U_{AG_Y} = V_T \beta + V_T \psi - V_{X'} \cos \bar{\Lambda} + V_{Y'} \sin \bar{\Lambda} + L_X \dot{\psi} \qquad (17)$$

In this equation ψ, $V_{X'}$, and $V_{Y'}$ normally come from the platform and hence are always measured in the horizontal plane in earth reference axes. However, β is measured by the probe in lateral airplane axes as described by equation (5). For an accurate measurement of U_{AG_Y}, β should be measured in lateral earth axes instead of airplane axes. Hence a β_Y proportional to the vane normal force F_{N_Y} is required so that effects of the roll angle, ϕ, must be considered. Referring to the diagram adjacent to equation (12).

$$F_{N_Y} = F_{N_\beta} \cos \phi - F_{N_\alpha} \sin \phi$$

where

$$F_{N_Y} = C_{N_\beta} \beta_Y q S_V$$

$$F_{N_\beta} = C_{N_\beta} \beta q S_V$$

$$F_{N_\alpha} = C_{N_\alpha} \alpha q S_V$$

$$C_{N_\beta} = C_{N_\alpha}$$

dividing by $C_{N_\beta} q S_V$ gives

$$\beta_Y = \beta \cos \phi - \alpha \sin \phi$$

Assuming ϕ is small,

$$\beta_Y = \beta - \alpha\phi$$

so that equation (17) becomes

$$U_{AG_Y} = V_T \beta - V_T \alpha\phi + V_T \psi - V_X, \cos \bar{\Lambda} + V_Y, \sin \bar{\Lambda} + L_X \dot{\psi}$$

For zero mean data, $\Delta\beta = \beta - \bar{\beta}$, $\Delta\psi = \psi - \bar{\psi}$, $\Delta V_X, = V_X, - \bar{V}_X,$, etc., hence

$$\Delta U_{AG_Y} = V_T \Delta\beta - V_T \Delta\alpha \Delta\phi + V_T \Delta\psi - \Delta V_X, \cos \bar{\Lambda} + V_Y, \sin \bar{\Lambda} + L_X \Delta\dot{\psi} \quad (18)$$

If platform velocities are unavailable, then the acceleration, a_Y, may be substituted as follows:

$$\Delta U_{PG_Y} = - \int_o^t a_Y \, dt$$

Since a_Y is not available from the platform it must be computed using the measured acceleration at the center-of-gravity. Note that L_X now becomes the yawing moment arm between the cg accelerometer and the probe.

$$a_Y = a_S \cos \psi$$

where

a_S = horizontal acceleration perpendicular to the reference heading axes.

and

$$a_S = a_L \cos \phi + a_N \sin \phi$$

then

$$a_Y = (a_L \cos \phi + a_N \sin \phi) \cos \psi$$

and for ϕ and ψ small,

$$a_Y = a_L + a_N \phi$$

which for zero mean data is approximately

$$\Delta a_Y = \Delta a_L + a_N \Delta\phi = \Delta a_L + (g + \Delta a_N)\,\Delta\phi$$

Thus equation (18) becomes

$$U_{AG_Y} = V_T \Delta\beta + V_T \Delta\alpha\,\Delta\phi + V_T \Delta\psi - \int_o^t [\Delta a_L + (g + \Delta a_N)\,\Delta\phi]\,dt + L_X \Delta\dot{\psi}$$

where L_X is now the yawing moment arm between the airplane center-of-gravity and the gust probe.

Longitudinal Gust Velocity Equation

The equation for the longitudinal gust measurement in the horizontal plane is

$$U_{AG_X} = U_{AP_X} + U_{PG_X} \qquad (19)$$

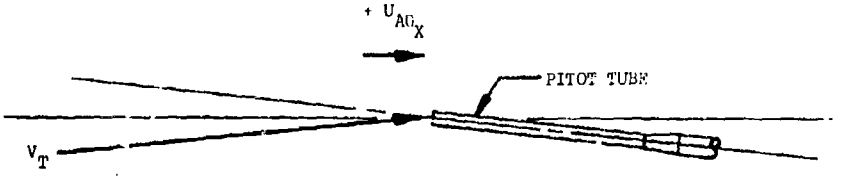

The diagram shows the pitot tube at a slight positive pitch attitude angle with respect to the horizontal. The instantaneous true airspeed, V_T, is also shown slightly inclined to the horizontal. V_T is determined from pitot-static differential pressure measurements and consequently is relatively unaffected by small angular flow changes with respect to the tube.

Consequently,

$$U_{AP_X} = V_T$$

Since positive gusts are directed aft

$$U_{PG_X} = -[V_{X'} \sin\bar{\Lambda} + V_{Y'} \cos\bar{\Lambda}] \quad \text{(from equation 6)}$$

hence

$$U_{AG_X} = V_T - V_{X'} \sin \bar{\Lambda} - V_{Y'} \cos \bar{\Lambda}$$

and for zero mean data

$$\Delta V_T = V_T - \bar{V}_T, \quad \Delta V_{X'} = V_{X'} - \bar{V}_{X'},$$

and

$$\Delta V_{Y'} = V_{Y'} - \bar{V}_{Y'}$$

so that

$$U_{AG_X} = \Delta V_T - \Delta V_{X'} \sin \bar{\Lambda} - \Delta V_{Y'} \cos \bar{\Lambda} \qquad (20)$$

If the platform velocity components are not available, then they may be approximated by integrating the acceleration component, a_X, as follows:

$$\Delta U_{PG_X} = - \int_0^t a_X \, dt$$

where

$$a_X = a_F \cos \theta - a_N \sin \theta$$

where

a_F = measured cg longitudinal acceleration in airplane axes.

Since θ is normally very small,

$$a_X = a_F - a_N \theta$$

which for zero mean data is approximately

$$\Delta a_X = \Delta a_F - a_N \Delta\theta = \Delta a_F - (g + \Delta a_N) \Delta\theta$$

hence equation (20) becomes

$$U_{AG_X} = \Delta V_T - \int_0^t [\Delta a_F - (g + \Delta a_N) \Delta\theta] \, dt$$

Appendix IV

For each of the gust velocity equations derived above an alternate method for determining the incremental aircraft velocity with respect to the ground has been provided should the platform velocities be unavailable. If all the platform angular measurements are unavailable then the angular changes must be determined by integration of the angular rates from the rate gyros.

$$\theta = \int_o^t \dot{\theta}\, dt$$

$$\phi = \int_o^t \dot{\phi}\, dt$$

$$\psi = \int_o^t \dot{\psi}\, dt$$

WIND VELOCITY DETERMINATION

The average wind velocity, $\bar{U}_{AG}$, is determined from the average true airspeed, $\bar{V}_T$, and the aircraft average ground speed $\bar{U}_{PG}$. The vector diagram shows how these quantities are related when the average or reference heading angle, $\bar{\Lambda}$, and the average ground track angle, $\bar{Z}$, are known.

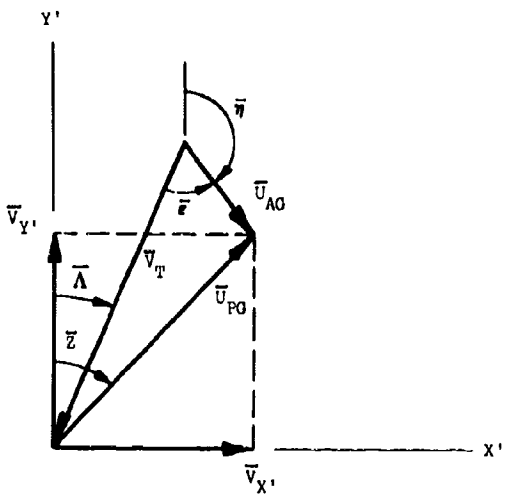

$$V_T = \frac{1}{T_n} \int_o^{T_n} V_T\, dt$$

$$\bar{\Lambda} = \frac{1}{T_n} \int_o^{T_n} \Lambda\, dt$$

where

T_n = time over which average is computed, usually the length of the run (sec).

$$\bar{U}_{PG} = \sqrt{\bar{V}_{X'}^2 + \bar{V}_{Y'}^2} \quad ; \quad \bar{Z} = \tan^{-1} \frac{\bar{V}_{X'}}{\bar{V}_{Y'}}$$

where

$\bar{V}_{X'}$ = aircraft average easterly velocity relative to the ground from LN-3 inertial platform (knots).

$\bar{V}_{Y'}$ = aircraft average northerly velocity relative to the ground from LN-3 inertial platform (knots).

then from the law of cosines

$$\bar{U}_{AG} = \sqrt{\bar{V}_T^2 + \bar{U}_{PG}^2 - 2\,\bar{V}_T\,\bar{U}_{PG}\cos(\bar{Z} - \bar{\Lambda})}$$

$$\bar{n} = 180^\circ - \bar{\varepsilon} + \bar{\Lambda}$$

where

$\bar{n}$ = average wind direction (deg).

$\bar{\varepsilon}$ = angle between the aircraft average velocity vector and the wind vector (deg).

$$\bar{\varepsilon} = \sin^{-1}\left[\frac{\bar{U}_{PG}}{\bar{U}_{AG}}\sin(\bar{Z} - \bar{\Lambda})\right] .$$

Appendix IV

REFERENCES

1. Hildreth, William W. Jr., et al, High Altitude Clear Air Turbulence, Aeronautical Systems Division Technical Documentary Report No. ASD-TDR-63-440 (LR 16816), June 1963, Unclassified.

2. Coleman, Thomas L.; Steiner, Roy, Atmospheric Turbulence Measurements Obtained from Airplane Operations at Altitudes Between 20,000 and 75,000 Feet for Several Areas in the Northern Hemisphere, NASA TN D-548, October 1960, Unclassified.

3. United States Air Force. Research Investigation of High Altitude Clear Air Turbulence in the Altitude Layer of 50,000 to 80,000 Feet. Contract No. AF33(615)-3639, Systems Engineering Group, Research and Technology Division, Air Force Systems Command, Wright-Patterson Air Force Base, Ohio; 1 March 1966. Unclassified.

4. Saunders, K. D., B-66B Low Level Gust Study, Volume XIII. Instrumentation. Wright Air Development Division Technical Report 60-305, March 1961. Unclassified.

5. Crooks, Walter M. High Altitude Clear Air Turbulence. Air Force Flight Dynamics Laboratory, Research and Technology Division, Technical Report No. AFFDL-TR-65-144. (LR 18794) September 1965. Unclassified.

6. United States Air Force. High Altitude Critical Atmospheric Turbulence (HI-CAT) Contract No. F33615-67-C-1461. System Engineering Group, Research and Technology Division, Air Force Systems Command, Wright-Patterson Air Force Base, Ohio; 13 March 1967 Unclassified.

7. Pratt, Kermit G. and Walker, Walter G. A Revised Gust-Load Formula and a Re-evaluation of V-G Data Taken on Civil Transport Airplanes from 1933 to 1950. NACA Report 1206, 1954. (Supersedes NACA TN's 2964 by Kermit G. Pratt and 3041 by Walter G. Walker.) Unclassified.

8. Military Specification. Airplane Strength and Rigidity Flight Loads, MIL-A-8861(ASG). 18 May 1960. Unclassified.

9. Strom, J. A.; Weathermon, T. G. B-66B High Altitude Gust Survey Technical Analysis, Technical Documentary Report ASD-TDR-63-145, Vol 1. April 1963. Unclassified.

10. Burns, Anne; Rider, C. K. Project TOPCAT - Power Spectral Measurements of Clear Air Turbulence Associated with Jet Streams. Royal Aircraft Establishment Technical Report No. 65210, September 1965. Unclassified.

11. Taylor, J. Manual on Aircraft Loads. AGARDograph 83. Pergamon Press Ltd., New York, 1965. Unclassified.

12. Lappe, U. Oscar: Low-Altitude Turbulence Model for Estimating Gust Loads on Aircraft. Journal of Aircraft, Vol. 3, No. 1, Jan-Feb. 1966, pp 41-47.

REFERENCES

13. Saunders, K. D. B-66B Low Level Gust Study. WADD-TR 60-305, Vol. I, Technical Analysis, March 1961. Unclassified.

14. Wilson, E. Bright Jr. An Introduction to Scientific Research. McGraw-Hill Book Company, Inc., New York, 1952.

15. Prophet, D. T. A Mechanism for Clear Air Turbulence Development. Lockheed Report 20428, Lockheed-California Company, Burbank, California. January 1967. Unclassified.

16. HICAT PCM Telemetry Ground Station, Operation and Maintenance Instructions, Volumes I and II, Lockheed Electronics Co., Los Angeles, California. January 1966.

17. Airborne PCM Telemetry System, Model 5302, Operation and Maintenance Manual, Volumes I and II, Dynatronics Inc., Orlando, Florida, November 1965.

18. Acceptance Test Procedures, Airborne PCM Telemetry System, Model 5302, Dynatronics Inc., Orlando, Florida, October 1965.

19. United States Air Force. Technical Manual Field Maintenance, LN-3-2A Inertial Navigation System, USAF TO 5F1-6-2-2, 1 April 1963. Unclassified.

20. M. A. Martin, Digital Filters for Data Processing, G E Technical Information Series, 62SD484, October 1962.

21. R. J. Graham, Determination and Analysis of Numerical Smoothing Weights, NASA TR R-179, 1963.

22. H. Press and J. W. Tukey, Power Spectral Methods and their Application to Problems in Airplane Dynamics, AGARD Flight Test Manual, Vol. IV, Part IVC.

23. R. B. Blackman and J. W. Tukey, The Measurement of Power Spectra, Dover Publications Inc., 1959

Unclassified

Security Classification

DOCUMENT CONTROL DATA - R&D

(Security classification of title, body of abstract and indexing annotation must be entered when the overall report is classified)

1. ORIGINATING ACTIVITY (Corporate author)	2a. REPORT SECURITY CLASSIFICATION
Lockheed-California Company Burbank, California	Unclassified 2b. GROUP

3. REPORT TITLE

PROJECT HICAT AN INVESTIGATION OF HIGH ALTITUDE CLEAR AIR TURBULENCE

4. DESCRIPTIVE NOTES (Type of report and inclusive dates)

Final Report/12 February 1965 to 10 July 1967.

5. AUTHOR(S) (Last name, first name, initial)

Crooks, Walter M.; Hoblit, Frederic M.; Prophet, David T., et al

6. REPORT DATE	7a. TOTAL NO. OF PAGES	7b. NO. OF REFS
November 1967	255	23

8a. CONTRACT OR GRANT NO.	9a. ORIGINATOR'S REPORT NUMBER(S)
AF33(657)-11143 b. PROJECT NO. 1469	Lockheed Report 20771
c. Task No.	9b. OTHER REPORT NO(S) (Any other numbers that may be assigned this report)
d. BPS No. 3(6399-6510)	AFFDL-TR-67-123, Vol I

10. AVAILABILITY/LIMITATION NOTICES

This document is subject to special export control and each transmittal to foreign governments or foreign nationals may be made only with prior approval of AFFDL (FDTE), Wright-Patterson AFB, Ohio 45433.

11. SUPPLEMENTARY NOTES	12. SPONSORING MILITARY ACTIVITY
None	AF Flight Dynamics Laboratory Research and Technology Division Air Force Systems Command Wright-Patterson AFB, Ohio

13. ABSTRACT

This report describes the high altitude clear air turbulence (HICAT) flight investigation with primary emphasis upon the results achieved since 15 February 1965. On this date the program was redirected to utilize a new digital instrumentation system for the measurement of CAT in the wavelength range from about 100 feet to 60,000 feet. The program effort required the measurement of CAT velocity components at altitudes of 45,000 to 70,000 feet in seven geographic areas. Instrumentation carried aboard the HICAT aircraft, an Air Force U-2, consisted of a PCM System, an Inertial Navigation System, aerodynamic and aircraft response sensors including a fixed vane gust probe, oscillograph recorder, and a digital magnetic tape recorder.

The program objective is to determine the statistical characteristics of high altitude CAT so as to improve structural design criteria. Overall, 29.2 hours of high altitude CAT were located and recorded in flights covering over 256,000 miles from bases in California, Massachusetts, Alaska, Hawaii, Puerto Rico, New Zealand, and Australia. Actual vertical, lateral, and longitudinal gust velocity time histories have been calculated from the measurements and used to obtain gust velocity power spectra. Derived equivalent gust velocities were also calculated and peak counted. Meteorological factors were considered in categorizing and correlating data. Time histories and power spectra are found in Volume II of this report, while meteorological data and flight track maps are included in Volume III.

DISTRIBUTION OF THIS ABSTRACT IS UNLIMITED.

DD FORM 1 JAN 64 1473

Unclassified

Security Classification

Unclassified
Security Classification

14. KEY WORDS	LINK A		LINK B		LINK C	
	ROLE	WT	ROLE	WT	ROLE	WT
Turbulence						
Clear Air Turbulence						
Critical Atmospheric Turbulence						
Atmospheric Turbulence						
HICAT (High Altitude Clear Air Turbulence)						

INSTRUCTIONS

1. ORIGINATING ACTIVITY: Enter the name and address of the contractor, subcontractor, grantee, Department of Defense activity or other organization *(corporate author)* issuing the report.

2a. REPORT SECURITY CLASSIFICATION: Enter the overall security classification of the report. Indicate whether "Restricted Data" is included. Marking is to be in accordance with appropriate security regulations.

2b. GROUP: Automatic downgrading is specified in DoD Directive 5200.10 and Armed Forces Industrial Manual. Enter the group number. Also, when applicable, show that optional markings have been used for Group 3 and Group 4 as authorized.

3. REPORT TITLE: Enter the complete report title in all capital letters. Titles in all cases should be unclassified. If a meaningful title cannot be selected without classification, show title classification in all capitals in parenthesis immediately following the title.

4. DESCRIPTIVE NOTES: If appropriate, enter the type of report, e.g., interim, progress, summary, annual, or final. Give the inclusive dates when a specific reporting period is covered.

5. AUTHOR(S): Enter the name(s) of author(s) as shown on or in the report. Enter last name, first name, middle initial. If military, show rank and branch of service. The name of the principal author is an absolute minimum requirement.

6. REPORT DATE: Enter the date of the report as day, month, year; or month, year. If more than one date appears on the report, use date of publication.

7a. TOTAL NUMBER OF PAGES: The total page count should follow normal pagination procedures, i.e., enter the number of pages containing information.

7b. NUMBER OF REFERENCES: Enter the total number of references cited in the report.

8a. CONTRACT OR GRANT NUMBER: If appropriate, enter the applicable number of the contract or grant under which the report was written.

8b, 8c, & 8d. PROJECT NUMBER: Enter the appropriate military department identification, such as project number, subproject number, system numbers, task number, etc.

9a. ORIGINATOR'S REPORT NUMBER(S): Enter the official report number by which the document will be identified and controlled by the originating activity. This number must be unique to this report.

9b. OTHER REPORT NUMBER(S): If the report has been assigned any other report numbers *(either by the originator or by the sponsor)*, also enter this number(s).

10. AVAILABILITY/LIMITATION NOTICES: Enter any limitations on further dissemination of the report, other than those imposed by security classification, using standard statements such as:

(1) "Qualified requesters may obtain copies of this report from DDC."

(2) "Foreign announcement and dissemination of this report by DDC is not authorized."

(3) "U. S. Government agencies may obtain copies of this report directly from DDC. Other qualified DDC users shall request through _____."

(4) "U. S. military agencies may obtain copies of this report directly from DDC. Other qualified users shall request through _____."

(5) "All distribution of this report is controlled. Qualified DDC users shall request through _____."

If the report has been furnished to the Office of Technical Services, Department of Commerce, for sale to the public, indicate this fact and enter the price, if known.

11. SUPPLEMENTARY NOTES: Use for additional explanatory notes.

12. SPONSORING MILITARY ACTIVITY: Enter the name of the departmental project office or laboratory sponsoring *(paying for)* the research and development. Include address.

13. ABSTRACT: Enter an abstract giving a brief and factual summary of the document indicative of the report, even though it may also appear elsewhere in the body of the technical report. If additional space is required, a continuation sheet shall be attached.

It is highly desirable that the abstract of classified reports be unclassified. Each paragraph of the abstract shall end with an indication of the military security classification of the information in the paragraph, represented as *(TS)*, *(S)*, *(C)*, or *(U)*.

There is no limitation on the length of the abstract. However, the suggested length is from 150 to 225 words.

14. KEY WORDS: Key words are technically meaningful terms or short phrases that characterize a report and may be used as index entries for cataloging the report. Key words must be selected so that no security classification is required. Identifiers, such as equipment model designation, trade name, military project code name, geographic location, may be used as key words but will be followed by an indication of technical context. The assignment of links, rules, and weights is optional.

Unclassified
Security Classification